COMMUNICATIONS OF THE GEOLOGICAL SURVEY OF NAMIBIA

VOLUME 23
2021

CONTENTS

Cover Image

The richly fossiliferous late Eocene Tufa Dome at Eocliff, Sperrgebiet, Namibia, viewed from the east

(Image: Martin Pickford)

A Reference Section for the Otavi Group (Damara Supergroup) in Eastern Kaoko Zone near Ongongo, Namibia

P.F. Hoffman[1,2,*], S.B. Pruss[3], C.L. Blättler[4], E.J. Bellefroid[5] & B.W. Johnson[6]

[1]*School of Earth & Ocean Sciences, University of Victoria, Victoria, BC, Canada, V8P 5C2*
[2]*Department of Earth & Planetary Sciences, Harvard University, Cambridge, MA 02138, USA*
[3]*Department of Geosciences, Smith College, Northampton, MA 01065, USA*
[4]*Department of Geophysical Sciences, University of Chicago, Chicago, IL 60637, USA*
[5]*Department of Earth & Planetary Sciences, McGill University, Montreal, QC, Canada, H3A 0E8*
[6]*Department of Geological & Atmospheric Sciences, Iowa State University, Ames, IA 50011-1027, USA*
* *1216 Montrose Ave., Victoria, BC, Canada, V8T 2K4. email: <paulfhoffman@gmail.com>*

Abstract : A reference section for the Otavi Group (Damara Supergroup) in the East Kaoko Zone near Ongongo is proposed and described. The section is easily accessible, well exposed, suitable for field excursions, and well documented in terms of carbonate lithofacies, depositional sequences and stable-isotope chemostratigraphy. The late Tonian Ombombo Subgroup is 355 m thick above the basal Beesvlakte Formation, which is not included in the section due to poor outcrop and complex structure. The early-middle Cryogenian Abenab Subgroup is 636 m thick and the early Ediacaran Tsumeb Subgroup is 1020 m thick. While the section is complete in terms of formations represented, the Ombombo and lower Abenab subgroups have defined gaps due to intermittent uplift of the northward-sloping Makalani rift shoulder. The upper Abenab and Tsumeb subgroups are relatively thin due to erosion of a broad shallow trough during late Cryogenian glaciation and flexural arching during post-rift thermal subsidence of the carbonate platform.

Introduction

The Otavi Group (Fig. 1) is a folded neritic carbonate succession of Neoproterozoic age. In northern Namibia, it is 1.5-3.5 km thick and covers the Congo craton (Northern Platform) east of the Kaoko belt and north of the Damara belt (Miller, 2008). Continuations of the same former carbonate platform occur in the West Congo and Zambian fold belts (Miller, 2013; Delpomdor *et al.* 2016; Cailteaux & De Putter, 2019) as well as in subsurface in the Congo Basin (Kadima *et al.* 2011). The original extent of the shallow-marine carbonate bank was on the order of 5 million square kilometres.

The type area of the Otavi Group is the Otavi Mountainland (SACS, 1980; Hedberg, 1979; King, 1994; Kamona & Günzel, 2007; Miller, 2008). Regrettably, the formations defined in that area (Fig. 1E) were detailed only in unpublished reports (Söhnge, 1953, 1957). There are few modern descriptions of the carbonate sedimentology (Krüger, 1969; Hegenberger, 1987; Bechstädt *et al.* 2009; Delpomdor *et al.* 2018), and existing stable isotope data from the Otavi Mountainland have low stratigraphic resolution (Kaufman *et al.* 1991) except for the youngest formation (Cui *et al.* 2018). Moreover, the oldest of three subgroups making up the revised Otavi Group (Hoffmann & Prave, 1996) is not preserved in the Otavi Mountainland (Fig. 1).

Major upgrades of vehicle route D3710 (Fig. 2) made accessible one of the most complete and conveniently exposed sections of the Otavi Group (2.02 km) in the Eastern Kaoko Zone (Miller, 2008). The top of the section is located 2.2 km east of the spring at Ongongo, 5 km north

of route C43 at Warmquelle (Fig. 2). The purpose of this paper is to present a composite section from Ongongo as a reference section for the Otavi Group in the western part of the platform. As a 2-3-day field excursion, it complements the correlative foreslope section (Swakop Group) at Fransfontein, 170 km to the southeast (Hoffman *et al.* 2021). High-resolution carbonate δ^{13}C and δ^{18}O records have been obtained from the Ongongo section and its basin-scale setting is well documented (Hoffman *et al.* 2021). A field guide for the Ongongo section with illustrations different from those in this paper is available as supplementary on-line information SOI S3.12, appended to Hoffman *et al.* (2021).

Structure

The Ongongo section (Fig. 3) is exposed on the western limb of a doubly-plunging anticlinal culmination. The structural culmination is situated at the southern tip (lateral tip-line) of an eastward-vergent thin-skinned thrust-stack exposed in oblique section (Fig. 2). A little over 12 km north-northeast of the culmination, basal Devede Formation is thrust over middle Elandshoek Formation (Fig. 1), a stratigraphic duplication of 1.4 km. The thrust is rooted in a detachment zone that is coextensive with the marly and argillaceous Beesvklate Formation (Fig. 1), exposed in a nest of possible sheath folds north of Okakuyu (Fig. 2).
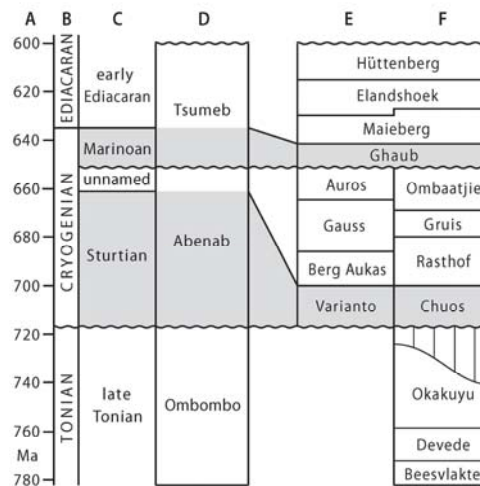

Figure 1. Geologic time scale and Otavi Group formations and subgroups in the Otavi Mountainland and Eastern Kaoko zone. (A) Age in 10^6 years before present (Ma). (B) Periods (Gradstein *et al.* 2012; Shields-Zhou *et al.* 2016). (C) Epochs, with panglacial (snowball) epochs indicated by grey shade. (D) Subgroups of Otavi Group (SACS, 1980; Hoffmann & Prave, 1996). (E) Formations as defined in the Otavi Mountainland (Söhnge, 1957; Hedberg, 1979; SACS, 1980; King, 1994; Hoffmann & Prave, 1996). (F) Formations as defined in the Eastern Kaoko zone (Hedberg, 1979; Hoffman & Halverson, 2008; Hoffman *et al*, 2021). Note that the early Ediacaran and unnamed middle Cryogenian inter-snowball epoch are expanded in E and F relative to the time scale in A-D. Epoch time boundaries: early Cryogenian (Sturtian snowball onset) at 717 Ma (Macdonald *et al*. 2018; MacLennan *et al*. 2018; Lan *et al*. 2020); middle Cryogenian (Sturtian snowball termination) at 661 Ma (Rooney *et al*. 2015, 2020); late Cryogenian (Marinoan snowball onset) at 651 Ma (Prave *et al*. 2016; Bao *et al*. 2018; Nelson *et al*. 2021); early Ediacaran (Marinoan snowball termination) at 635 Ma (Rooney *et al*, 2015; Zhou *et al*, 2019). Top of the Otavi Group is constrained to be ≤600 Ma by D1 metamorphic (^{39}Ar/^{40}Ar phengite) ages in Otavi Group-correlative Swakop Group in the Northern Damara zone (Lehmann *et al*. 2016). The top of the Devede Fm is 760 Ma (Halverson *et al*, 2005; Hoffman *et al*, 2021) based on U-Pb (ID-TIMS) ages for igneous zircon from an airborne volcanic ash layer 37 km NNW of the Ongongo section (Fig. 2).

The thin-skinned thrusts and associated short-wavelength (2-3 km) folds (D1) were subsequently deformed by long-wavelength (20-30 km) thick-skinned structures (D2) of oblique NNW-SSE trend. Major D2 structures include the Sesfontein Thrust and the associated Warmquelle footwall syncline (Fig. 2), and Kamanjab basement anticline and its autochthonous cover of Nosib Group arkosic terrestrial clastics. Structural relief in the area (Fig. 2) owes much to the opposing plunges of the first-order D2 structures, Kamanjab anticline and Warmquelle syncline (Guj, 1970; Hedberg, 1979).
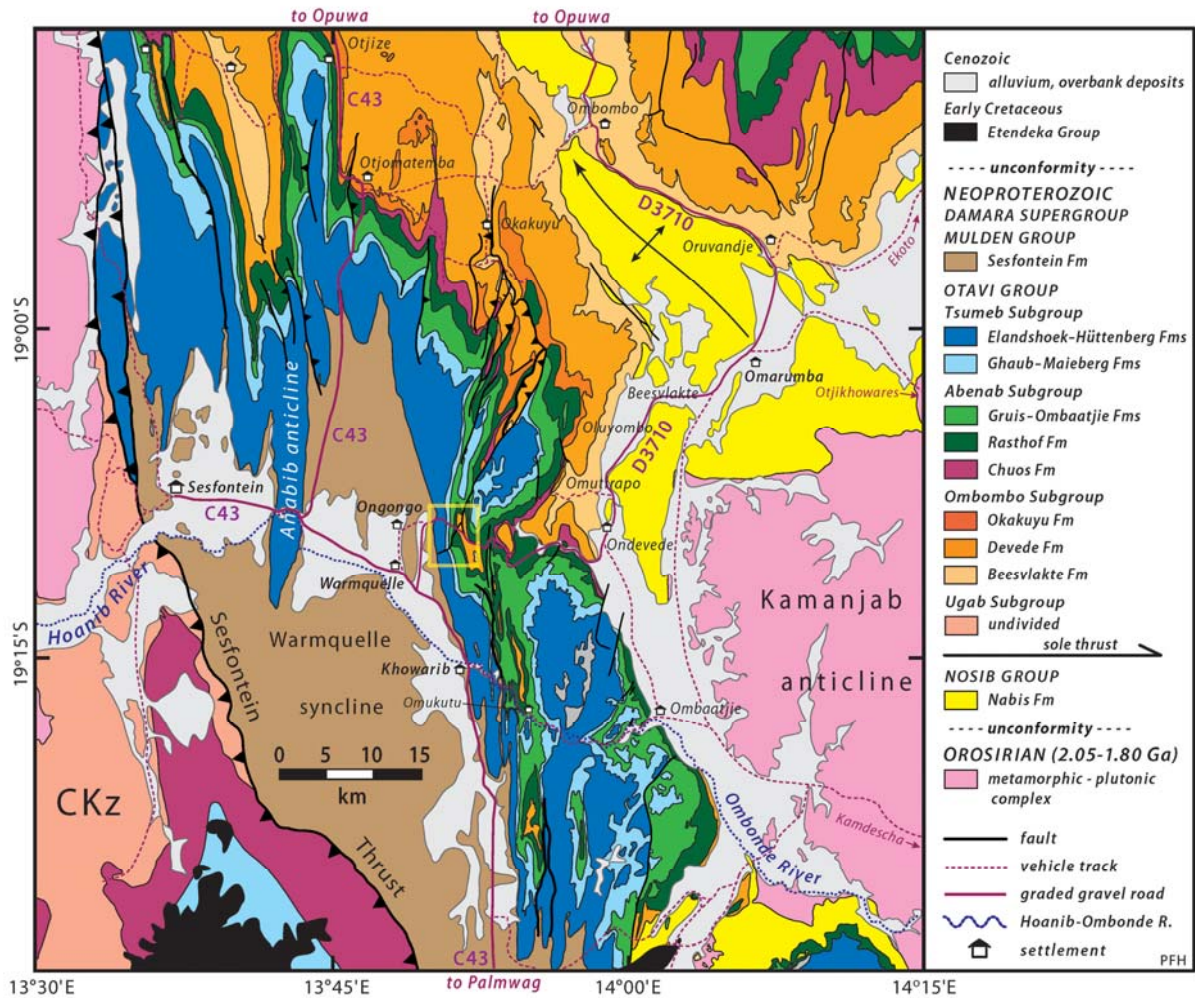
Figure 2. Bedrock geology of the upper Hoanib River area (Hoffman *et al.* 2021). The area of the proposed reference section east of Ongongo is indicated by the yellow box.

The structural culmination east of Ongongo (yellow box, Fig. 2) is aligned with a WSW-ENE line of structural highs. This transverse structural welt is oriented parallel to the Damara belt. A wave train of plunge reversals extends southwards along strike from the culmination east of Ongongo (Fig. 2). These transverse waves could be a far-field response to terminal Damara collision (D3) at ~550 Ma in Southern (Khomas) Zone (Miller, 2008; Goscombe *et al.* 2018).

3

Basin-scale setting

Ongongo is situated on the inner platform (IPz) of the Otavi Group, 85 km north of the southern foreslope (Hoffman & Halverson, 2008; Hoffman *et al.* 2021). Its distance from the western platform edge is unknown because the Sesfontein Thrust occludes the shelf break. The distance could not have been less than 70 km, assuming 50% W-E tectonic shortening in the train of tight D1 folds and thrusts between Ongongo and the Sesfontein Thrust (Fig. 2).

Subsidence accommodating Otavi Group occurred in two stages: syn-rift and post-rift. The transition coincides with the top of the Gruis Formation (Fig. 1), allowing for minor fault reactivation in the lower Ombaatjie Formation. In terms of stratigraphic thickness at Ongongo, 36% (733 m) of the section is syn-rift and 64% (1285 m) is post-rift. The nearest major rift structure was the northward-tilted dip-slope of Makalani rift-shoulder (Hoffman & Halverson, 2008; Hoffman *et al.* 2021), the crest of which was 70 km south of Ongongo. Terrigenous clastics in the Ombombo and Abenab subgroups at Ongongo were likely derived from the Makalani dip-slope according to palaeocurrents and spatial grain-size variation (Hoffman & Halverson, 2008; Hoffman *et al.* 2021).

Erosional disconformities of glacial origin define the base of the Abenab and Tsumeb subgroups (Fig. 1). Minimum depths of erosion and thicknesses of lost strata can be estimated from subglacial palaeotopographies constructed from measured sections throughout the area (Hoffman *et al.* 2021). The late Tonian Okakuyu Formation (Fig. 1) is relatively thin (45 m) at Ongongo, implying Sturtian erosion of ≥350 m compared with the Okakuyu area 25 km to the north (Fig. 2). Ongongo is situated at the western margin of Omarumba trough (Hoffman *et al.* 2021), a wide shallow NNE-SSW trending glacial trough of Marinoan age. As a result, ≥60 m of uppermost Ombaatjie Formation (Fig. 1) has been lost at Ongongo relative to areas outside the Omarumba trough.

Total post-rift stratigraphic thickness varies significantly S-N across the platform. Thickness minima mark the crest of an arch, the Khowarib arch (Hoffman *et al.* 2021), located ~75 km north of the southern margin and ~30 km south of Ongongo. Thinning over the arch affects the Ombaatjie, Maieberg, Elandshoek and Hüttenberg formations (Fig. 1) in roughly equal proportion (Hoffman *et al.* 2018, 2021). This implies that thinning is not the result of erosion but does reflect spatial variation in long-term subsidence, apparently including a component of lithospheric flexure (e.g. Watts *et al.* 1982). The post-rift succession at Ongongo is 34% thicker (1285 vs 958 m) than the same succession at the crest of the arch, but is only half as thick as sections 60 km to the north - 2560 m at Ohumbameya (Hoffman *et al.* 2018) or 2690 m in the northern Otavi Mountainland (King, 1994). Isopach data compiled by Hedberg (1979) suggest that the Khowarib arch may project eastwards to the southern Otavi Mountainland. South of the arch, the post-rift succession thickens to an estimated 2075 m (61% thicker than at Ongongo) on farm Neuland 541 near the shelf break, 23.5 km west of Outjo.

Location and Access

The Ongongo section is most easily reached from regional route C43 (Fig. 2) between Khorixas and Opuwa. The intersection with D3710 is at 19.1972°S/13.8229°E, 9.0 km NNW of Khowarib. Turn north onto D3710 and proceed 7 km angling toward the near-vertical dolomite before turning eastward into the drainage gap (Fig. 3). The road, as it progresses upstream from bank to bank, descends stratigraphically through 2.02 km of carbonate strata.

There are two structural kinks in the overall west-facing fold limb. At the elevation of the drainage, the short dip reversals are in the Devede and Maieberg formations (Fig. 1). These minor folds may relate to the lateral tip-line of the D1 thrust to the north (Fig. 2).

The riverbed through the section (Fig. 3) is bouldery and not suitable for camping. A cozy and convenient campsite for a small party is located at the small magenta circle in Figure 3. Stop on road D3710 at 19.1457°S/13.8595°E and

turn northeast, perpendicular to the road. Cross the secondary drainage channel and turn left (NNW) onto a seldom-used vehicle track for 0.11 km to the campsite at 19.1449°S/13.8596°E. The entire section is within easy walking distance from this campsite.
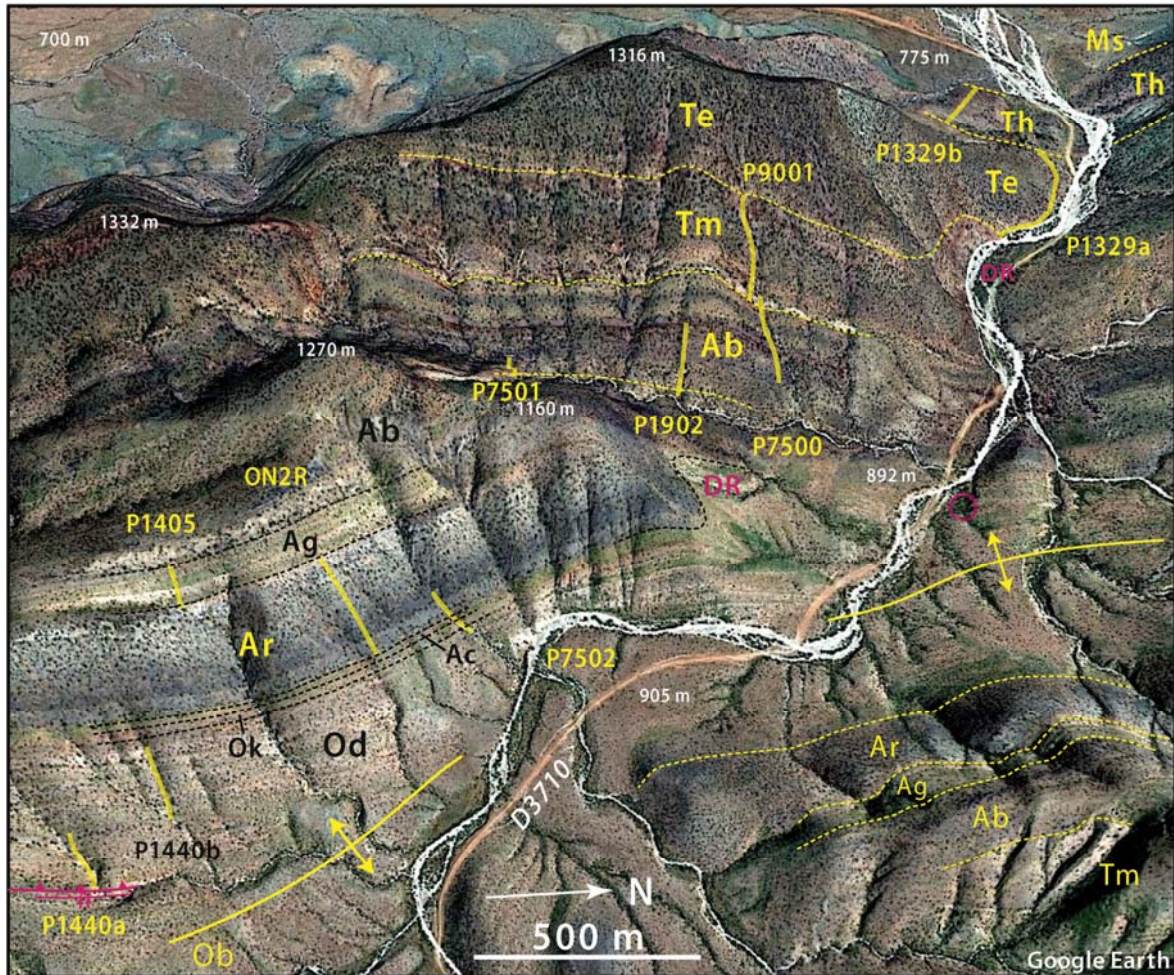
Figure 3. Oblique satellite image looking westward at the proposed Otavi Group reference section on route D3710. Dashed lines indicate formation boundaries and solid yellow lines are the numbered measured sections. Abbreviations (Fig. 1): Ab, Ombaatjie Fm; Ac, Chuos Fm; Ag, Gruis Fm; Ar, Rasthof Fm; DR (magenta), dip reversal; Ms, Sesfontein Fm (Mulden Group); Ob, Beesvlakte Fm; Od, Devede Fm; Ok, Okakuyu Fm; Te, Elandshoek Fm; Th, Hüttenberg Fm; Tm, Maieberg Fm. Magenta circle (centre right) is a convenient campsite. Spot elevations (relative to sea level) in white. Google Earth Image © 2021 Maxar Technologies.

For larger parties, a prepared rest camp at the spring (swimming hole) in Ongongo is located 2.2 km west of the stratigraphic top of the section. At 19.1411°S/13.8370°E on D3710, turn west onto a small dirt track. Follow this track westward, bearing right at forks 0.89 km, 1.53 km and 2.47 km beyond the turnoff. The last fork is at 19.1450°S/13.8155°E. Cross the river at 19.1462°S/13.8130°E and drive north and then northeast for 1.23 km around to the rest camp reception area near 19.1398°S/13.8190°E. Cross back over the river at 19.1405°S/13.8187°E to reach the camping area at 19.1403°S/13.8194°E near the swimming hole on the south side of the river. The campsite can also be reached directly from Warmquelle, 5.8 km to the south on route C43 (Fig. 2).

Lithofacies terminology and carbon isotope excursions

Carbonate lithofacies are categorised as described and illustrated previously (Halverson *et al.* 2002; Hoffman & Halverson, 2008; Hoffman, 2011a; Hoffman *et al.* 2021). 'Rhythmite' is flat-laminated micrite lacking evidence of wave or traction-current action, but may include turbidites and debrites. 'Ribbonite' is thin-bedded (<0.3 m) lutite with wave- or traction-current bedforms including low-angle cross-stratification. 'Stromatolite' refers to laminated microbial-sedimentary structures, typically dendroidal or columnar, occurring both as mounded and tabular bodies. 'Grainstone' is thick-bedded (>0.3 m) arenite, commonly cross-bedded, composed of intraclasts and/or ooids with intergranular void-filling cement and authigenic chert where dolomitized. 'Microbialaminite' refers to microbial-sedimentary deposits with low-relief undulatory laminations characterized by small-scale disconformities, tabular intraclasts, and 'tepee' structures representing polygonal pressure ridges caused by expansive cementation driven by evaporative pumping, indicative of subaerial exposure (Assereto & Kendall, 1978; Kendall & Warren, 1987). In the order given, the five lithofacies are considered to represent a sequence of decreasing water depth at a given location, or a seaward to landward transect across a prograding shelf and coastal system. Microbial lithofacies in the middle Ar2 member of Rasthof Formation (Fig. 1) do not fit comfortably in the general lithofacies scheme. Distinct lithofacies unique in the Otavi Group to Rasthof Formation are described under that formation.

Carbon isotope excursions (CIEs) are significant departures from long-term mean $\delta^{13}C$ values. They are numbered from the base of the Cryogenian and Ediacaran Periods, with odd numbers for negative excursions (lower $\delta^{13}C$) and even numbers for positive excursions (higher $\delta^{13}C$) following Quaternary marine $\delta^{18}O$ stages (Pillans & Gibbard, 2012). Five Cryogenian (Cn1-Cn5) and four Ediacaran (En1-En4) CIEs are recognized in the Otavi Group. Many can be correlated with CIEs defined and named in other regions, as noted below.

Devede and Okakuyu formations (Ombombo Subgroup)

The Ombombo Subgroup (Hoffmann & Prave, 1996) is composed of three formations (Fig. 1), the oldest of which is poorly exposed in the core of the Ongongo anticline and no attempt was made to include it in the measured section (Fig. 4). Where it is best laid out, southeast of Oruvandje (Fig. 2), the Beesvlakte Formation consists of three members: a lower argillite, a middle argillite and a regressive set of upward-shoaling nearshore dolomite cycles (stromatolite, grainstone and intertidal microbialaminite), and an upper marly marble tectonite (Hoffman & Halverson, 2008).
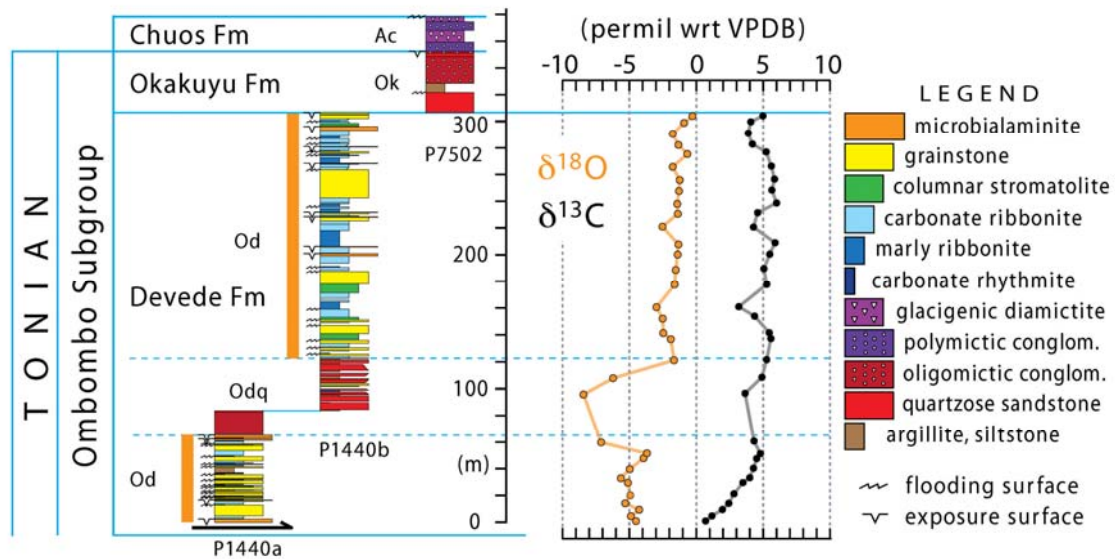
Figure 4. Late Tonian Ombombo Subgroup (Fig. 1) columnar sections P1440a, P1440b and P7502 (Fig. 3), with stable isotope records (Hoffman *et al*. 2021). Abbreviations as in Figure 3. Unit Odq is a northward-tapered siliciclastic tongue in the lower Devede Formation.

Section P1440a (Figs. 3 & 4) begins at 19.1717°S/13.8710°E on the hanging wall of a small eastward-vergent thrust, beneath which is a syncline of lower Devede Formation dolomite. Comparison with adjacent sections suggests that the hanging wall of the thrust at this location is close to the base of the Devede Formation, which is defined as the first dolomite ≥1.0 m thick. The Devede Formation is 310 m thick in P1440, which is a composite of two sections P1440a and b (Figs 3 & 4). Essentially, it is a stack of regressive nearshore dolomite cycles with a member (Odq) rich in siliciclastic (quartz-chert) rudite and arenite between 85 and 126 m stratigraphically above the datum. This mappable wedge of clastics thickens southward toward the Makalani rift shoulder and consists of resistant debris eroded from uplifted quartzarenite (Nabis Formation) and authigenic chert from the lower Devede dolomite (Hoffman & Halverson, 2008). It records SSE-down rift-faulting on the Makalani structure in early Devede Formation time with rift-shoulder uplift as an isostatic response. At the base of the siliciclastic member in P1440a is a 17-m-thick roundstone conglomerate, the top of which is easily walked out linking sections P1440a and b (Fig. 3). The top of the section 'a' is at 19.1724°S/13.8698°E and the base of section 'b' is at 19.1697°S/13.8693°E. The conglomerate contains clasts of quartz, quartzite, amphibolite and granodiorite, indicating formerly exposed basement on the Makalani dip-slope.

In total, the Devede Formation in P1440 contains approximately 52 depositional cycles, yielding an average thickness of 6.0 m per cycle. The cycles are strongly asymmetric with condensed transgressions and fulsome regressions in the (complete) sequence marly ribbonite (wavy dololutite), ribbonite, stromatolite, cherty grainstone (beds ≥0.4 m) and microbialaminite. Twelve of the cycles end at evident subaerial exposure surfaces (tepee structure, Assereto & Kendall, 1978; Kendall & Warren, 1987) and the rest at marine flooding surfaces (36) or erosive scours (4). There are eleven columnar stromatolite beds ranging from 0.3 to 6.8 m thick (average 1.5 m), the more developed of which exhibit divergent to prone branching typical of the morphotype *Tungussia* Semikhatov (Hofmann, 1969). Commonly pale pinkish in colour, the bedding-parallel branches give these stromatolite beds a nodular appearance in outcrop.

In most other sections, there is a 150-m-thick interval dominated by pink *Tungussia* stromatolite biostromes near the top of the Devede Formation (Hoffman & Halverson, 2008; Hoffman *et al*. 2021). This interval is missing at

7

Ongongo. Because the Devede Formation at Ongongo is 100-180 m thinner than other sections (n=4) within 20 km distance (to the northeast, Fig. 2), erosion beneath the disconformity at the base of the overlying Okakuyu Formation (Fig. 4) is the simplest explanation for the missing thick stromatolite biostrome interval. The disconformity has 4.0 m of local relief at the top of section P1440b (19.1701°S/13.8676°E).

The Okakuyu Formation is only 5.6-9.6 m thick in section P1440b, so a thicker (45.4 m) section at P7502 (Fig. 3) was utilized in the composite section (Fig. 4). The base of the Okakuyu Fm in P7502 is at 19.1614°S/13.8634°E and the section consists of two units each of quartz-quartzite-chert-pebble conglomerate and cross-bedded sandstone of the same composition, and a single unit of thin-bedded argillaceous siltstone (Fig. 4). The top of the Okakuyu Formation at 19.1615°S/13.8632°E is poorly exposed, but the basal Chuos conglomerate can be distinguished from the underlying Okakuyu conglomerate by the presence of dolomite clasts, more abundant chert clasts and a less well-sorted matrix. Since the Okakuyu Formation is 300-350 m thick 25 km north of Ongongo (Hoffman & Halverson, 2008), we must assume that in the Ongongo section it is ≥85% erosionally truncated beneath the sub-Chuos Formation disconformity/ unconformity. Northward younging toplaps beneath the Okakuyu and Chuos formations suggest repeated late Tonian (post-760 Ma) reactivations of the Makalani rift shoulder.

Chuos and Rasthof formations (Abenab Subgroup)

The Sturtian glacigenic Chuos Formation was measured in section P7502 and its cap-carbonate sequence, the Rasthof Formation was documented in section ON2R (Figs 3 & 5). The Rasthof Formation $\delta^{13}C$ data are from Pruss et al. (2010).

The 26-m-thick Chuos Formation consists of two conglomerates, each overlain by diamictite (Fig. 5). Both conglomerates carry clasts of dolomite, chert, quartzite and quartz, the older (7.0 m) being stratified and the younger (6.3 m) fining upward. The diamictites are matrix-supported polymictic rudites with clast types similar to the conglomerates but with the addition of basement granodiorite clasts in the older, thicker (8.8 m) and more massive of the two diamictites. This older diamictite has a mud-rich greywacke matrix and both rounded and angular cobbles. The younger diamictite (3.8 m) is weakly stratified, clast-size graded and Fe-enriched. The base of the Chuos Formation is at 19.1615°S/13.8632°E in P7502 and its top is at 19.1616°S/13.8631°E.
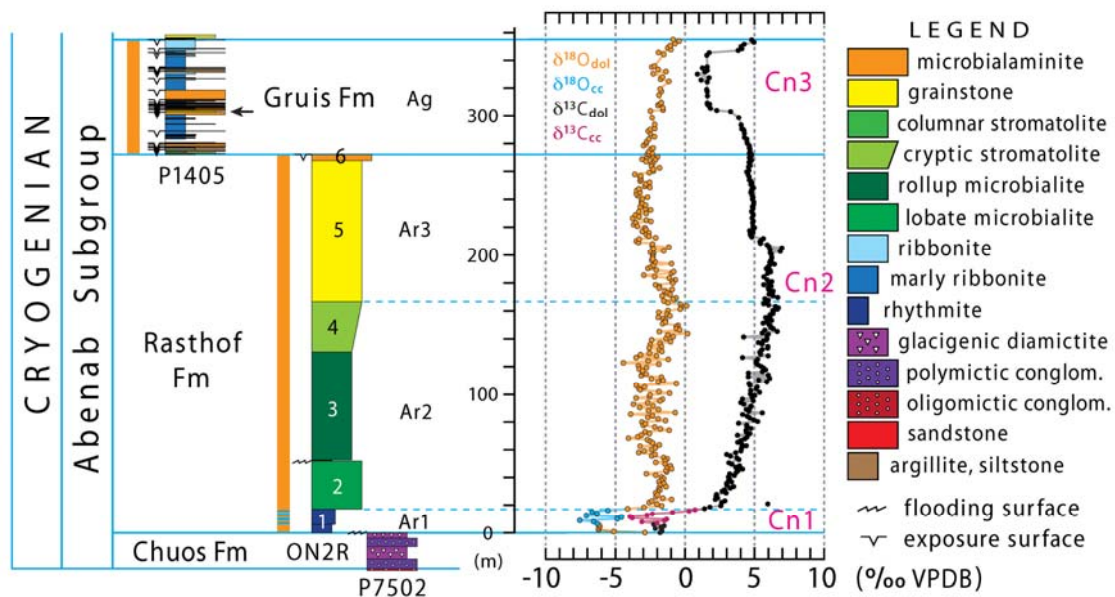
Figure 5. Cryogenian lower Abenab Subgroup (Fig. 1) columnar sections P7502 (Chuos Fm), ON2R (Rasthof Fm) and P1405 (Gruis Fm), with stable isotope records (Hoffman *et al*. 2021). See Figure 3 for section locations. The Rasthof Formation is divisible into three members (Ar1-3) and six lithofacies units (see text). Note colour coding for dolomite (orange and black) and calcite (blue and purple) isotope data points.

The 271.5-m-thick Rasthof Formation is essentially an inflated highstand depositional sequence divided into six lithofacies units (Fig. 5). The deepest-water facies is at the base of the formation and the shallowest is at the top, with but a single flooding surface within the sequence. Much of the postglacial accommodation space required for highstand Rasthof accumulation would have been provided by net Sturtian erosion - 255-305 m of Okakuyu Formation eroded (see previous section) less 26 m of Chuos Formation deposited.

Unit 1 (Ar1, Fig. 5) is 17.0 m thick in section ON2R and consists of dark grey parallel-laminated abiotic dolomite rhythmite with spaced 5-30-cm-thick limestone turbidites and fine-grained debrites in the upper 10 m. Its basal contact with Fe-rich diamictite is knife-sharp, and its upper contact with lobate microbialite (unit 2) is gradational over ~0.5 m.

Unit 2 ('lobate microbialite,' Fig. 5) is 35.0 m thick in ON2R and corresponds to the 'thickly-laminated' facies (Pruss *et al*. 2010; Bosak *et al*. 2011; Dalton *et al*. 2013). A medium grey dolomite, it is a laminated microbialite characterised by 10-20-cm-scale convexities that

expand upwards in any fixed direction, climbing obliquely above an inclined zone of tightly deformed laminae with abundant 'chambered' void-filling sparry cement (Pruss *et al*. 2010; Le Ber *et al*. 2013; Wallace *et al*. 2014). In cross-section, these microbial 'lobes' resemble anticlines developed over thrust ramps, but unlike tectonic structures their directions of lateral growth have no preferred azimuth. A possible cause of non-directional compression (constrict-tion) in the horizontal plane is microbial growth expansion, with lobes being an expression of the free surface. Microbial growth expansion has been invoked to explain 'microbial polygons' in productive tidal ponds on the littoral coast of the United Arab Emirates (Lokier *et al*. 2018). Unlike the Persian/Arabian Gulf microbial structures, the 'lobate microbialites' in the Rasthof Formation lack evidence of desiccation or current action. A small percentage of the lobes develop sharp secondary crests that aggrade vertically (Hoffman *et al*. 2021). These are the only suggestions of phototropism in what, from its sequence stratigraphic position, is inferred to be a deep sublittoral environment. An oddity of unit 2 is that from a distance it appears to be

9

regularly bedded on a 2-m-scale, but at the outcrop this bedding is cryptic.

Unit 3 ('rollup microbialite,' Fig. 5) is 78.5 m thick in ON2R and corresponds to the 'thinly-laminated' facies (Pruss *et al.* 2010; Bosak *et al.* 2011; Dalton *et al.* 2013). Its top is gradational but its base is a prominent flooding surface, underlain by a 20-cm drape of quartzose silty dolomite with low-angle cross-stratification and overlain by 0.6 m of marly dolomite ribbonite. Unit 3 microbialite is a smoothly laminated dolomite which at a distance has the darkest grey colour within the Rasthof Formation (Fig. 3), but which actually consists of alternating dark and light laminae averaging 13 couplets per cm. The dark laminae become paler with stratigraphic height such that the top of unit 3 is less a loss of laminae than a loss of colour contrast.

'Rollups' are the iconic structure in unit 3 and consist of delaminated flaps, generally 2-6 couplets thick, that were folded and refolded on the seafloor (Hoffman *et al.* 1998a; Hoffman & Halverson, 2008; Pruss *et al.* 2010; Bosak *et al.* 2013; Le Ber *et al.* 2013). The rollups indicate that the sediment was cohesive but pliable when folding occurred, presumably because of microbial binding. How the flaps were originally torn is usually conjectural, but in some cases, it is related to intermittent fluid or gas expulsion from neptunian dykes (Pruss *et al.* 2010; Bosak *et al.* 2013; Hoffman *et al.* 2021). Some such dykes are bordered by stacks of flaps that were successively back-flipped away the dyke, flap after flap. The dykes themselves are typically filled by microbialite intraclasts and void-filling cement.

Insoluble residues from samples of units 2 and 3 in ON2R contain variable concentrations of microscopic, organic-rich, regularly-sized, elliptical bodies (110 x 70 μm) and tubular structures, interpreted as the agglutinated tests of protistan heterotrophs (Pruss *et al.* 2010; Bosak *et al.* 2011, 2012; Dalton *et al.* 2013). Biological agglutination of detrital grains is supported by mineralogical investigation of post-Sturtian cap-carbonate sequences in Zambia (Kakontwe Formation) and Mongolia (Tayshir Formation) containing similar microfossils (Moore *et al.* 2017).

Unit 4 is 35 m thick in ON2R and is gradational with units 3 and 5 (Fig. 5). Palimpsest microbial lamination is evident basally and mechanical layering at the top. The term 'cryptic stromatolite' alludes to ghost-like columnar structures in which vertically aggraded cuspate arches are separated by concave 'dish' structures. In other sections, unit 4 contains spaced, mostly non-branching columnar stromatolites with indistinct convex internal laminations and encrusted sidewalls, resembling the morphotype *Boxonia* Korolyuk (Hofmann, 1969).

Unit 5 is 102 m thick in ON2R and consists of light grey dolomite grainstone with low- to high-angle cross-bedding and increasing amounts of authigenic white chert towards the top. Unit 6 is 3.8 m thick and ends at a heavily-silificied sequence boundary beneath which are 1.6 m of dolomite microbialaminite with tepee structures indicating subaerial exposure. The sequence boundary marks a colour change from grey to pink dolomite. In section P1405 (Fig. 5), there are two 0.5-m-thick tepeed microbialam-inite horizons 2 and 3 m below the heavily-silicified sequence boundary marking the top of the Rasthof Formation.

Gruis Formation (Abenab Subgroup)

The Gruis Formation (Hedberg, 1979; Hoffman & Halverson, 2008) was measured and sampled in section P1405 (Fig. 3), the base of which is at 19.1688°S/13.8641°E. Recessive, thin-bedded and straw-coloured on exposed surfaces, it differs in almost every respect from the underlying Rasthof Formation. In a total thickness of 114.2 m (Fig. 6) there are no fewer than 40 depositional cycles (2.86 m per cycle), 29 of which end at subaerial exposure surfaces marked by well-developed tepee structures. Not surprisingly, the formation is highly oxidized overall and its dolomite is typically pinkish on fresh surfaces. Marly ribbonite is the most common lithology in aggregate, followed by microbialaminite, ribbonite and grainstone in declining order. A 1.0-m-thick grainstone bed 35 m above the datum (black arrow in Fig. 6) carries fist-size nodules of authigenic white chert. The same chert marker bed is observed at virtually the

same position (±2.0 m) with respect to the δ¹³C record (i.e. CIE Cn3 downturn, Fig. 6) over an area the size of Fig. 2, but shifted 30 km eastward (Hoffman *et al*. 2021).
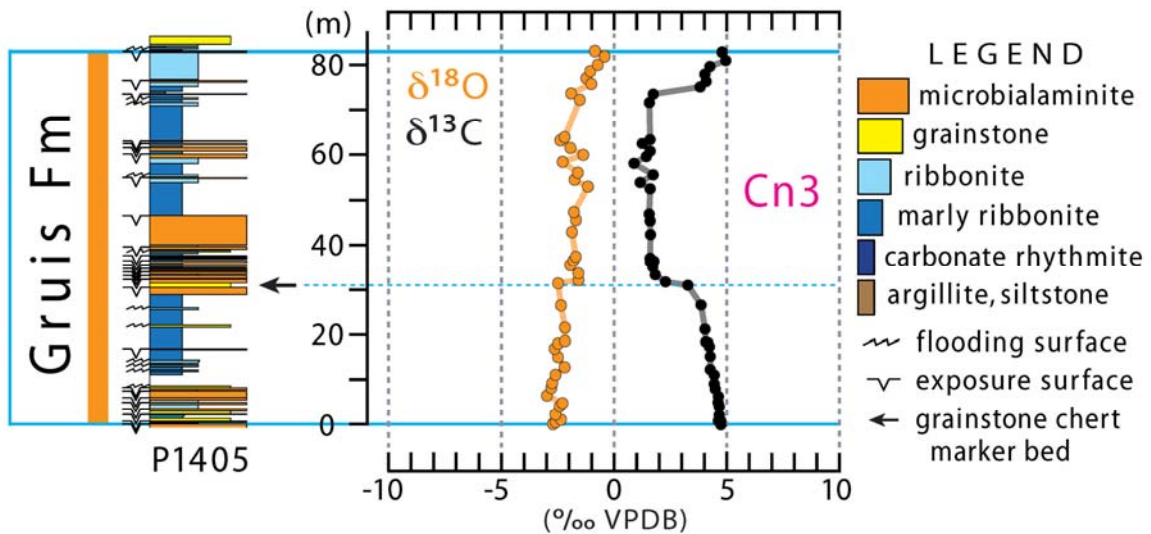

Figure 6. Gruis Formation (Fig. 1) enlarged columnar section and stable isotope record from section P1405 (Fig. 3). Horizontal arrow indicates the nodular chert grainstone marker bed that regionally coincides with the δ¹³C downturn of CIE Cn3 (Hoffman *et al*. 2021). Cn3 appears to be a blunted expression of the Tayshir CIE in Mongolia (Johnston *et al*. 2012; Bold *et al*. 2016).

In the terminology of Schlager (2005), the Rasthof Formation was a 'catch-up' sequence and the Gruis Formation a 'keep-up' one. In Rasthof time, sedimentation had to catch-up with subsidence accommodation generated during the 56-Myr Sturtian glaciation when little sediment-ation occurred because of the weak hydrologic cycle (Partin & Sadler, 2016). Once it did catch up, at the Rasthof top sequence boundary, it was able to keep pace with subsidence on orbital (cycle?) time scales thereafter. The marly impurity of the Gruis Formation is a distal manifestation of the last major episode in the 100-Myr uplift history of the Makalani rift-shoulder, where 60 km southeast of Ongongo the Gruis Formation oversteps the Rasthof Formation onto the crystalline basement complex and contains ≤150 m of basement-derived alluvial fan-glomerate (Hoffman & Halverson, 2008; Hoffman *et al*. in press).

Ombaatjie Formation (Abenab Subgroup)

The δ¹³C/δ¹⁸O records from the Ombaatjie Formation (Hoffmann & Prave, 1996; Hoffman & Halverson, 2008) are composites from sections P7501 and P7500 (Figs 3 & 7). The datum for P7501 is at 19.1586°S/13.8548°E where the contact with Gruis Formation is well exposed. Section P7500 begins at 19.1502°S/13.8552°E and ends at the top of the Ombaatjie Formation at 19.1510°S/13.8530°E (Figs 7 & 8A). A complete section (P1902) of the lower Ombaatjie Formation (units b1-b3) was measured but not sampled (Fig. 9B). Eight parallel sections of the upper Ombaatjie Formation (units b4-b8) were measured (two sampled) at Ongongo as a test of km-scale lateral variability of the cycles (Figs 8A & 9A).

The Ombaatjie Formation is an aggradational stack of upward-shoaling deposit-ional cycles. An influx of quartz sand at the base of unit b4 (Fig. 9A), evident from afar as a dark-brown band of desert 'varnish' (Fig. 8A), serves to separate the formation into two natural divisions. Taking section P1902 (Fig. 9B) to represent the lower division (units b1-b3) and P7500 (Fig. 9A) the upper (units b4-b8), gives a total to 27 depositional cycles in 280 m of strata,

for an average cycle thickness of 10.4 m. Comparison with Gruis Formation (2.86 m average cycle) and Elandshoek Formation (7.2 m) suggests rapid acceleration in tectonic subsidence rate between Gruis and Ombaatjie time and a gradual decline in subsidence rate thereafter. While consistent with a transition from rift to post-rift thermal subsidence at the Gruis-Ombaatjie boundary, the relation between cycle thickness and subsidence rate assumes that the same orbital period resonated with depositional cycle dynamics.

Most lower Ombaatjie cycles (12 of 15) end at marine flooding surfaces (i.e. abrupt increases of inferred water depth) above intraclast and/or ooid grainstone (Fig. 9B). In contrast, most upper Ombaatjie cycles (9 of 12) end at subaerial exposure surfaces above microbialaminite with tepees (Fig. 9A). The cycle stack in this area is somewhat regressive overall. Perhaps as a result, the upper Ombaatjie Formation is more thoroughly dolomitized than the lower Ombaatjie (Fig. 7). For this reason, we hesitate to compare cycle thickness between the lower and upper Ombaatjie Formation. Limestone has been preferentially thinned stratigraphically relative to dolomite by tectonic flattening across the steeply-dipping cleavage
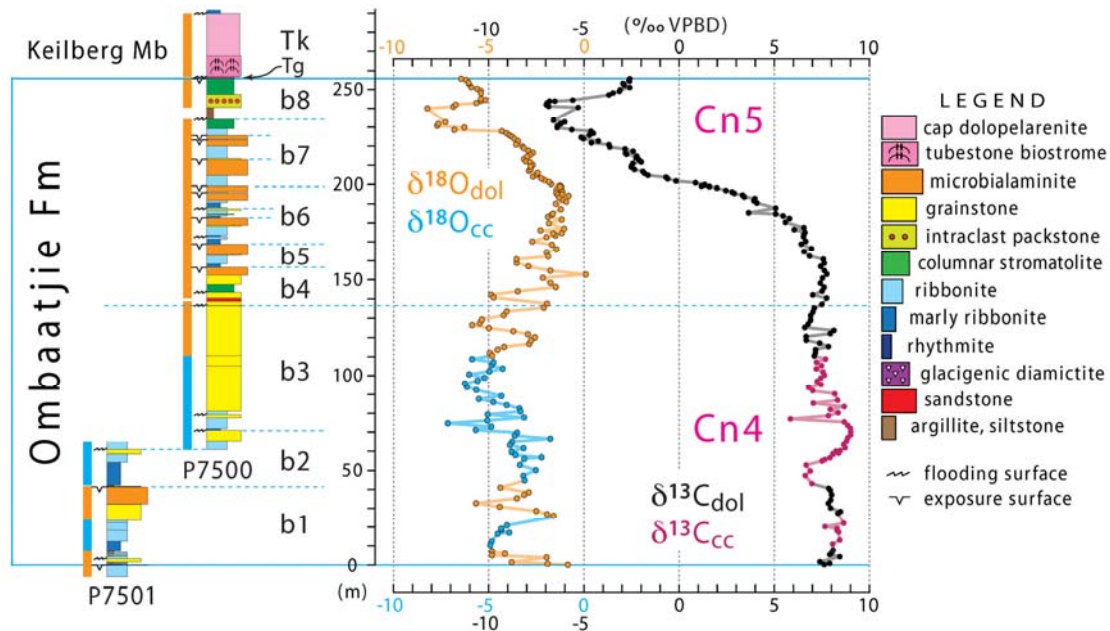
Figure 7. Ombaatjie Formation (Fig. 1) columnar sections P7501 and P7500 (Figs. 3 & 8A), with stable isotope records (Hoffman *et al*. in press). Note offset $\delta^{18}O$ (blue & orange) and $\delta^{13}C$ (black) scales. Dolomite and calcite are colour coded as in Figure 5. The formation is divided into eight units b1-b8 and two members at the base of unit b4 (see text). An unbroken b1-b3 section (without isotope data) is shown in Figure 9B. CIE Cn4 is correlated with Keele peak (Kaufman *et al*. 1997) and Cn5 with Trezona CIE (Rose *et al*. 2012).

Units b7 and b8 are associated with the Cn5 C-isotope excursion (Figs 7 & 9A), which is correlated with the immediate pre-Marinoan Trezona CIE (Halverson *et al*. 2002; Rose *et al*. 2012). Unit b8 and the top of unit b7 are also notable for a proliferation of large (multi-metre) stromatolite mounds composed internally of cm-scale columns with strongly divergent dendroid branching (form-group *Tungussia* Semikhatov,

Hofmann, 1969). The stromatolite proliferation was cited as evidence for elevated carbonate saturation in support of a biogeochemical model in which the C-isotope excursion was driven by enhanced rates of anaerobic relative to aerobic respiration, presumably in response to increased delivery of sulfate and/or ferric Fe as electron acceptors (Tziperman *et al*. 2011).

Unit b8 is also notable for the occurrence of 'intraclast packstone' (Fig. 9A). This unusual lithotype is found on the outer and inner platform but only in unit b8 (Hoffman *et al*. in press). It consists of oligomictic rounded granules of Fe-rich carbonate (ankerite) up to a few millimeters in diameter. The coarse grains are set in a fine-grained carbonate mud matrix of similar composition. The packstone is mechanically bedded, even cross-bedded, implying that the muddy matrix was emplaced post-depositionally by infiltration. Authigenic FeS_2 nodules are common and formed after the matrix was emplaced. The palaeoenvironmental significance of intraclast packstone in b8 remains an unsolved mystery, but the Fe-rich carbonate was likely authigenic in origin at its source (i.e. before erosion and redeposition as bedded granules). Enhanced authigenic carbonate production would be consistent with the anaerobic respiration model for CIE Cn5 (Tziperman *et al*. 2011).

Ghaub and Maieberg formations (Tsumeb Subgroup)

The main repository for Marinoan glacial deposits (Ghaub Formation, Hoffmann & Prave, 1996) was on the foreslope of the carbonate platform near the ice grounding zone (Hoffman, 2004, 2011a, b; Domack & Hoffman, 2011). Only scraps of carbonate-clast diamictite, interpreted as lodgement tillite, are found on the glaciated top of the platform (Hoffman *et al*. in press). Of nine sections at Ongongo that cross the Cryogenian-Ediacaran boundary (Fig. 8A), only five preserve any Ghaub Formation (unit Tg, Fig. 9A - P9000 (0.3 m), P9001 (0.2 m), P7500 (≤0.6 m), E1403 (0.8 m) and E1402 (2.4 m). No clast fabric data (Dowdeswell *et al*. 1985) were obtained at Ongongo, but strongly preferred NNE-SSW azimuthal long-axis orientations are documented in Ghaub diamictite 23 km south-southeast of P7500 (Hoffman *et al*. in press). This fabric is compatible with south-southwest-directed Marinoan glacial flow in present coordinates.
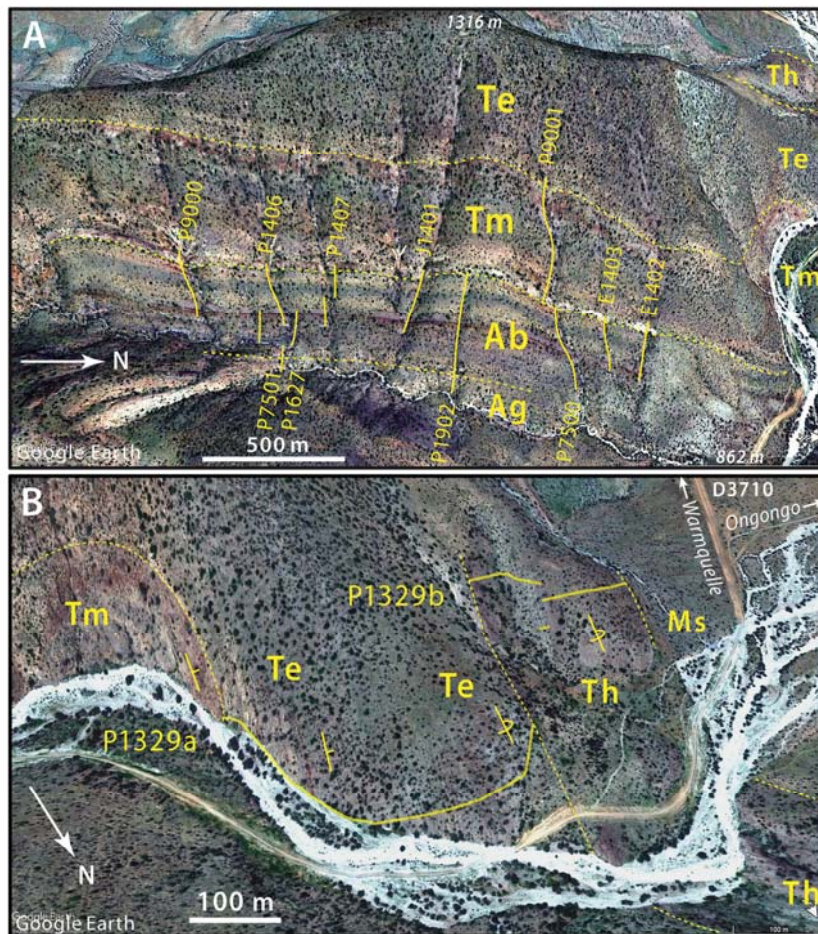
Figure 8. Oblique satellite images: **(A)** Ombaatjie (Ab) and Maieberg (Tm) formation sections (solid yellow) shown in Figures 7, 9 and 10; **(B)** Elandshoek (Te) and Hüttenberg (Th) formation sections shown in Figures 11 and 12. Google Earth Images © 2021 Maxar Technologies.

The basal Ediacaran cap-carbonate sequence (Maieberg Formation, Hoffman & Halverson, 2008) was measured and sampled in two parts: the Keilberg Member (unit Tk) in P7500 and the rest (units Tm2 and Tm3) in P9001 (Figs 3, 8A & 10). The base of the Keilberg Member in P7500 is at 19.1511°S/13.8530°E and the base of Tm2 in P9001 is at 19.1516°S/ 13.8526°E (Figs 8A & 10).

The ever-present Keilberg Member (Hoffmann & Prave, 1996; Hoffman *et al*. 2007) represents the basal Ediacaran cap dolomite observed globally in marine sequences (Knoll *et al*. 2006; Narbonne *et al*. 2012). It is 33.1 m thick in P7500 (30.0 m in P9001) and stands out as a very pale-grey to white flinty dolomite with a palimpsest peloidal texture and a knife-sharp basal contact. The basal 0.5 m is mechanically stratified with low-angle cross-bedding. It is overlain by 5.5 m (P9001) to 10.7 m (P7500) of weakly developed tubestone stromatolite (Hegenberger, 1987; Hoffman, 2011b). Above the stromatolitic interval is peloidal grainstone featuring hummocky cross-stratification (HCS) with low-angle downlaps, but no giant wave ripples or sand volcanoes as occur elsewhere on the platform in the same interval (Allen & Hoffman, 2005; Crockford *et al*. 2021; Hoffman *et al*. in press). In the uppermost Keilberg Member, bedding becomes thin and tabular (Fig. 10). The contact with limestone rhythmite (locally dolomitized) of member Tm2 is well defined, but lacks any evident break in sedimentation. Benthic crystal fans, pseudomorphic after cm-scale seafloor aragonite cement, begin at the base of Tm2 (e.g. P9001 and

14

E1403, Fig. 8A) but are never observed in the Keilberg Member. As an upward-deepening sequence, Keilberg Member is interpreted as the relatively expanded transgressive systems tract in the Maieberg depositional sequence (Hoffman & Halverson, 2008; Hoffman, 2011b).
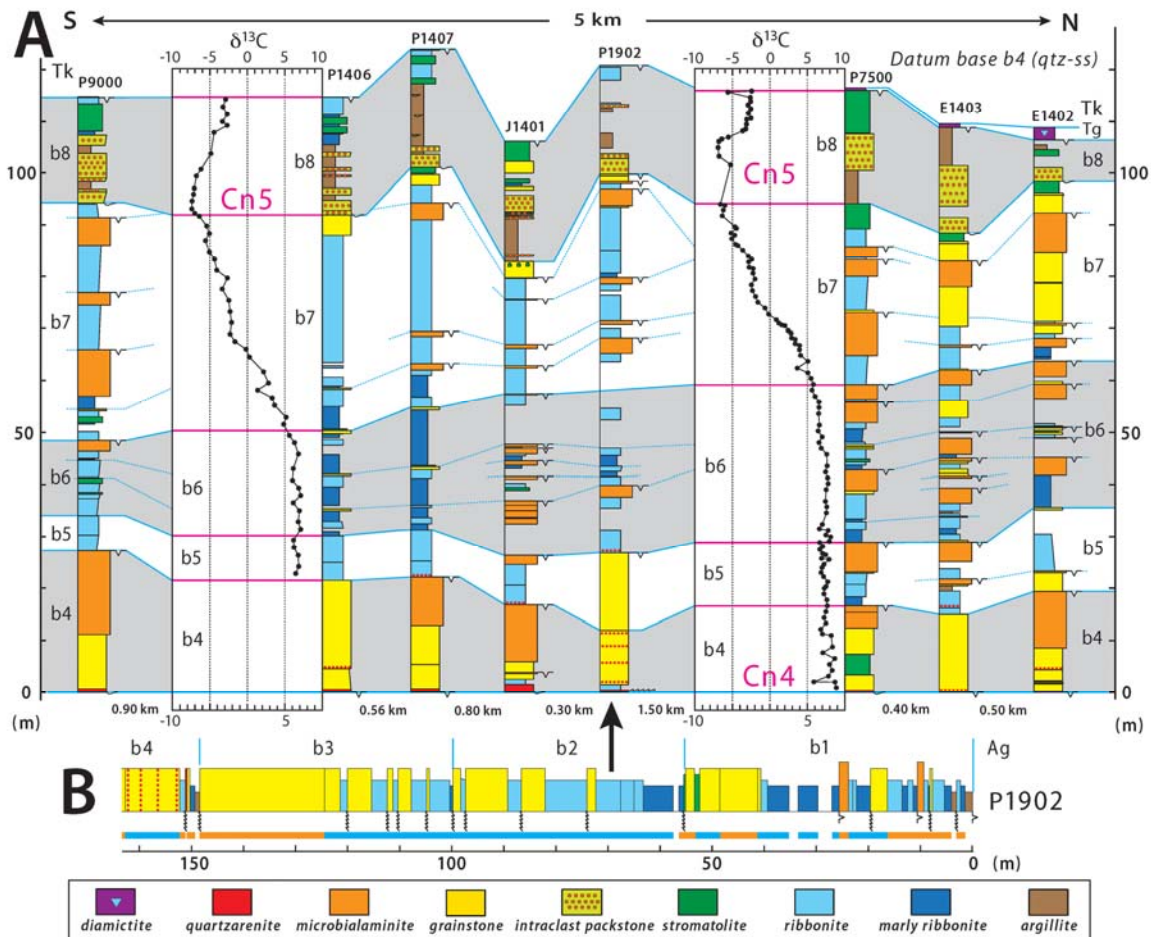
Figure 9. (A) Upper Ombaatjie Formation (units b4-b8) closely-spaced columnar sections (Fig. 8A) with $\delta^{13}C$ records (Hoffman *et al*. in press) from P1406 and P7500 (see Fig. 7 for $\delta^{18}O$ record). **(B)** Lower Ombaatjie Formation (units b1-b3) columnar section P1902 (Fig. 8A).

The middle Tm2 member of the Maieberg Formation (Hoffman *et al*. in press) consists of limestone/dolomite rhythmite and marly rhythmite deposited below storm wave base. It encompasses the maximum flooding and lower highstand parts of the post-Marinoan depositional sequence. It is analogous to the Brachina Formation in South Australia (Preiss & Forbes, 1981), the Sheepbed Formation in northwest Canada (Aitken, 1982), the Guia Formation in southwest Brazil (Nogueira *et al*. 2007) and the C2 (Bulu) Formation of the Schisto-Calcaire Subgroup in the West Congo Supergroup (Delpomdor *et al*. 2016). Benthic crystal fans (former aragonite) occur abundantly in the first 52 m of Tm2 in P9001, which is their maximum development on the inner platform. Spaced prismatic fans ≤16 cm in length (palaeovertical) occur in the lower half of this interval and bunched clusters the size of cabbages in the upper half. Because of tectonic strain, their morphology is better preserved where dolomitized (Fig. 10). On the foreslope and outer margin of the platform, Tm2 crystal fans are

spatially associated with seafloor topography, implicating enhanced vertical mixing in their occurrence (Hoffman & Halverson, 2008; Hoffman, 2011a). At Ongongo, vertical mixing may have been localized by the sidewall of a Marinoan glacial trough (Omarumba Trough, Hoffman *et al*. in press).
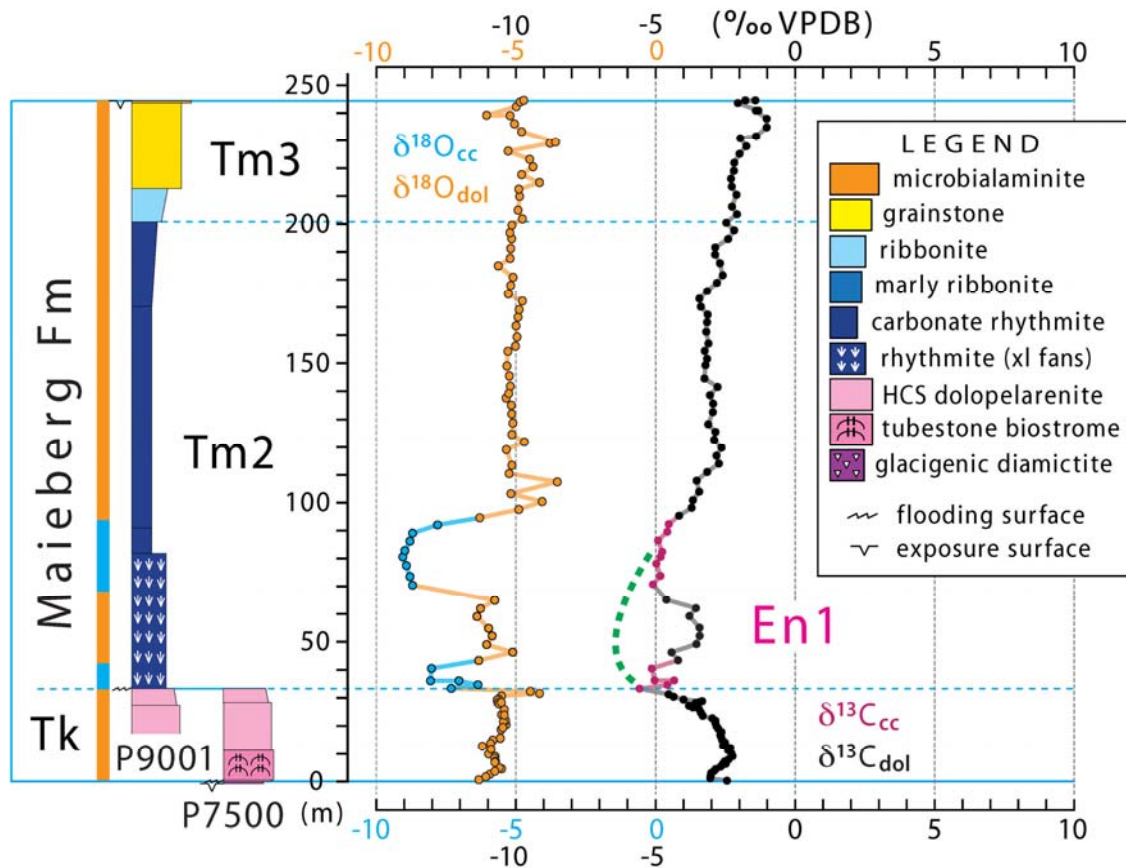

Figure 10. Earliest Ediacaran Maieberg Formation (Fig. 1) columnar section P9001 (Figs. 3 & 8A) with stable isotope records (Hoffman *et al*. in press). Note offset $\delta^{18}O$ (blue & orange) and $\delta^{13}C$ (black) scales. Dolomite and calcite are colour coded as in Figure 5. The formation is divisible into three members Tm1-Tm3. Note dolomite-calcite isotopic fractionations, consistent with low-temperature equilibrium fractionations (Friedman & O'Neil, 1977), not observed in Ombaatjie Formation (Fig. 7). Green dashed line indicates $\delta^{13}C$ trajectory in undolomitized lower Tm2 sections (Hoffman *et al*. in press).

The Maieberg Formation is the only formation in the Otavi Group that exhibits consistent $\delta^{13}C$ and $\delta^{18}O$ fractionations between coexisting dolomite and calcite (Hoffman, 2011b). The lower part of Tm2 includes the nadir of the first Ediacaran negative C-isotope excursion En1 (Fig. 10). P9001 is interesting because En1, which is normally expressed in limestone, is partly dolomitized. Both $\delta^{18}O$ and $\delta^{13}C$ are shifted to heavier values where dolomitized (Fig. 10). Similar shifts are associated with dolomitization of the post-Marinoan cap-carbonate sequence (Ol Formation) of the Zavkhan terrane in western Mongolia (Bold *et al*. 2020).

The Upper Maieberg member Tm3 begins with the first bedforms indicating wave or traction current action. They are preceded in upper Tm2 by fine-grained debrites. Tm3 dolomite ribbonite grades upwards into massive or cross-bedded grainstone (Fig. 10). Authigenic silicification increases in intensity upwards towards the terminal sequence boundary above a thin veneer of microbialaminite with tepees.

The Maieberg Formation is exceptionally thick as a single transgressive-highstand depositional sequence without higher-order cycles or parasequences. This reflects a large accommodation generated through rapid (early post-rift) tectonic subsidence and net erosion of the platform during Marinoan glaciation (Hoffman *et al.* 1998a, b). In contrast, because of its location near the crest of the Khowarib arch (Hoffman *et al.* in press) the Maieberg Formation is relatively thin, 240.1 m, at Ongongo. This compares with an average 385 m (n=11) for all Maieberg sections on the platform, or 370 m (n=9) with the thickest and thinnest (outliers) ignored. From a thermal subsidence model an average sediment accumulation rate of 65 m/Myr was estimated for the Ombaatjie Formation (Halverson *et al.* 2002). This serves as a maximum bound on accumulation rates during the combined Marinoan and Maieberg Formation, yielding a minimum of (370/65) 5.7 Myr duration for Marinoan glaciation and Maieberg deposition combined. If the Maieberg Formation underwent compaction after its accumulation - stylolites are characteristic of upper Tm2 - the minimum combined duration would be longer. Since lithofacies such as tubestone stromatolite (Cloud *et al.* 1974; Corsetti & Grotzinger, 2005; Bosak *et al.* 2013) and benthic crystal fans (Lasaga, 1998; Grotzinger & James, 2000; Vieira *et al.* 2015) imply rapid accumulation for the Maieberg Formation, a multi-million year duration for Marinoan glaciation appeared probable (Hoffman *et al.* 1998a, b). In retrospect, more was learned regarding the fundamental nature of Cryogenian glaciation from the Rasthof and Maieberg cap-carbonate sequences than from the Chuos and Ghaub diamictites.

Elandshoek and Hüttenberg formations (Tsumeb Subgroup)

The base of section P1329a (Fig. 8B) is at 19.1409°S/13.8482°E where the Maieberg-Elandshoek transition (Figs 10 & 11) is a reprise of the Rasthof-Gruis 'catch-up-keep-up' transition (Fig. 5). The basal Te1 member of the Elandshoek Formation (Fig. 11) is a stack of thin (average 2.86 m) regressive cycles, most of which (7 out of 11) end at subaerial exposure surfaces marked by tepees or tepee-breccias above pinkish dolomite microbialaminite. In Te2 and Te3 (Fig. 11), most cycles (40 of 43) end at marine flooding surfaces and only three have evidence of subaerial exposure. As a whole, the Elandshoek Formation is 389 m thick in P1329a (Fig. 8B) and consists of 54 ribbonite-grainstone cycles with an average thickness of 7.2 m. The average thickness is likely overestimated because of cycle undercounting. Cryptic flooding surfaces within grainstone units went unrecorded and stromatolite beds in ribbonite were not counted as cycle boundaries. Member Te2 contains 17 beds (average 0.37 m) of laterally-linked prolate stromatolites ('Tuten', Krüger, 1969), many of which are heavily silicified. The top of the Elandshoek Formation is a prominent flooding surface above an upper member (Te3) dominated by grainstone (Fig. 11).

The base of section P1329b (Fig. 8B) is at 19.1412°S/13.8434°E and the Hüttenberg Formation is divisible into three members (Fig. 12). Th1 is dominated by ribbonite with subordinate stromatolite; Th2 is dominated by marly ribbonite with subordinate ribbonite, and Th3 is dominated by grainstone. There are eight stromatolite beds in Th1, of which the fourth is the thickest (3.3 m) and the average is 1.0 m. Th2 is recessive and the section (Fig. 12) is a composite (Fig. 8B). A 1.4-m-thick silicified bed of laterally-linked stromatolites occurs near the top of Th2. Grainstone in the lower half of Th3 is cross-bedded. A sharp disconformity separates the top of the Hüttenberg Formation from synorogenic foredeep clastics (greywacke semi-pelite) in the Sesfontein Formation of the Mulden Group (Guj, 1970; Hedberg, 1979; SACS, 1980).

Figure 11. Early Ediacaran Elandshoek Formation (Fig. 1) columnar section P1329a (Fig. 8B) with stable isotope records (Hoffman *et al*. in press). Note offset $\delta^{18}O$ (orange) and $\delta^{13}C$ (black) scales. The formation is divisible into three members Te1-3.

The composite $\delta^{13}C$ record from P9001 and P1329 (Figs 10 & 11) is remarkable in that values remain well below 0.0‰ (VPDB) until the top of the Elandshoek Formation, 605 m above the base of the Ediacaran. This suggests that the Otavi Group platform and the Death Valley area of California (Petterson *et al*. 2011) have the most expanded early Ediacaran sections known (Hoffman *et al*. in press). The positive CIE En4 in the lower-middle Hüttenberg Formation (Fig. 12) is less enriched and prolonged than in correlative strata in the Otavi Mountainland (Cui *et al*. 2018; Hoffman & Lamothe, 2019) but it shares the same large point-to-point variability, the significance of which remains to be revealed and declining accumulation rates alone do not explain.
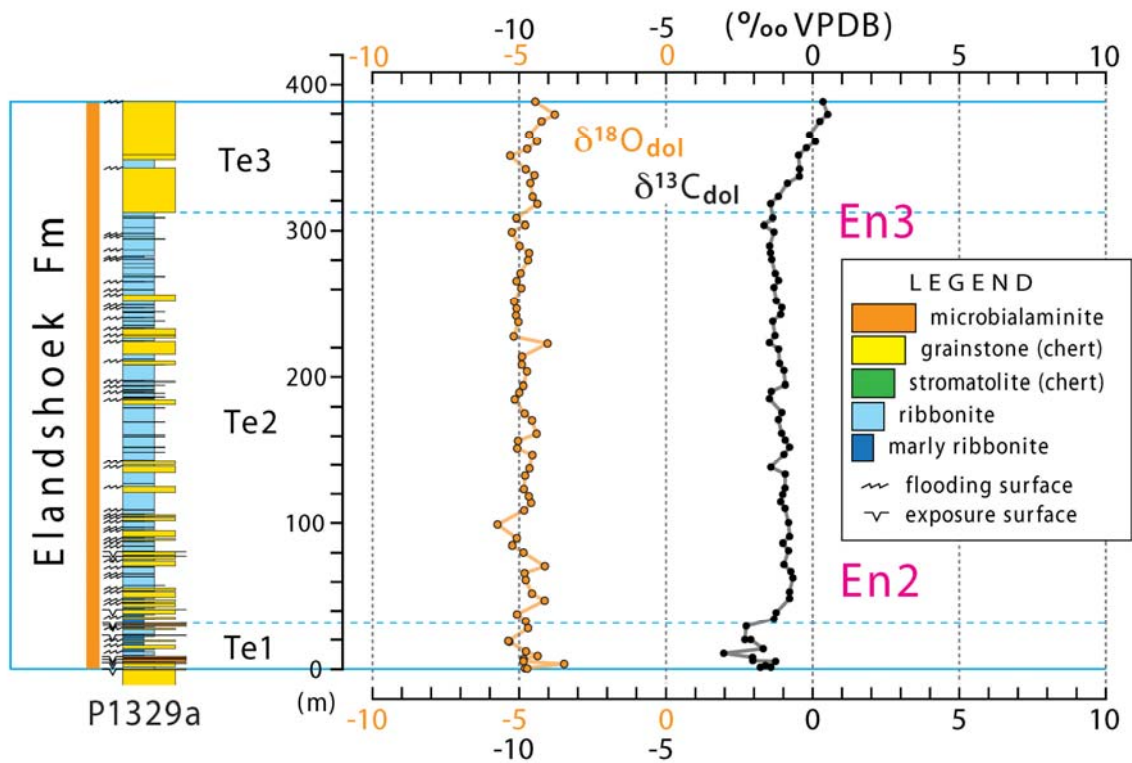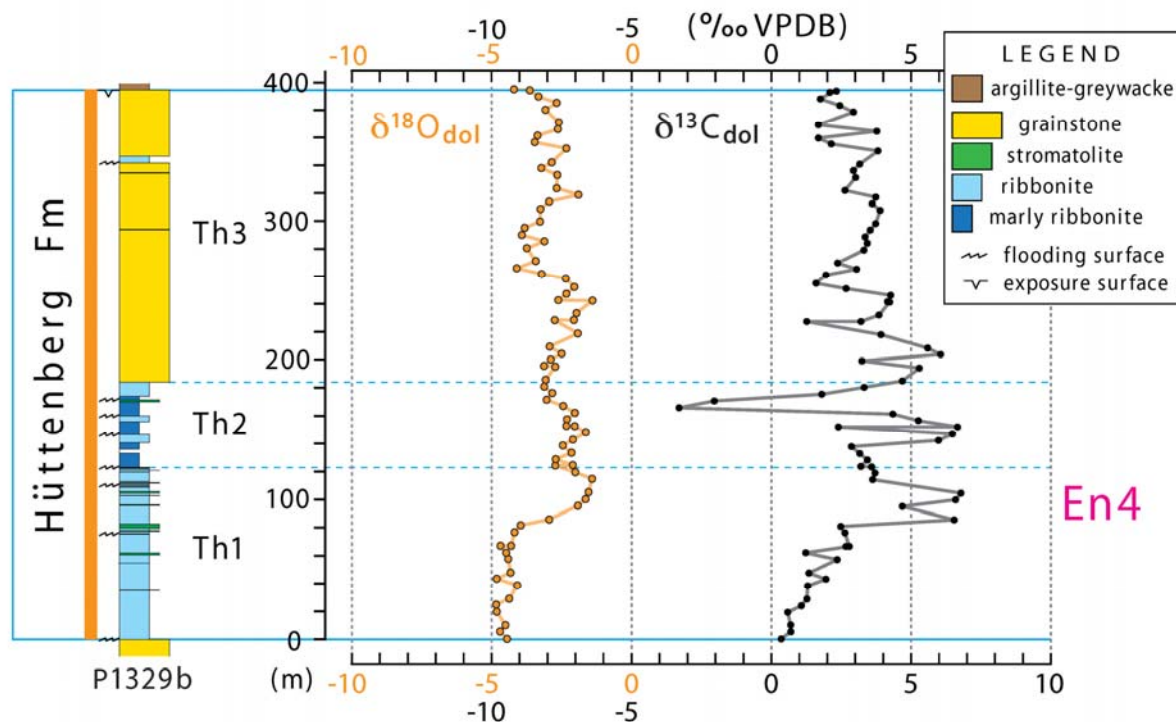
Figure 12. Early Ediacaran Hüttenberg Formation (Fig. 1) columnar section P1329b (Fig. 8B) with stable isotope records (Hoffman *et al*. in press). Note offset $\delta^{18}O$ (orange) and $\delta^{13}C$ (black) scales. The formation is divisible into three members Th1-Th3. CIE En4 is correlated with the Hüttenberg CIE in the northern Otavi Mountainland (Cui *et al*. 2018).

Summary and Discussion

The complete composite section from Ongongo and its $\delta^{18}O$ and $\delta^{13}C$ records are assembled in Figure 13. The Rasthof and Maieberg formations (cap-carbonate sequences) stand out from the other five carbonate formations in their lack of m-scale depositional cycles. This is most easily explained by deep unfilled accommodation generated during the preceding glacial epochs from tectonic subsidence and net erosion. The Cryogenian $\delta^{13}C$ record from the Abenab Subgroup has long been a global standard (Halverson *et al*. 2005, 2010; Halverson & Shields-Zhou, 2011).

A reference section for the Otavi Group in the Eastern Kaoko Zone is not a substitute for one in the Otavi Mountainland. The formation-scale sequences are somewhat different in the two areas (Hedberg, 1979), particularly in the middle Abenab Subgroup. Stable isotope records from the Otavi Mountainland are needed to resolve uncertain correlations of inter-snowball form-ations between the two areas (Fig. 1). They are also needed to test different interpretations of sub-Marinoan stratigraphic relations-synglacial tectonics in the Otavi Mountainland (Bechstädt *et al*. 2018) or subglacial erosion in the Eastern Kaoko Zone (Hoffman & Halverson, 2008; Hoffman *et al*. in press). Different geology or different interpretations?
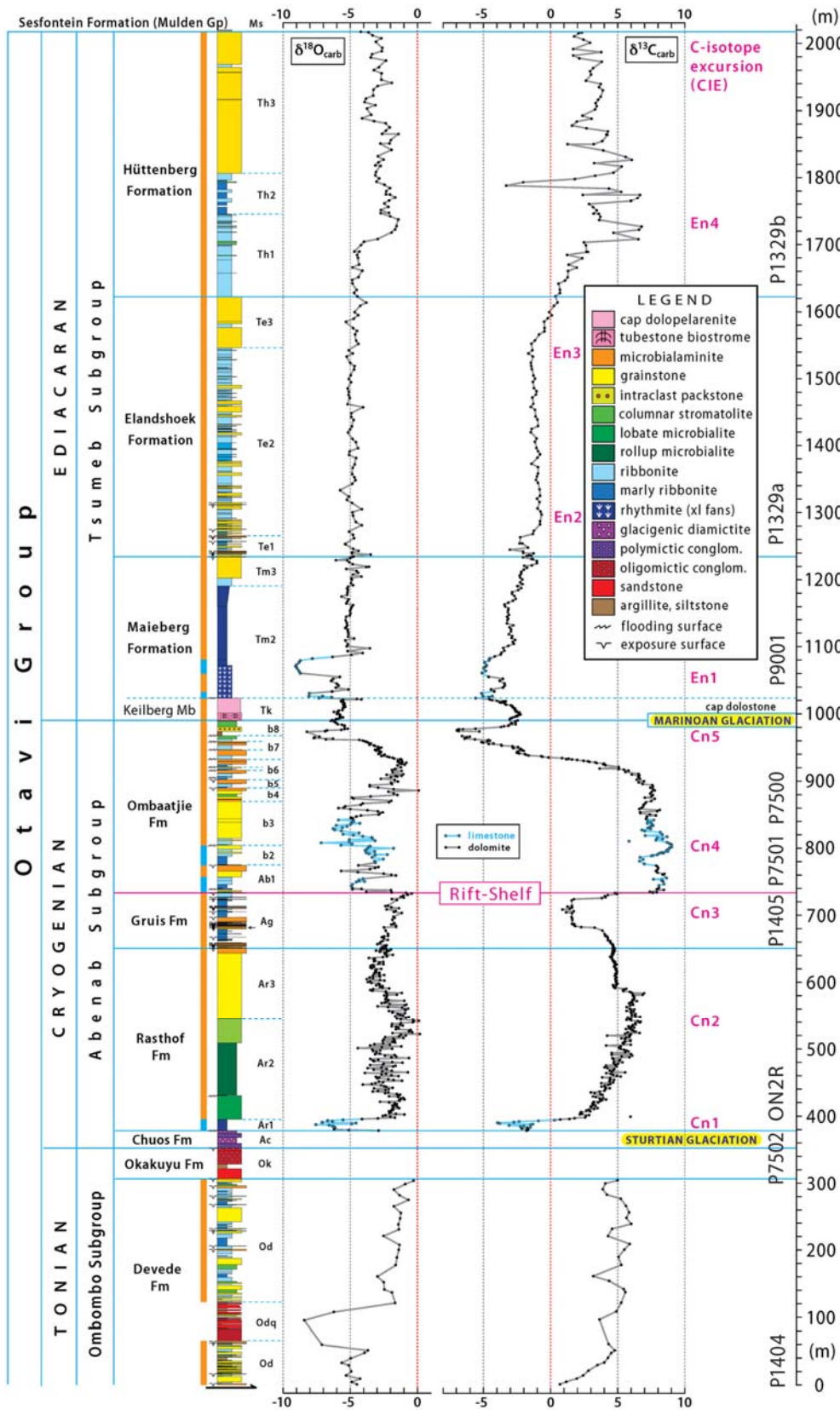
Figure 13. Composite Otavi Group columnar section (Fig. 3) with stable isotope records (tabulated by section number in Hoffman *et al.* in press). The rift-shelf transition is placed after the last major uplift episode of the Huab and Makalani rift shoulders of the outer (southern) platform (Hoffman & Halverson; 2008, Hoffman *et al.* in press). Rift-related structural rotations continued into the late Cryogenian (Marinoan) time in the Swakop Group on the distal foreslope of the Otavi platform and in the Northrn Damara belt (Hoffman *et al.* in press).

Acknowledgements

References

Aitken, J.D. 1982. Precambrian of the Mackenzie fold belt - a stratigraphic and tectonic overview. *In:* Hutchison, R.W., Spence, C.D., Franklin, J.M. (Eds) *Precambrian Sulfide Deposits*, *H.S. Robinson Memorial Volume*. Geological Association of Canada Special Paper, **25**, 149-161.

Allen, P.A. & Hoffman, P.F. 2005. Extreme winds and waves in the aftermath of a Neoproterozoic glaciation. *Nature*, **433**, 123-127.

Assereto, R.L.A.M. & Kendall, C.G.StC. 1978. Nature, origin and classification of peritidal tepee structures and related breccias. *Sedimentology*, **24**, 153-210.

Bao, X.J., Zhang, S.H., Jiang, G.Q., Wu, H.C., Li, H.Y., Wang, X.Q., An, Z.Z. & Yang, T.S. 2018. Cyclostratigraphic constraints on the duration of the Datangpo Formation and the onset age of the Nantuo (Marinoan) glaciation in South China. *Earth and Planetary Science Letters*, **483**, 52-63.

Bechstädt, T., Jäger, H., Rittersbacher, A., Schweisfurth, B., Spence, G., Werner, G. & Boni, M. 2018. The Cryogenian Ghaub Formation of Namibia - New insights into Neoproterozoic glaciations. *Earth-Science Reviews*, **177**, 678-714.

Bechstädt, T., Jäger, H., Spence, G. & Werner, G. 2009. Late Cryogenian (Neoproterozoic) glacial and post-glacial successions at the southern margin of the Congo craton, northern Namibia: facies, palaeogeography and hydrocarbon perspective. *In:* Graig, J., Thurow, J., Thusu, B., Thitham, A. & Abutarruma, Y. (Eds) *Global Neoproterozoic Petroleum Systems: The Emerging Potential in North Africa*. Geological Society of London Special Publication, **326**, 255-287.

Bold, U., Crüger Ahm, A.-S., Schrag, D.P., Higgins, J.A., Jamsran, E. & Macdonald, F.A. 2020. Effect of dolomitization on isotopic records from Neoproterozoic carbonates in southwestern Mongolia. *Precambrian Research*, **350**, 105902, 1-19.

Bold, U., Smith, E.F., Rooney, A.D., Bowring, S.A., Buchwaldt, R., Dudás, F.Õ., Ramezani, J., Crowley, J.L., Schrag, D.P. & Macdonald, F.A. 2016. Neoproterozoic stratigraphy of the Zavkhan terrane of Mongolia: the backbone for Cryogenian and early Ediacaran chemostratigraphic records. *American Journal of Science*, **316**, 1-63.

Bosak, T., Lahr, D.J.G., Pruss, S.B., Macdonald, F.A., Dalton, L. & Matys, E. 2011. Agglutinated tests in post-Sturtian cap carbonates of Namibia and Mongolia. *Earth and Planetary Science Letters,* **308**, 29-40.

Bosak, T., Lahr, D.J.G., Pruss, S.B., Macdonald, F.A., Gooday, A.J., Dalton, L. & Matys, E.D. 2012. Possible early foraminiferans in post-Sturtian (716-635 Ma) cap carbonates. *Geology*, **40**, 67-70.

Bosak, T., Mariotti, G., Macdonald, F.A., Perron, J.T. & Pruss, S.B. 2013. Microbial sediment-ology in Neoproterozoic cap carbonates. *In:* Bush, A.M., Pruss, S.B. & Payne, J.L. (Eds) *Ecosystem Paleobiology and Geobiology*. Paleontological Society Papers, **19**, 1-25.

Cailteaux, J.L.H. & De Putter, T. 2019. The Neoproterozoic Katanga Supergroup (D. R. Congo): State-of-the-art and revisions of the lithostratigraphy, sedimentary basin and

geodynamic evolution. *Journal of African Earth Sciences*, **150**, 522-531.

Cloud, P., Wright, L.A., Williams, E.G., Diehl, P. & Walter, M.R. 1974. Giant stromatolites and associated vertical tubes from the upper Proterozoic Noonday Dolomite, Death Valley region, eastern California. *Geological Society of America Bulletin*, **85**, 1869-1882.

Corsetti, F.A. & Grotzinger, J.P. 2005. Origin and significance of tube structure in Neoproterozoic post-glacial cap carbonates: example from the Noonday Dolomite, Death Valley, United States. *Palaios*, **20**, 348-362.

Crockford, P.W., Mehra, A., Domack, E.W. & Hoffman, P.F. 2021. Report: An occurrence of radially symmetric sedimentary structures in the basal Ediacaran cap dolostone (Keilberg Member) of the Otavi Group. *Geological Survey of Namibia Communications*, **23**, 26-38.

Cui, H., Kaufman, A.J., Peng, Y.B., Liu, X.M. & Plummer, R.E. 2018. The Neoproterozoic Hüttenberg δ13C anomaly: Genesis and global implications. *Precambrian Research*, **313**, 242-262.

Dalton, L.A., Bosak, T., Macdonald, F.A., Lahr, D.J.G. & Pruss, S.B. 2013. Preservational and morphological variability of assemblages of agglutinated eukaryotes in Cryogenian cap carbonates of northern Namibia. *Palaios*, **28**, 67-79.

Delpomdor, F., Eyles, N., Tack, L. & Préat, A. 2016. Pre- and post-Marinoan carbonate facies of the Democratic Republic of the Congo: Glacially- or tectonically-influenced deep-water sediments? *Palaeogeography, Palaeoclimatology, Palaeoecology*, **457**, 144-157.

Delpomdor, F., Schröder, S., Préat, A., Lapointe, P. & Blanpied, C. 2018. Sedimentology and chemostratigraphy of the late Neoproterozoic carbonate ramp sequences of the Hüttenberg Formation (northwestern Namibia) and the C5 Formation (western central Democratic Republic of Congo): Record of the late post-Marinoan marine transgression on the margin of the Congo Craton. *South African Journal of Geology*, **121**, 23-42.

Domack, E.W. & Hoffman, P.F. 2011. An ice grounding-line wedge from the Ghaub glaciation (635 Ma) on the distal foreslope of the Otavi carbonate platform, Namibia, and its bearing on the Snowball Earth hypothesis. *Geological Society of America Bulletin*, **123**, 1448-1477.

Dowdeswell, J.A., Hambrey, M.J. & Wu, R.T. 1985. A comparison of clast fabric and shape in Late Precambrian and modern glacigenic sediments. *Journal of Sedimentary Petrology*, **55**, 691-704.

Friedman, I. & O'Neil, J.R. 1977. Compilation of stable isotope fractionation factors of geochemical interest. *In:* Fleischer, M. (Ed.) *Data of Geochemistry, Sixth Edition.* United States Geological Survey Professional Paper, **440-KK**, 1-12 and 49 figures.

Goscombe, B., Foster, D.A., Gray, D. & Wade, B. 2018. The evolution of the Damara orogenic system: A record of West Gondwana assembly and crustal response. *In:* Siegesmund, S., Basei, M.A.S., Oyhantçabal, P. & Oriolo, S. (Eds) *Geology of Southwest Gondwana.* Springer International, Berlin, pp. 303-352.

Gradstein, F.M., Ogg, J.G., Schmitz, M.D. & Ogg, G.M. 2012. *The Geologic Time Scale 2012.* Elsevier, Amsterdam, 1176 pp.

Grotzinger, J.P. & James, N.P. 2000. Precambrian carbonates: evolution of understanding. *In:* Grotzinger, J.P. & James, N.P. (Eds) *Carbonate Sedimentation and Diagenesis in the Evolving Precambrian World.* SEPM (Society for Sedimentary Geology) Special Publication, **67**, 3-20.

Guj, P. 1970. The Damara Belt in the southwestern Kaokoveld, South West Africa. *University of Cape Town Precambrian Research Unit Bulletin*, **8**, 168 pp. + 4 map sheets (scale 1:125,000) + cross-sections.

Hedberg, R.M. 1979. Stratigraphy of the Ovamboland Basin, South West Africa. *University of Cape Town Precambrian Research Unit Bulletin*, **24**, 325 pp. + 6 map sheets (scale 1:250,000).

Hegenberger, W. 1987. Gas escape structures in Precambrian peritidal carbonate rocks. *Communications of the Geological Survey of Namibia*, **3**, 49-55.

Halverson, G.P., Hoffman, P.F., Schrag, D.P. & Kaufman, A.J. 2002. A major perturbation of the carbon cycle before the Ghaub glaciation (Neoproterozoic) in Namibia: Prelude to snowball Earth? *Geochemistry Geophysics Geosystems*, **3**, doi: 10.1029/2001GC000244.

Halverson, G.P., Hoffman, P.F., Schrag, D.P., Maloof, A.C. & Rice, A.H.N. 2005. Toward a Neoproterozoic composite carbon-isotope record. *Geological Society of America Bulletin*, **117**, 1181-1207.

Halverson, G.P. & Shields-Zhou, G. 2011. Chemostratigraphy and the Neoproterozoic glaciations. *In:* Arnaud, E., Halverson, G.P. & Shields-Zhou, G. (Eds) *The Geological Record of Neoproterozoic Glaciations*. Geological Society of London Memoir, **36**, pp. 51-66.

Halverson, G.P., Wade, B.P., Hurtgen, M.T. & Barovich, K.M. 2010. Neoproterozoic chemostratigraphy. *Precambrian Research*, **182**, 337-350.

Hoffman, P.F. 2011a. Glacigenic and associated strata of the Otavi carbonate platform and foreslope, northern Namibia: evidence for large base-level and glacioeustatic changes. *In:* Arnaud, E., Halverson, G.P., Shields-Zhou, G. (Eds) *The Geological Record of Neoproterozoic Glaciations*. Geological Society of London Memoir, **36**, 195-209.

Hoffman, P.F. 2011b. Strange bedfellows: glacial diamictite and cap carbonate from the Marinoan (635 Ma) glaciation in Namibia. *Sedimentology*, **58**, 57-119.

Hoffman, P.F. & Halverson, G.P. 2008. Otavi Group of the western Northern Platform, the eastern Kaoko Zone and the western Northern Margin Zone. *In:* Miller, R. McG. (Ed.) *The Geology of Namibia, Vol. 2*. Geological Survey of Namibia, pp. 13.69-13.136.

Hoffman, P.F., Halverson, G.P., Domack, E.W., Husson, J.M., Higgins, J.A. & Schrag, D.P. 2007. Are basal Ediacaran (635 Ma) post-glacial "cap dolostones" diachronous? *Earth and Planetary Science Letters*, **258**, 114-131.

Hoffman, P.F. Halverson, G.P., Schrag, D.P., Higgins, J.A., Domack, E.W., Macdonald, F.A., Pruss, S.B., Blättler, C.L., Crockford, P.W., Hodgin, E.B., Bellefroid, E.J., Johnson, B.W., Hodgskiss, M.S.W., Lamothe, K.G., LoBianco, S.L.C., Busch, J.F., Howes, B.J., Greenman, J.W., Nelson, L.L., In press. Snowballs in Africa: sectioning a long-lived Neoproterozoic carbonate platform and its bathyal foreslope (NW Namibia). *Earth-Science Reviews*. https://doi.org/10.1016/j.earscirev.2021.103616.

Hoffman, P.F., Kaufman, J.A. & Halverson, G.P. 1998a. Comings and goings of global glaciations on a Neoproterozoic carbonate platform in Namibia. *GSA Today*, **8**, 1-9.

Hoffman, P.F., Kaufman, A.J., Halverson, G.P. & Schrag, D.P. 1998b. A Neoproterozoic snowball Earth. *Science*, **281**, 1342-1346.

Hoffman, P.F., Lamothe, K.G. & Greenman, J.W. 2018. Report: Stratigraphic investigations of the Neoproterozoic Otavi/Swakop Group in the southern Kunene Region. *Communications of the Geological Survey of Namibia*, **20**, 100-113.

Hoffmann, K.-H. & Prave, A.R. 1996. A preliminary note on a revised subdivision and regional correlation of the Otavi Group based on glaciogenic diamictites and associated cap dolomites. *Communications of the Geological Survey of Namibia*, **11**, 77-82.

Hofmann, H.J., 1969. Attributes of stromatolites. *Geological Survey of Canada Paper*, **69-39**, 58 pp.

Johnston, D.T., Macdonald, F.A., Gill, B.C., Hoffman, P.F. & Schrag, D.P. 2012. Uncovering the Neoproterozoic carbon cycle. *Nature*, **483**, 320-323.

Kadima, E., Delvaux, D., Sebagenzi, S.N., Tack, L. & Kabeya, S.M. 2011. Structure and geological history of the Congo Basin: an integrated interpretation of gravity, magnetic and reflection seismic data. *Basin Research*, **23**, 499-527.

Kamona, A.F. & Günzel, A. 2007. Stratigraphy and base metal mineralization in the Otavi Mountain Land, Northern Namibia - a review and regional interpretation. *Gondwana Research*, **11**, 396-413.

Kaufman, A.J., Hayes, J.M., Knoll, A.H. & Germs, G.J.B. 1991. Isotopic compositions of carbonates and organic carbon from upper Proterozoic successions in Namibia: stratigraphic variation and the effects of diagenesis and metamorphism. *Precambrian Research*, **49**, 301-327.

Kaufman, A.J., Knoll, A.H. & Narbonne, G.M. 1997. Isotopes, ice ages, and terminal Proterozoic earth history. *Proceedings of the U.S. National Academy of Sciences*, **94**, 6600-6605.

Kendall, G.St.C. & Warren, J. 1987. A review of the origin and setting of tepees and their

associated fabrics. *Sedimentology*, **34**, 1007-1027.

King, C.H.M. 1994. Carbonates and mineral deposits of the Otavi Mountainland. *Geological Survey of Namibia International Conference on Proterozoic Crustal & Metallogenic Evolution Excursion*, **4**, 40 pp.

Knoll, A.H., Walter, M.R., Narbonne, G.M. & Christie-Blick, N. 2006. The Ediacaran Period: a new addition to the geologic time scale. *Lethaia*, **39**, 13-30.

Krüger, L. 1969. Stromatolites and oncolites in the Otavi Series, South West Africa. *Journal of Sedimentary Petrology*, **39**, 1046-1056.

Lan, Z.W., Huyskens, M.H., Lu, K., Li, X.H., Zhang, G.Y., Lu, D.B. & Yin, Q.Z. 2020. Toward refining the onset age of Sturtian glaciation in South China. *Precambrian Research*, **338**, 105555, 1-8.

Lasaga, A. 1998. *Kinetic Theory in the Earth Sciences*. Princeton University Press, NJ. 822 pp.

Le Ber, E., Le Heron, D.P., Winterleitner, G., Bosence, D. & Vining, B.A. 2013. Microbialite recovery in the aftermath of the Sturtian glaciation: Insights from the Rasthof Formation, Namibia. *Sedimentary Geology*, **294**, 1-12.

Lehmann, J., Saalmann, K., Naydenov, K.V., Milani, L., Belyanin, G.A., Zwingmann, H., Charlesworth, G. & Kinnaird, J.A. 2016. Structural and geochronological constraints on the Pan-African tectonic evolution of the northern Damara Belt, Namibia. *Tectonics*, **35**, 103-135.

Lokier, S.W., Andrade, L.L., Court, W.M., Dutton, K.E., Head, I.M., van der Land, C., Paul, A. & Sherry, A. 2018. A new model for the formation of microbial polygons in a coastal sabkha setting. *Depositional Record*, **3**, 201-208.

Macdonald, F.A., Schmitz, M.D., Strauss, J.V., Halverson, G.P., Gibson, T.M., Eyster, A., Cox, G., Mamrol, P. & Crowley, J.L. 2018. Cryogenian of Yukon. *Precambrian Research*, **319**, 114-143.

MacLennan, S., Park, Y., Swanson-Hysell, N., Maloof, A., Schoene, B., Gebreslassie, M, Antilla, E., Tesema, T., Alene, M. & Haileab, B. 2018. The arc of the Snowball: U-Pb dates constrain the Islay anomaly and the initiation of the Sturtian glaciation. *Geology*, **46**, 539-542.

Miller, R.McG. 2008b. *The Geology of Namibia: Vol. 2, Neoproterozoic to Lower Palaeozoic*. Geological Survey of Namibia, Windhoek.

Miller, R.McG. 2013. Comparative stratigraphic and geochronological evolution of the Northern Damara Supergroup in Namibia and the Katanga Supergroup in the Lufilian Arc of Central Africa. *Geoscience Canada*, 40, http://dx.doi.org/10.12789/geocanj.2013.40.007

Moore, K.R., Bosak, T., Macdonald, F.A., Lahr, D.J.G., Newman, S., Settens, C. & Pruss, S.B. 2017. Biologically agglutinated eukaryotic microfossil from Cryogenian cap carbonates. *Geobiology*, **15**, 499-515.

Narbonne, G.M., Xiao, S.H. & Shields, G.A. 2012. The Ediacaran Period. *In:* Gradstein, F.M., Ogg, J.G., Schmitz, M.D. & Ogg, G.M. (Eds) *The Geologic Time Scale 2012*. Elsevier, Amsterdam, pp. 413-435.

Nelson, L.L., Smith, E.F., Hodgin, E.B., Crowley, J.L., Schmitz, M.D. & Macdonald, F.M. 2021. Geochronological constraints on Neoproterozoic rifting and onset of the Marinoan glaciation from the Kingston Peak Formation in Death Valley, California (USA). *Geology*, **48**, https://doi.org/10.1130/G47668.1

Nogueira, A.C.R., Riccomini, C., Sial, A.N., Moura, C.A.V., Trindade, R.I.F. & Fairchild, T.R. 2007. Carbon and strontium isotope fluctuations and paleoceanographic changes in the late Neoproterozoic Araras carbonate platform, southern Amazon craton, Brazil. *Chemical Geology*, **237**, 168-190.

Partin, C.A. & Sadler, P.M. 2016. Slow net sediment accumulation sets snowball Earth apart from all younger glacial episodes. *Geology*, **44**, 1019-1022.

Petterson, R., Prave, A.R., Wernicke, B.P. & Fallick, A.E. 2011. The Neoproterozoic Noonday Formation, Death Valley region, California. *Geological Society of America Bulletin*, **123**, 1317-1336.

Pillans, B. & Gibbard, P. 2012. The Quaternary Period. *In:* Gradstein, F.M., Ogg, J.G., Schmitz, M.D. & Ogg, G.M. (Eds) *The Geologic Time Scale 2012, Vol. 2*. Elsevier, Amsterdam, pp. 979-1010.

Prave, A.R., Condon, D.J., Hoffmann, K.-H., Tapster, S. & Fallick, A.E. 2016. Duration and nature of the end-Cryogenian (Marinoan) glaciation. *Geology*, **44**, 631-634.

Preiss, W.V. & Forbes, B.G. 1981. Stratigraphy, correlation and sedimentary history of Adelaidean (Late Proterozoic) basins in Australia. *Precambrian Research*, **15**, 255-304.

Pruss, S.B., Bosak, T., Macdonald, F.A., McLane, M. & Hoffman, P.F. 2010. Microbial facies in a Sturtian cap carbonate, the Rasthof Formation, Otavi Group, northern Namibia. *Precambrian Research*, **181**, 187-198.

Rooney, A.D., Strauss, J.V., Brandon, A.D. & Macdonald, F.A. 2015. A Cryogenian chronology: Two long-lasting synchronous Neoproterozoic glaciations. *Geology*, **43**, 459-462.

Rooney, A.D., Yang, C., Condon, D.J., Zhu, M.Y. & Macdonald, F.A. 2020. U-Pb and Re-Os geochronology tracks stratigraphic condensation in the Sturtian snowball aftermath. *Geology*, **48**, 625-629.

Rose, C.V., Swanson-Hysell, N.L., Husson, J.M., Poppick, L.N., Cottle, J.M., Schoene, B. & Maloof, A.C. 2012. Constraints on the origin and relative timing of the Trezona δ^{13}C anomaly below the end-Cryogenian glaciation. *Earth and Planetary Science Letters,* **319-320**, 241-250.

SACS (South African Committee for Stratigraphy) 1980. Damara Sequence. *In:* Kent, L.E. (Ed.) *Stratigraphy of South Africa Part 1: Lithostratigraphy of the Republic of South Africa, South West Africa/Namibia and the Republics of Bophuthatswana, Transkei and Venda*. Geological Survey of South Africa Handbook, **8**, pp. 415-438.

Schlager, W. 2005. Carbonate Sedimentology and Sequence Stratigraphy. *SEPM (Society for Sedimentary Geology) Concepts in Sedimentology and Paleontology*, **8**, 200 pp.

Shields-Zhou, G.A., Porter, S. & Halverson, G.P. 2016. A new rock-based definition for the Cryogenian Period (circa 720 - 635 Ma). *Episodes*, **39** (**1**), 3-8.

Söhnge, P.G. 1953. Review of the geology of the Otavi Mountain Land, South West Africa. Unpublished Report, Tsumeb Corporation Ltd, Tsumeb.

Söhnge, P.G., 1957. Revision of the geology of the Otavi Mountainland, South West Africa (with 1958 amended stratigraphic table). Unpublished Report, Tsumeb Corporation Ltd, Tsumeb.

Tziperman, E., Halevy, I., Johnston, D.T., Knoll, A.H. & Schrag, D.P. 2011. Biologically induced initiation of Neoproterozoic snowball-Earth events. *Proceedings of the U.S. National Academy of Sciences*, **108** (**37**), 15,091-15,096.

Vieira, L.C., Nédélec, A., Fabre, S., Trindade, R.I.F. & Paes de Almeida, R. 2015. Aragonite crystal fans in Neoproterozoic cap carbonates: a case study from Brazil and implications for the post-snowball Earth coastal environment. *Journal of Sedimentary Research*, **85**, 285-300.

Wallace, M.W., Hood, A.v.S., Woon, E.M.S., Hoffmann, K.-H. & Reed, C.P. 2014. Enigmatic chambered structures in Cryogenian reefs: The oldest sponge-grade organisms? *Precambrian Research*, **255**, 109-123.

Watts, A.B., Karner, G.D. & Steckler, M.S. 1982. Lithospheric flexure and the evolution of sedimentary basins. *Philosophical Transactions of the Royal Society of London Series A*, **305** (**1489**), 249-281.

Zhou, C.M., Huysken, M.H., Lang, X.G., Xiao, S.H. & Yin, Q.Z. 2019. Calibrating the terminations of Cryogenian global glaciations. *Geology*, **47**, 251-254.

An occurrence of radially symmetric sedimentary structures in the basal Ediacaran cap dolostone (Keilberg Member) of the Otavi Group

P.W. Crockford[1,2], A. Mehra[3,4], E. Domack[5,a] & P.F. Hoffman[2,6]

[1]Department of Earth and Planetary Sciences, Weizmann Institute of Science Rehovot 76100 Israel. email:
peter.crockford@weizmann.ac.il
[2]Department of Earth and Planetary Sciences, Harvard University, Cambridge MA 02138, USA
[3]Department of Geoscience, Princeton University, Princeton NJ 08544, USA
[4]Department of Earth Sciences, Dartmouth College, Hanover NH 03755, USA
[5]College of Marine Science, University of South Florida, St Petersburg FL 33701, USA
[6]School of Earth and Ocean Sciences, University of Victoria, Victoria BC V8W 2Y2, Canada
[a]Deceased

Abstract : Snowball Earth cap carbonate sequences provide an archive of what are likely the most dramatic climate transitions in all of Earth history. One approach to gain insight into these events is the detailed observation of sedimentary structures within these post-glacial units. Here, we report on newly discovered radially symmetric sedimentary structures within the Keilberg Member post-Marinoan 'cap dolostone' from the Otavi Group of northwest Namibia. We describe the local expression of over 60 decimeter-scale cymbal or disc structures from a single location. We interpret these features, which we name Zildjian structures, to be of likely abiotic origin. Through morphological comparisons, we suggest that Zildjian structures are most similar to *Astropolithon*, a pseudofossil that formed as a result of fluid or gas expulsion.

Introduction

Persuasive geological and geochemical evidence suggests that the Neoproterozoic Era was punctuated by a pair of 'Snowball Earth' glaciations - the Marinoan (646 +/- 5 to 635 Ma; Kendall *et al.* 2006; Prave *et al.* 2016; Condon *et al.* 2005) and the Sturtian (717 to 661 Ma; Macdonald *et al.* 2010; MacLennan *et al.* 2017; Rooney *et al.* 2014) - during which time the oceans were covered from pole to pole by dynamic ice sheets (Kirshvink 1992; Hoffman & Schrag, 2002; Hoffman *et al.* 2017; Hoffman *et al.* in press). The transitions out of these extreme climate states are documented by so called 'cap dolostones', which (in the case of the Marinoan) are layers of organic-poor micro-clotted, pseudo-peloidal (also described as micropeloidal or dolopelarenite) dolomite overlying glacial deposits and glacial erosion surfaces. These post-glacial carbonates have been observed to range in thickness from 10s of centimetres to 100s of metres (Grotzinger & Knoll, 1995; Hoffman *et al.* 1998, 2011; Hoffman & Li, 2009). Cap dolostones are found on virtually all palaeocontinents and palaeogeographic reconstructions place deposition typically at ≤ 50° palaeolatitude (Hoffman & Li, 2009). These units represent the transgressive systems tract (i.e. post-glacial flooding) of thick depositional sequences that may have formed because of prolonged subsidence in a slow sedimentation regime (Partin *et al.* 2016).

Cap dolostones contain many unusual (and, in certain cases, enigmatic) sedimentological features, including tubestone stromatolites (Corsetti & Grotzinger, 2005), digitate and fanning barites (Bao *et al.* 2008; Crockford *et al.* 2016, 2018, 2019), trochoidal bedforms interpreted as giant wave ripples (Allen &

Hoffman, 2005; Lamb *et al.* 2012), and sheet cracks filled with fibrous isopachous dolomite cement (Hoffman & Macdonald, 2010; also cf. Hoffman, 2011 for an in-depth review of cap dolostone sedimentology). In fact, Marinoan cap dolostones are so distinctive in character and setting that they defined the base of the Ediacaran Period (Knoll *et al.* 2006) before their age and synchroneity were known radiometrically (Rooney *et al.* 2015; Zhou *et al.* 2019).
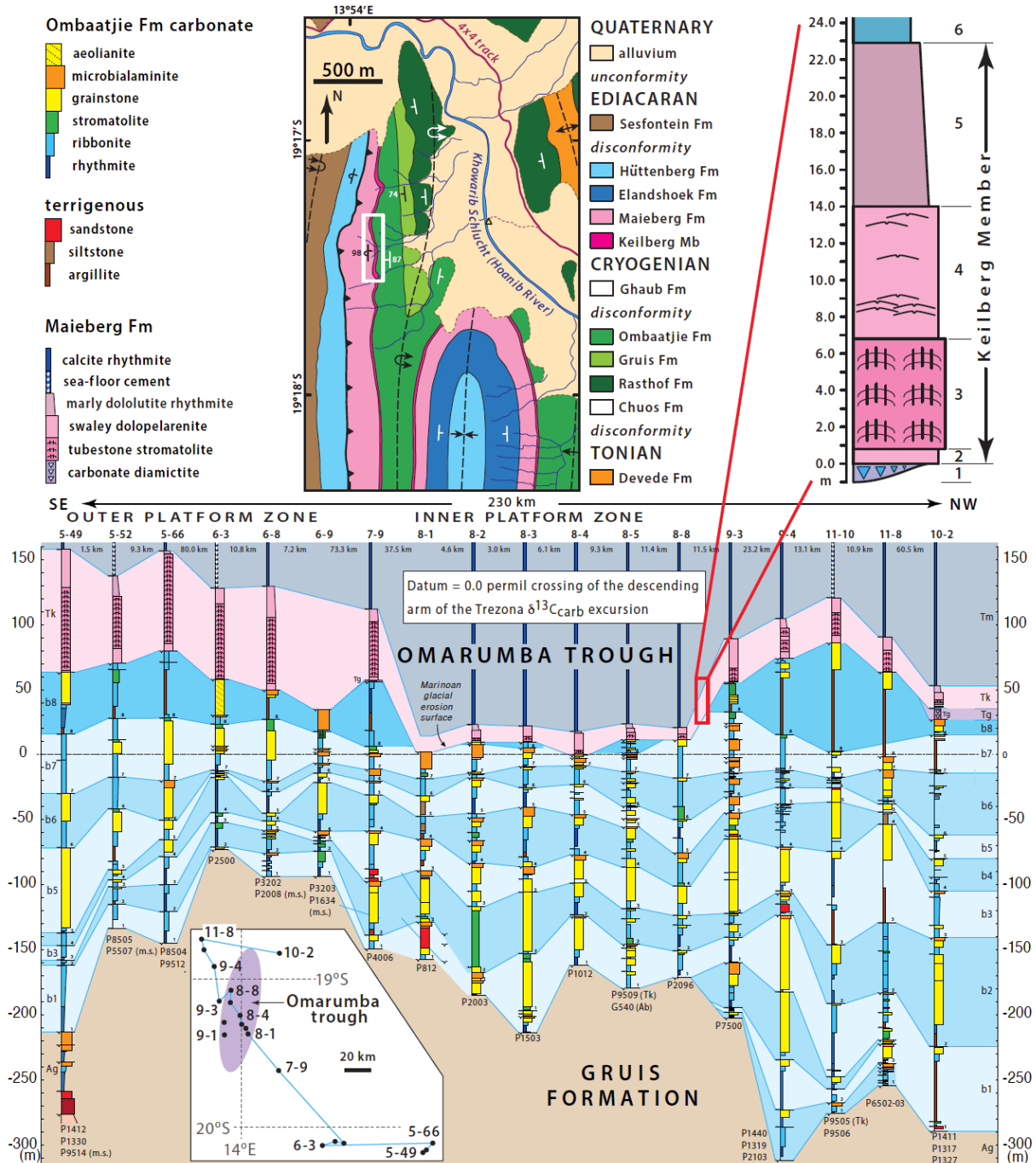

Figure 1. Geology and representative columnar section of the Keilberg Member in the study area. A legend is provided in the top left of the figure.

In the top centre map panel of Figure 1, the area bearing the Zildjians in the foreland thrust-fold belt of the Ediacaran Kaoko orogen is outlined by the white rectangle. Bedrock includes pre-orogenic carbonate formations of the Otavi Group (770-600 Ma) and synorogenic clastics of the Sesfontein Formation (Mulden Group). The Glacigenic Chuos and Ghaub formations are too thin to show at this scale. The white rectangle is in the W-facing but E-dipping limb of an anticline in the hanging wall of a W-directed backthrust. Local topographic relief is 425 m relative to the Hoanib River, which has perennial flowing surface water in this area. A vehicle track (purple line) connects westward to Khowarib and eastward to Omukutu and Ombaatjie. The field campsite is indicated by a small yellow triangle. In the top right panel, a representative columnar section of Keilberg Member cap dolostone in the white rectangular area of the map panel and red rectangle of the cross section in the lower panel are presented. Numbered lithologic units: 1 - Ghaub Formation (Marinoan) carbonate diamictite inferred to be a lodgement tillite derived from underlying upper Ombaatjie Formation (left panel); 2 - low-angle cross-stratified dolopelarenite (peloid grainstone); 3 - tubestone stromatolite (Corsetti & Grotzinger, 2005); 4 - low-angle cross-stratified dolopel-arenite with peloidal sand volcanoes at horizons indicated; 5 - thin planar-laminated dolomicrite with argillaceous partings increasing upward; 6 - marly calcite rhythmite. Stratigraphic height is in metres above the base of the Keilberg Member (0.0 m). In the lower cross section panel, selected Ombaatjie Fm sections are plotted from the OPz and IPz which outline the Omarumba Trough. The insert map at the bottom of the panel shows relative section locations. Palaeotopography is reconstructed assuming as a datum when carbonate carbon isotope values from previous studies cross 0.0 per mil in cycle b7 (Hoffman *et al*. in press), which, elsewhere, is supported by correlation of Keilberg Member thickness with stratigraphic height above this datum (Hoffman *et al*., in press). The Omarumba trough has been inferred to be a subglacial bedrock trough formed via partial removal of the b8 and b7 cycles via Marinoan glacial erosion (Hoffman *et al*. in press).

One way to gain new perspectives on cap dolostone depositional processes is through the careful accounting and analysis of sedimentary features within them. Such features - from millimetre-scale wave ripples to metre-scale microbial buildups and kilometre-scale mud volcanoes - represent a record of physical forcings that can be used to understand past environmental conditions (Hoffman & Macdonald, 2010; Lamb *et al.* 2012). With such analyses in mind, we present a description of decimetre-scale radially symmetrical sediment-ary cymbal-shaped structures that are located within the Keilberg Member cap dolostone of the Congo craton in modern day Namibia. Due to their size and shape, we call these cymbal-like structures "Zildjians", after an Armenian-Turkish-American family of cymbal manufacturers since 1618.

Geological Setting

The focus of this study is the Keilberg Member of the Maieberg Formation (Hedberg, 1979; SACS, 1980; Hoffman & Halverson, 2008), which is the basal Ediacaran formation within the Otavi Group. The study site is located near the village of Omukutu on the upper Hoanib River east of Khowarib, in the Kunene Region of northwest Namibia (S19°17'20.04" E13°54'5.4"; Fig. 1). At the study location, the Maieberg Fm is exposed as sub-vertically dipping, slightly overturned beds that face to the west. The Keilberg Member documents the initial post-glacial transgression from the Marinoan glaciation (Hoffman *et al.* 1998, 2011; Hoffman *et al*. in press) across northwest Namibia and correlates with other, globally distributed formations that record similar geological events (Hoffman *et al.* 2017). The Omukutu area is situated on the inner Otavi Group carbonate platform at the western sidewall of the Omarumba Trough (Fig. 1), a broad shallow depression cut by south-southwestward-flowing Marinoan ice. In this location, the Keilberg Member directly overlies the glacial erosion

28

surface, marked by scraps of lodgement tillite, and passes gradationally upwards into marly limestone rhythmite of the middle Maieberg Formation postglacial maximum-flooding interval. The Keilberg Member at Omukutu is ≈23 m thick. Regionally, sections within the Omarumba Trough range between 10-20 m in thickness but outside the trough they can expand to between 30 and 100 m (Fig. 1).

Field observations

Sixty-one different Zildjian structures were recorded in the Omukutu area (Fig 2). Most structures were observed to be between 7.8 and 9.1 m above the base of the Keilberg Member, although several were also found at 11.2, 13.0 and 13.5 m above the base of the section (Table 1). The stratigraphic interval containing the Zildjian structures was deposited above 'tubestone' stromatolites (Corsetti & Grotzinger, 2005) and is comprised of dolomitized micropeloidal grainstone (i.e. dolopelarenite) characterized by swaley low-angle cross-stratification (Fig. 1). The Zildjians were identified as concentric circular ridges and depressions (Fig. 2). As previously mentioned, in the Omukutu area, the beds are slightly overturned. Therefore, field measurements of Zildjians were made on the undersides of the structures (Fig. 2). Although the preservation of Zildjian structures varied across the outcrop (due to differential weathering), we applied a consistent measurement scheme to document those instances that we were safely able to reach.

In total, we were able to study approximately half of the 61 observed structures (n = 35). In what follows, we present observations as if observing Zildjian structures from right-way-up in horizontal beds unless otherwise specified. For each Zildjian, we measured an outer rim diameter (D_1), an inner trough diameter (D_2), a central axial pit diameter (D_3), and the distance to the next closest Zildjian (from center to center; S), all parallel to bedding (Fig. 3C; Table 1).

We also measured an overall vertical relief where the undersides of structures protrude down from the bedding plane (H) and stratigraphic height (Z), both normal to bedding (Fig. 3C; Table 1). These measurements yielded a mean D_1 of 0.29 m [range: 0.12-0.70 m; n=29]; a mean D_2 of 0.09 m [range: 0.04-0.14 m; n=33]; a mean D_3 of 0.045 m [range: 0.015-0.075 m; n=33]; a mean H of 0.023 m [range: 0.005-0.048 m; n=24]; and a mean S of 1.07 m [range: 0.33-2.63; n=14] (Table 1). As observed, none of the structures exhibited any markings radiating away from the axial pit. Such observations have been documented in a number of interpreted Ediacaran and Cryogenian circular fossil imprints (MacGabhann, 2007; Inglez *et al.* 2019; Burzinski *et al.* 2020). We note that many of the Zildjian structures displayed a slight depression beyond the D_1 perimeter, approaching, in some cases, one metre in diameter. This slight depression radiating away from the underside of the Zildjian structures implies a slight doming of the bedding plane (Fig. 2A). Together, these measurements depict a regularity of Zildjian dimensions as well as somewhat regular spacings between them
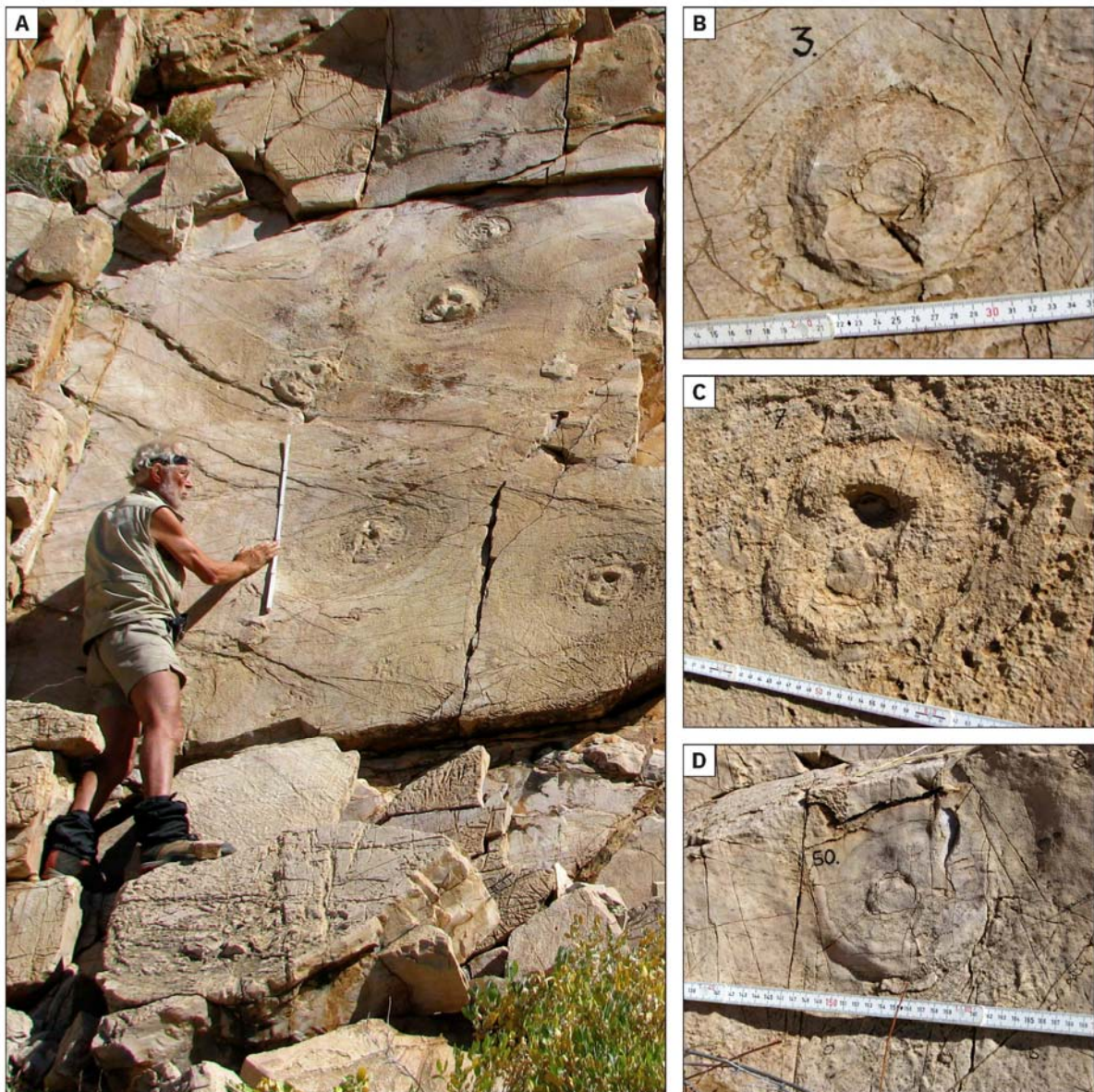
Figure 2. Sedimentological expression of the undersides of Zildjian structures in overturned beds in the Omukutu area. (A) Bedding plane image of undersides of multiple Zildjian structures at the outcrop (ruler in images is in cm). Note that in (A) Zildjians are surround by a slight depression beyond D_1 diameter and that since beds are slightly overturned this suggests a doming of the bedding plane. (B-D) Three examples of Zildjian structures.

Two weathered blocks of float provided cross-sectional views of the Zildjian structures (Fig. 3A & 3B) thereby allowing a more detailed description of their sedimentological characteristics. In these two samples, we observed regular laminations in grainstone parallel to the bedding plane away from the structures. Moving towards the center of the structure, laminations deflected downward, reaching an angle of $\approx$ 45 degrees. Further inward, laminations curved back up toward the axial zone of the structures. In the axial zone, in the lower portion of the structures, the laminations appeared to stop and were replaced by infill (likely micritic) which in one sample displayed convex layering (Fig. 3B & 3D). Tracing the axial zone further up, however, laminations do bridge across the structures (Fig.

30

3D). This finding is consistent with continued sedimentation that draped over the resulting Zildjian bedform. In cross-section, we observed that, when vertically tracing the axial zone downwards (~ 10 cm), D_2 and D_3 varied. A possibility for the vertical heterogeneity of inter-Zildjian widths is differential exposure (i.e. differences in where the bedding plane intersects with different Zildjians) rather than true size dissimilarities between structures.
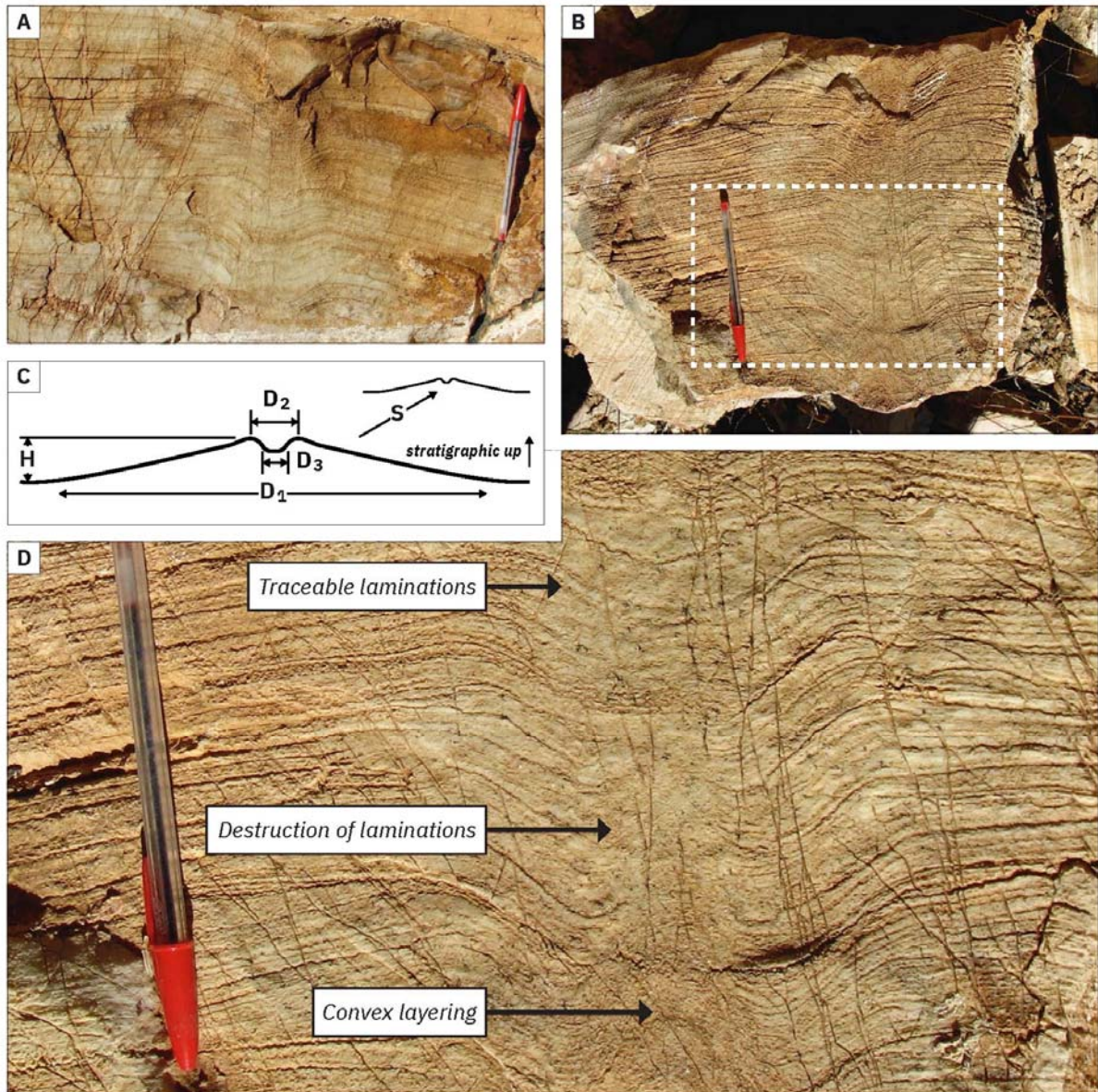
Figure 3. Cross sectional view of Zildjian structures from two float samples. (A, B) Photos of two Zildjian cross sections of float samples in the Omukutu area. Note that photos are presented in interpreted stratigraphic up orientation and that the Bic crystal pen length (scale) is 14.9 cm. A cross sectional schematic provided in (C) where D_1 outer diameter, D_2 diameter at upper lip, D_3 diameter in axial pit, H synoptic height and S lateral spacing between discs is shown. (D) a zoomed in view of a portion of one of the Zildjian cross sections (denoted by the white dashed box in B) is presented where convex beds under the structure, destruction of laminations and traceable laminations across the structure are shown.

Interpretation

In what follows, we compare the Zildjian structures to reported discoidal sedimentary features of both abiotic and biotic interpreted sedimentary origins. Specifically, we focus on some of the key features highlighted above: the regular spacing between the Zildjians, the dimensions of the structures, the partial destruction of laminations in the axial pit, and the slight doming outside the D_1 diameter. We utilise these observations to consider a biological versus abiotic origin for these structures. We would like to note, however, that further research, utilizing analyses such as detailed petrography and/or microscopy,will be needed to conclusively rule out particular interpretations.

There are several instances of documented sedimentary features that are both morphologically similar to Zildjians and have inferred biological origins. Examples of such features include Ediacaran and Cryogenian discoidal fossils such as *Aspidella* (MacGabhann, 2007), rooting or frond structures (Luzhnaya & Ivantsov 2019), Cambrian medusae (Young & Hagadorn, 2010) or features formed via microbial mats. Importantly, slight outer doming analogous to that observed in the Zildjian structures beyond the D_1 diameter (see above), has not been described in any of these examples. Zildjian structures have a decimetre-scale range of outer rim diameters (i.e. from 0.12 to 0.7 m) which is considerably larger than the range of diameters reported for Ediacaran discoidal fauna imprints (maximum diameter of < 0.15 m, with many reported in the sub-cm range; MacGabhann, 2007; Inglez *et al.* 2019; Burzinski *et al.* 2020) or the frond-like Petalonamae *Ediacaria flindersi* Sprigg (outer diameter of < 0.02 m; see Luzhnaya & Ivantsov, 2019) or so called 'scratch circles' (Jensen *et al.* 2018). While Cambrian medusoids can reach similar sizes to the Keilberg Zildjians (Young & Hagadorn, 2010) other morphological characteristics disprove such an affinity. In particular, the destruction of bedding in the axial pit rules out an interpretation of Zildjians as surficial impressions resulting from a dead medusa-like organism. Additionally, the observed regular spacing of Zildjians is inconsistent with the expected spatial distribution of a death assemblage of medusae (i.e. maximum

concentration in local troughs, Hagadorn & Miller, 2011). While such regular spacing may be induced via holdfasts of fronds, again, the magnitude of relief of the Zildjians is unlike reported scratch circles and the size of these structures does not match reported imprints from frond-bearing organisms. The final possibility is that Zildjians formed as a direct result of microbial construction such as a stromatolite. A challenge to this interpretation is that Zildjians are of different scale and morphology from documented stromatolite occurrences of this age (James *et al.* 2001; Bosak *et al.* 2013). While some instances of slightly crinkly laminations (Fig. 3) away from the axial zone may conform to expectations of microbial laminite morphology, the spacing (i.e. a lack of lateral contact) of Zildjians and relief is very different from documented domal microbial laminite occurrences (Romero *et al.* 2020). In sum, the outer doming, size, vertical disruption, and regular spacing of the Keilberg Zildjian structures do not match those of previously reported Neoproterozoic or early Cambrian fauna, flora or microbial structures. Therefore, the lack of overlap of these key observations motivates consideration of an abiotic origin.

If the Keilberg Zildjian structures are unlikely to be of biological origin, then what sort of processes led to their formation? The shape, size, axial pit and distribution of Zildjians are very different from discoidal features produced by diagenetic concretions (Schwid *et al.* 2021) but are similar to interpreted gas and fluid escape structures (Dionne, 1973; Lowe, 1975) such as sand volcanoes. In particular, the structures exhibit a striking morphological resemblance to the pseudofossil *Astropolithon*, which is characterised by positive convex relief, a central sediment plug, circular shape, and a diameter of several millimetres to tens of centimetres (Pickerill & Harris, 1979). *Astropolithon* has been documented elsewhere in time and space (Walter, 1972; Mount, 1993; Seilacher & Goldring, 1996; Seilacher *et al.* 2002; Hagadorn & Miller, 2011), but, in contrast to the Zildjian structures, they have typically been reported in siliciclastic-dominated units. Indeed, this difference in host-lithology may be responsible

for the spectacular preservation (i.e. clearly visible deformation of laminations in cross section) of Zildjian structures in the Omukutu area. Initially *Astropolithon* was interpreted to be a trace fossil by Dawson (1878) but later investigations noted how the pseudofossil bears the same characteristics as sand or mud volcanoes (Seilacher *et al.* 2002). Thus, *Astropolithon* are now considered to be genetically similar to those sedimentary structures, forming as a result of the expulsion of over-pressurized gases or fluids (contained within pore spaces) out of a breach in the sediment-water interface (Lowe, 1975; Pickerill & Harris, 1979). The only suggested distinction between sand or mud volcanoes and *Astropolithon* is the presence of a less permeable surface layer in the latter, which results in slight doming beyond the central vent or aperture (Seilacher *et al.* 2002). In the case of a Silurian example from the Kufra Basin (Seilacher *et al.* 2002), this less-permeable surface layer was suggested to be a 'biomat'. A potential point of contrast between *Astropolithon* and the Zildjian structures reported here, are that no evidence for an organic-rich seal was found in our study location. That said, at this time we cannot rule out the possibility of a microbial mat acting as a seal or impermeable layer. Additionally, we note that rapid cementation of carbonate laminae may have had a similar sealing effect where deformation then occurred within partially lithified sediments. With these considerations in mind, we explore further the potential origins of Zildjian structures below.

If the Zildijian structures are indeed *Astropolithon*-like constructions, they formed because of either gas or fluid escape from sediments and, in turn, these physical events were likely triggered by either degradation of organic matter, seismic activity, or rapid sediment loading (Fig. 4).
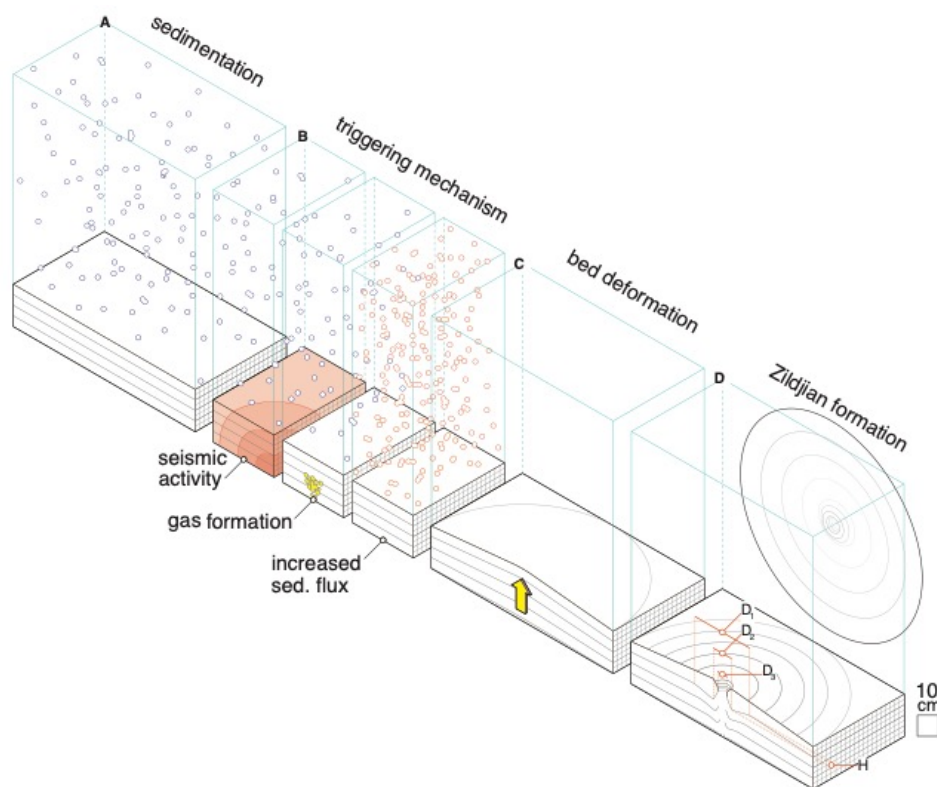

Figure 4. Representation of possible Zildjian formation mechanisms. (A) Initial sedimentation; (B) triggering mechanisms; (C) deformation of beds; (D) Zildjian formation including a cross-sectional, plan and underside view of the structures. A scale is provided on the lower right of the figure.

Table 1. Dimensional data on cymbal-like structures in stratigraphic order (top to bottom). All measurements in metres: #, structure number; Z, stratigraphic height with respect to base of Keilberg Mb; D_1, disc outer diameter; D_2, inner rim diameter; D_3, axial pit diameter; H, overall vertical relief; S, distance to nearest structure at same horizon. Total thickness of Keilberg Member, 18.2 m. Base of tubestone stromatolite, 0.5-1.2 m; top of tubestone stromatolite, 6.5-9.4 m (with respect to the base of the Keilberg Mb). Remainder of Keilberg Member composed of laminated dolopelarenite with low-angle hummocky cross-stratification. D_1 average 0.296 m [0.12-0.70] n=29; D_2 average 0.093 m [0.04-0.14] n=33; D_3 average 0.0415 m [0.015-0.075] n=33; H average 0.231 m [0.010-0.048] n=24; S average 1.07 m [0.33-2.63] n=14.

#	Z	D_1	D_2	D_3	H	S
60	13.5	-	0.12	0.033	0.015	
62	13.0	0.70	0.08	0.07	0.03	
52	11.25	-	0.067	0.040	0.005	
17	9.1	0.40	0.08	0.035	0.014	
50	9.1	0.21	0.07	0.035		1.32
51	9.05	0.3	0.110	0.05	0.013	
2	8.7	0.20	0.11		0.016	2.63
3	8.7	0.28	0.07	0.040	0.018	0.84
10	8.7	-	0.04	0.015		
22	8.65	0.224	0.092	0.066		0.72
23	8.65	0.12	0.046	0.028		0.86
30	8.65					
31	8.65					
32	8.61	0.275	0.116	0.058	0.018	1.6
1	8.6	0.28	0.12	0.06	0.025	
19	8.55	0.28	0.07	0.051	0.03	0.76
20	8.55	0.26	0.12	0.072	0.048	0.52
21	8.55	0.20	0.078	0.055	0.014	
25	8.55	-	0.130	0.035		0.33
26	8.55	0.15	0.090	0.030		1.16
27	8.55	0.275	0.165	0.065	0.017	
29	8.55	0.190	0.080	0.050	0.015	1.33
18	8.3	0.26	0.07	0.05		
53	8.3	-	0.09	0.03		
6	8.25	0.50	0.09	0.04	0.023	1.03
7	8.25	0.46	0.11	0.04	0.032	
8	8.25	0.55	0.10	0.05	0.04	1.04
9	8.25	0.34	-	0.06	0.03	
11	8.25	0.40	0.04	0.03		
15	8.25	0.5	0.14	0.055	0.04	0.86
4	8.2	0.16	0.04	0.015	0.020	
24	8.2	0.270	0.140	0.030	0.010	
28	8.11	0.245	0.135	0.075	0.048	
5	7.8	0.20	0.08	0.051	0.013	
16	float	0.23	0.12	0.05		
61	float	0.12	0.06	0.03	0.02	

Multiple exposed horizons make selecting a definitive set and order of genetic events challenging. We first consider gas escape. A possible formation mechanism is the degradation of organic matter, which may have produced pockets of gases that pooled in place until sudden expulsion through beds occurred. Previous work has suggested that 'balloon' structures in sands (Hilbert-Wolf *et al.* 2016) are a key feature of gas escape. However, such features are absent from our study area. Although a difference in host lithology may be responsible for the lack of balloon structures, their absence potentially supports fluid escape versus gas escape as the primary expulsion events resulting in Zildjian structures.

A second potential piece of evidence in support of fluid escape is the upward deflection of beds into the axial pit; similar features have been shown in fluid-escape experiments conducted in siliciclastic sand and silt (Nichols *et al.* 1994). While there are many documented examples of fluidization structures with inferred relationships to seismicity, we did not observe, nor can we correlate, episodes of faulting or other physical indicators that would pinpoint a seismic trigger. Moreover, the appearance of the Keilberg Zildjians in multiple beds, as well as the possibility of the variation of the D_2 and D_3 diameters at the outcrop being caused by multiple expulsion episodes, appears to require a mechanism for repeated triggering. The combination of post-glacial sea level rise and

glacial unloading could potentially produce seismic activity in the study area. However, further work is needed to identify and link such observations. An alternative possibility is that rapid loading may have been the underlying cause of the Keilberg Zildjians. Indeed, rapid sedimentation events have been suggested as the most common cause of fluid-escape structures in the sedimentary record (Lowe, 1975). However, this hypothesis is negated if fine mm-scale laminations in cross section require slower sedimentation. In sum, through morphological comparison Zildjians appear to bear the most similarity to *Astropolithon* and are likely the result of fluid or gas escape from sediments, however further work is warranted in order to constrain their origins at this time more precisely.

Conclusions

Here we have described a new sedimentary feature within post-Marinoan cap carbonate in the Omukutu area of Namibia. The features most closely resemble the pseudofossil *Astropolithon* indicating fluid or gas expulsion and are therefore unlikely to be the result of a fossil imprint or direct microbial construction. At this time, further interpretation is challenging without detailed petrography, microscopy, and geochemical analyses, which are greatly encouraged in future work. Importantly, if such structures resulted from fluid escape, they may

provide support for models of rapid cap dolostone sedimentation. The lack of prior reports of Zildjian structures, and their discovery in the Omukutu area within the most extensively studied Cryogenian field area that has been developed to date, is potentially due to their exposure in vertically dipping beds with well-exposed bedding planes. Indeed, there may be many other roughly time-equivalent occurrences of Zildjians or similar structures within post-Marinoan strata and therefore further exploration is warranted.

Acknowledgements

References

Allen, P.A. & Hoffman, P.F. 2005. Extreme winds and waves in the aftermath of a Neoproterozoic glaciation. *Nature*, **433**, 123-127. https://doi.org/10.1038/nature03176.

Bao, H., Lyons, J.R. & Zhou, C. 2008. Triple oxygen isotope evidence for elevated CO2 levels after a Neoproterozoic glaciation. *Nature*, **453** (**7194**), 504-506. https://doi.org/10.1038/nature06959.

Bosak, T., Mariotti, G., MacDonald, F.A., Perron, J.T. & Pruss, S.B. 2013. Microbial sedimentology of stromatolites in Neoproterozoic cap carbonates. *The Paleontological Society Papers*, **19**, 51-76. doi: 10.1017/s1089332600002680.

Burzynski, G., Dececchi, T.A., Narbonne, G.M. & Dalrymple, R.W. 2020. Cryogenian *Aspidella* from northwestern Canada.

Precambrian Research, **336**, 105507. https://doi.org/10.1016/j.precamres.2019.1055 07.

Condon, D., Zhu, M., Bowring, S., Wang, W., Yang, A. & Jin, Y. 2005. U-Pb ages from the Neoproterozoic Doushantuo Formation, China. *Science*, **308** (**5718**), 95-98. doi: 10.1126/science.1107765.

Corsetti, F.A. & Grotzinger, J.P. 2005. Origin and significance of tube structures in Neoproterozoic post-glacial cap carbonates: example from Noonday Dolomite, Death Valley, United States. *Palaios*, **20** (**4**), 348-362. https://doi.org/10.2110/palo.2003.p03-96.

Crockford, P.W., Cowie, B.R., Johnston, D.T., Hoffman, P.F., Sugiyama, I., Pellerin, A., Bui, T.H., Hayles, J., Halverson, G.P., Macdonald, F.A. & Wing, B.A. 2016. Triple oxygen and multiple sulfur isotope constraints on the evolution of the post-Marinoan sulfur cycle. *Earth and Planetary Science Letters*, **435**, 74-83. https://doi.org/10.1016/j.epsl.2015.12.017.

Crockford, P.W., Hodgskiss, M.S., Uhlein, G.J., Caxito, F., Hayles, J.A. & Halverson, G.P. 2018. Linking paleocontinents through triple oxygen isotope anomalies. *Geology*, **46** (**2**), 179-182. https://doi.org/10.1130/G39470.1.

Crockford, P.W., Wing, B.A., Paytan, A., Hodgskiss, M.S., Mayfield, K.K., Hayles, J.A., Middleton, J.E., Ahm, A.S.C., Johnston, D.T., Caxito, F. & Uhlein, G. 2019. Barium-isotopic constraints on the origin of post-Marinoan barites. *Earth and Planetary Science Letters*, **519**, 234-244. https://doi. org/10.1016/ j.epsl.2019.05.018

Dawson J.W. 1878. Supplement to the second edition of *Acadian Geology*. *In*: Acadian Geology, the geological structure, organic remains and mineral resources of Nova Scotia, New Brunswick and Prince Edward Island. 3rd Edition. MacMillan, London, 102 pp.

Dionne, J.C. 1973. Monroes; a type of so-called mud volcanoes in tidal flats. *Journal of Sedimentary Research*, **43** (**3**), 848-856.

Grotzinger, J.P. & Knoll, A.H. 1995. Anomalous carbonate precipitates; is the Precambrian the key to the Permian? *Palaios*, **10** (**6**), 578-596.

Hagadorn, J. & Miller, R. 2011. Hypothesized Cambrian medusae from Saint John, New Brunswick, reinterpreted as sedimentary structures. *Atlantic Geology*, **47**, 66-80. doi: 10.4138/atlgeol.2011.002.

Hedberg, R.M. 1979. Stratigraphy of the Ovamboland Basin, South West Africa. *University of Cape Town Precambrian Research Unit Bulletin*, **24**, 325 p. and 6 map sheets scale 1:125,000.

Hilbert-Wolf, H.L., Roberts, E.M. & Simpson, E.L. 2016. New sedimentary structures in seismites from SW Tanzania: Evaluating gas- vs. water-escape mechanisms of soft-sediment deformation. *Sedimentary Geology*, **344**, 253-262. https://doi.org/10.1016/j.sedgeo.2016.03.011.

Hoffman, P.F. 2011. Strange bedfellows: glacial diamictite and cap carbonate from the Marinoan (635 Ma) glaciation in Namibia. *Sedimentology*, **58** (**1**), 57-119. https://doi.org/ 10.1111/j.1365-3091.2010.01206.x.

Hoffman, P.F., Abbot, D.S., Ashkenazy, Y., Benn, D.I., Brocks, J.J., Cohen, P.A., Cox, G.M., Creveling, J.R., Donnadieu, Y., Erwin, D.H. & Fairchild, I.J. 2017. Snowball Earth climate dynamics and Cryogenian geology-geobiology. *Science Advances*, **3** (**11**), p.e1600983. DOI: 10.1126/sciadv.1600983.

Hoffman, P.F. & Halverson, G.P. 2008. Otavi Group of the western Northern Platform, the eastern Kaoko Zone and the western Northern Margin Zone. *In:* Miller, R. McG. (Ed.) *The Geology of Namibia, Volume 2.* Geological Survey of Namibia, 13.69-13.136.

Hoffman, P.F., Halverson, G.P., Schrag, D., Higgins, J.A., Domack, E.W., Macdonald, F.A., Pruss, S.B., Blattler, C.L., Crockford, P.W., Hodgin, E.B., Bellefroid, E.J., Johnson, B.W., Hodgskiss, M.S.W., Lamothe, K.G., LoBianco, S.J.C., Busch, J.F., Howes, B.J., Greenman, J.W., Nelson, L.L. (in press). Snowballs in Africa: sectioning a long-lived Neoproterozoic carbonate platform and its bathyal foreslope (NW Namibia). *Earth-Science Reviews*. https://doi.org/10.1016/j.earsci rev.2021.103616.

Hoffman, P.F., Kaufman, A.J., Halverson, G.P. & Schrag, D.P. 1998. A Neoproterozoic snowball earth. *Science*, **281** (**5381**), 1342-1346. DOI: 10.1126/science.281.5381.1342.

Hoffman, P.F. & Li, Z.X. 2009. A palaeogeographic context for Neoproterozoic glaciation. *Palaeogeography, Palaeoclimat*

ology, Palaeoecology*, **277** (**3-4**), 158-172. https://doi.org/10.1016/j.palaeo.2009.03.013.

Hoffman, P.F. & Macdonald, F.A. 2010. Sheet-crack cements and early regression in Marinoan (635 Ma) cap dolostones: Regional benchmarks of vanishing ice-sheets? *Earth and Planetary Science Letters*, **300** (**3-4**), 374-384. https://doi.org/10.1016/j.epsl.2010.10.027.

Hoffman, P.F. & Schrag, D.P. 2002. The snowball Earth hypothesis: testing the limits of global change. *Terra nova*, **14** (**3**), 129-155.https://doi.org/10.1046/j.1365-3121.2002.00408.x.

Inglez, L., Warren, L.V., Okubo, J., Simões, M.G., Quaglio, F., Arrouy, M.J. & Netto, R.G. 2019. Discs and discord: The paleontological record of Ediacaran discoidal structures in the south American continent. *Journal of South American Earth Sciences*, **89**, 319-336. https://doi.org/10.1016/j.jsames.2018.11.023.

James, N.P., Narbonne, G.M. & Kyser, T.K. 2001. Late Neoproterozoic cap carbonates: Mackenzie Mountains, northwestern Canada: precipitation and global glacial meltdown. *Canadian Journal of Earth Sciences*, **38** (**8**), 1229-1262.

Jensen, S., Högström, A.E., Almond, J., Taylor, W.L., Meinhold, G., Høyberget, M.A.G.N.E., Ebbestad, J.O.R., Agić, H.E.D.A. & Palacios, T. 2018. Scratch circles from the Ediacaran and Cambrian of Arctic Norway and southern Africa, with a review of scratch circle occurrences. *Bulletin of Geosciences*, **93**, 287-304.

Kendall, B., Creaser, R.A. & Selby, D. 2006. Re-Os geochronology of postglacial black shales in Australia: Constraints on the timing of "Sturtian" glaciation. *Geology*, **34** (**9**), 729-732. https://doi.org/10.1130/G22775.1.

Kilner, B., Niocaill, C. & Brasier, M. 2005. Low-latitude glaciation in the Neoproterozoic of Oman. *Geology*, **33** (**5**), 413-416. https://doi.org/10.1130/G21227.1.

Kirschvink, J.L. 1992. Late Proterozoic low-latitude global glaciation: the snowball Earth Earth. *In*: Schopf, J.W., Klein, C. & Des Maris, D. (Eds) *The Proterozoic Biosphere: A Multidisciplinary Study*, Cambridge University Press, pp. 51-52.

Knoll, A., Walter, M., Narbonne, G. & Christie-Blick, N. 2006. The Ediacaran Period: a new addition to the geologic time scale. *Lethaia*, **39** (**1**), 13-30. https://doi.org/10.1080/00241160500409223.

Lamb, M.P., Fischer, W.W., Raub, T.D., Perron, J.T. & Myrow, P.M. 2012. Origin of giant wave ripples in snowball Earth cap carbonate. *Geology*, **40** (**9**), 827-830. https://doi.org/10.1130/G33093.1.

Lowe, D.R. 1975. Water escape structures in coarse-grained sediments. *Sedimentology*, **22** (**2**), 157-204. https://doi.org/10.1111/j.1365-3091.1975.tb00290.x.

Luzhnaya, E.A. & Ivantsov, A.Y. 2019. Skeletal Nets of the Ediacaran Fronds. *Paleontological Journal*, **53** (**7**), 667-675. https://doi.org/10.1134/S0031030119070050.

MacGabhann, B.A. 2007. Discoidal fossils of the Ediacaran biota: a review of current understanding. *Geological Society, London, Special Publications*, **286** (**1**), 297-313. https://doi.org/10.1144/SP286.21.

MacLennan, S., Park, Y., Swanson-Hysell, N., Maloof, A., Schoene, B., Gebreslassie, M., Antilla, E., Tesema, T., Alene, M. & Haileab, B. 2018. The arc of the Snowball: U-Pb dates constrain the Islay anomaly and the initiation of the Sturtian glaciation. *Geology*, **46** (**6**), 539-542. https://doi.org/10.1130/G40171.1.

Mount, J.F. 1993. Formation of fluidization pipes during liquefaction: examples from the Uratanna Formation (Lower Cambrian), South Australia. *Sedimentology*, **40** (**6**), 1027-1037. https://doi.org/10.1111/j.1365-3091.1993.tb01378.x.

Nichols, R.J., Sparks, R.S.J. & Wilson, C.J.N. 1994. Experimental studies of the fluidization of layered sediments and the formation of fluid escape structures. *Sedimentology*, **41** (**2**), 233-253.https://doi.org/10.1111/j.1365-3091.1994.tb01403.x.

Partin, C.A. & Sadler, P.M. 2016. Slow net sediment accumulation sets snowball Earth apart from all younger glacial episodes. *Geology*, **44** (**12**), 1019-1022. https://doi.org/10.1130/G38350.1.

Pickerill, R.K. & Harris, I.M. 1979. A reinterpretation of *Astropolithon hindii* Dawson 1878. *Journal of Sedimentary Research*, **49** (**3**), 1029-1036. https://doi.org/

10.1306/212F78AB-2B24-11D7-8648000102C1865D.

Prave, A.R., Condon, D.J., Hoffmann, K.H., Tapster, S. & Fallick, A.E. 2016. Duration and nature of the end-Cryogenian (Marinoan) glaciation. *Geology*, **44** (**8**), 631-634. https://doi.org/10.1130/G38089.1.

Raub T. 2008. *Prolonged Deglaciation of "Snowball Earth*, Thesis, Yale University.

Romero, G.R., Sanchez, E.A., Soares, J.L., Nogueira, A.C.R. & Fairchild, T.R. 2020. Waxing and waning of microbial laminites in the aftermath of the Marinoan glaciation at the margin of the Amazon Craton (Brazil). *Precambrian Research*, **348**, p.105856. https://doi.org/10.1016/j.precamres.2020.105856.

Rooney, A.D., Macdonald, F.A., Strauss, J.V., Dudás, F.Ö., Hallmann, C. & Selby, D. 2014. Re-Os geochronology and coupled Os-Sr isotope constraints on the Sturtian snowball Earth. *Proceedings of the National Academy of Sciences*, **111** (**1**), 51-56. https://doi.org/10.1073/pnas.1317266110.

Rooney, A.D., Strauss, J.V., Brandon, A.D. & Macdonald, F.A. 2015. A Cryogenian chronology: Two long-lasting synchronous Neoproterozoic glaciations. *Geology*, **43** (**5**), 459-462. https://doi.org/10.1130/G36511.1.

SACS (South African Committee for Stratigraphy) 1980. Damara Sequence. *In:* Kent, L.E. (Ed.) *Stratigraphy of South Africa Part 1: Lithostratigraphy of the Republic of South Africa, South West Africa/Namibia and the Republics of Bophuthatswana, Transkei and Venda*. Geological Survey of South Africa Handbook, **8**, 415-438.

Seilacher, A. & Goldring, R. 1996. Class Psammocorallia (Coelenterata, Vendian-Ordovician): Recognition, systematics, and distribution. *GFF, Journal of the Geological Society of Sweden*, **118** (**4**), 207-216. https://doi.org/10.1080/11035899609546256.

Seilacher, A., Lüning, S., Martin, M.A., Klitzsch, E., Khoja, A. & Craig, J. 2002. Ichnostratigraphic correlation of lower Palaeozoic clastics in the Kufra Basin (SE Libya). *Lethaia*, **35** (**3**), 257-262. https://doi.org/10.1111/j.1502-3931.2002.tb00083.x

Schwid, M.F., Xiao, S., Nolan, M.R. & An, Z. 2021. Differential Weathering of Diagenetic Concretions and the Formation of Neoproterozoic Annulated Discoidal Structures. *Palaios*, **36** (**1**), 15-27. https://doi.org/10.2110/palo.2020.018.

Walter, M.R. 1972. Tectonically deformed sand volcanoes in a Precambrian greywacke, Northern Territory of Australia. *Journal of the Geological Society of Australia*, **18**, 395-399. https://doi.org/10.1080/00167617208728777.

Young, G.A. & Hagadorn, J.W. 2010. The fossil record of cnidarian medusae. *Palaeoworld*, **19** (**3-4**), 212-221. https://doi.org/10.1016/j.palwor.2010.09 .014.

Zhou, C., Huyskens, M.H., Lang, X., Xiao, S. & Yin, Q.Z. 2019. Calibrating the terminations of Cryogenian global glaciations. *Geology*, **47** (**3**), 251-254. https://doi.org/10.1130/G45719.1.

Notes on traverses across the Khorixas-Gaseneirob Thrust, Southern Khorixas and Outjo Districts, Namibia

Roy McG. Miller

Consulting Geologist, P.O. Box 11222, Windhoek, 11009, Namibia (e-mail: roymm36@mweb.com.na)

Abstract : Local algalaminites in the pre-Chuos Saturn Formation suggests deposition of parts of this unit in shallow water south of the northern boundary fault of the deep Nosib-age rift of the Northern Zone but mass-flow carbonate layers with stromatolitic reef debris and sandstone layers with transported oolites interbedded with the Chuos diamictites point to much deeper water during Chuos times. Mass flows and rhythmites in the Tsumeb Subgroup rocks on the Fransfontein Ridge are indicative of slope deposition that passed southwards into numerous mass flows and rhythmites of the coeval Karibib Formation in much deeper water of the deepening Northern Zone rift. Quartzites interbedded with the schists of the Kuiseb Formation west of Khorixas show evidence of small-scale regressions and transgressions.

D1 was intense in the Kaoko Belt and folded the northern margin of the Damara Belt. Erosional debris was deposited in intramontane valleys along this margin as the molasse of the Mulden Group. Intense D2 deformation, however, folded the Swakop Group succession into a series of NE-SW to ENE-WSW folds which were then thrust up and over the northern boundary fault of the deep Nosib-age rift of the Northern Zone and onto the Mulden molasse as a series of thrusts successively overstepping each other from west to east to form the front of the Khorixas-Gaseneirob Thrust, the floor thrust of a duplex system of thrusts. Nappes of Swakop Group and deep-water Otavi Group rocks were thrust onto the Mulden phyllites. D2 produced the E-W foliation in the Mulden phyllites and caused north-verging folding and thrusting in the Otavi rocks of the Fransfontein Ridge. In the Kuiseb schists west of Khorixas, zones of intense bedding-parallel D2 deformation and quartzite disruption suggest the presence of several thrusts within the schists. D2 stretching lineations point to a thrust transport direction between 320° and 360° (magnetic).

Introduction

The notes that follow have been extracted from a programme of observations made in 2010 along seven traverses that started at the base of the Damara succession in the Fransfontein Ridge and continued through to the top of the Karibib Formation or into the Kuiseb Formation a few kilometres south of the Khorixas-Gaseneirob Thrust. The locations of Traverses 2-4 are shown in Figure 1 and that of Traverse 1 in Figure 1.1. The observations have built on the work of Frets (1969) and Clifford (2008).
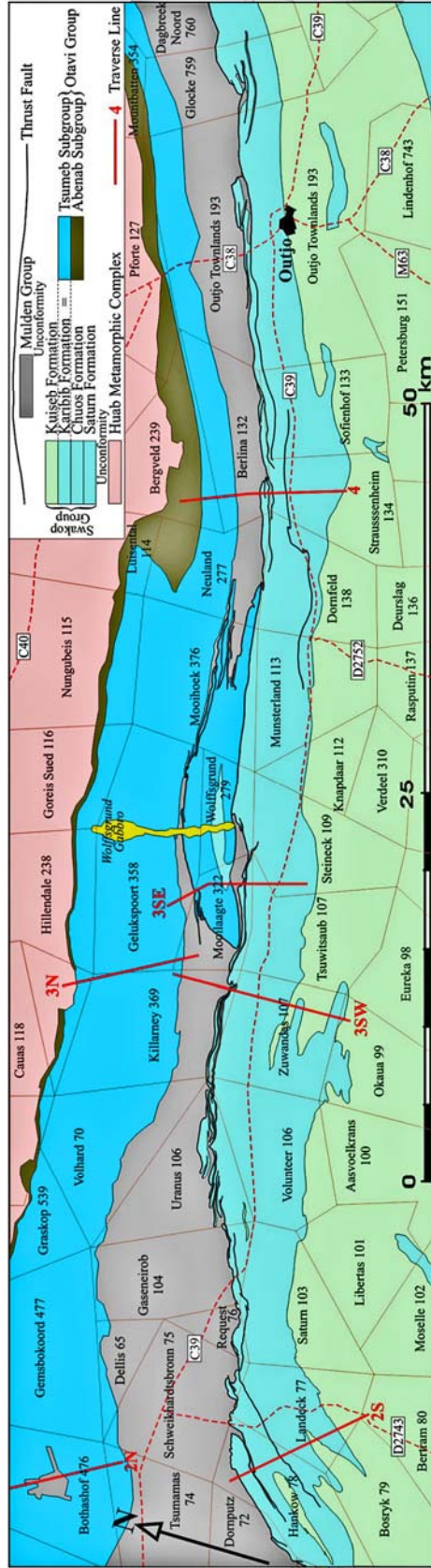
Figure 1. Simplified map of the geology east of Outjo (superficial cover omitted) showing the stepped D2 thrust front of the Khorixas-Gaseneirob Thrust along which the lower and middle Swakop Group (Saturn to Karibib formations) has been thrust onto Mulden Group phyllites. A nappe of deep-water Otavi Group carbonate rocks with an overlying nappe of Swakop Group rocks was also thrust onto the Mulden phyllites during the same D2 event. The locations of Traverses 2-4 are shown. Based on mapping by Clifford (2008) and the compilation by Schreiber (2004).

40

Definitions and Methods

In the descriptions that follow, a **grainstone** is a carbonate sandstone or siltstone (i.e. all carbonate grains) which can be limestone or dolomite; a **ribbonite** is a carbonate grainstone deposited below wavy base but having a thin, wavy, flaser-like bedding that can have internal, cross-bed-like laminations; a **rhythmite** is a stack of laminated or thicker, identical looking grainstone beds, generally graded and turbiditic in nature, that accumulated on the continental rise. Rhythmites can consist of limestone alone, dolomite alone, silici-clastics alone or combinations of these. Thickness of rhythmite layers can vary from a few millimetres to one metre.

All dip readings listed are followed by the reading of dip direction; readings are magnetic and uncorrected to true north, e.g. 45/160, dip 45°, dip direction 160°. These notes will hopefully encourage remapping of the sedimentology and structure of the Damaran rocks in Figure 1 in order to provide a better understanding of depositional conditions and post-Mulden structural evolution.

General Summary of Geology, Stratigraphy, Sedimentary Structures and Structure

Stratigraphy

Otavi Group rocks build the Fransfontein Ridge east of the farm Bothashof 476. The Abenab Subgroup at the base is thin. Not all formations are present. The Tsumeb Subgroup forms the main unit with a thickness of 7 km. The Ghaub Formation at the base is only locally preserved as is the tan-coloured Keilberg Member dolostone, its cap carbonate that forms the basal unit of the overlying Maieberg Formation limestones. The thickest unit by far is the Elandshoek Formation which followed by the Hüttenberg Formation at the top of the succession.

The Swakop Group occurs south of the Khorixas-Gaseneirob Thrust. It consists of the Saturn Formation at the base followed by the Chuos Formation with a prominent iron formation layer in the upper half. Thin equivalents of the Okonguarri and Ghaub Formations may be present at the top of the sequence assigned to the Chuos Formation by Clifford (2008). Limestones, dolomites and thin interbedded schists of the overlying Karibib Formation are followed by the thick schistose metagreywacke succession of the Kuiseb Formation. Post-Kuiseb Mulden Group phyllites fill the valley and plains between the Fransfontein Ridge and the Swakop Group rocks as well as some karst structures in the Elandshoek Formation. Red, Kalahari-age sandstones containing solution-collapse carbonate fragments fill a few small dolines in the Fransfontein Ridge.

Sedimentary Structures

Between the Summas Mountains and Outjo, sedimentary structures are poorly preserved in the pre-Chuos Saturn Formation (Basal Swakop Group) mainly as a result of the intense D2 deformation. The Chuos Formation is generally poorly exposed and is extensively covered by calcrete. However, mass-flow carbonate and sandstone layers, the former with stromatolitic reef debris in places and the latter with transported silicified oolites, do form better outcrops than the interbedded diamictites and schist layers. Mass flows, some with fibrous isopachous cement surrounding carbonate clasts, and rhythmite in the Tsumeb Subgroup of the Fransfontein Ridge suggest deposition on the continental slope as it deepened southwards. The coeval Karibib Formation, deposited south of the northern boundary fault of the Northern

Zone rift in still deeper water starts with 2 m of tan dolostone of the Keilberg Member, the cap carbonate to the Ghaub Formation diamictite. Above that are two carbonate facies of the Karibib Formation separated south of the roof thrust of the Khorixas-Gaseneirob Thrust duplex thrust complex by a schist horizon. The lower carbonate facies is intensely foliated but Clifford (2008) records local mass-flow layers (his intraformational breccias) and some graded bedding. The upper carbonate facies contains numerous mass-flow layers with grey limestone and pale brown dolomite clasts in a limestone or pale brown dolomite grainstone matrix. The limestone clasts are often highly flattened where bedding and the s2 foliation are parallel. The dolomite clasts do not deform as easily. Additionally, some mass-flow layers contain clasts of silicified oolites. The mass-flow layer at the top of the Hüttenberg Formation in the Fransfontein Ridge and that at the top of the Karibib Formation appear to be one and the same layer, both having the largest, least deformed clast suite which includes fragments of silicified oolite layers.

Structure

Fransfontein Ridge: No clear evidence of pre-Mulden D1 deformation was found but post-Mulden D2 deformation was intense, particularly south of the Khorixas-Gaseneirob Thrust front. The southward dip of the Fransfontein Ridge is variably steep to moderate with minor open folds with E-W axes and local, small-scale north-recumbent folds in the Hüttenberg Formation. Bedding-parallel shear zones, interpreted as thrusts, occur locally at or near the base and top of the Otavi Group succession in the Fransfontein Ridge. Traverses 2N and 3N encountered flattened stromatolite columns the orientation of which point to a northward transport direction of the thrust. Down-dip orientation of the axes of minor folds in or close to shear zones suggest small-scale sheath folding in the same northward transport direction. These indicators suggested transport in the direction between 340° and 360° (magnetic).

Swakop Group: D2 N-S compression folded the Swakop Group succession into upright to steeply north-vergent isoclinal folds which have a NE-SW orientation just NE of the Summas Mountains but gradually swing around to an ENE orientation towards the east. This change in orientation is believed to be controlled by the orientation of the huge, buttress-like scarp of northern boundary fault of the Northern Zone rift which had a throw of almost 7 km on it during eruption of the late- Nosib Naauwpoort volcanics just to the southwest (Miller, 2008). This fault was the boundary between the Otavi Group succession and a much thicker Swakop Group to the south. It was against this buttress that the Swakop Groups rocks were initially compressed and then thrust up and over it as a thrust duplex complex onto the Mulden phyllites along the Khorixas-Gaseneirob Thrust. The fault is now deeply buried beneath the Swakop Group rocks and may not be too far south of the thrust front. The axial planar s2 foliation is intense in the limbs of folds but is less strongly developed in fold closures. Clifford (2008) recognised some north-directed thrusts and younger strike-slip faults. Rather than being a single thrust, the Khorixas-Gaseneirob Thrust is a complex of thrusts that successively overstep each other from west to east (Fig. 1). Most of the thrusts are vertical or dip steeply to the south. On the farm Neuland 277 and east thereof, Clifford (2008) mapped a zone of what he called "rib rock" (Fig. 4.7) at the thrust front with some parallel stringers extending into the Karibib Formation carbonates just behind the front. This so-called "rib rock" consists of long, parallel, rib-like cleavage mullions of chert in the thrust-front carbonates. Each thrust forming the thrust front is a massive sheath fold in which the cleavage mullions have been rotated into parallelism with the

transport direction of the thrust (transport direction 320° magnetic). Stretching lineations in the Karibib carbonates close to the thrust further west point to a 330° (magnetic) transport direction (Traverse 3SE).

D2 also thrust a nappe consisting of the Chuos Formation and intensely foliated Karibib dolomite (the Wolffsgrund Nappe) onto a less deformed nappe of deep-water Tsumeb Subgroup rocks consisting of the Maieberg, Elandshoek and Hüttenberg Formations (the Mooilaagte Nappe). This stack of two nappes was then thrust onto the Mulden phyllites ahead of the Khorixas-Gaseneirob Thrust. A similar nappe system may be present further east on the farms Nettleton 355, Neins West 178, Sitrusdal 723 and Neins 179, and possibly still further east under calcrete on Valhal 331.

Traverse 1: Huab Metamorphic Complex, Kuiseb Formation; farms Kaoko Kroon 487, Inhoek 482

Summary of the Geology

The traverse is located on the southern edge of the Welwitschia Inlier southwest of Khorixas and extends from the Khorixas-Gaseneirob Thrust southwards through the Kuiseb Formation (Fig. 1.1). Mapping of the area was carried out by Frets (1969).

Stratigraphy

Only the gneisses of the Huab Metamorphic Complex and schists and minor quartzites of the Kuiseb Formation occur along the traverse

Sedimentology of the Kuiseb Formation

Graded metagreywacke turbidites form the bulk of the Kuiseb Formation. Most of the interbedded quartzites were deposited during small-scale regression and transgression cycles.

Structure

The gneisses of the Huab Metamorphic Complex are intensely sheared as a result of overthrusting of the Kuiseb Formation along the Khorixas-Gaseneirob Thrust. The gneiss is highly brecciated for about 100 m north of the thrust. The main thrust is vertical or dips steeply southwards, strike 110°.

F1 structures in the Kuiseb Formation are not obvious (known from the wider regional context to have been open and orientated E-W (Miller, 1980)) but the Kuiseb schists have a subtle bedding-parallel s1 foliation dated at ~590 Ma (Lehmann *et al.*, 2015). Regional tight to isoclinal F2 folds with a well-developed, axial planar s2 foliation follow the curvilinear trend of the contact with the Welwitschia Inlier. The s2 mineral fabric is coarsest close to the thrust where bedding has been totally disrupted. The intensity of s2 is variable further south but is generally most intense where bedding and cleavage are parallel. D2 ductility contrast between the quartzites and the enclosing schist is apparent such that the schist can be intensely foliated and the quartzite layers totally disrupted suggesting thrusting in the schist succession. Autobrecciation of the schist or transposition of thin quartzite layers into relatively isolated fold mullions or even into totally isolated lumps of quartzite has taken

43

place. Numerous small-scale drag folds in the quartzites have resulted in thickness of individual layers varying considerably. F2 folds are overturned towards the NE with the axial planar s2 foliation dipping mainly between 55° and 65° to the SW. D3 produced a gentle buckling along a NE-trending axis and a spaced s3 fracture cleavage. Along the traverse, the main trend of bedding and foliation was WNW with fold structures defined by the main quartzite layers.

Figure 1.1. Google image of the region covered by Traverse 1, mainly farms Kaoko Kroon 486 and Inhoek 482. Localities numbered. The line of the schematic section of Figure 1.6 is shown in red.

Huab Metamorphic Complex

44

Locality 1 (UTM 33k0488714, 77483227), Farm Kaoko Kroon 487: The Khorixas-Gaseneirob Thrust. The gneisses against the thrust are intensely sheared, foliated and finely comminuted but with small drawn-out pods in which the originally gneissic texture and mineralogy is still recognisable. There are a few thin (10 cm thick) lenses of yellow or brown carbonate in the shear zone. The gneiss is highly brecciated for about 100 m north of the thrust but also contains thin (5-30 cm thick) phyllitic shear zones subparallel to the main thrust plane. The main thrust is vertical or dips steeply south, strike 110°.

Kuiseb Formation

Locality 2 (UTM 33k0489686, 77485742), Farm Inhoek 482: Intensely foliated chlorite-muscovite Kuiseb schist, dip of foliation 75/200 (Fig. 1.2). Bedding in the single s0/s2 fabric is indicated by rare, short lenses of sheared out white quartzite up to 1 cm thick. There are also laminae up to 1 mm thick of brown carbonate parallel to the foliation as well as rare foliation-parallel quartz veins up to 1 cm wide. Local quartz veins up to 1 m wide are parallel to and cross cut the foliation. The locally developed fracture cleavage (s3), dip 85/345, has a red, ferruginous staining which is not present on the s2 cleavage.

Figure 1.2. Intensely foliated Kuiseb schist with an s3 fracture cleavage associated with gentle buckling of the s0/s2 foliation. Farm Inhoek 482.

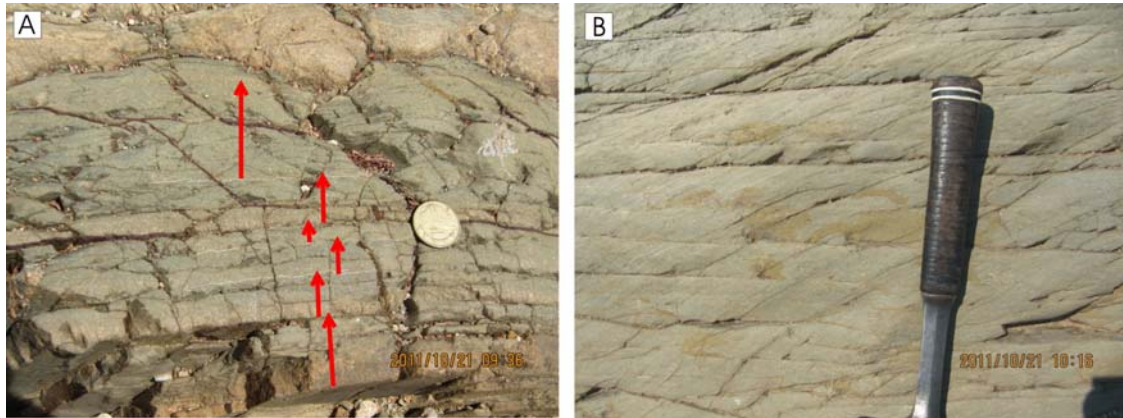Locality 3 (UTM 33k0489731, 7744899) (Fig. 1.3): Graded beds in Kuiseb schist.

Figure 1.3. Turbidite layers in the Kuiseb schist: **(A)** Turbidite couplets: thin light brown quartzite base, up to 7 cm thick with grey fine-grained tops between 1 cm and several cm thick, each layer marked with a red arrow; coin diameter 22 mm; **(B)** Subtly graded beds; beds 0.5-5 cm thick; bedding perpendicular to hammer handle. Farm Inhoek 482.

Locality 5 (UTM 33k0489312, 7744574) (Figs. 1.4, 1.5): Ridge of light brown quartzite. The main quartzite layer is 3 m thick, dip 48/208. Above and below the main layer are several thinner layers of quartzite interbedded with the schist. Most of these thinner layers have many very thin quartzite layers immediately above and below them (Figs. 1.4A, B). The packages of very thin quartzite layers with a single thicker layer (4-12 cm thick) in the middle probably represent small-scale regression and transgression cycles. Several such cycles occur above and below the main, ridge-forming quartzite layer. Some thin quartzite layers were totally disrupted during deformation and consist only of pebble-like pieces of quartzite floating in tectonic mélange of schist fragments (Fig. 1.5) in which the s2 foliation is well developed. The intensity of s2 varies across the outcrop. The B2 lineation plunges 38/268. s3 is also well developed at this locality as are disharmonic minor folds of the quartzites; fold axes plunges 43/305.
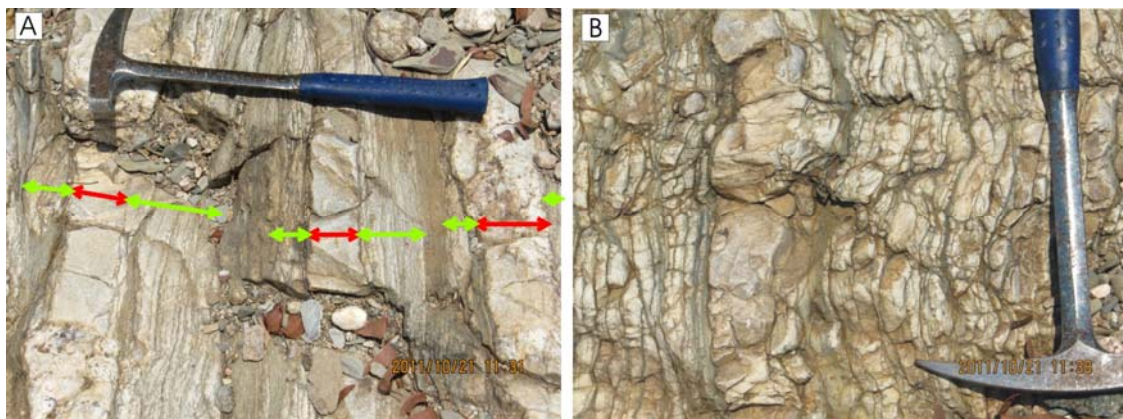
Figure 1.4. (A) Single thin layers of quartzite (red arrows) sandwiched between packages of very thin layers of quartzite (green arrows) suggesting cycles of regression and transgression; **(B)** Close-up view of a cyclical quartzite package as shown in 'A'. Farm Inhoek 482.

Figure 1.5. Intense dismemberment of quartzite layer during D2 deformation such that the quartzite layer is represented only by pebble-like blobs of quartzite floating in a tectonic schist mélange. Farm Inhoek 482.

Locality 6 (UTM 33k0489568, 7740179): Thick ridge-forming quartzite layer. Complex minor folds and ductility contrasts between the quartzite and the enclosing schist have caused the thickness of this quartzite layer to vary between 0 m and 10 m with an average of about 5 m. Parts of the quartzite are gritty but no grading was observed. There are a few thin quartz veins in the quartzite.
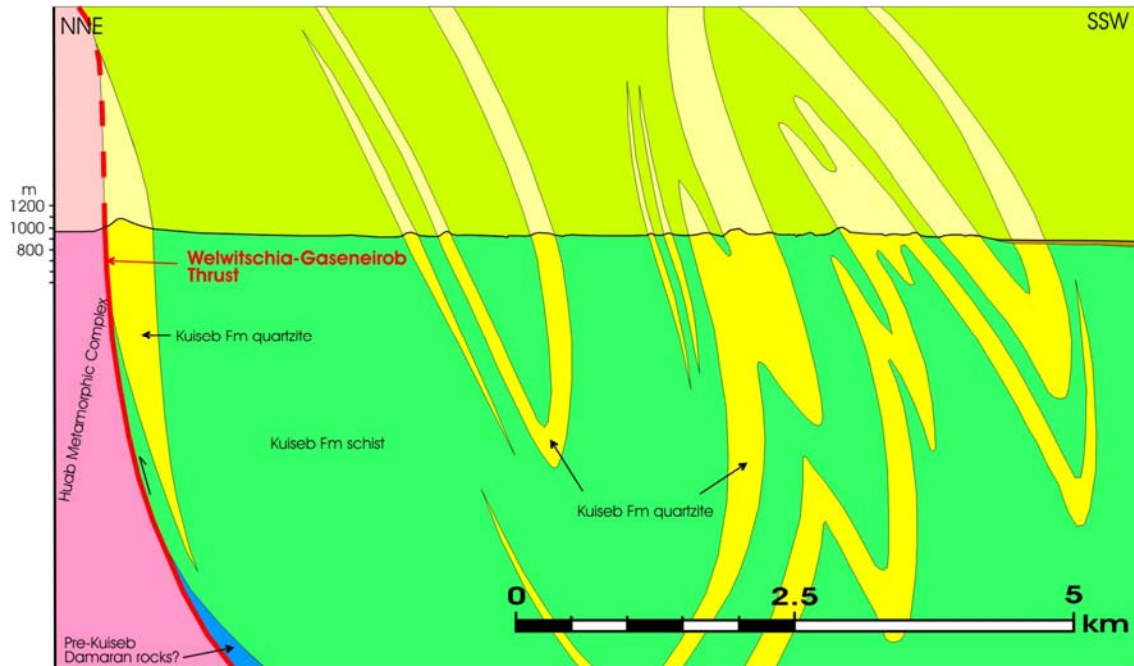
Figure 1.6. Schematic section along Traverse 1 incorporating structural data from Frets (1969).

Traverse 2N, Otavi Group; farms Danube 59, Bothashof 476

Stratigraphy

The traverse starts near the southern border of the farm Danube 59 at the base of the Otavi Group of the Fransfontein Ridge in a thin section of the Gruis and Ombaatjie Formations of the Abenab Subgroup. It continues through Tsumeb Subgroup rocks on Bothashof 476 and ends in calcrete-covered Mulden rocks. Although most recent publications refer to the carbonate succession above the Abenab Subgroup on the southern flank of the Fransfontein Ridge as the Karibib Formation, the lithology is similar to that of the Tsumeb Subgroup and the formation names from this subgroup are used for this section. For detail of the Abenab Subgroup at this locality, the reader is referred to Hoffman (2010).

Sedimentology

The Abenab Subgroup contains photic zone stromatolite layers as well as deeper water slope deposits of alternating phyllites and graded carbonate grainstone rhythmites.

A thin, tan dolostone of the Keilberg Member, the cap to the Ghaub Formation, forms the base of the Maieberg Formation of the Tsumeb Subgroup. The Maieberg Formation passes upwards from massive grey limestone with white jaspilite (coarse-grained chert) veins and lumps into slope deposits of laminated, turbiditic grey limestone rhythmite with cappings of pale grey, very fine-grained, pelagic dolomite. One mass-flow layer containing only Maieberg fragments occurs near the top of the Maieberg Formation. The overlying Elandshoek Formation consists largely of whitish to very pale grey, massive to thickly bedded dolomite with a few thin zones of thin to laminated bedding. There are patches of intense white jaspilite veining which is typical of the Elandshoek Formation.

48

Thinner bedding generally prevails in the upper 1/3rd of the Elandshoek Formation but zones of massive dolomite, deep-water laminated rhythmites and mass-flow breccias alternate. Fragments in the mass-flow breccias are usually enclosed in a veneer of white chert outboard of which is a 4-7 mm thick rim of white, fibrous isopachous cement (Fig. 2.8). This texture is typical of the Gauss Formation in the Otavi Mountainland. The Hüttenberg Formation consists of grey thin- to medium-bedded limestone with thin bedding-parallel layers of brown-weathering chert in the lower part and laminated grey grainstone rhythmites with some very thin, pale grey pelagic dolomite cappings in the upper part.

The Mulden Group cuts unconformably into the top of the Hüttenberg Formation and fills a large post-D1 karst cavity in the Elandshoek Formation. The Mulden is post D1 and pre D2. The basal conglomerate of the karst fill is overlain by layers of grey, foliated phyllite and brown siltstone.

A few younger dolines are filled with structureless, brown to reddish, fragment-filled sandstone of Kalahari age.

Structure

The whole Otavi Group succession on the Fransfontein Ridge was thrust northwards on two thrusts during regional D2. Adjacent to that at the base of the succession, stromatolites have been deformed into bedding-parallel lozenges (Fig. 2.2). Axes of minor folds associated with the other near the base of the Elandshoek Formation have been rotated by the thrusting and plunge down the SSE dip direction of nearby bedding. These suggest the transport direction of the thrust was 340° (magnetic). Minor folds near the top of the Hüttenberg Formation have been overturned to the north. The foliation in the Mulden phyllite is D2 in age.
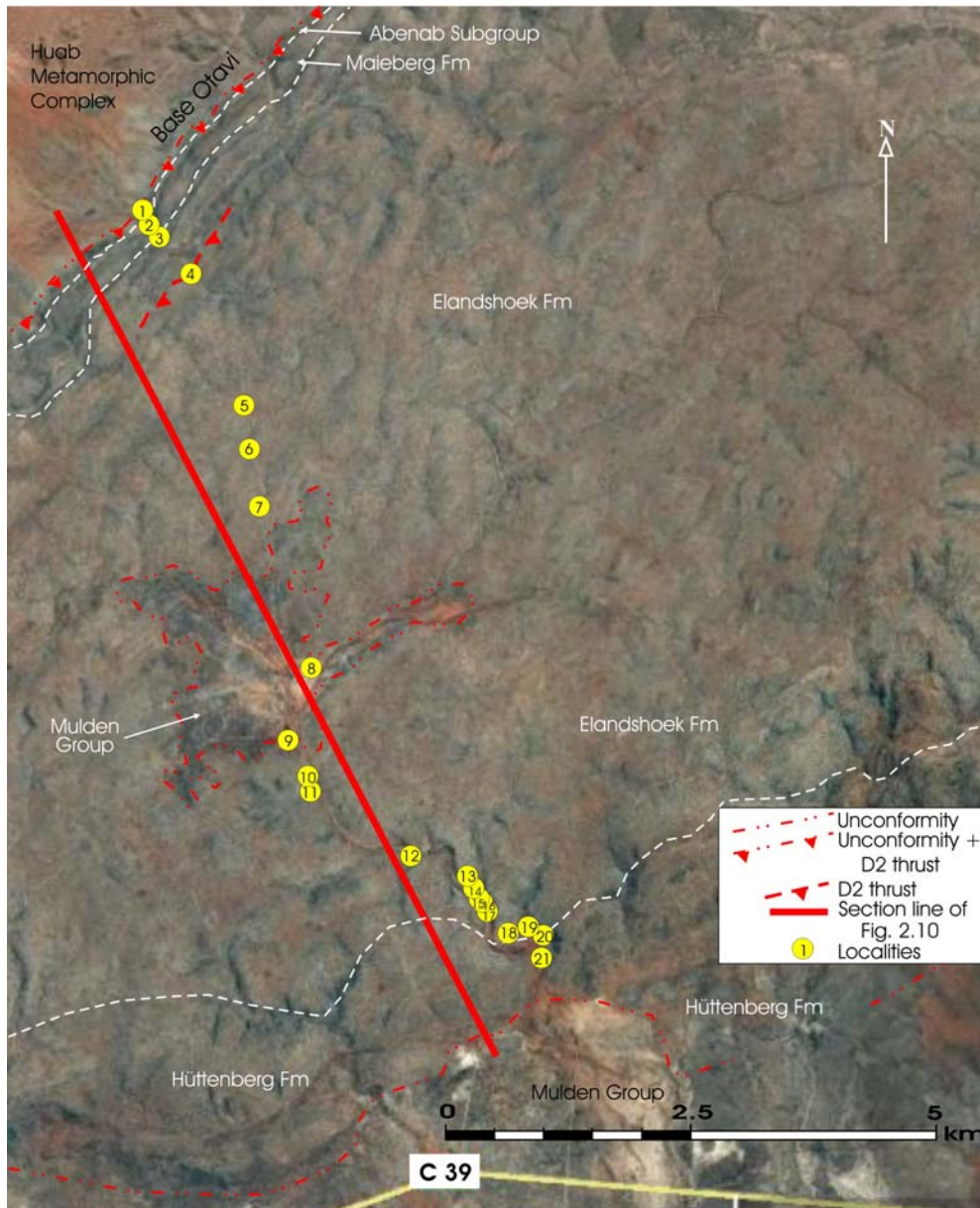
Figure 2.1. Google image of the region covered by the Traverse 2N, mainly farm Bothashof 476. The line of the section in Figure 2.10 is also shown (red line).

Abenab Subgroup, Gruis Formation, *5 m thick*

Locality 1 (UTM 33k0536323, 7772659), Fig. 2.1: Base of the Otavi Group on farm Danube 59. Basal brown-weathering dolomite with numerous very thin stringers of muscovite-chlorite phyllite.

Thrusting has strongly deformed the columnar stromatolites adjacent to phyllite layers into elongate lozenges ± 10 cm thick (Fig. 2.2). Bedding dip 50/150.

50

Figure 2.2. Stromatolites intensely transposed and deformed into bedding-parallel lozenges. Thin jaspilite veins (coarser grained than chert but finer grained than vein quartz - TCL terminology) in the stromatolites.

Ombaatjie Formation, *true thickness 130 m*

This consists of alternating layers of variable thickness of intensely foliated phyllite, foliation 72/130 with foliation steeper than bedding, and grey dolomite ribbonite (grainstone with flaser-like bedding, deposited below wave base - Fig. 2.3) with local stromatolites and thin, laminated, brown-weathering, calcareous sandstone layers. Detail of this section is given by Hoffman (2010).
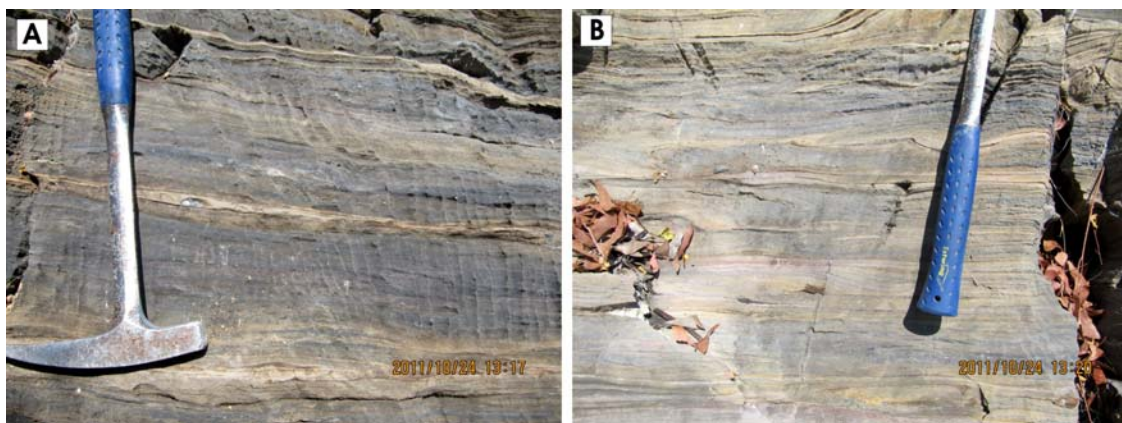
Figure 2.3. Dolomite ribbonite grainstones of cycle b7 (?) of the Ombaatjie Formation near the boundary between the farms Danube 59 and Bothashof 476. Some of the units in **(A)** are slightly argillaceous.

Tsumeb Subgroup, Maieberg Formation

Locality 2 (UTM 33k0536434, 7772561): Layer of tan dolostone about 0.5 m thick (Fig. 2.4) at the base of the Maieberg Formation, which is the cap dolostone to the Ghaub Formation (Keilberg Member - nowhere near as thick as shown by Hoffman, 2010). No Ghaub Formation is present on this farm but it is present further

51

east on Bergveld 239. The tan dolostone is overlain by about 27 m of grey, massive Maieberg limestone, which is cut by numerous white jaspilite veins and contains irregular lumps of massive white jaspilite up to 2 m across. Above this is typical grey, laminated, deep-water Maieberg rhythmite (laminae of grey limestone turbidite alternating with thinner, light grey laminae of very fine-grained pelagic dolomite). This contains much fewer white jaspilite veins. Bedding dip 74/140. One 50 cm-thick mass flow unit, containing only Maieberg fragments, occurs near the top of the Maieberg. Bedding dip at top of Maieberg 52/130.

Figure 2.4. 0.5 m-thick tan dolostone of the Keilberg Member at the base of the Maieberg Formation.

Elandshoek Formation

Locality 3 (UTM 33k0536458, 7772445): Contact between grey laminated Maieberg Formation and typical whitish massive to thickly bedded Elandshoek Formation. Bedding dip near base, 35/135, i.e. bedding becoming less steep. A few zones with very thin bedding. Irregular pods of massive white jaspilite and zones with intense veining by white jaspilite - a typical feature of the Elandshoek Fm.

Locality 4 (UTM 33k0536787, 7772009): A 12 m thick (true thickness) shear zone in the Elandshoek Fm, dip of shear zone foliation 48/136, probable thrust. Bedding just below the shear zone 42/160 but undulating, axes of minor folds within the shear zone plunge down the bedding, plunge direction 160°.

Locality 5 (UTM 33k0537338, 7770735): Elandshoek Fm. Massive but some zones 2 m thick with thin bedding, bedding dip 63/165 but undulating southerly.

Locality 6 (UTM 33k0537407, 7770180): Elandshoek Fm. Broad open synclinal axis, bedding dip 34/260.

Locality 7 (UTM 33k0537472, 7769613) (Fig. 2.5): Elandshoek Fm. Typical thick to massive bedding of the whitish upper Elandshoek Fm with faint, discontinuous, internal bedding laminae in places, some silicified. Some thin beds totally silicified.

Figure 2.5. Typical thick to massive bedding of the whitish upper Elandshoek Formation. Dark layers are thin silicified beds. Farm Bothashof 476.

Locality 8 (UTM 33k0538026, 7767981): Basal conglomerate of the Mulden Group filling post-D1 - pre-D2 karst cavity in Elandshoek Fm; Bothashof house located within this inlier.

Locality 9 (UTM 33k0537817, 7767345): Basal conglomerate of the Mulden Group karst fill just south of Bothashof house (Fig. 2.6). The basal conglomerate is overlain by cleaved Mulden phyllite. Within the karst, the basal part of the conglomerate contains numerous angular to subrounded blocks of Elandshoek dolomite (Fig. 2.7A) but the clasts in the top of the conglomerate are mainly quartz with very few of dolomite; brown to reddish sandy to silty matrix to the conglomerate. Parts of the conglomerate look like a solution-collapse breccia. The uppermost part of the karst fill consists of brown, very thinly bedded to laminated siltstone with some small dolomite and quartz fragments (Fig. 2.7B).

Figure 2.6. South side of the Mulden-filled depression surrounding the farm house on Bothashof 476. Brown areas in the lower slopes are comprised of the Mulden basal conglomerate, whitish Elandshoek dolomite higher up hill.
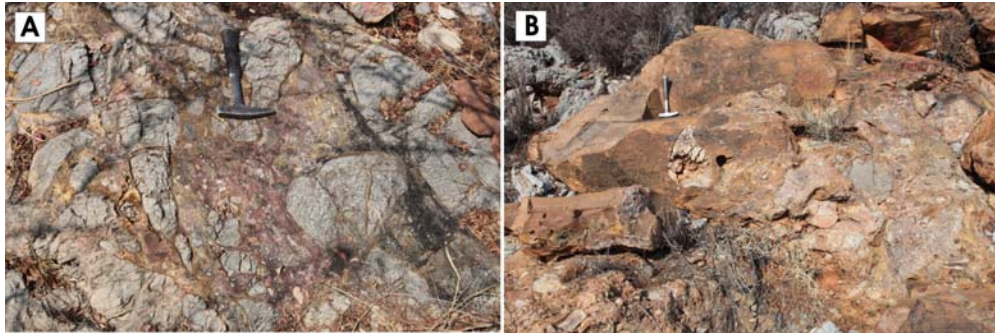
53

Figure 2.7. Close up views of the basal Mulden lithology filling the large karst structure shown on Fig. 2.1. **(A)** Basal conglomerate: clasts of Elandshoek dolomite in a brown sandy to silty matrix; **(B)** Brown, thinly bedded to laminated siltstone at the top of the Mulden karst fill.

Locality 10 (UTM 33k0537998, 7766781): Elandshoek Fm with thin brown layers of silicified oolites or grainstone; bedding dip 36/195. Plunge of minor fold axes 14/278.

Locality 11 (UTM 33k0538014, 7766718): Elandshoek Fm; bedding dip same as previous locality. Elongate karst filling about 10 m wide of highly silicified red-brown siltstone with a few siltstone and quartz clasts in the centre and dolomite clasts along the margin. Elongate in direction 260°. Possibly of Kalahari age.

Locality 12 (UTM 33k0539064, 7766028): Elandshoek Fm; bedding dip 24/300. Bedding dips mainly gently south but undulates about the horizontal with some gentle northerly dips.

Locality 13 (UTM 33k0539726, 7765682): Towards the top of the Elandshoek Fm; medium grey weathered surface but very light grey fresh surface. Extensive area of small-fragment slump breccia with platy Elandshoek fragments. Fragments have a very thin silica (jasperoid?) coating enclosed in an outer coating of a fibrous isopachous cement 4-7 mm thick (Fig. 2.8A). In places, the platy fragments were deposited subparallel to bedding so that the layers of fibrous isopachous cement are roughly parallel to bedding in adjoining undeformed layers (Fig. 2.8B). These slump breccias occur between layers of typical massive, unbrecciated Elandshoek dolomite. This texture is very similar to that described for the Gauss Formation in the Otavi Mountainland.

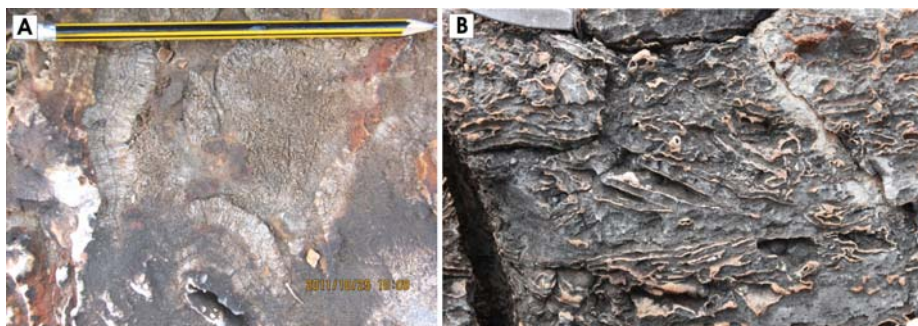**Figure 2.8.** Small-fragment slump breccia with Elandshoek fragments enclosed in thin veneers of silica and an outer rim of fibrous isopachous cement. **(A)** Close up view showing the radiating fibers of the outer rim; **(B)** Platy fragments of Elandshoek dolomite lying subparallel to bedding. Fragments are enclosed in weather-resistant rims of isopachous cement. Towards the top of the Elandshoek Formation on Bothashof 476.

Locality 14 (UTM 33k0539664, 7765771): Elandshoek Fm; Laminated, very light grey Elandshoek rhythmites, i.e. deep water. Many small-scale, tight chaotic folds which may be due to slumping.

Locality 15 (UTM 33k0539706, 7765733): Elandshoek Fm; Base of a zone of medium to dark grey weathering Elandshoek dolomite breccia with abundant fibrous isopachous cement.

Locality 16 (UTM 33k0539706, 7765733): Elandshoek Fm; Same grey-weathering Elandshoek dolomite but thickly bedded to massive, overlies the main breccia zones with fibrous isopachous cement. Still some small patches of fibrous isopachous cement. Bedding dip 10/250.

Locality 17 (UTM 33k0539852, 7765453): Elandshoek Fm; Top of grey-weathering Elandshoek dolomite. Consists entirely of rhythmite with some minor mass flow layers. Overlain by rhythmite that weathers to a very light grey colour. Deep-water deposit on continental rise.

Locality 18 (UTM 33k0540070, 7765215): Elandshoek Fm; rhythmite, bedding dip 17/150. 20 cm-wide fault filled with abundant white calcite, fault dip 77/210.

Locality 19 (UTM 33k0540262, 7765286): Elongate Kalahari-filled doline in very light grey to whitish weathering Elandshoek Fm; fill is red-brown, highly silicified Kalahari siltstone with some quartz grit and small fragments of Elandshoek dolomite and chert, fragments most abundant along edges of doline.

Locality 20 (UTM 33k0540419, 7765211): Hüttenberg Fm limestone; northern part of Farm Tsumamas 74. Thin- to medium-bedded Hüttenberg Fm (Fig. 2.9) weathers medium grey, slightly lighter grey on fresh surface. Base of Hüttenberg Fm about 40 m below this locality.

Locality 21 (UTM 33k0540410, 7764945): Hüttenberg Fm limestone; rhythmites with laminae of limestone turbidite and a few very thin light grey pelagic dolomite laminae, bedding dip 28/128; tight minor folds overturned to the north, fold axial plane dip 47/140, strike of fold hinges 54° - 43°, i.e. south to north compression and overturning. Zones of silicified laminae, some bands of light to dark grey, brown-weathering chert (latter typical for Hüttenberg) parallel to bedding.

Figure 2.9. Typical thin to medium bedding of grey Hüttenberg Formation limestone, often with internal rhythmite laminations. Brown silicified beds. Farm Tsumamas 74.
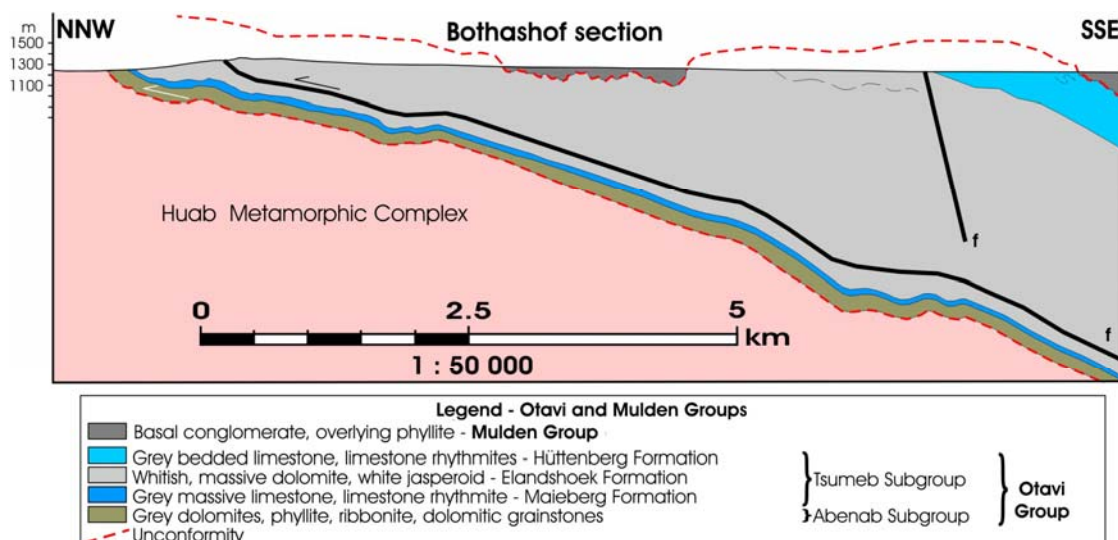
Figure 2.10. Section along the northern part of Traverse 2N.

Traverse 2S; Swakop Group; farm Landeck 77

Stratigraphy

This traverse is a continuation of Traverse 2N. It starts in the poorly exposed Mulden Group and continues in the Swakop Group rocks on Hankow 78 and Landeck 77 and thence to the poorly exposed Kuiseb schists towards the southern border of Landeck 77 (Fig. 2.11). For the Swakop Group rocks, reference is made to Clifford (2008). Clifford's Saturn Formation corresponds to Miller's (2008) Ugab Subgroup, his Landeck Formation corresponds to the combined Chuos, Okonguarri and Ghaub Formations (the latter two were unknown at the time he was mapping in the 1960s and are not mapped out separately), Clifford's Bergfriede

Formation corresponds to the Karibib Formation and his Okaua Formation corresponds to the Kuiseb Formation. Clifford considered the Okaua Formation in the south and the Mulden Group north of the Khorixas-Gaseneirob Thrust to be one and the same unit. Localities recorded for Traverse 2S and the section line for Figure 2.28 are shown in Figure 2.11. The detailed map of Clifford (2008) has been used as a lithological guide but the sedimentology, the Chuos, Okonguarri and Ghaub Formations and internal structure of layers need remapping throughout the area that he mapped.

Sedimentology

The entire Swakop Group succession was deposited in deep water south of the huge fault scarp that formed the northern boundary of the deep Nosib-age rift which encompassed the Northern Zone and the northern Central Zone.

Bedding and sedimentary structures are generally poorly developed in the Saturn

Formation although Clifford (2008) does record the presence of algal structures.

Carbonate layers and some siliciclastic layers in the Chuos Formation are mass flows or thinly bedded turbiditic grainstone rhythmites. Some contain abundant stromatolite fragments and others transported silicified oolites. Although

56

locally well-exposed, the formation is poorly exposed for the most part. The presence of the iron formation, again poorly exposed, is indicated by float.

Three facies of the Karibib Formation are present. One occurs between the roof and sole thrusts shown in Figures 2.11 and 2.28 and contains some mass flows and graded beds (Clifford, 2008). The other two, apparently more distal than the first, consist of a lower and upper facies separated from each other by a phyllitic schist marker and located south of the roof thrust (Figs. 2.11, 2.28). The lower facies starts with 2 m of tan dolostone of the Keilberg Member, the cap carbonate to the glaciogenic Ghaub Formation, followed by grey limestone. Bedding and some graded bedding (Fig. 2.19) can be distinguished in places but generally an intense bedding-parallel foliation obscures much of the original sedimentary detail. The third facies, the upper Karibib Formation, is comprised of numerous, readily distinguishable mass-flow layers of varying thickness and with varying clast sizes. Many of these have a strong

bedding-parallel foliation and intensely flattened limestone clasts. Dolomite clasts do not deform as readily. Thin interbeds of thinly bedded turbiditic grainstone rhythmites are common (Figs. 2.20 - 2.23). It should be possible to follow out individual mass-flow layers laterally until they pinch out. Several beds of grey limestone nodules set in a pale grey dolomite grainstone matrix occur near the top of the formation. The uppermost mass-flow layer contains the largest and least deformed clasts, some highly oolitic. This layer is considered to be the same layer that occurs at the top of the Hüttenberg Formation in Traverse 2N.

On this traverse, the Kuiseb Formation is not exposed but near the Summas Mountains to the SW it consists of turbiditic greywackes.

The Mulden Group is a syn- to post-D1, intramontane deposit consisting predominantly of grey chlorite-muscovite phyllites with a strong, steep to vertical, ENE-WSW foliation that formed during regional D2 compression.

Structure

Clifford (2008) recognised a late-sedimentary - pre-tectonic slump, the Saturn Slide, of Ugab, Chuos and Karibib stratigraphy onto the same stratigraphic units further down slope.

Clifford (2008) recognised a D1 phase of thrusting (Figs. 2.11, 2.28) but an s1 axial planar foliation, which would be best displayed in D2 fold closures, was not discernable. Further to the west, Miller (1980) recognised large, open E-W folds but s1 is a bedding-parallel micaceous fabric in the Kuiseb schists (Lehmann et al., 2015). Clifford (2008) recognised D2 thrusts east of Traverse 2S but most of his large faults along this traverse are reinterpreted here as thrusts. D2 deformation took place during

intense D2 N-S to NW-SE compression and folding. The succession was tightly compressed against and then over the massive buttress of the fault scarp that formed the northern boundary of the Northern Zone rift (Fig. 2.28). The Khorixas-Gaseneirob Thrust is the floor thrust to the stacked succession of duplex-like thrusts of which there may be more than indicated, particularly along contacts between rocks of contrasting ductility. Much of the bedding is vertical or near vertical with an intense s2, bedding-parallel foliation. The orientation of the fault scarp probably controlled the orientation of the D2 structures. The intense compression steepened up structures during and after D2 thrusting.
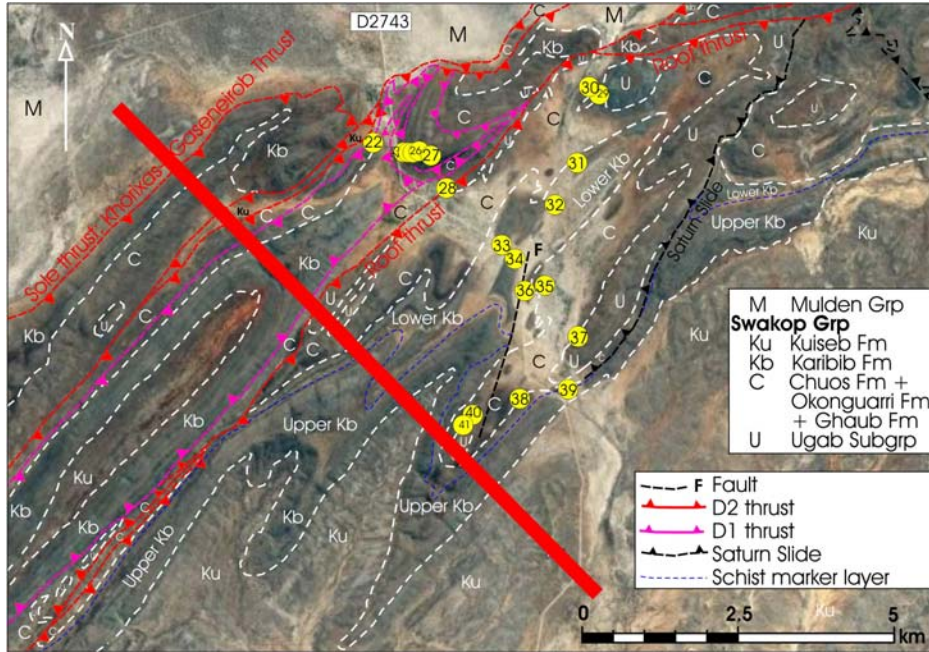
Figure 2.11. Google image of the region covered by Traverse 2S, mainly farm Landeck 77. The red line is the section line in Figure 2.28. Stratigraphy and structure are modified from Clifford (2008).

Locality 2.22 (UTM 33k0544006, 7756727): Karibib Formation; farm Hankow 78. Highly complex structure in this area immediately adjacent to the Khorixas-Gaseneirob Thrust. There are more thrust dislocations than shown, particularly along schist layers. Bedding vertical to N-vergent; N-vergent isoclinal folds, axial plane dip 66/225, plunge of axis 34° in direction 280° (Fig. 2.12). Siliceous iron formation float in areas of Chuos Fm outcrop and subcrop.

Figure 2.12. Steeply N-vergent isoclinal folds in Karibib Formation limestone adjacent to the Khorixas-Gaseneirob Thrust on farm Hankow 78.

Locality 2.23 (UTM 33k0544530, 7756473): Chuos Formation; farm Landeck 77. Hill with interbedded zones of dolomite, limestone and siliciclastic units. At this locality, thickly bedded, very dark grey dolomite, tight minor folds, two 20-30 cm

thick slump breccias made up of fragments of this same dolomite. May be near the stratigraphic top of the Chuos Fm.

Locality 2.24 (UTM 33k0544593, 7756465): Same hill, Chuos Formation, next carbonate layer stratigraphically lower down. The whole of this light grey unit is comprised of stacked, graded, turbiditic dolomite grainstones, individual layers between <1 cm and 12 cm thick (Fig. 2.13A). The lower part of unit consists mostly of slump folds (Fig. 2.13B) and slump breccias with clasts of light grey, thinly to very thinly bedded dolomite (Figs. 2.14A, B). Younger solution collapse breccias in this slump breccia cemented by white to black sparry calcite (Fig. 2.15). This dolomite is underlain by blue-grey limestone.
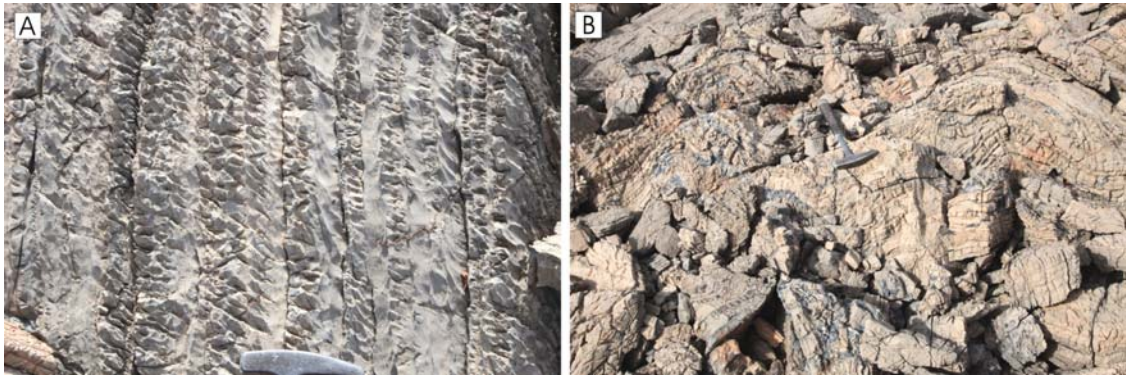
Figure 2.13. (A) Dolomite zone within the Chuos Formation made up entirely of stacked, graded dolomite turbidite layers between <1 cm and 12 cm thick. Top to right, fine-grained tops form the smoother layers; **(B)** Layer of small-scale slump folds in the dolomite grainstone turbidite sequence of 'A', cavity fillings of white sparry calcite. Farm Landeck 77.

Figure 2.14. (A) Mass flow or slump breccia layer of very thinly bedded light grey dolomite; **(B)** Mass-flow layer within the succession of thin, stacked, dolomite turbidite grainstones shown in Fig. 2.13A. Fragments are all derived from these thin turbidite layers.

Figure 2.15. Post-deformation solution collapse breccia in syn-sedimentary slump breccia, cement of white to black sparry calcite.

Locality 2.25 (UTM 33k0544712, 7756508): Same hill, Chuos Formation. Zone of highly foliated phyllite with thin siltstone beds. Clifford marks a D1, bedding-parallel thrust at this level that was folded by F2. Phyllite underlain by a dolomite layer which is a mass flow containing many small dolomite fragments and very finely laminated fragments of small stromatolites. The southern edge of this layer (i.e. top) is made up of small *in situ* stromatolites 5-10 cm in diameter and 20 cm in height all perpendicular to bedding.

Locality 2.26 (UTM 33k0544772, 7756560): Same hill, Chuos Formation. Next dolomite layer down in the stratigraphy – also a mass flow.

Locality 2.28 (UTM 33k0544920, 7756527): Same hill, Chuos Formation. Next dolomite layer down in the stratigraphy - also a mass flow. Platy dolomite fragments, some fragments of small stromatolites and many lumps of silicified material.

Locality 2.28 (UTM 33k0545191, 7756006): Saturn Fm, farm Landeck 77. Core of NE-trending anticline that is cut off

on its NW flank by the long NE-trending roof thrust shown on Fig. 2.28. The core of this structure is a brown-weathering dolomite that is very light grey when fresh. This is cut by numerous calcite and quartz-rich veins with rather abundant limonite dodecahedra after pyrite. The marginal layer is a breccia (mass flow?) with blocks of brown-weathering dolomite and limestone set in a sparse, sparry calcite cement.

Locality 2.29 (UTM 33k0547535, 7757541): Chuos Formation, farm Landeck 77, near NE corner. An anticline cored by massive, light coloured Saturn Fm dolomite. This locality is on the first carbonate layer within the basal siliciclastics of the overlying Chuos Fm. The carbonate layer is a mass flow composed almost entirely of small fragments up to 10 cm across of stromatolites (reef debris). There are also some scattered fragments of grey, fine-grained dolomite from 1 cm to 50 cm in size (Fig. 2.16). There is a siliceous Fe formation layer lower down in the Chuos (i.e. stratigraphically below this mass flow) but above the Saturn dolomite. Bedding vertical, strike NE.

Figure 2.16. Lowest carbonate layer in Chuos Formation at locality 2.29. This is a mass flow composed almost entirely of light grey stromatolitic reef debris and a few large angular fragments of grey dolomite, NE Landeck 77.

Locality 2.30 (UTM 33k0547472, 7757614): Chuos Formation, farm Landeck 77, near NE corner. Next carbonate layer up in the Chuos Fm. Also a mass flow. Immediately overlain by a brown, slightly feldspathic sandstone containing layers and scattered grit-size grains of white silicified oolites and a few fragments of brown dolomite up to 3 cm across, i.e a mass-flow sandstone (Fig. 2.17). Interbedded with the sandstone is a black, very fine-grained graphitic metapelite that is foliated in places and massive in others - weathered surface light grey. There is also an associated, highly feldspathic layer speckled by tiny red Fe-stained spots. This is a recrystallised acid volcanic containing numerous tiny acicular and euhedral crystals of zircon. The same graphitic phyllite and speckled feldspathic volcanic rock occur at the copper prospect at locality 2.40.

Figure 2.17. Gritty, feldspathic mass-flow sandstone in the Chuos Fm containing well-sorted, grit-sized grains of white silicified oolites and a few small clasts of brown dolomite up to 3 cm across (one at hammer head). Farm Landeck 77.

61

Locality 2.31 (UTM 33k0547247, 7756215): Lower Karibib Formation, farm Landeck 77. Intense bedding-parallel foliation of grey Karibib Fm limestone containing some white streaks and calc-silicate layers. The outcrop consists of vertical, small-scale antiforms, most of which are defined by calc-silicate layers, separated from each other by narrow zones of shearing (Fig. 2.18).

Figure 2.18. Vertical, small-scale anticlinal folds in Karibib Formation limestone. Synclines sheared out. Farm Landeck 77.

Locality 2.32 (UTM 33k0546668, 7755804): Base Karibib Formation, farm Landeck 77. Tan-coloured Keilberg Member dolostone 2 m thick at the base of the Karibib Formation. There is abundant very coarsely crystalline brown calcite at the contact between the Keilberg Member and the underlying Chuos Fm.

Locality 2.33 (UTM 33k0546235, 7754887): Karibib Formation, farm Landeck 77. Traverse from base to middle of Karibib Fm limestone - an intense bedding-parallel foliation throughout.

Locality 2.34 (UTM 33k0546264, 7754854): Karibib Formation, farm Landeck 77. Graded limestone beds 3-10 cm thick near base of Karibib Formation (Fig. 2.19).

Figure 2.19. Graded limestone beds 3-10 cm thick near the base of the Karibib Formation.

Locality 2.35 (UTM 33k0546508, 7754350): Base Karibib Formation, farm Landeck 77. Undulating but gently dipping brown dolomite of the Keilberg Member at the base of the Karibib Fm. Beds dip 10-22/280.

Locality 2.36 (UTM 33k0546446, 7754356): Karibib Formation, farm Landeck 77. Karibib Fm about 50 m above the Keilberg Member. Beds dip 54/270 but dip undulates considerably.

Locality 2.37 (UTM 33k0547309, 7753595): Saturn Fm, farm Landeck 77. Massive, structureless, featureless, light brown weathering dolomite.

Locality 2.38 (UTM 33k0546338, 7757373): Karibib Formation limestone, farm Landeck 77. Lower part of Karibib Fm below negatively weathering and valley-forming marker phyllitic schist layer. Intense bedding-parallel foliation in limestone except in closures of minor folds where foliation is scarcely developed. No mass-flow layers seen in this traverse across the lower Karibib Fm.

Locality 2.39 (UTM 33k0547132, 7752753): Upper Karibib Formation, farm Landeck 77. North to south traverse across the outcrop from near the top of the marker layer of phyllitic schist to the top of the Karibib Formation.

Top of phyllitic schist: A limestone layer near the top of the schist is a clast-bearing mass-flow unit.

The upper Karibib limestone unit above the phyllitic schist marker: This consists of numerous mass flows layers interbedded with varying thicknesses of laminated rhythmite and grainstone flows of varying grain sizes. The laminated rhythmite is comprised of grey limestone turbidite laminae, some of which are capped by thinner, light grey pelagic dolomite layers. The rhythmite lamination becomes very indistinct in places. The mass flows vary from centimetres to several metres in width. Most clasts in the mass flows are flattened and drawn out fragments of grey or, less commonly, white limestone. Dolomite clasts are light grey, distinctly less numerous and less deformed than the limestone clasts. Some flows contain only clasts smaller than about 5 cm in size. The largest clasts in other flows are generally not much larger than about 25 cm. In some flows, the clast size fines upwards. Figure 2-20 is from a 10 m-thick, medium grey, limestone mass-flow layer with white, drawn-out limestone clasts and less deformed, brown-grey dolomite clasts. Layer thickness, clast size and proportions of grey limestone and light grey dolomite clasts vary from layer to layer (Figs. 2.21A, B).

Towards the top of the unit is a zone of very thin mass-flow layers, individually 6-7 cm thick but also up to 15 cm thick, many of which have platy grey limestone clasts set in a light grey-brown dolomite grainstone matrix. Some of these contain some light grey dolomite clasts or consist almost entirely of light grey dolomite clasts in a grey limestone grainstone matrix (Figs.2.22A, B, 2.23A, B). Closely associated with these thinly bedded flows are a few layers of small, grey limestone nodules set in a light grey dolomite matrix (Fig. 2.24). The penultimate layer at the top of the formation is a 7 m-thick mass-flow unit containing dark grey and grey limestones clasts with very few, very light grey dolomite clasts. The matrix of the lower 4 m is grey limestone and that of the upper 3 m is light grey dolomite (Fig. 2.25). The uppermost few metres of the Karibib Fm consist of limestone with an intense bedding-parallel foliation. The Kuiseb Fm schists occur above this but are not exposed.

Figure 2.20. 10 m thick limestone mass-flow layer in the middle of the upper Karibib Fm containing white, drawn-out limestone clasts and less deformed brown-grey dolomite clasts. Note the intense foliation which is almost bedding-parallel. Southern part of Landeck 77.
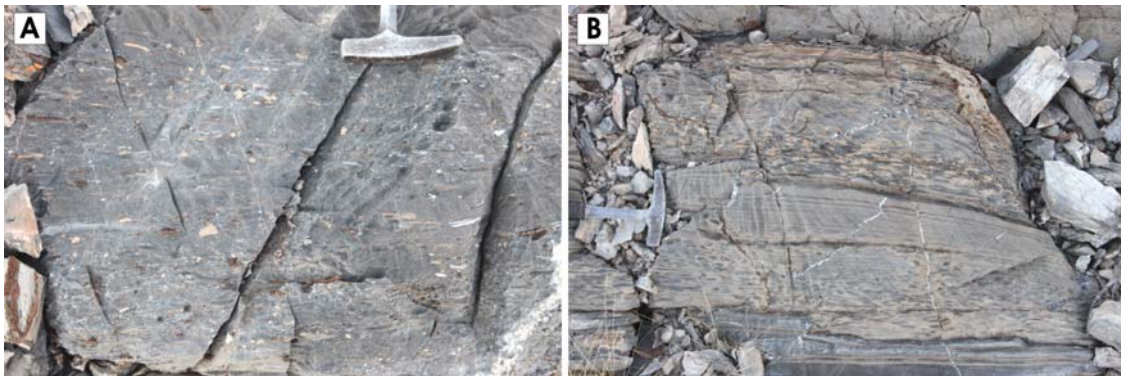

Figure 2.21. Mass-flow layers in the Karibib Fm stratigraphically above the layer of Figure 2.20. **(A)** Large platy, deformed clasts of grey limestone and small clasts of less deformed, white and brown dolomite; **(B)** Two mass-flow layers with grey limestone clasts in a very light grey dolomite grainstone matrix. These two layers are underlain and separated by laminated rhythmite, i.e. thin, deep-water turbidites.

Figure 2.22. Mass-flow layers: **(A)** Platy clasts of grey to whitish limestone orientated parallel to bedding and set in a very light grey dolomite grainstone matrix. Mass flows are separated by laminated layers of limestone or dolomite: 1 - Graded limestone turbidite with a very thin capping of positively weathering pelagic dolomite; 2 - Turbiditic and pelagic dolomite; 3 - as for 1. **(B)** Close up view o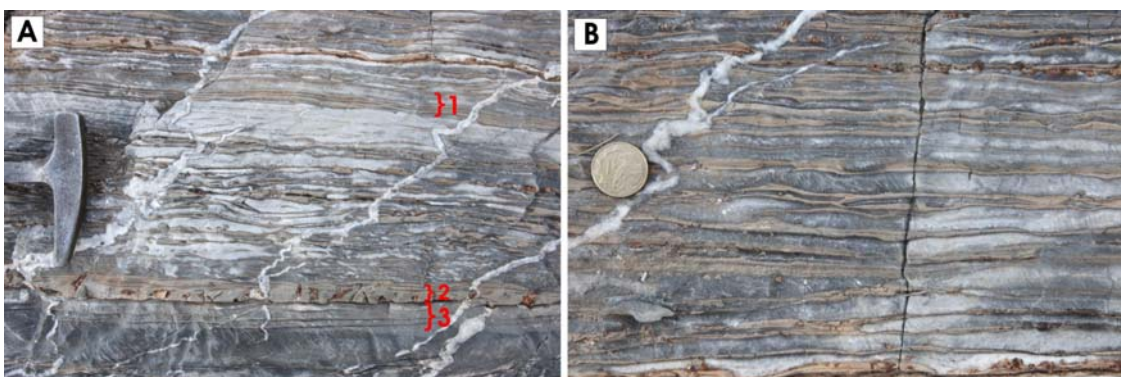f a mass-flow layer with platy clasts of grey to whitish limestone orientated parallel to bedding and set in a very light grey-brown, positively weathering dolomite grainstone matrix.
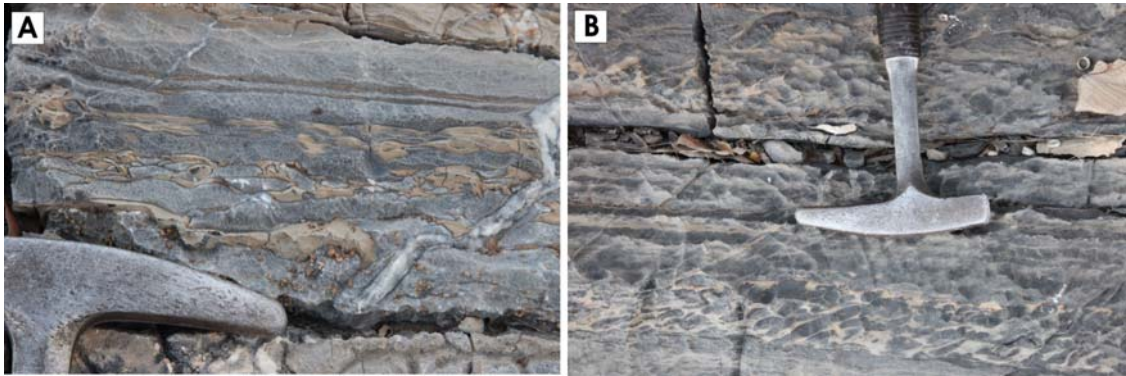
64

Figure 2.23. Mass-flow layers: **(A)** Close up view of a thin mass-flow layer in which individual larger and smaller, bedding-parallel platy limestone clasts are readily distinguishable in the very light grey dolomite grainstone matrix. **(B)** Two mass-flow layers with an imbrication-like orientation of the limestone clasts. Both orientations may be primary depositional features; the tectonic foliation is not apparent in the rock.
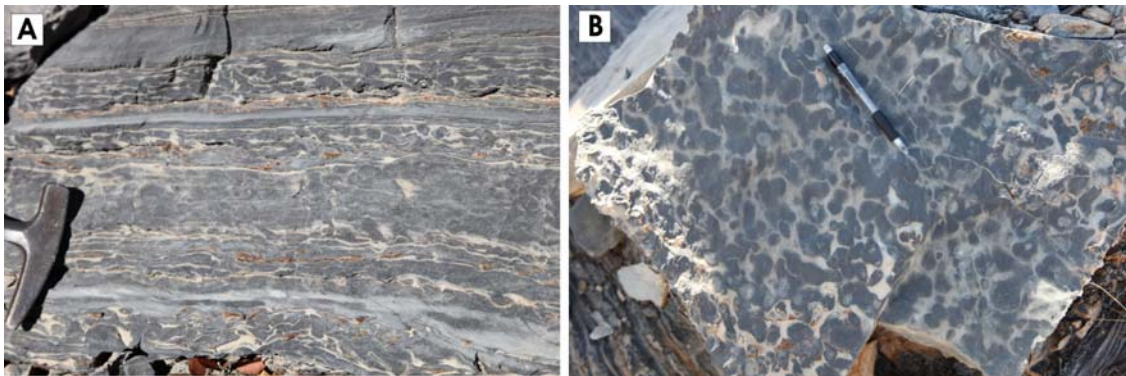
Figure 2.24. Layers with limestone nodules: **(A)** Thin layers of grey limestone nodules set in a light grey dolomite matrix; **(B)** As for A but plan view of a bedding plane surface displaying the shape of the limestone nodules.
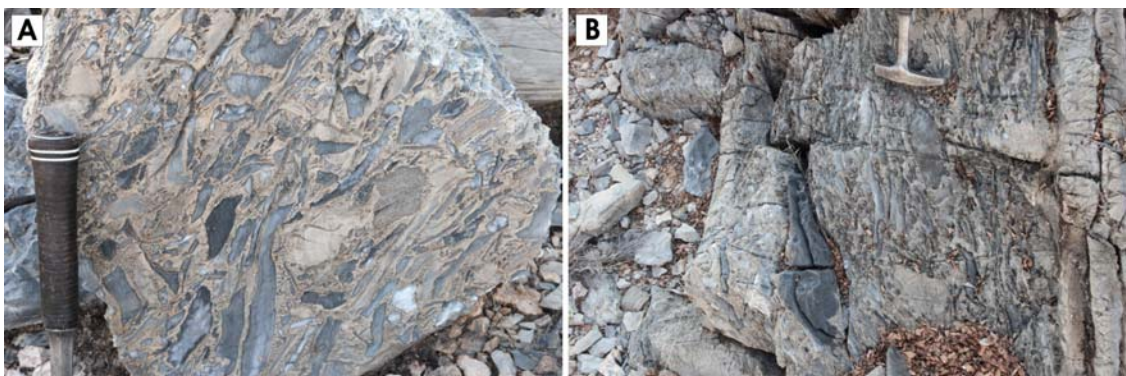
Figure 2.25. Uppermost, 7 m-thick mass flow just below the top 3m of the Karibib Fm. Blocky and platy angular clasts of grey limestone are set in a grainstone matrix of very light grey dolomite. A few almost white dolomite clasts. **(A)** View onto a surface subparallel to bedding give the impression of being undeformed; **(B)** View of the bedding of the same layer shows that there is a rather strong bedding-parallel orientation of clasts and foliation in the matrix.

Locality 2.40 (UTM 33k0545592, 7752345): Chuos Formation, farm Landeck 77. Copper prospect on western Landeck. In Chuos Fm, same graphitic phyllite and speckled volcanic rock as at locality 2.30. Bedding tightly undulating about horizontal, ferruginous gossan composed mainly of ramifying veins of limonite after pyrite with some malachite, chrysocolla and rare azurite (Fig. 2.26). Gossan appears to be largely horizontal.

Figure 2.26. Malachite and chrysocolla associated with veins of limonite after pyrite in the Chuos Formation on the western part of Landeck 77.

Locality 2.41 (UTM 33k0545487, 7752143): Top of Saturn Fm. Thin to very thin layers of brown dolomite interbedded with layers of schist of similar thickness (Fig. 2.27). Very similar to the top of the Ugab Subgroup on the eastern edge of the Summas Mountains near the spring at the northern edge of the farm Löwenfontein.

Figure 2.27. Thin interbedded layers of brown dolomitic grainstone and schist at the top of the Saturn Fm.
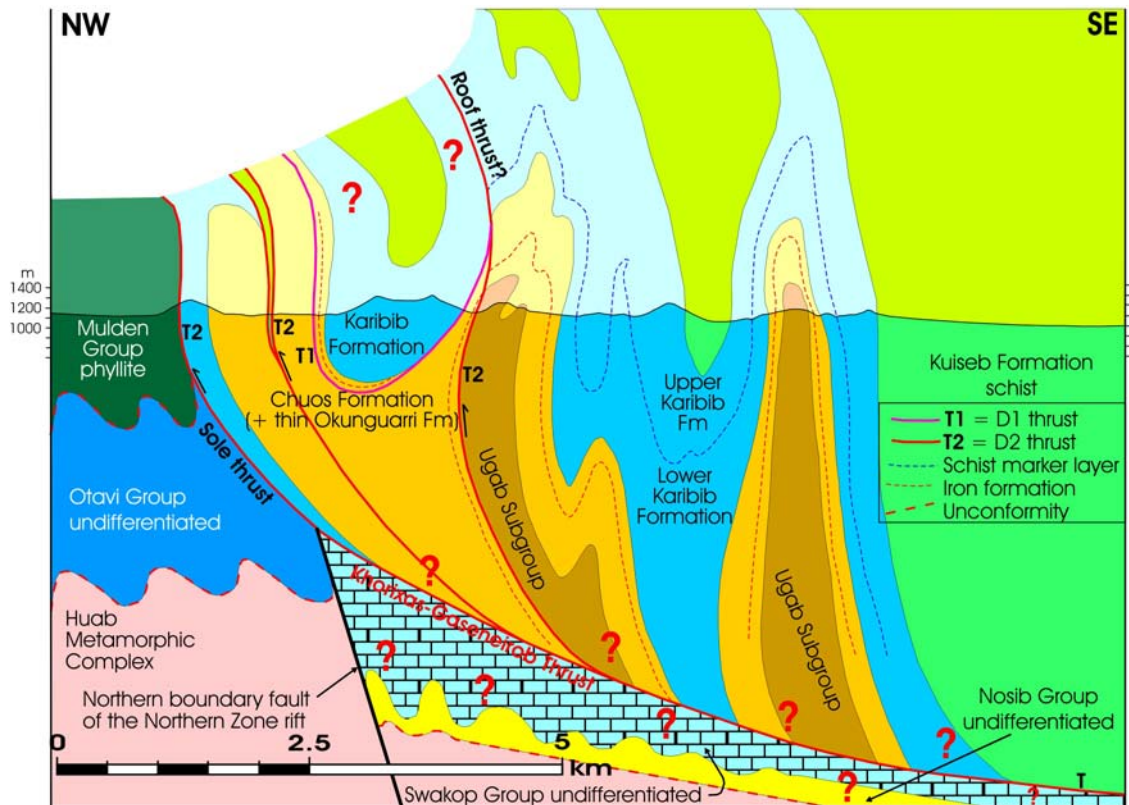
Figure 2.28. Section along the southern part of Traverse 2S incorporating modified stratigraphic and structural data from Clifford (2008).

Traverse 3N; farms Hillendale 238, Gelukspoort, 349, Mooilaagte 322

Stratigraphy

The base of the Otavi Group occurs on the southern edge of the farm Hillendale 238. Most of the guest farm Gelukspoort 358 is underlain by rocks of the Otavi Group. The top of the Otavi Group occurs just south of the southern border of Gelukspoort on the farm Mooilaagte 322. Here the Otavi Group is overlain unconformably by the post-D1 - pre-D2 molasse of the Mulden Group.

The basal part of the Fransfontein Ridge is composed of rocks of the Berg Aukas Formation, the cap carbonate to the Chuos Formation. Along strike from this locality are minor occurrences of the Chuos

Formation (Miller & Grote, 1988; Miller, 2008). The Ghaub Formation also occurs along strike to the east and west but is absent at the traverse locality (erroneously marked as Chuos by Miller & Grote, 1988). Above the Ghaub, the three formations of the Tsumeb Subgroup are present.

The Mulden Group lies unconformably on, and has cut into, the top of the Hüttenberg Formation.

There is a ridge of silicified breccia of uncertain age as well as red, breccia- and sand-filled and silicified dolines of Kalahari age.

67

Sedimentology

The Berg Aukas Formation consists of laminated grey dolomite with thin slump breccias near the base.

The Maieberg Formation consists of very light grey to off-white, massive to thickly bedded limestone. The thick Elandshoek Formation consists mainly of very light grey to off-white, massive dolomite in which bedding or laminae are rarely present. A few mass-flow and oolite layers are present. Near the base of the formation are a few stromatolites but these become much more abundant in the upper quarter of the formation. Oolites and stromatolites indicate shallow-water depos-ition. Some stromatolites and oolite layers are foetid. White jaspilite silicification with some of pink to red colour in places, occurs throughout the formation but is most common in the lower half. This silicification seems to be early diagenetic since jaspilite fragments occur in some of the upper mass-flow layers. The Hüttenberg Formations starts with rhythmites suggesting a marked change in water depth. Slumping is evident in the formation. The top of the Hüttenberg is a mass flow with large fragments of dark grey limestone.

The Mulden Group consists of phyllites.

Structure

In contrast to Travers 2N, the whole Fransfontein Ridge succession in this traverse is steely inclined to the south. The contact between the Elandshoek and Hüttenberg Formations is 3 m above a D2 thrust. For several metres below the thrust the stromatolite domes are flattened parallel to bedding. All are orientated updip suggesting northward transport of the thrust in the direction 340° (magnetic). Above the thrust, axes of minor F2 folds are orientated down dip. The l2 stretching lineation parallels these axes, both suggestive of sheath folding associated with the thrust in the direction 360° (magnetic). A second thrust fault occurs half way up in the Hüttenberg Formation. Some bedding-parallel chert layers are boudinaged. The overlying Mulden phyllites have a vertical foliation.
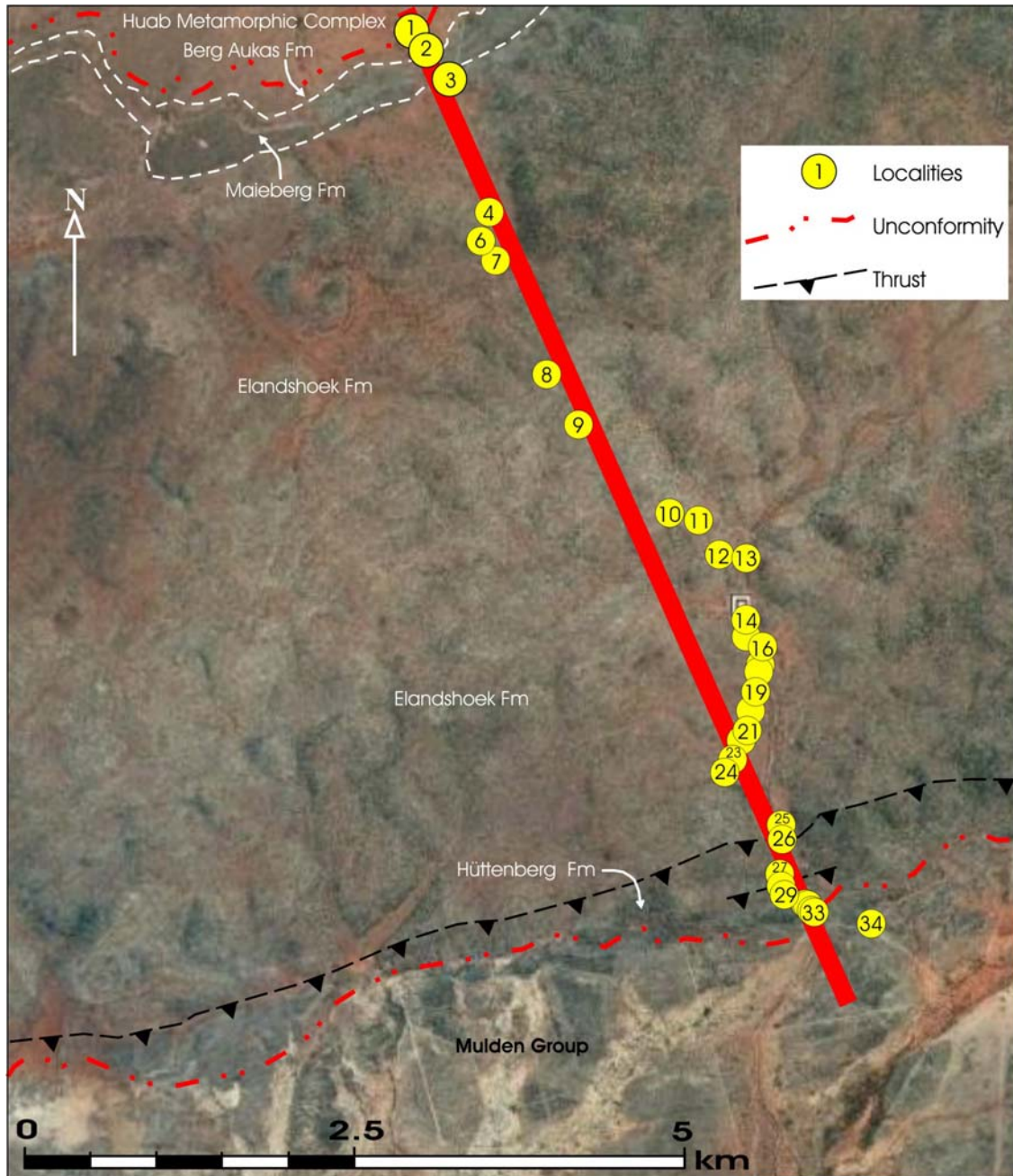
Figure 3.1. Google map of the localities on Traverse 3N. Location of section line of Figure 3.11 also shown (thick red line).

Locality 1 (UTM 33k0570476, 7775853): The basal 2.5 km of the succession is vertical to very steeply southerly dipping. Berg Aukas Formation: about 500 m thick, consists of laminated grey dolomite of the cap dolostone to the Chuos Formation. This forms the base of the sequence. Thin layers of slump breccia occur near the base of the formation. The other Abenab Subgroup formations are missing.

Locality 2 (UTM 33k0570366, 7775753): Maieberg Formation: Very light grey to almost white, massive to thickly

bedded limestone. Basal tan-coloured Keilberg Member is missing. The Maieberg Formation is about 1 km thick.

Locality 3 (UTM 33k0570241, 7775592): The Maieberg is overlain by the very light grey to whitish dolomites of the Elandshoek Formation.

Locality 4 (UTM 33k0570084, 7774496): Northern border of Gelukspoort 358. Massive, almost unbedded very light grey to whitish dolomite of the Elandshoek Fm with a few scattered stromatolites in places. Abundant, very coarse filigree-like

white jaspilite silicification that is typical of the Elandshoek Fm (Fig. 3.2A) (Jaspilite - a term used by TCL for silica that is too coarse grained to be called chert and too fine grained to be called quartz). Faint lamination in places, dip 88/65, i.e. beds slightly overturned. Many silicification stringers are parallel or subparallel to the lamination (Fig. 9.2B). Some of the ramifying jaspilite veins appear to enclose fragments of a hydraulic breccia (i.e. no disorientation of fragments) but they may also simply be filling ramifying fractures.
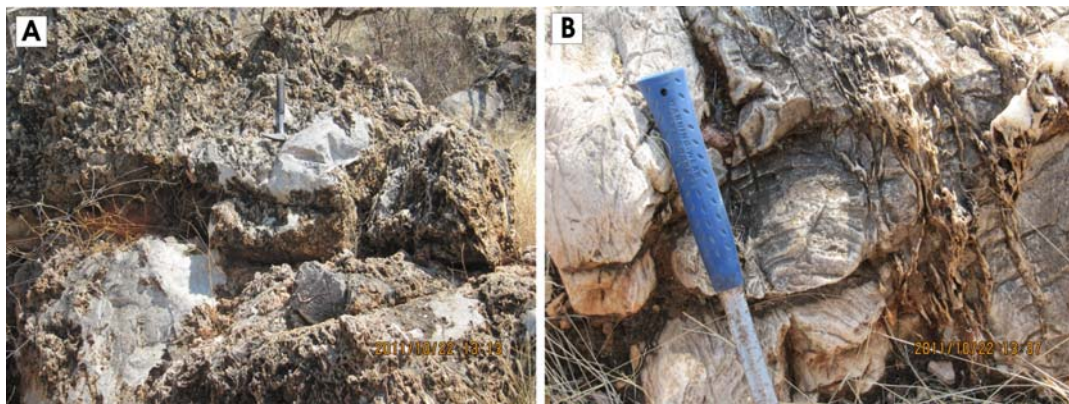
Figure 3.2. Silicification in the Elandshoek Formation. **(A)** Irregular bodies of massive silicification, some with a very coarse filigree-like texture. **(B)** Silicification stringers parallel to steeply dipping bedding lamination. Note the stromatolite beneath the hammer handle.

Locality 5 (UTM 33k0569944, 7774314): Northern Gelukspoort 358. Large elongate, hard, weather-resistant, ridge-forming body of brecciated white jaspilite

cemented by red, yellow, pink and white jaspilite (Fig. 3.3). Samples of red and yellow parts for analysis. Breccia is about 600 m long and subparallel to bedding.
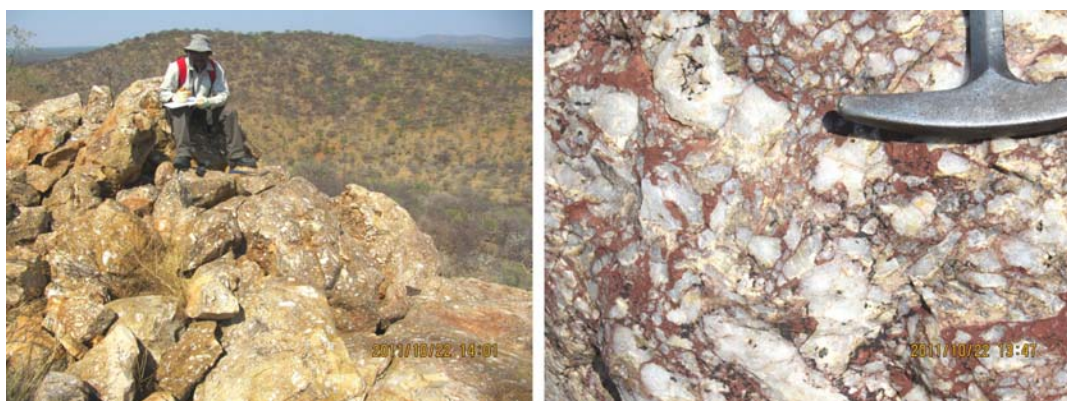
Figure 3.3. Photographs of ridge-forming body of brecciated white jaspilite fragments cemented by red and yellow jaspilite.

70

Locality 6 (UTM 33k0570026, 7774269): Northern Gelukspoort 358. Bedding-parallel breccia with abundant highly ferruginous calcite.

Locality 7 (UTM 33k0570157, 7774141): Northern Gelukspoort 358. Doline 5 x 10 m in diameter in Elandshoek dolomite. Filled with red, highly silicified Kalahari sand with patches of red jasper. Patches of manganese wad or pyrolusite (?) around the edges of the doline. Veins of the red silicified Kalahari sand radiate into the dolomite away from the doline.

Locality 8 (UTM 33k0570534, 7773278): Northern Gelukspoort 358.

Vertical lamination, strike 58°. White jaspilite still present but less abundant than lower down in the stratigraphy.

Locality 9 (UTM 33k05707065, 7772900): Northern Gelukspoort 358. Elandhoek Fm, several bedding-parallel jaspilite bands, bedding 58-85/160, i.e. undulating southerly dip.

Locality 10 (UTM 33k0571489, 7772203): Northern Gelukspoort 358. Narrow, intermittent, bedding-parallel zone of red jasper veining in the Elandshoek Fm, possibly breccia cementing (Fig. 3.4).

Figure 3.4. Bedding-parallel zone of red jasper veining in the Elandshoek Formation.

Locality 11 (UTM 33k0571657, 7772153): Northern Gelukspoort 358. The Rooikop. 100 m-diameter area of intense veining of the Elandshoek dolomite by red jasper, layered in places by variably intense silicification. Probably of Kalahari age.

Locality 12 (UTM 33k0571818, 7771888): Gelukspoort 358. Same dolomite and red jasper veining.

Locality 13 (UTM 33k0572034, 7771885): Gelukspoort 358. Red jasper veining of dolomite in hillsides to east and west of this locality.

Locality 14 (UTM 33k0572066, 7771348): Gelukspoort 358. Bedding in

Elandshoek dolomite 65/136. A few broad domal stromatolites in this area.

Locality 15 (UTM 33k0572012, 7771200): Gelukspoort 358. Elandshoek Fm. A 1 metre thick grainstone made up of carbonate oolites and pisolites, each individually enclosed in a thin coating of silica.

Locality 16 (UTM 33k0572122, 7770995): Gelukspoort 358. Elandshoek. Some slightly foetid stromatolites.

Locality 17 (UTM 33k0572106, 7770968): Gelukspoort 358. Elandshoek but with less white jaspilite than usual, bedding 80/180. Layer of silicified oolites (Fig. 3.5); also foetid.

Figure 3.5. Layer of foetid silicified oolites near the top of the Elandshoek Fm, carbonate oolites weathered out of a silica cement that has replaced the original matrix to the oolites.

Locality 18 (UTM 33k0572089, 7770856): Gelukspoort 358. 60 cm-thick mass flow in Elandshoek Fm, fragments mostly Elandshoek dolomite but also some fragments of white jaspilite, i.e. jaspilite silicification was synsedimentary to early diagenesis and took place during continued Elandshoek deposition. Several zones or patchy occurrences of variously silicified oolites between this and the last locality.

Locality 19 (UTM 33k0572038, 7770601): Gelukspoort 358. Massive Elandshoek dolomite is medium grey on weathered surfaces but is still very light grey to whitish on fresh surfaces, not foetid. Some white jaspilite still present. Clear bedding planes rare.

Locality 20 (UTM 33k0571736, 77710401): Gelukspoort 358. E-W elongate doline in very light grey Elandshoek dolomite, 40 x 70 m in diameter and filled with red, highly silicified Kalahari sandstone and siltstone. Bedding dip in the dolomite 70/174. Some stromatolites in the dolomite.

Locality 21 (UTM 33k0571734, 77710344): Southern Gelukspoort 358. Stacked stromatolites in Elandshoek dolomite (Fig. 3.6). Dolomite foetid.

Figure 3.6. Stromatolite near the top of the Elandshoek Fm, near southern border of farm Gelukspoort 358.

Locality 22 (UTM 33k0571848, 7770248): Southern Gelukspoort 358. Stromatolites fairly numerous between this and Locality 26. Occasional layer of grey to dark grey dolomite that is very light grey when fresh.

Locality 23 (UTM 33k0572271, 7769835): Southern Gelukspoort 358. Elandshoek Fm. Layers of silicified oolites; some very slightly foetid stromatolites. Brown silicification of some layers. Bedding 43/184.

Locality 24 (UTM 33k0572293, 7769727): Southern Gelukspoort 358. Elandshoek Fm, very light grey to whitish on fresh surfaces but light grey on weathered surfaces. Some white jaspilite. Silicification often in thin laminae and often defining the laminae in numerous stromatolites. 15 m-wide zone of strongly transposed stromatolites. These initially formed upright, parallel columns but at this locality are all bent parallel to bedding which dips 70/160 (Fig. 3.7). Transport direction seems to be approximately up dip. Oolites occur between the stromatolite columns; slightly foetid. Above this 15 m-wide zone there are fewer stromatolites but they are all deformed in the same way. Between the layers containing stromatolites there are some lensoid layers with sugary silicification but no obvious oolites.
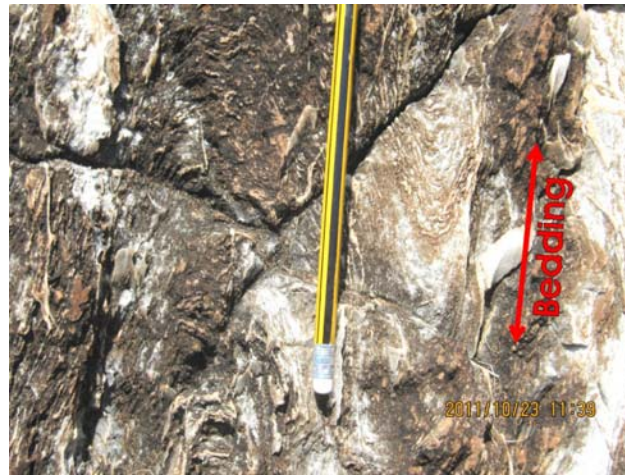
Figure 3.7. Part of a 15 m-wide zone of strongly transposed silicified stromatolites so that they are all orientated parallel to bedding which dips 70/160.

Locality 25 (UTM 33k0572325, 7769523): Southern Gelukspoort 358. Approaching the top of the Elandshoek Fm, very light grey to whitish on fresh surfaces but light grey on weathered surfaces. Abundant unsilicified oolitic grainstones, bedding 54/175. Veins of white jaspilite.

Locality 26 (UTM 33k0572326, 7769472): Southern Gelukspoort 358. Top of Elandshoek Fm and base of Hüttenberg Fm. 4 m-wide shear zone which may be a thrust (Figs. 3.8, 3.11). Overlain by 3m of very light grey Elandshoek dolomite with some cross-cutting veins of white jaspilite. The base of the Hüttenberg Fm consists of 15 m of limestone rhythmite. The rhythmite consists of graded laminae of turbiditic limestone and thinner, finer-grained laminae of pelagic dolomite. This is the first zone of continuous well-developed bedding encountered since stating at the base of the Elandshoek Fm and appears to mark a sharp change from shallow-water upper Elandshoek Fm deposition to deep-water Hüttenberg deposition. Bedding 40/164. There are two rhythmite zones separated and overlain by massive, light grey dolomite which is white with faint pink patches on the fresh surface.

Figure 3.8. Strong foliation in a 4 m-wide shear zone within 3 m of the top of the Elandshoek Fm.

Locality 27 (UTM 33k0572313, 7769343): A 40 m-thick mass flow with angular fragments of very fine-grained dark grey dolomite set in a rather abundant matrix cement of white sparry calcite (Fig. 3.9). This mass flow may be the result of very passive, short-distance slumping because there are parts in it with scarcely any disruption but these also contain a few patches of the sparry calcite. This scarcely broken zone is interlayered with more broken zones with much sparry calcite.

Figure 3.9. Mass flow or slumped layer consisting of angular fragments of dark grey dolomite cemented by sparry calcite cement.

Locality 28 (UTM 33k0572349, 7769321): Shear zone with lozenge-shaped fragments of dark grey dolomite with chert veins and various internal textures (Fig. 3.10A). Black to dark grey, bedding-parallel chert layers in the grey dolomite above the shear zone, typical of the Hüttenberg Fm (Fig.3.10B). Bedding 51/175.
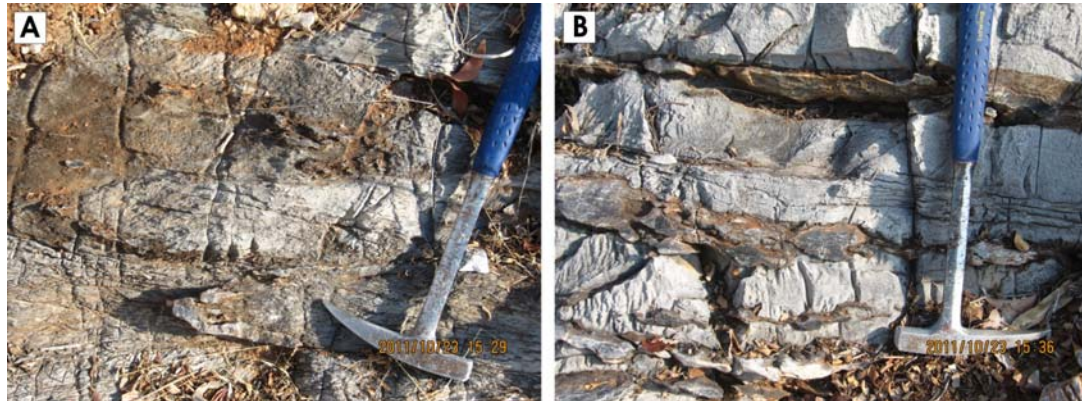
Figure 3.10. Hüttenberg Formation: **(A)** Shear zone with lozenge-shaped fragments of dark grey dolomite with various internal textures and chert veins. **(B)** Grey, bedded Hüttenberg dolomite with boudinaged, bedding-parallel lenses of dark grey to black chert.

Locality 29 (UTM 33k0572457, 7769257): Hüttenberg Formation. Minor folds in Hüttenberg. Bedding 52/165, axial plane of minor fold 75/156, stretching lineation parallel to minor fold axis - plunge 53° in direction 180°.

Locality 30 (UTM 33k0572475, 7769252): Hüttenberg Formation. Eight stacked, thinly to very thinly bedded limestone turbidites, very light grey on the weathered surface but dark grey on fresh surfaces. Rest of the outcrop massive or with rare bedding planes or laminations.

Locality 31 (UTM 33k0572509, 7769197): Hüttenberg Formation. Top 10 m of the Hüttenberg Fm is a mass flow containing fragments of dark grey limestone.

Locality 32 (UTM 33k0572536, 7769179): Hüttenberg Formation. End of Hüttenberg outcrop. Base of Mulden Group on Hüttenberg. Mulden covered and not exposed. Farm Mooilaagte 322.

Locality 33 (UTM 33k0572974, 7769103): Mulden Group, farm Mooilaagte 322. Weathered Mulden phyllite, some layers tan coloured, others silvery grey, some dark grey to black. Phyllite - vertical, strike 82°.

Locality 34 (UTM 33k0538026, 7767981): Mulden Group. At farm house on Mooilaagte 322. Very dark grey Mulden phyllite, carbonaceous?
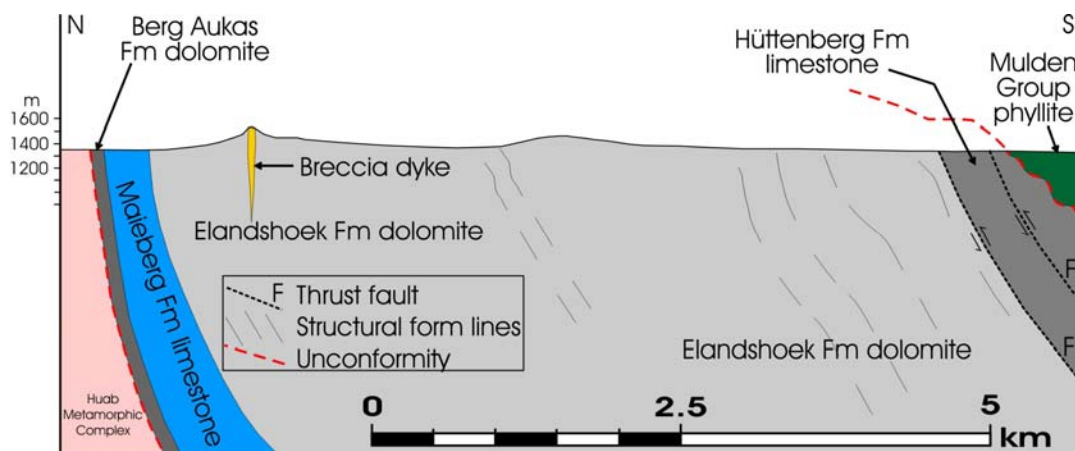

Figure 3.11. Section along Traverse 3N.

Stratigraphy

The Khorixas-Gaseneirob Thrust is the boundary between contrasting stratigraphies, Otavi, Mulden and Swakop Groups on the northern side and only Swakop Group on the southern side. At the northern end of both traverses Mulden Group phyllites unconformably overlie the top unit of the Tsumeb Subgroup, the Hüttenberg Formation, of the Fransfontein Ridge. But the Mulden Group is also overlain by a thrust sheet, the Mooilaagte Nappe consisting of the full, 3-formation Tsumeb Subgroup succession. This nappe is tectonically overlain by the Wolffsgrund Nappe consisting of the Chuos and Karibib Formations of the Swakop Group.

The Swakop Group south of the Khorixas-Gaseneirob Thrust consists of the Chuos, Karibib and Kuiseb Formations. The Chuos Formation is poorly exposed on Tsuwandas and the Kuiseb Formation is not exposed at all. Drilling and float in the calcrete indicate that the Karibib Formation is not as extensive as shown on Clifford's (2008) map and the cores of the southern anticlines have more Chuos than he shows (F. Bockmühl, farm owner of Tsuwandas, pers. comm., 2011). For clarification of the structure and the sections, the traverse is divided into southwestern (3SW - Fig. 3.15) and southeastern parts (3SE - Fig. 3.16).

Sedimentology

The reader is referred to Traverse 3N for an indication of the sedimentology of the Otavi Group rocks in the Mooilaagte Nappe but this is a deeper water facies of that on the Fransfontein Ridge and the sedimentology needs to be mapped in detail. Limestones and dolomites of the Maieberg Formation are overlain by dolomites of the Elandshoek Formation, the latter being overlain by limestone and dolomite of the Hüttenberg Formation.

Iron formation float indicates the presence of this ferruginous layer in the Chuos Formation around the base of the Snake Head Mountain. Best exposures of the Chuos are in the Snake Head Mountain where it is massive but zones of different sized clasts of granite and gneiss suggest a crude layering.

Two facies of the Karibib Formation occur as in the Landeck area of Traverse 2S. The facies north of the roof thrust (Fig. 3.15) is thickly bedded to massive and lacks sedimentary features except for thin ribbonites at the top and bottom of the formation in the Snake Head Mountain. The southern facies is thinly to thickly bedded with zones of ribbonite and many mass-flow layers. As with the Landeck area, the sedimentology of the Karibib Formation needs to be mapped in detail. It may be possible to map out the lateral extent of individual mass-flow lobes.

Structure

Two stages of nappe development took place. First the intensely deformed Wolffsgrund Nappe was thrust northwards onto the deep-water facies of the Tsumeb Subgroup, either during D1 or early D2. Then the deep-water Tsumeb Subgroup facies with its piggy-back of the Wolffsgrund Nappe was thrust during late D2 onto the Mulden Group phyllites during northward thrusting along the Khorixas-Gaseneirob Thrust. The Otavi Group rocks in the D2 Mooilaagte Nappe are far less

deformed than those of the overlying Swakop Group rocks in the Wolffsgrund Nappe. Nevertheless, their structures need mapping, particularly the segmented northern edge of the Mooilaagte Nappe which may be a series of sheath folds that could reveal the transport direction of the nappe.

The Swakop Group rocks are intensely deformed in the D2 structures further south. Except in tight D2 fold closures, there is an intense vertical bedding-parallel foliation in the Karibib marbles which tends to obscure detail in thinly bedded ribbonites and stretches out clasts in the mass-flow layers. Close to the Khorixas-Gaseneirob Thrust, the stretching lineation plunges down the dip direction of the foliation, i.e. 150°, which suggests a thrust transport direction of 330°. The area requires detailed structural mapping.
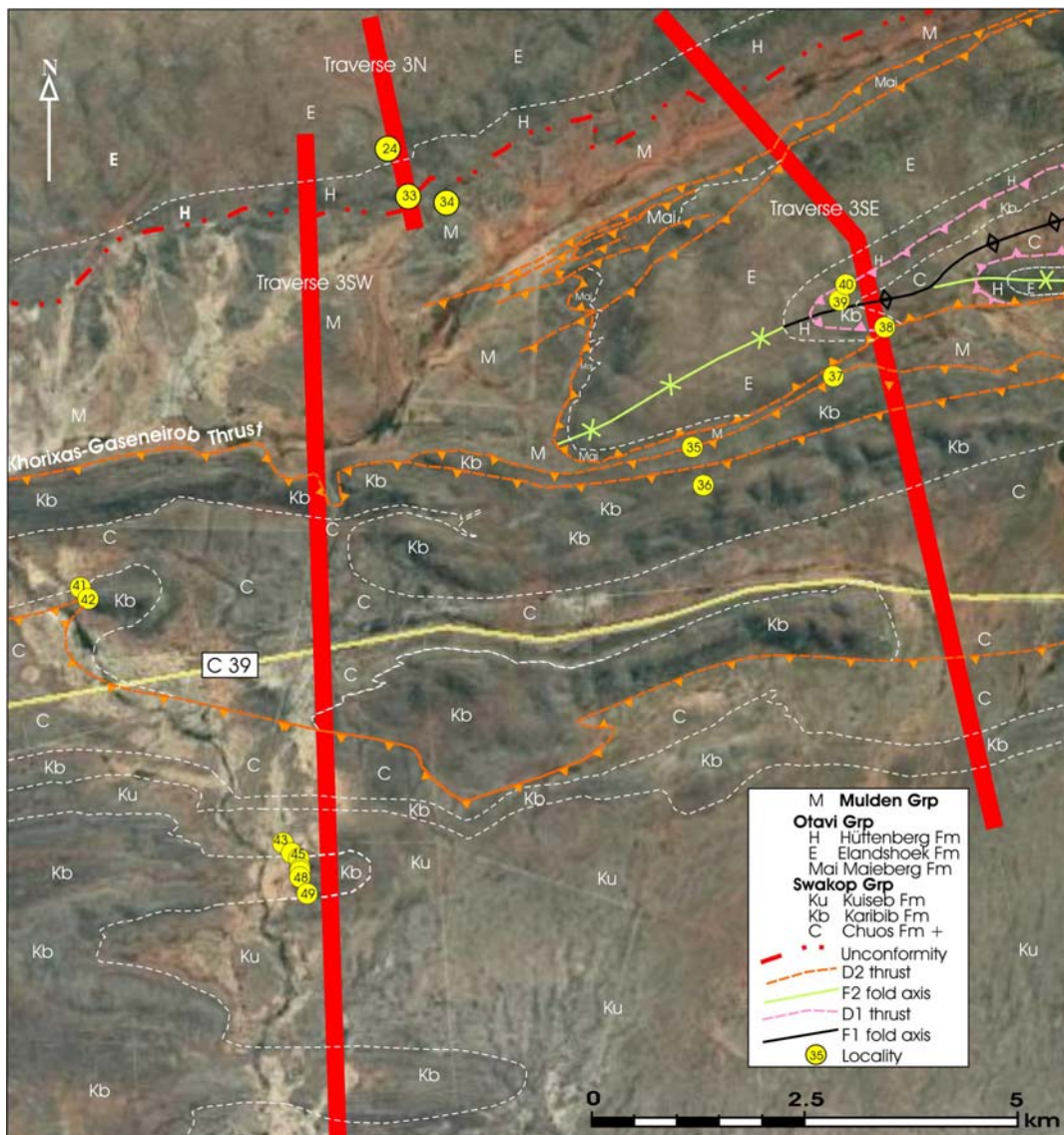

Figure 3.12. Google image of the region covered by Traverses 3SW and 3SE, farms Killarney 369, Tsuwandas 107, Mooilaagte 322, Zuwitsaub 108 and Steineck 109. The lines of the sections in Figures 3.15 and 3.16 are also shown (red lines). Stratigraphy and structure modified from Clifford (2008).

Locality 35 (UTM 33k0575878, 7766209): Karibib Fm, farm Mooilaagte 322. Intensely foliated, medium grey Karibib limestone, foliation dip 65/170. This locality just above the Khorixas-Gaseneirob Thrust which dips parallel to the foliation. The Karibib limestone is intensely foliated for the entire distance between this and the next locality.

Locality 36 (UTM 33k0575997, 7765770): Karibib Fm, farm Mooilaagte 322. Intensely foliated Karibib limestone, foliation dip 65/180, poorly developed stretching lineation plunge 57° in direction 150°. Rare very thin layers of parallel laminations that may be rhythmites.

Locality 37 (UTM 33k0577541, 7767037 (39) - Karibib Fm, farm Mooilaagte 322. Intensely foliated siliceous Karibib marble just above Khorixas-Gaseneirob Thrust where Karibib Fm thrust over Mulden phyllites. Foliation dip 80/146, plunge of stretching lineation on the foliation 75° in direction 150°, i.e. stretching lineation almost exactly down dip.

Locality 38 (UTM 33k0578131, 7767647): Karibib Fm, farm Mooilaagte 322. Intensely foliated Karibib Fm limestone. Foliation dip 83/160.

Locality 39 (UTM 33k0577605, 7767990): Karibib Fm, farm Mooilaagte 322. Intensely foliated Karibib Fm limestone. Foliation vertical, strike 90°. The Chuos Fm with tillite containing granite clasts occurs below the Karibib marble between localities 38 and 40. The Chuos and the Karibib marble between localities 38 and 40 form a D1 anticline that was tightened during D2 overthrusting. A very narrow strip of Karibib Fm(?) phyllites separates this locality from locality 40.

Locality 40 (UTM 33k0577660, 7768125): Hüttenberg Fm, farm Mooilaagte 322. Topmost layer of Hüttenberg. Chaotic mass flow with clasts of grey limestone, grey chert and silicified oolite and pisolite. Not strongly foliated. This layer forms the top of the Hüttenberg Fm and is the same mass flow layer that occurs at the top of the Hüttenberg Fm on the Fransfontein Ridge and at the equivalent stratigraphic level at the top of the Karibib Fm on the southern part of Landeck 77 (Fig. 2.25).

A D1 thrust separates localities 39 and 40; i.e. the Karibib/Chuos succession has been thrust over the underlying Otavi rocks forming the Wolffsgrund Nappe. D2 then thrust the Otavi rocks of the Mooilaagte Nappe with its Wolffsgrund Nappe piggy-back northwards onto the Mulden phyllites. Further D2 compression folded the D1 thrust, tightened the Karibib/Chuos D1 anticline and formed the Otavi syncline underneath.

Locality 41 (UTM 33k0568699, 7764525): Karibib and Chuos formations, farm Tsuwandas 107, Snake Head Mountain. Chuos Fm tillite with numerous pebbles and boulders of granite and gneiss. 5 m of rhythmite form the basal 5 m of the Karibib Fm. Above this the formation is thickly bedded to massive with no sedimentary structures.

Locality 42 (UTM 33k0568784, 7764437): Top of Snake Head Mountain. There may be thin ribbonites in the Karibib Fm at this locality

Farm Tsuwandas 107 south of the main tar road. Only Chuos, Karibib and Kuiseb formations present, extensive parts of the Karibib Fm are covered by calcrete. The Chuos and Kuiseb formations are covered by calcrete or soil, but iron formation float and occasional thin bands of carbonate that stick up through the calcrete help to delineate the Chuos Fm. Water boreholes indicate that the Chuos Fm is more extensive than shown by Clifford (2008) on the southern part of the farm where it is largely covered by calcrete.

Locality 43 (UTM 33k0571206, 7761392): Karibib Fm, farm Tsuwandas 107. Thinly to thickly bedded Karibib Fm dolomite, extensive karsting along joints. No sedimentary structures. Bedding dip 28/275.

Locality 44 (UTM 33k0571247, 7761346): Karibib Fm, farm Tsuwandas 107. Rapid change in dip to 86/184. Strongly developed bedding-parallel foliation.

Locality 45 (UTM 33k0571268, 7761298): Karibib Fm, farm Tsuwandas 107. Thinly bedded Karibib Fm limestone with very thin mass-flow layers 0.5 to 4 cm thick consisting of tabular, dark grey limestone clasts set in a light grey matrix of dolomite grainstone. (Identical to the very thin mass flow layers seen on the southern part of Landeck). There is a strong bedding-parallel cleavage and clasts in mass-flow layers are drawn out in the foliation. Bedding dip vertical, strike 90°. A few metres further up in the succession are more mass-flow layers up to 3 m thick containing a variety of clasts, all of which are strongly drawn out in the foliation (Fig. 3.13).

Figure 3.13. Mass flow near the top of the Karibib Formation on the southern part of farm Tsuwandas 107. Note intense flattening of clasts in the bedding-parallel foliation.

Locality 46 (UTM 33k0571277, 7761125): Karibib Fm, farm Tsuwandas 107. 3 m-thick mass flow. Bedding vertical, strike 90°.

Locality 47 (UTM 33k0571287, 7761159): Karibib Fm, farm Tsuwandas 107. Vertical isoclinal folds near the top of the Karibib Formation limestone (Fig. 3.14). Fold axes strike 90°.

Locality 48 (UTM 33k0571276, 7761100): Karibib Fm, farm Tsuwandas 107. Layers of single oolites in thinly bedded Karibib limestone; oolites probably emplaced by mass flow. Bedding vertical, strike 90°.

Figure 3.14. Vertical isoclinal folds near the top of the Karibib Formation limestone. Southern part of farm Tsuwandas 107.

Locality 49 (UTM 33k0571354, 7760958): Karibib Fm, farm Tsuwandas 107. Top of Karibib Fm and end of outcrop. Karibib is here overlain by the Kuiseb Fm but this is covered by calcrete. A few thin bands of carbonate up to 40 cm wide poke up through the calcrete.
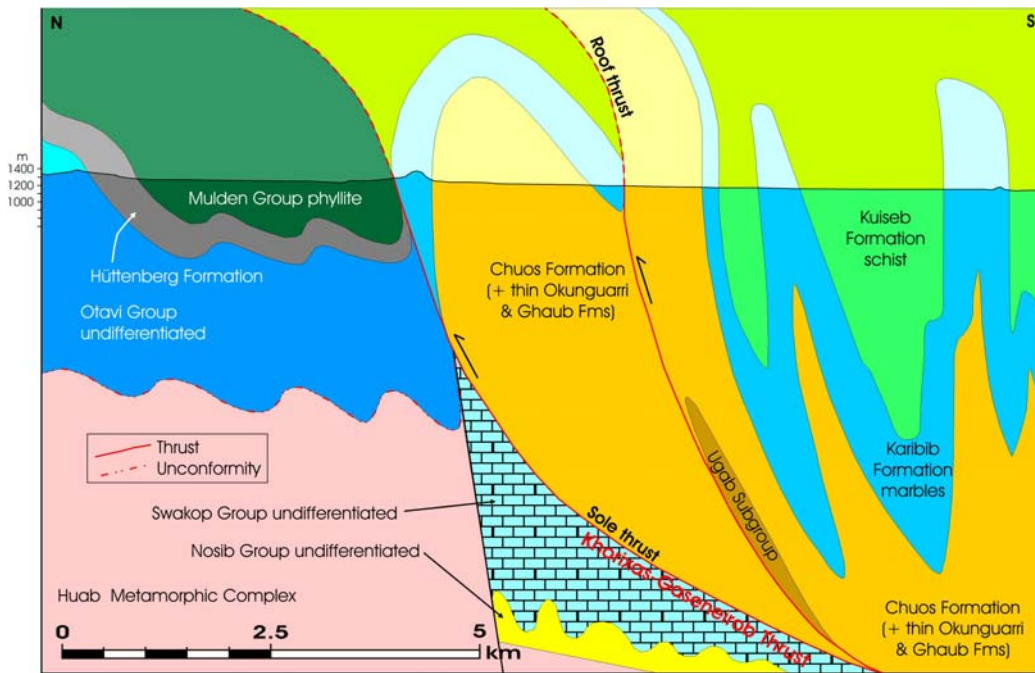

Figure 3.15. Geological section for Traverse 3SW showing D2 structures.
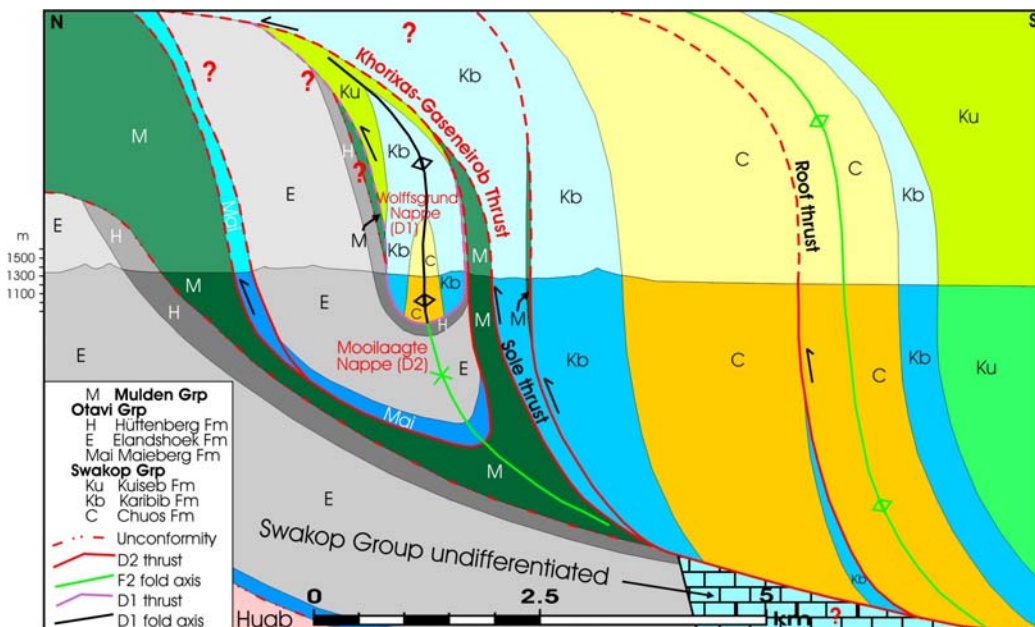

Figure 3.16. Geological section for Traverse 3SE showing D1 and D2 structures.

80

Traverse 4; farms Bergveld 239, Belina 132 and Straussenheim 134.

This traverse starts at the base of the Otavi Group succession in the eastern Fransfontein Ridge, continues up through the Otavi rocks and crosses the calcrete and soil-covered valley underlain by the Mulden Group. South of the Mulden the traverse crosses the Khorixas-Gaseneirob Thrust into rocks of the Swakop Group. The rocks of the Fransfontein Ridge were mapped by Tsumeb Corporation geologists and their subdivision of the stratigraphy has been used for the 1:500 000 Geological Map of the Damara Orogen (Miller & Grote, 1988). Of the Abenab Subgroup rocks in this traverse, only the Gauss Formation is represented. There is no Berg Aukas Formation and no Auros Formation. The Swakop Group rocks have been thrust over the Mulden Group along the Khorixas-Gaseneirob Thrust and occur to the south of this thrust. Exposures are generally poor on Staussenheim 134 south of the northernmost ridge of Karibib Formation marble. The location of the traverse is shown in Figure 4.1.

Stratigraphy

On the Fransfontein Ridge, the Gauss Formation of the Abenab Subgroup is overlain by the Ghaub Formation of the Tsumeb Subgroup followed by the Maieberg, Elandshoek and Hüttenberg formations. Unconformably above the latter are the phyllites of the Mulden Group.

South of the Khorixas-Gaseneirob Thrust the stratigraphy consists of the Saturn, Chuos and Karibib formations of the Swakop Subgroup.

Sedimentology

Otavi Group in the Fransfontein Ridge

The lower part of the Gauss Formation is massive to faintly laminated, very light grey dolomite but the bulk of the formation consists of a slump breccia in which fragments are enclosed in rims of fibrous isopachous cement. The texture is identical to that of the Gauss Formation in the Otavi Mountainland.

The glaciogenic Ghaub Formation contains mainly carbonate clasts with some chert and some stromatolite clasts. The Maieberg Formation consists of limestone rhythmites. Above it, the Elandshoek Formation is made up of very light grey to whitish, massive dolomite with some white jaspilite veining near the base and zones of laminated bedding and a mass-flow layer cemented by white jaspilite in the upper 300 m. The dolomite is foetid in places. The base of the Hüttenberg Formation consists of medium-grey, laminated to massive dolomite with white jaspilite veins and nodules and grey and black chert lenses. Several dolomite grainstone mass-flow layers with clasts of limestone, reef debris and white silicified oolites occur higher up. The upper 100 m of the Hüttenberg Formation consists of laminated rhythmites. Mulden phyllites lie unconformably on the Hüttenberg Formation.

Swakop Group south of Khorixas-Gaseneirob Thrust front

The Saturn Formation consists of strongly foliated, pale grey dolomite. Above it, the only exposures of the Chuos Formation are thinly bedded to intensely foliated layers of grey dolomite, one of which contains tremolite needles. An intense foliation in the Karibib Formation generally obscures sedimentary structures but locally thinly bedded rhythmites and grainstones are evident.

81

Structure

The Fransfontein ridge has an undulating southerly dip of between 30° and 79°. There is a bedding-parallel shear zone at the top of the Ghaub Formation suggestive of a thrust. Small-scale, N-vergent isoclinal folds occur at the top of the Elandshoek Formation.

Up against the Khorixas-Gaseneirob Thrust, the Karibib Formation has an intense foliation that dips steeply south. East and west of the traverse line and eastwards almost to the C68, the main road to Etosha, Clifford (2008) records a layer of what he calls 'rib rock' (Figs. 4.6, 4.7) all along the Khorixas-Gaseneirob Thrust with short, parallel extensions in the Karibib marbles in places. The 'ribs' are ling, thin, rib-like cleavage and fold mullions of chert layers that have been rotated into the transport direction by sheath folds that characterise the thrust. The orientation of the mullions indicates a 320° (magnetic) transport direction. The lateral extensions of the 'rib rock' into the marbles mark the locations of parallel thrusts. The Khorixas-Gaseneirob Thrust is the frontal or floor thrust of a stacked sequence of duplex thrusts, many of which may be along lithological contacts and have not been recognised (Fig. 4.8).

South of the thrust, the Saturn dolomites, much of the Karibib marble and dolomite layers in the Chuos Formation, are vertical and intensely foliated.
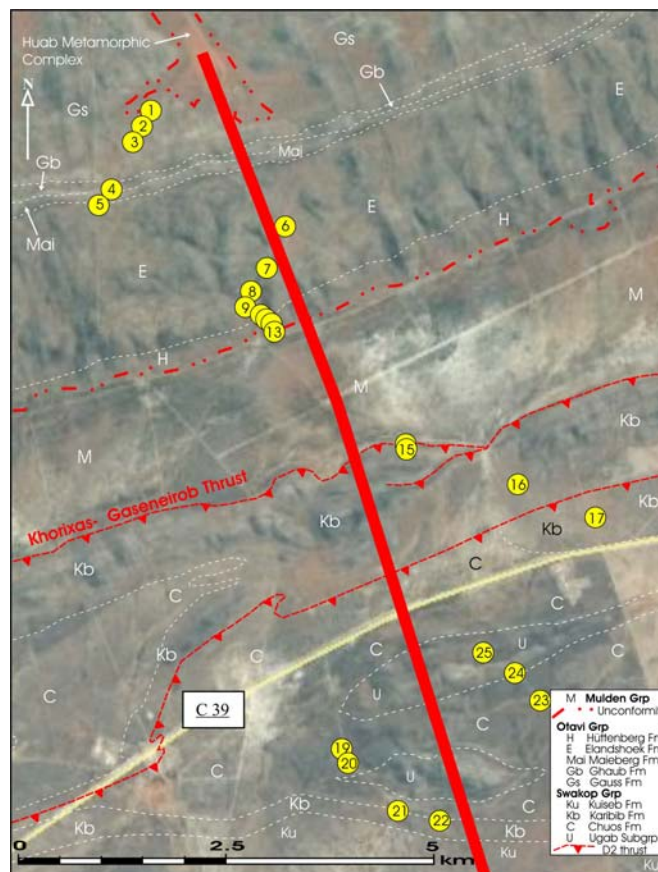

Figure 4.1. Google image of the region covered by Traverse 4, mainly farms Bergveld 239, Belina 132 and Straussenheim 134. The line of the section in Figure 4.8 is also shown (red line). Stratigraphy and structure modified slightly from Clifford (2008).

Abenab Subgroup, Gauss Formation

Locality 1 (UTM 33k0600297, 7776913): Basal Otavi Group, farm Bergveld 239. Near base of Otavi (base not exposed). Massive to faintly laminated, very light grey dolomite that weathers to medium or light grey. Difficult to determine bedding. Rare stromatolites.

Locality 2 (UTM 33k0600201, 7776663): Very light grey dolomite, bedding dip 54/196.

Locality 3 (UTM 33k0600091, 7776525): Very light grey dolomite, jointing that may be bedding or shearing, dip 79/170. Colloform texture, i.e. early diagenetic, sub sea floor, fibrous isopachous cement enclosed fragments of a slump breccia which constitutes the bulk of the formation. This is the typical texture of the Gauss Formation in the Otavi Mountainland. Dip of bedding just below the Ghaub Formation is 48/185.

Tsumeb Subgroup, Ghaub Formation

Locality 4 (UTM 33k0599827, 7775973): Ghaub Formation containing mainly carbonate clasts with some chert and some stromatolite clasts. Largest clast is 40 cm across but most are much smaller than this. The matrix of the top 10 m of the formation is sheared suggesting a possible thrust, foliation dip 47/185. The top half of

this shear zone has a pink matrix and contains mainly small clasts. The intensity of the foliation decreases downwards and the centre of the formation is unfoliated. True thickness of the formation is about 75 m. Overlain by Maieberg Fm, Keilberg Member missing.

Tsumeb Subgroup, Maieberg Formation

Locality 5 (UTM 33k0599691, 7775788): Maieberg Fm limestone rhythmites, medium grey on weathered surfaces, light grey when fresh, bedding dip

30/180. Nearby is a Kalahari doline filled with red, highly silicified Kalahari siltstones.

Tsumeb Subgroup, Elandshoek Formation

Locality 6 (UTM 33k0601941, 7775531): Elandshoek Fm, northwestern part of Belina 132. Very light grey to whitish, massive Elandshoek dolomite with some white jaspilite veining but not as abundant as on Traverse 3N. Dolomite slightly foetid in places.

Locality 7 (UTM 33k0601704, 7775007): Elandshoek Fm. Open fold in Elandshoek, bedding dip 20/240.

Locality 8 (UTM 33k0601520, 7774630): Elandshoek Fm. Bedding dip in Elandshoek 62/170.

Locality 9 (UTM 33k0601529, 7774522): Elandshoek Fm. 20 m thick mass flow of Elandshoek fragments in a white jaspilite cement - poor exposure.

Locality 10 (UTM 33k0601665, 7774481): Elandshoek Fm. Some laminations. Minor, tight, N-vergent isoclinal folds; bedding dip variable, average 72/145.

Tsumeb Subgroup, Hüttenberg Formation

Locality 11 (UTM 33k0601689, 7774431): Base Hüttenberg Fm. Medium

grey laminated to massive dolomite that weathers dark grey, white jaspilite veins and

nodules. Local intense silicification of the laminations. Grey and black chert lenses. Two mass-flow layers a little higher in the stratigraphy.

Locality 12 (UTM 33k0601718, 7774321): Hüttenberg Fm. 4 m-thick mass flow with abundant stromatolitic reef debris, some silicified (Fig. 4.2). Also fragments of layers of silicified oolites (Fig. 4.3 A) and loose oolites and pisolites in the matrix (Fig. 4.3B). The upper ¾ of the Hüttenberg Fm apart from the uppermost 100 m, is intensely silicified, the remainder consists of numerous grainstones containing abundant oolites (Fig. 4.4). Bedding dip 55/165.

Figure 4.2. Mass flow in the Hüttenberg Formation containing abundant fragments of silicified and unsilicified reef debris and silicified oolites and pisolites; curved laminae of silicified stromatolite fragment at top left of photograph; farm Belina 132.
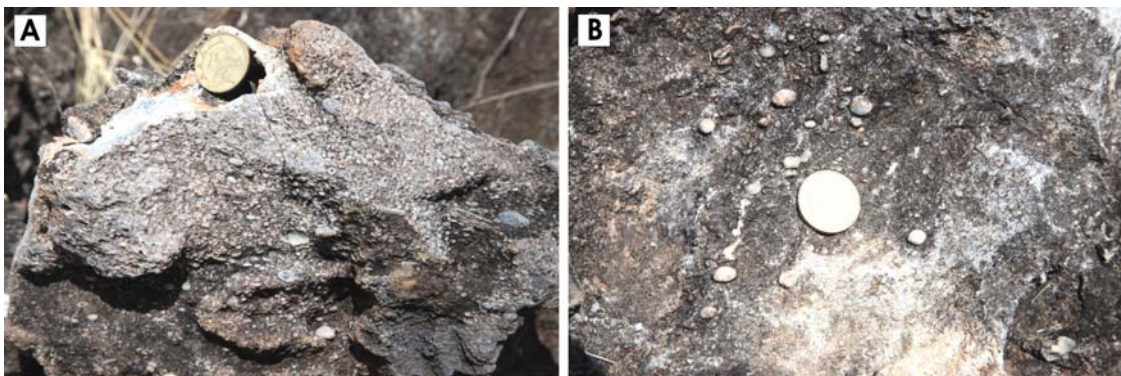
Figure 4.3. (A) Fragment of a layer of silicified oolites in the mass flow of Figure 4.2. **(B)** Abundant silicified oolites and some pisolites scattered through the dolomite grainstone matrix of the mass flow of Figure 4.2.

Figure 4.4. Dolomite grainstone with abundant detrital silicified oolites in upper Hüttenberg Formation, farm Belina 132.

Figure 4.5. Flaser bedding in the top 100 m of the Hüttenberg Formation on Belina 132. The light layers are composed of detrital silicified oolites. The dark layers consist of dolomite grainstone containing scattered detrital oolites.

Locality 13 (UTM 33k0601718, 7774321): Hüttenberg Fm. The uppermost 100 m of the Hüttenberg Fm consists of finely laminated flaser beds and rhythmites (Fig. 4.5). A 10 m-thick, small-fragment mass flow occurs about 30 m from the top. Farm Belina 132.

Mulden Group

Between Localities 13 and 14. Not exposed, calcrete and soil covered. Farm Belina 132. Clifford (2008) indicates phyllite in places.

Swakop Group, Karibib Formation

Locality 14 (UTM 33k0603364, 7772891): Karibib Fm, southern border of farm Belina 132. Locality situated in intensely foliated Karibib marble immediately against the Khorixas-Gaseneirob Thrust. Foliation dip 72/184.

Locality 15 (UTM 33k0603364, 7772891): Karibib Fm, southern border of farm Belina 132. "Rib rock" of Clifford (2008) (Figs. 4.6, 4.7). This "rib rock" formed when the silicified layers in the Karibib Formation were disrupted during deformation into fold or cleavage mullions. As deformation progressed, these mullions were rotated into the transport direction of the deformation and became extended in that direction. All these siliceous mullions have been so stretched out that they are like sword blades or "ribs", i.e. flat, 2-3 cm wide and long. They are all parallel and plunge down and define the stretching lineation (Fig. 4.7A). The axes of minor fold mullions are also parallel to the stretching lineation (Fig. 4.7B). Such intense deformation and rotation of mullions is typical of sheath folding associated with major overthrusting. Thus, the Karibib Fm all along the northern limit of its outcrop where Clifford has mapped "rib rock" has been deformed into sheath folds. From Clifford's map it would appear that the whole northern half of this ridge of Karibib Fm marbles, if not the entire width of the ridge, is deformed into sheath folds. Plunge of stretching lineation 50° in direction 140° which is indicative of a 320° (magnetic) transport direction.

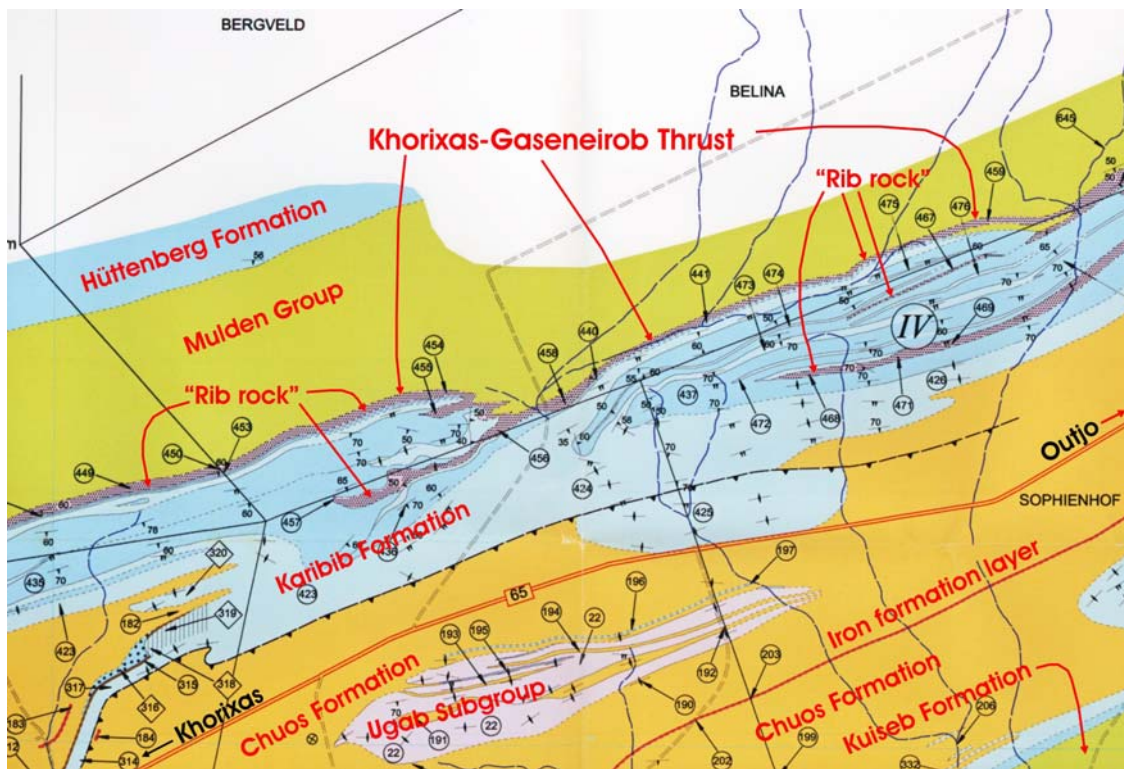**Figure 4.6.** Copy of geological map by Clifford (2008) of the ridge of Karibib Formation marble along the boundary between the farms Belina 132 and Straussenheim 134/Sophienhof 133. Note the locations of his strike-parallel "rib rock" at the northern margin of the Karibib marble and at places within the marble where it is also strike parallel. Published with permission of the Geological Society of South Africa.
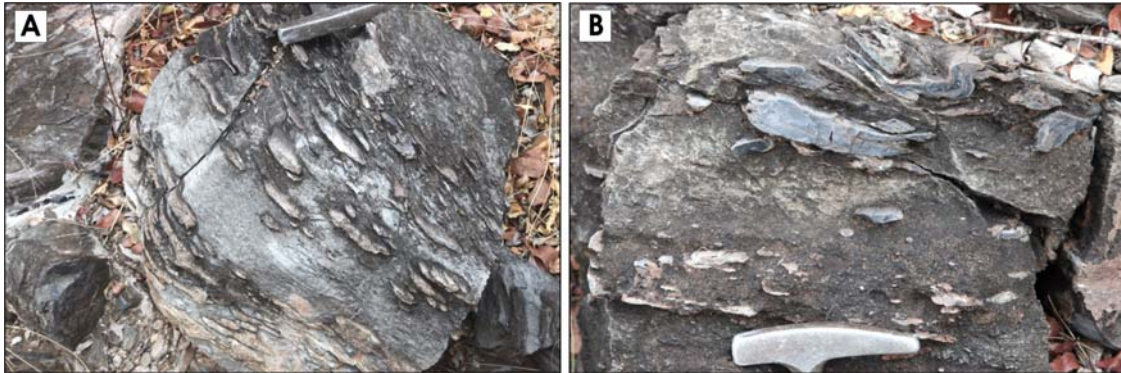
Figure 4.7. So-called "rib rock" of Clifford (2008). **(A)** Flattened cleavage-mullions of disrupted chert layers in the Karibib Formation immediately adjacent to the Khorixas-Gaseneirob Thrust front. Each flattened mullion is stretched out like a sword blade. All are parallel and define the stretching lineation indicating that this part of the Karibib Formation, and possibly the whole ridge of Karibib marbles, consists of sheath folds. Near the southern border of farm Belina 132. **(B)** Fold mullion of chert, the axis of which extends down the mullion and is orientated parallel to the stretching lineation. Same locality as Figure 4.7A.

Locality 16 (UTM 33k0604701, 7772395): Karibib Fm, northern part of farm Strausssenheim 134. Bedding vertical, strike 140°.

Locality 17 (UTM 33k0605641, 7771985): Karibib Fm, northern part of farm Strausssenheim 134. Layers of thin limestone turbidites, 4 mm to 12 cm thick. Bedding vertical, strike 85°.

Swakop Group, Chuos Formation

Locality 18 (UTM 33k0602635, 7769090): Chuos Formation, farm Straussenheim 134 south of the main road. Near the base of the Chuos Formation: A few thin layers of thinly to thickly bedded, dark grey or brown dolomite separated from each other by several metres of calcrete. No other features in the dolomites. Bedding dip 55/340, i.e. nose of fold structure.

Locality 19 (UTM 33k0602599, 7769214): Chuos Formation, farm Strauss-enheim 134. Dolomite layer protruding through calcrete, bedding dip 71/135.

Locality 20 (UTM 33k0602583, 7769187): Chuos Formation, farm Straussenheim 134. Tremolite needles in poorly exposed dolomite layer.

Swakop Group, Karibib Formation

Locality 21 (UTM 33k0603275, 7768452): Karibib Formation, farm Straussenheim 134, at farm house. Thinly bedded grainstones, Bedding vertical, strike 130°.

Locality 22 (UTM 33k0603767, 7768340): Karibib Formation, farm Straussenheim 134. Bedding obscured by intense foliation, foliation dip 85/185.

Swakop Group, Chuos and Saturn formations

Locality 23 (UTM 33k0604957, 7769792): Chuos Fm, eastern part of farm Straussenheim 134. Very dark grey dolomite

(fresh and weathered), partly massive, partly finely laminated, steep southerly dip. Some loose blocks appear to have stretching

lineations so the laminations may be a tectonic foliation.

Locality 24 (UTM 33k0604664, 7770111): Saturn Fm, eastern part of farm Straussenheim 134. Very strongly foliated light grey Saturn Fm dolomite, foliation dip 80/160.

Locality 25 (UTM 33k0604284, 7770365): Saturn Fm, eastern part of farm Straussenheim 134. Featureless, light grey Saturn Fm dolomite that weathers both light and dark grey. Intense foliation that oscillates about vertical and strikes 90°. Whole ridge like this.
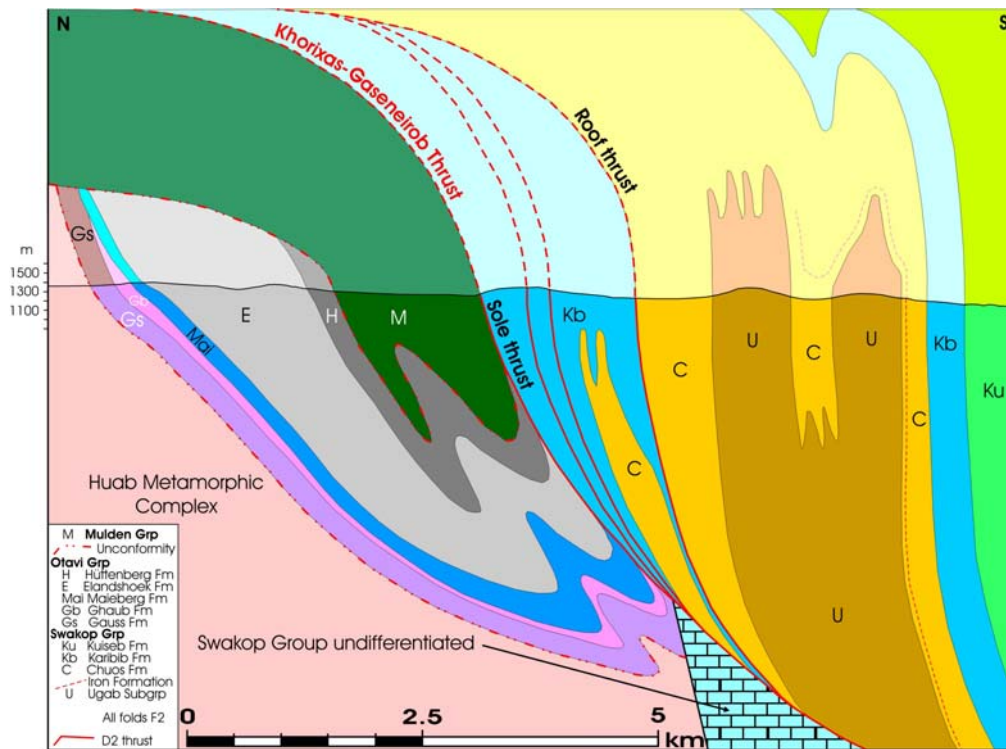
Figure 4.8. Section along traverse 4, includes stratigraphic and structural data from geological maps of Clifford (2008) for the Swakop Group rocks.

Conclusions

The unit above the Ghaub Formation in the Fransfontein Ridge is not well mapped and has been referred to as the Maieberg Formation (i.e. Otavi Group) in Figure 13.76 of Hoffman & Halverson (2008) and Karibib Formation (i.e. Swakop Group) in their Figure 13.77. This unit consists of the three formations of the Tsumeb Subgroup of the Otavi Group. Furthermore, it has been affected by the large-scale thrusting just to the south. All along the Fransfontein Ridge this unit needs careful stratigraphic, sedimentological and structural mapping.

The northern boundary fault of the Northern Zone Rift had a throw of at least 6.6 km (Miller, 1980, 2008). It must also have been the location of a huge growth fault during deposition of the Swakop Group which was approximately 16 km thick in the Okonguarri area (Ugab Subroup + Chuos + Okonguarri + Karibib + Kuiseb formations). This separated the Otavi facies on the top of the fault scarp from Swakop Group facies below the scarp. Although deformation has now tightly compressed the Swakop Group succession and thrust it northwards, detailed facies analyses may reveal the present

88

location of that part of the Swakop Group succession that was closest to the growth fault.

Acknowledgements

References

Clifford, T.N. 2008. The geology of the Neoproterozoic Swakop-Otavi transition zone in the Outjo District, northern Damara Orogen, Namibia. *South African Journal of Geology,* **111**, 117-140.

Frets, D.C. 1969. Geology and structure of The Huab-Welwitschia area South West Africa. *Bulletin of the Precambrian Research Unit, University of Cape Town*, **5**, 235 pp.

Hoffman, P.F. 2010. Strange bedfellows: glacial diamictite and cap carbonate from the Marinoan (635 Ma) glaciation in Namibia. *Sedimentology*, **58**, 57-119.

Hoffman, P.F. & Halverson, G.P. 2008. Otavi Group of the western Northern Platform, the eastern Kaoko Zone and the western Northern Margin Zone. *In:* Miller, R. McG. *The Geology of Namibia*, Volume **2**, pp. 13.69 - 13.136.

Lehmann, J., Saalmann, K., Naydenov, K.V., Milani, L., Belyanin, G.A., Zwingmann, H., Charlesworth, G. & Kinnaird, J.A. 2015. Structural and geochronological constraints on the Pan-African tectonic evolution of the northern Damara Belt, Namibia. *Tectonics*, **34**, 103-135.

Miller, R.McG. 1980. Geology of a portion of central Damaraland, South West Africa/Namibia. *Memoir of the Geological Survey of South Africa, South West Africa, Series*, **6**, 78 pp.

Miller, R.McG. 2008. *The Geology of Namibia*, **2**, 13-1 - 13-410.

Miller, R.McG. & Grote, W. 1988. Geological Map of the Damara Orogen, 2 A0 sheets. *Geological Society of South Africa*, Available from Geological Survey, Windhoek.

Schreiber, U.M. 2004. Geological map Fransfontein, Sheet 2014. 1:250,000 series. *Geological Survey of Namibia.*

Micro-cursorial mammals from the late Eocene tufas at Eocliff, Namibia

Brigitte Senut & Martin Pickford

Centre de Recherche en Paléontologie - Paris (CR2P), Muséum national d'Histoire naturelle, CNRS, Sorbonne Université, CP 38, 8 rue Buffon, 75005, Paris (brigitte.senut@mnhn.fr, martin.pickford@mnhn.fr)

Abstract : Fossils of macroscelideans, or micro-cursorial mammals, are common and diverse at Eocliff in the Sperrgebiet, Namibia, a complex of tufa deposits of Bartonian-Priabonian age. Associated mammals comprise rodents, insectivorans (tenrecoids, chrysochlorids) and hyracoids. The nearby tufa at Eoridge has yielded large mammals (anthracothere, hyracoid) that indicate a late Eocene age for the deposits. The few rodents from Eoridge are the same as those from Eocliff, indicating that the tufas at the two localities are penecontemporaneous. The diversity of macroscelideans at Eocliff is high (six taxa) with four brachyodont to semi-hypsodont taxa and two hypselodont taxa. None of the Eocliff macroscelideans is closely related to Palaeogene North African herodotiines which possess divergent molar morphology including the presence of buccal cingula in upper molars, a structure that is unknown in the Eocliff genera. The aim of this paper is to describe and interpret the Eocliff macroscelideans.

Introduction

The tufa deposits at Eocliff, Namibia, have yielded a rich assemblage of small mammals (Pickford, 2015a-d, 2020) among which macroscelideans are well represented with more than 750 dentognathic and over 400 postcranial specimens. Fossil birds are quite common in the tufas (Mourer-Chauviré *et al*, 2014, 2018) while large mammals are rare (Pickford, 2015e, 2015f) but are important for biochronological correlations. Morphological and metric data indicate that there are at least six taxa of micro-cursorial mammals in the tufas, of which four are abundant and two are rare. The smallest taxon is poorly represented.

Traditionally, the micro-cursorial mammals of Africa have been attributed to Macroscelidea, but the Eocliff fossils indicate that, by the late Eocene, there were already deep divisions within this order, with three groups exhibiting markedly divergent cranial and dental anatomy. Four of the Eocliff taxa are brachyodont to semi-hypsodont and possess impressive facial fossa just above the alveolar margin of the maxilla and large infra-orbital foramina above the P4/, whereas two are hypselodont, have no facial fossae and possess small ant-orbital foramina positioned high on the face above the cervical end of the P4/, close to the superior rostral margin of the orbit. Most

of the Eocliff macroscelidean taxa have a steeply oriented ascending ramus of the mandible, but one species has the ramus slanting markedly posteriorly as in extant *Rhynchocyon* (Evans, 1942). Only one of the Eocliff macroscelidean taxa has suppressed the m/3, all the other taxa possess both upper and lower third molars.

The postcranial bones indicate that all of the Eocliff lineages possessed typical macroscelidean ankle morphology, with the distal tibia and fibula solidly fused early in ontogeny, and a conspicuous cotylar fossa in the talus. However, many of the distal tibio-fibular epiphyses are not fused to the diaphysis, possibly because the individuals were juvenile at the time of death.

It is likely that the bulk of the assemblage of micro-cursorial mammals from Eocliff represents the remains of regurgitation pellets of owls, which is why three of the four smaller taxa are common. The two larger taxa are more fragmentary and infrequent, probably because they were too large to be swallowed whole. The presence of two taxa of hypselodont macroscelideans at Eocliff suggests that there was grass present close to the site.

Unlike North African herodotiines, none of the Eocliff macroscelideans possesses

buccal cingula in the upper cheek teeth. In other respects none of the Eocliff micro-cursorial mammals is dentally close to any of the North African macroscelideans, all of which are bunodont and are endowed with buccal cingula, indicating that the latter may not represent stem-group macroscelideans as commonly thought.

An isolated upper molariform tooth of a macroscelidid from Silica North, Namibia (Pickford *et al*. 2008) resembles one of the rare taxa from Eocliff and it is reasonably close to it in dimensions, suggesting that the specimens from the two sites are likely to be conspecific.

Geological context and Age

The geological context and age of the Eocliff (Fig. 1, Table 1) and Eoridge tufas have been documented previously (Pickford, 2015a). The Eocliff tufas are estimated to correlate to the Bartonian-Priabonian (Pickford, 2020). Two of the large mammal taxa from the nearby tufas at Eoridge are related to species from Eo-Oligocene lineages that occur in the Fayum,

Egypt. *Bothriogenys fraasi* is an anthracothere (Pickford, 2015f) and *Rupestrohyrax palustris* is a titanohyracid hyracoid (Pickford, 2015e). The rodents from the nearby tufas at Eoridge, even though rare, are the same as those that occur in abundance at Eocliff (Pickford *et al*. 2014).
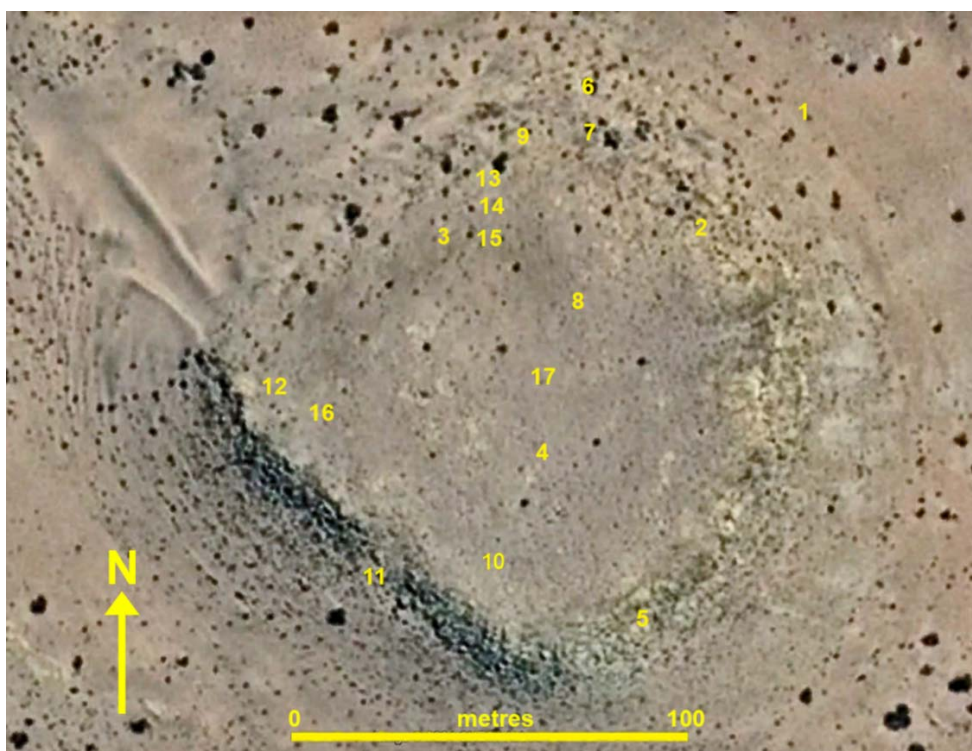
Figure 1. Vertical overhead view of Eocliff showing the location of discrete fossiliferous patches (Site abbreviation EC) EC1 and ECIbis were loose blocks collected from the northeastern slopes of the hill – the other deposits are *in situ* (image modified from Google Earth).

Table 1. GPS co-ordinates of fossiliferous patches at Eocliff (WGS 84 datum) Site abbreviation EC (in bold are localities from which collections have been made, the others remain to be sampled).

Eocliff	**1**	27°20'57.4"S	15°35'46.0"E
Eocliff	**2**	27°20'58.3"S	15°35'45.1"E
Eocliff	3	27°20'58.4"S	15°35'42.8"E
Eocliff	**4**	27°21'00.1"S	15°35'43.7"E
Eocliff	5	27°21'01.4"S	15°35'44.6"E
Eocliff	**6**	27°20'57.2"S	15°35'44.1"E
Eocliff	**7**	27°20'57.5"S	15°35'44.1"E
Eocliff	**8**	27°20'58.9"S	15°35'44.0"E

Eocliff	**9**	27°20'57.6"S	15°35'43.5"E
Eocliff	**10**	27°21'01.1"S	15°35'43.2"E
Eocliff	11	27°21'01.1"S	15°35'42.2"E
Eocliff	12	27°20'59.3"S	15°35'41.3"E
Eocliff	13	27°20'57.9"S	15°35'43.2"E
Eocliff	**14**	27°20'58.2"S	15°35'43.2"E
Eocliff	15	27°20'58.4"S	15°35'43.2"E
Eocliff	16	27°20'59.8"S	15°35'41.7"E
Eocliff	17	27°20'59.5"S	15°35'43.7"E

Fossil record of macroscelideans

Fossils attributed to macroscelideans have been found in African sediments ranging in age from the middle Eocene to Recent (Fig. 2). Some extant genera have been found in fossiliferous deposits, whereas others are unknown in the fossil record.
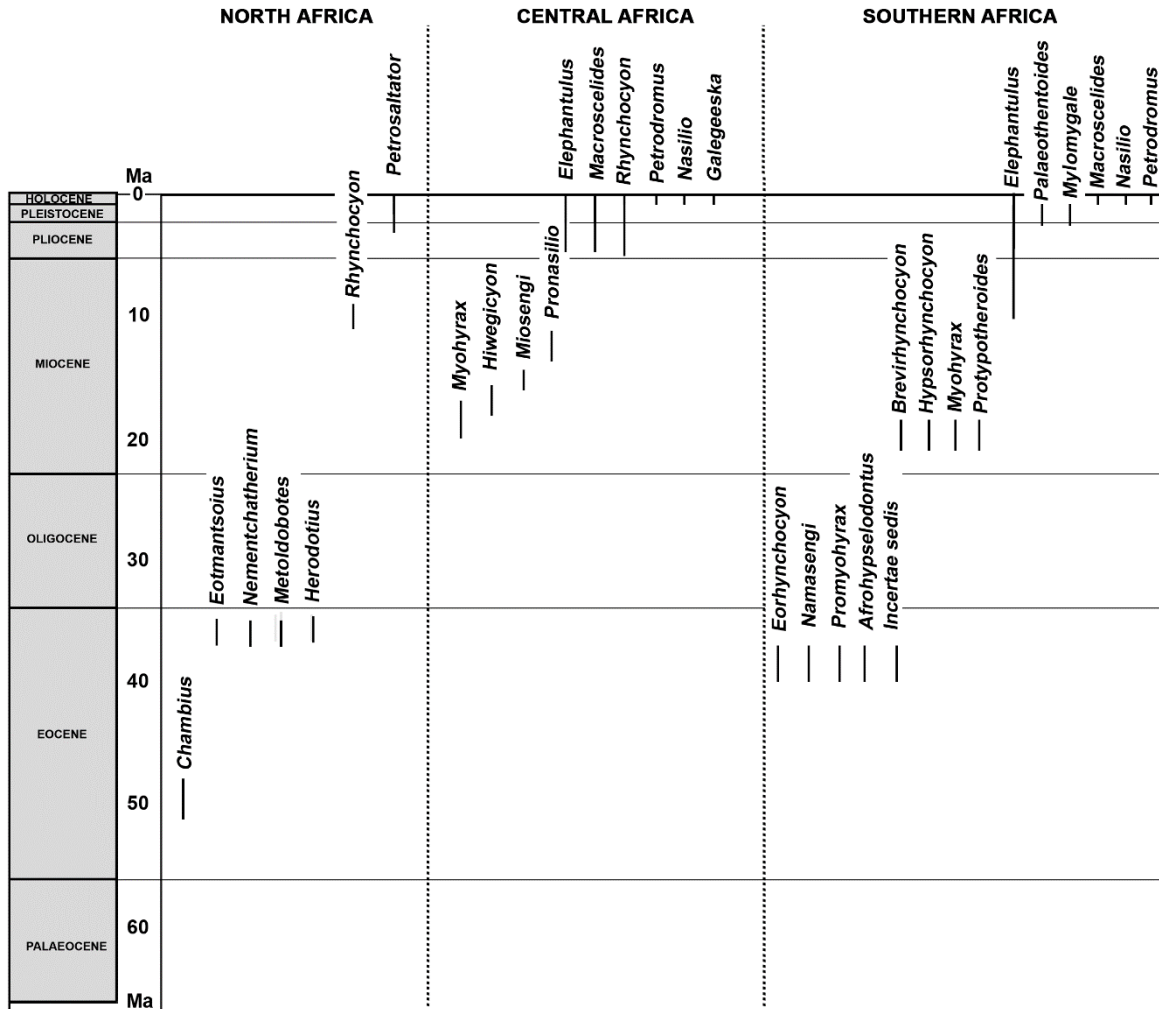
Figure 2. Distribution through time of genera attributed to macroscelideans in North, Central and Southern Africa. Age estimates are from Avery, 2019; Broom, 1948; Butler, 1969, 1987, 1995; Butler & Greenwood, 1976; Butler & Hopwood, 1957; Corvinus & Hendey, 1978; De Graaf, 1961; Grossman & Holroyd, 2009; Hendey, 1978; Holroyd, 2009, 2010; Hopwood, 1929; Mein *et al.* 2000; Pickford, 2015a, 2020; Schlosser, 1911; Seiffert, 2003, 2007; Senut, 2003, 2008; Senut *et al.* 1996; Stromer, 1926, 1931a; Tabuce, 2018; Tabuce *et al.* 2001; Wanas *et al.* 2009.

Materials and Methods

The methods of collection and extraction of fossils from the Eocliff tufa have been described in detail by Pickford (2020). Each fossiliferous patch was given a separate number in the order of discovery starting with EC1, and the GPS co-ordinates were recorded (Table 1). Small cairns were erected next to each of the fossiliferous patches. (Fig. 1).

The fossils are curated at the Earth Science Museum of the Geological Survey of Namibia (GSN), Windhoek. The locality abbreviation is EC. Catalogue numbers start with the locality (eg EC7) followed by a number denoting the size group of the fossils (eg EC7 1.1, 1.2, 2.1, 2.2 etc. depending on whether the specimen is from the upper jaw or lower jaw

respectively). Post-cranial bones carry the number 6 (eg EC7 6.1, 6.2 etc. depending on the skeletal part). When two specimens carry the same catalogue number they terminate with an alphabetical letter (eg EC7 2.1a, EC9 2.2b etc.).

Taphonomical note

The prevalence of juvenile specimens in the Eocliff micromammalian collection indicates that young mammals frequently fell prey to raptors, probably owls. The concentration of skeletal elements at some of the Eocliff fossiliferous patches suggests that they represent regurgitated owl pellets that accumulated beneath habitual roosting places, probably in trees that grew around the spring that deposited the tufa.

A goodly proportion of the Eocliff fossils are stained by patches of manganese, some in the form of dendrites and others by more extensive black films. In a few cases, rhizoliths are attached to the specimens. These black coatings suggest that, prior to being fossilised, some of the fossils may have been coated in microbial films such as algal mats. Taken together, this evidence indicates that some of the specimens may have fallen into water that was exposed to sunlight. A tufa dome setting, as has already been postulated for the Eocliff tufa deposits (Pickford, 2015a) accords with this scenario, as does the frequent presence of rhizoliths at diverse levels throughout the dome.

Dental nomenclature

The terminology used for describing the cusps and crests of the cheek teeth is depicted in figure 3. Terms related to crown heights (hypsodont, hypselodont, euhypsodont etc.) are based on White, 1959; Mones, 1982; Garcia-Lopez & Powell, 2011 and Von Koenigswald, 2020.
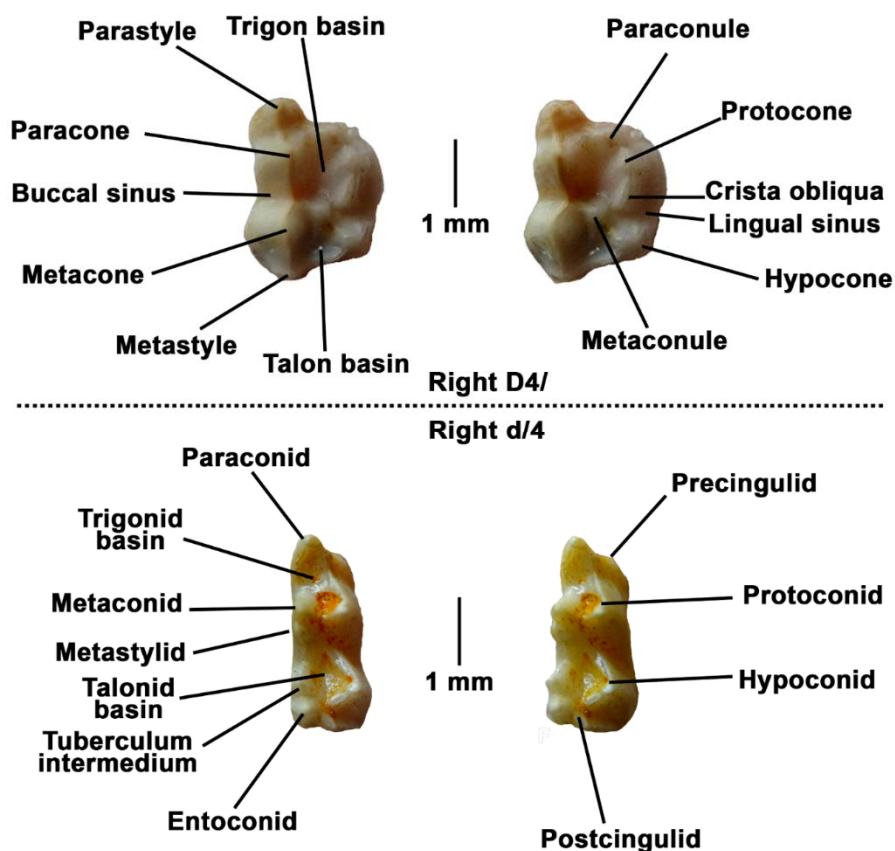

Figure 3. Terminology of upper and lower D4/ and d/4 (both teeth from the right side – stereo occlusal views).

In the order Macroscelidea, many recent authors recognise a single African family, Macroscelididae, with doubtful attribution of two Eurasian families to the order - Louisinidae and Apheliscidae (Hooker & Russell, 2012; Tabuce, 2018).

The African members of this family are currently arranged in several subfamilies – Rhynchocyoninae, Macroscelidinae, Herodotiinae, Metoldobotinae, Mylomygalinae and Myohyracinae (Holroyd, 2018).

The Eocliff fossils indicate however, that the morphological differences between these subfamilies are far deeper than previously reported and that they reflect differentiation at least at the family rank. For example, the dentognathic differences between the hypselodont, semi-hypsodont and brachyodont macroscelideans from Eocliff are greater than the differences documented between equids, tapirids and rhinocerotids among the Perissodactyla. We therefore classify the Eocliff and other macroscelidean taxa into different families rather than subfamilies. This, in essence, implies a change in rank which takes into account the morphological differences and thus the phylogenetically divergent relationships between the groups within the order. The Rhynchocyonidae were already markedly divergent from the Macroscelididae by Bartonian-Priabonian times, as were the Myohyracidae and the Afrohypselodontidae (new family).

Under the revised scheme, the Macroscelididae comprises four subfamilies, Macroscelidinae, Elephantulinae, Mylomygalinae and Namasenginae (nov.) while the Rhynchocyonidae comprise the extant genus *Rhynchocyon* together with fossil relatives *Miorhynchocyon*, *Brevirhynchocyon*, *Hypsorhynchocyon* and the Eocliff form described hereunder as *Eorhynchocyon*. Support for a higher ranking separation of these extant macroscelideans comes from molecular evidence as well as from anatomical arguments (Krásová *et al.* 2021; Heritage & Rayaleh, 2020; Rathbun & Dumbacher, 2016). The recent creation of two new genera (*Petrosaltator* and *Galegeeska*) for species previously included in *Elephantulus* highlight this tendency. The molecular analyses of Krásová *et al*. 2021, indicate a deep division between Macroscelididae and Rhynchocyonidae.

The systematic scheme utilised in this paper is as follows (in bold are new genera, subfamily and family erected in this paper).

Order Macroscelidea Butler, 1956

Family Rhynchocyonidae Gill, 1872
   Genus *Rhynchocyon* Peters, 1847
   Genus *Miorhynchocyon* Butler, 1984
   Genus *Brevirhynchocyon* Senut & Georgalis, 2014
   Genus *Hypsorhynchocyon* Senut, 2008
   Genus **Eorhynchocyon** nov.
Family Macroscelididae Bonaparte, 1838
  Subfamily Macroscelidinae Bonaparte, 1838
   Genus *Macroscelides* Smith, 1829
  Subfamily Elephantulinae Dumbacher *et al*. 2016
   Genus *Elephantulus* Thomas & Schwann, 1906
   Genus *Miosengi* Grossman & Holroyd, 2009
   Genus *Palaeothentoides* Stromer, 1931b
   Genus *Nasilio* Thomas & Schwann, 1906
   Genus *Pronasilio* Butler, 1984
   Genus *Hiwegicyon* Butler, 1984
   Genus *Petrodromus* Peters, 1846
   Genus *Petrosaltator* Rathbun & Dumbacher, 2016
   Genus *Galegeeska* Heritage & Rayaleh, 2020
  Subfamily Mylomygalinae Patterson, 1965
   Genus *Mylomygale* Broom, 1948

Subfamily **Namasenginae** nov.
    Genus *Namasengi* nov.
Family Myohyracidae Andrews, 1914
    Genus *Myohyrax* Andrews, 1914
    Genus *Protypotheroides* Stromer, 1922
    Genus *Promyohyrax* nov.
Family **Afrohypselodontidae** nov.
    Genus *Afrohypselodontus* nov.

Families of doubtful or uncertain macroscelidean affinities

Family Herodotiidae Simons, Holroyd & Bown, 1991
    Genus *Herodotius* Simons, Holroyd & Bown, 1991
    Genus *Chambius* Hartenberger, 1986
    Genus *Nementchatherium* Tabuce *et al.* 2001
    Genus *Eotmantsoius* Tabuce & Jaeger, 2012
Family Metoldobotidae Simons, Holroyd & Bown, 1991
    Genus *Metoldobotes* Schlosser, 1910
Family Louisinidae Sudre & Russell, 1982
Family Apheliscidae Matthew, 1915

Systematic Palaeontology

Order Macroscelidea Butler, 1956

Family Rhynchocyonidae Gill, 1872

Genus *Eorhynchocyon* nov.

Diagnosis :- Medium-sized macroscelidean in which the ascending ramus slants rearwards at a shallow angle; lower dental formula : incisors - 3, canine - 1, premolars - 4, molars - 2; lower canine with two partly to completely coalescent, roots; ventral profile of mandible convex throughout.

Type species :- *Eorhynchocyon rupestris* nov.

Etymology :- from the Greek, « *Eo* » in the sense of dawn, « *rhyncho* » for snout, « *cyon* » for dog.

Species *Eorhynchocyon rupestris* nov.

Diagnosis :- as for the genus.

Holotype :- EC7 7.2a, complete left mandible containing m/1 (Fig. 5A, Table 2).

Description

    Eocliff has yielded scarce remains of a macroscelidean that is intermediate in dimensions between *Nasilio* and *Petrodromus*. The total length of the mandible is 36.0 mm, and the alveolar process from i/1 to m/2 ranges in length from 21.4 to 22 mm.

Type locality and Age :- Eocliff 7, Namibia, Bartonian-Priabonian.

Etymology :- from the Greek, '*rupestris*' meaning near rocks.

    There are three P4/s in the Eocliff collection. Specimen EC6 2.1 is in a left maxilla fragment which preserves the infra-orbital canal and the facial fossa in front of it (Fig. 4). The P4/ crown is comprised of two lophs, a broad one mesially and a slightly narrower and shorter

one distally. The paracone and metacone are tall, the protocone and hypocone low. The trigon basin and talon basin are shallow. The hypocone is appreciably smaller than the other main cusps. There is a paraconule and a subtle metaconule expressed as a swelling between the trigon basin and the talon basin. At the mesial base of the protocone, there is a rounded knob of enamel, possibly a modified precingulum (or pericone). The tooth measures 2.3 x 1.8 mm so it is slightly larger than an isolated tooth from Silica North that shows similar crown morphology (Pickford *et al.* 2008). The latter tooth measures 1.8 x 1.7 mm. An isolated right P4/ from EC9 is added to the list of specimens despite its greater dimensions. The hypocone is appreciably smaller than the protocone, as in the other specimens.
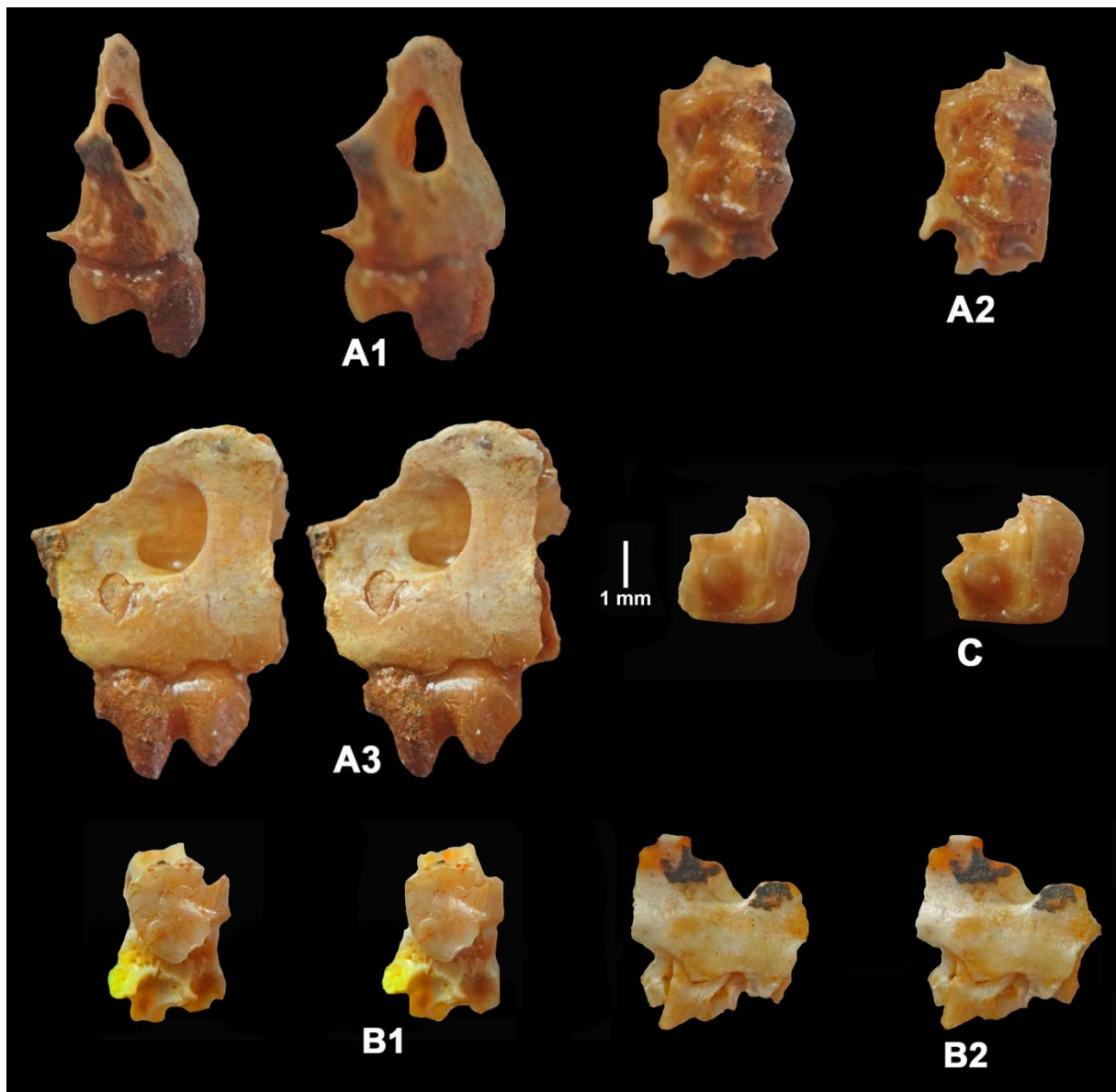
Figure 4. Stereo images of maxillae and an isolated upper tooth from Eocliff, Namibia, attributed to *Eorhynchocyon rupestris*. A) EC6 2.1, left maxilla fragment with P4/, A1 - anterior view to show the large infra-orbital canal, A2 - occlusal view (part of protocone broken off), A3 - lateral view to show infra-orbital foramen and facial fossa, B) EC7 5.1, left maxilla with damaged P4/, B1 - occlusal view, B2 - buccal view, C) EC9 5.1b, occlusal view of right P4/ lacking the parastyle and paracone (scale : 1 mm).

Figure 5. Stereo images of mandibles of *Eorhynchocyon rupestris* from Eocliff, Namibia. A) EC7 7.2a, holotype left mandible with m/1, A1 - buccal view, A2 - occlusal view, A3 - lingual view, B) EC7 7.2b, right mandible with fragment of p/2, worn m/1-m/2, B1 - lingual view, B2 - occlusal view with alveoli labelled, B3 - buccal view (scale : 10 mm).

There are two mandibles from Eocliff in which the ascending ramus slopes at a shallow angle to the rear, its root being well behind the last molar (Fig. 5). The shape of the jaw recalls that of the extant genus *Rhynchocyon* (Evans, 1942) and of early Miocene *Hypsorhynchocyon* Senut (2008). In occlusal view, the mandible is remarkably straight with no diastemata between the teeth and no lateral divergence of the ascending ramus. In buccal view, the mental foramina are located at about mid-height of the mandible, the anterior one being beneath the p/1 and the distal one beneath the p/4. Both fossil jaws retain all the alveoli, and it is clear that in this form there is no m/3 and the m/2 is reduced in dimensions compared to the m/1. The left and

right mandibles are unfused to each other, the scars for the ligamentous attachments that held the jaws together extending as far to the rear as the p/1, beneath the anterior mental foramen.

The lower canine in one specimen is double-rooted, the roots being confluent near the cervix, but separated at their apices and in the second specimen the roots are coalescent throughout. The mesial cuspid of the p/2 is preserved in the right mandible but the main cusp is broken off.

In both lower jaws the m/1 is preserved but is heavily worn, to the extent of eradicating much of the occlusal morphology (Table 2) and the right mandible also preserves the m/2. However, it is possible to discern that the m/1

was formed of two crescentids, of which the mesial one is slightly broader bucco-lingually than the distal one. The m/2 is formed of two lophids, the distal one narrower than the mesial one. The buccal sinusid is mesio-distally broad and quite deep, the lingual sinusid is shallow. The wear surfaces of the molars in both mandibles are horizontal, suggestive of a grinding dentition, already inferred from the wear pattern in the P4/s.

The left mandible from EC7 has an almost complete ascending ramus. The mandibular condyle is high above the occlusal surface of the teeth, estimated to be above the level of the roots of the upper cheek teeth. The coronoid process extends upwards and backwards but its apex is missing. What

remains suggests that it terminated above the mandibular condyle. The angle of the jaw terminates distally in an upwardly turned point slightly behind the level of the mandibular condyle. The anterior pole of the masseteric fossa terminates well behind the level of the m/2. The mandibular foramen is at the same level as the occlusal surface, but it is far back, 8.3 mm behind the distal alveolus of m/2. The ventral border of the mandible is gently convex throughout.

The alveoli indicate that the incisors were small, with i/1 and i/2 being procumbent in the jaw. The i/3 is small and steeply implanted. Behind it there are two alveoli (sometimes coalescent) for the lower canine as well as for all the teeth back to the m/2.

Table 2. Measurements (in mm) of teeth attributed to *Eorhynchocyon rupestris* from Eocliff, Namibia.

Catalogue	Tooth	Mesio-distal length	Bucco-lingual breadth
EC6 2.1	P4/ left	2.3	1.8
EC9 5.1b	P4/ right	3.1	2.7
EC7 7.2a (holotype)	m/1 left	3.3	2.2
EC7 7 2b	m/1 right	2.8	2.1
EC7 7.2b	m/2 right	2.7	1.7

Discussion

Eorhynchocyon rupestris is a medium-sized macroscelidean intermediate in dimensions between *Nasilio* and *Petrodromus*. It shares several features of the mandible with the extant genus *Rhynchocyon*, such as the shallow angle of the ascending ramus, the suppression of the m/3, and the convex profile of the entire ventral margin of the mandible.

In *Eorhynchocyon*, the straightness of the mandible in occlusal view, the convex ventral profile of the mandible in lateral view, the upwardly pointing angle, the position of the mandibular condyle and the form of the ascending ramus, all resemble the situation in Orycteropodidae, especially *Eteketoni* from the early Miocene of Napak, Uganda (Pickford, 2019). This fossil aardvark also has a reduced last molar, as in *Eorhynchocyon*, and the three known lower molars of the latter genus are bilophodont and, when worn, form an 8-shaped occlusal outline with little or no cusp relief remaining. There are however, differences between these genera - *Eteketoni* is considerably larger than *Eorhynchocyon*, the molars of *Eorhynchocyon* retain an enamel covering, and its mesial and distal roots are still separated from each other, but it is not beyond the realms of possibility that there is a

phylogenetic relationship between these two taxa. Similarities in the disposition of the bones in the orbito-temporal in *Rhynchocyon* and *Orycteropus* (Gregory, 1920) underline the possibility of a relationship between these lineages.

In this context it is interesting to note that the premaxilla of extant *Rhynchocyon* has a « largely or wholly edentulous premaxilla » (Patterson, 1965) although the presence or absence of upper incisors in this genus is variable (Corbet & Hanks, 1968). Aardvarks do not develop incisors. Likewise, the mandibles of the two taxa are not fused together.

Eorhynchocyon is a scarce element of the Eocliff macroscelidean fauna (5 specimens out of more than 1000) but it is important in that it indicates that the dichotomy between *Rhynchocyon* on the one hand and the other extant macroscelideans on the other (*Macroscelides*, *Elephantulus*, *Galegeeska Nasilio*, *Petrodromus*, *Petrosaltator*) had probably already occurred by the Bartonian-Priabonian. For this reason, it is considered likely that the differences between these two groups, which have traditionally been treated as denoting separation at the subfamilial rank,

implies a considerably deeper split, denoting at least a family rank distinction.

Family Macroscelididae Bonaparte, 1838

Subfamily Namasenginae nov.

Diagnosis : Small macroscelideans without palatal fenestration; steeply oriented ascending ramus of mandible; upper and lower dental formula : incisors - 3, canines - 1, premolars - 4, molars - 3; upper canine double-rooted.

Genus *Namasengi* nov.

Type species :- *Namasengi mockeae* nov.

Diagnosis :- Small macroscelidean slightly smaller than *Macroscelides* and *Elephantulus*; i/1-m/3 : 14.6-17.1 mm; large infra-orbital canal and facial fossa; upper and lower dental formula incisors - 3, canines - 1, premolars - 4, molars - 3; posterior dentition brachyodont; upper canine with two roots; P1/ and P2/ with single bucco-lingually compressed cusp; P3/ with four cusps (small hypoconid); P4/ fully molariform, largest tooth in the upper tooth row; upper molars with weak paraconule and metaconule, shallow trigon and talon basins; M3/ small with three roots; ascending ramus of mandible steeply oriented; moderately long retro-molar space; no coronoid foramen at the base of the ascending ramus; anterior lower premolars (p/1-p/3) bilaterally compressed with tall main cusp, prominent mesial stylid and low distal stylid; p/4 formed of two crescentids, the mesial one narrower than the distal one; lower molars with two sub-equal crescentids, with transversely oriented postprotocristid; m/3 reduced in size with two roots; D4/ with mesially projecting parastyle, large paraconule and metaconule; d/4 with prominent *tuberculum intermedium* mesial to the entoconid, and relatively small post-cingulid; metastylid distinct from the metaconid.

Differential diagnosis :- *Namasengi* differs from extant Macroscelididae (Macroscelidinae and Elephantulinae) by the lack of obvious fenestration of the palate. It differs from Rhynchocyonidae by the more steeply oriented coronoid process of the mandible and its much smaller dimensions.

Etymology :- Combination of *Nama* for « desert » and *sengi* Swahili word for elephant shrews, now the colloquial name in English.

Species *Namasengi mockeae* nov.

Diagnosis :- as for the genus.

Holotype :- EC10 1.1a, right maxilla containing C1/-M3/ (Fig. 6, Table 3).

Type locality and age :- Eocliff 10, Namibia, Bartonian-Priabonian.

Etymology :- the species is dedicated to Helke Mocke, Senior Geologist, Head of the Earth Science Museum of the Geological Survey of Namibia, who participated in the field surveys at Eocliff.

Description

Skull

The holotype right maxilla (EC10 1.1a) is slightly larger than those of extant *Macroscelides* and *Elephantulus* from Namibia. In lateral view the zygomatic process of the maxilla is observed to be overlain by the anterior process of the zygomatic which, although not preserved in the fossil, exhibits a sutural surface that extends anteriorly and dorsally to form the ventral and anterior margins of the orbit. The infraorbital canal pierces the maxilla at the level of the alveolar process to emerge above the P4/ in a prominent facial fossa that fades out anteriorly. The premaxilla is missing, but it shows a flange-like suture immediately anterior to the canine. The anterior margin of the orbit is in line with the rear of the P4/.

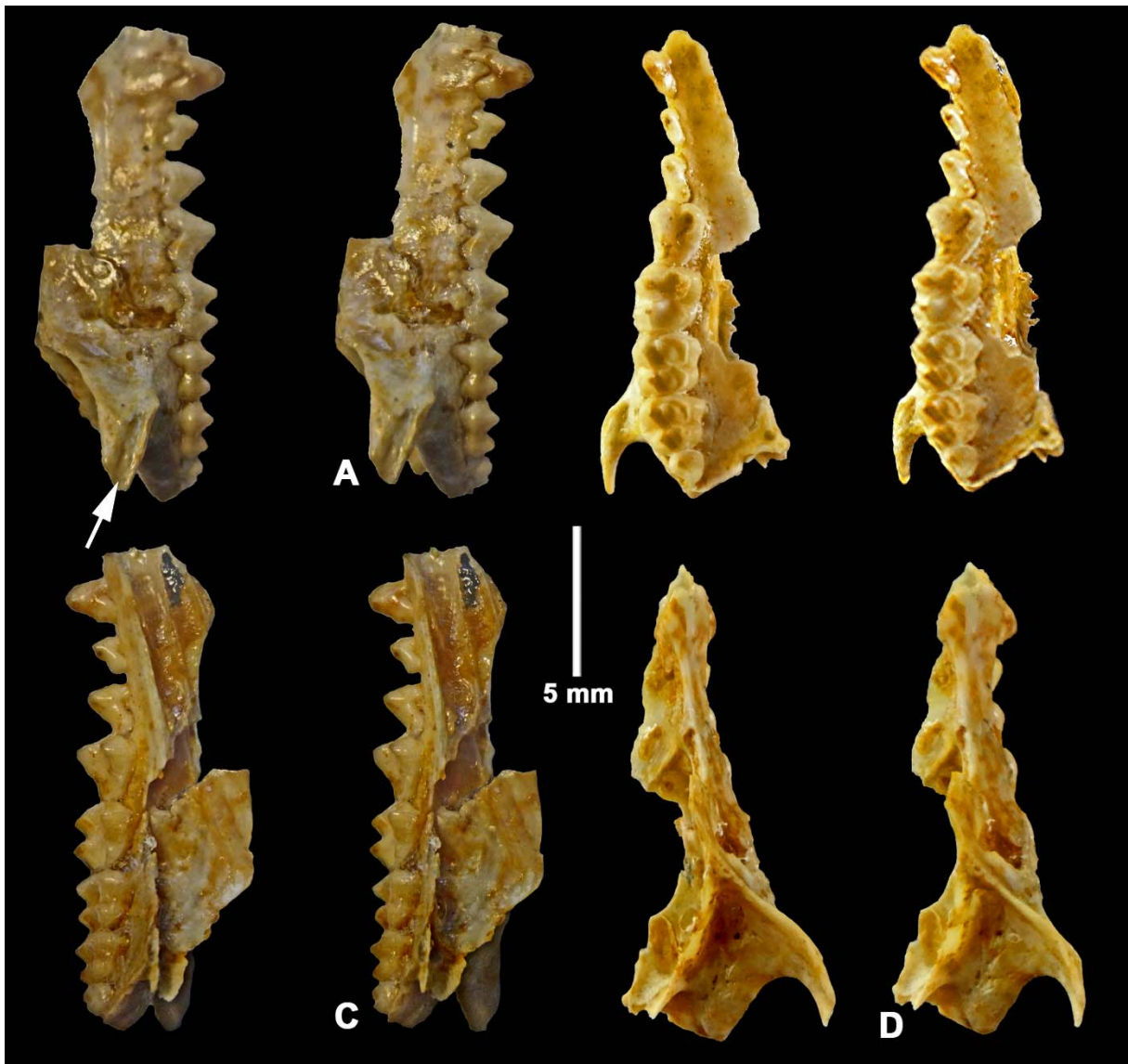**Figure 6**. Stereo images of EC10 1.1a, holotype right maxilla of *Namasengi mockeae* from Eocliff 10, with C1/-M3/. A) lateral view (arrow shows the suture for the zygomatic), B) occlusal view, C) lingual view, D) dorsal view (scale : 5 mm).

In ventral view, part of the palatine is preserved distally, extending anteriorly at least as far as the front of M2/. The zygomatic process of the maxilla departs abruptly from the

facial surface at the middle of M1/, the rear of the process being opposite the middle of M2/. The zygomatic process of the maxilla is robust at its root, but thins out where it meets the zygomatic, after which it extends a short distance distally as a narrow sliver of bone with a prominent lateral groove representing the maxillo-zygomatic suture.

In the preserved part of the palatal process of the holotype maxilla, there is no sign of fenestration, neither is there an obvious fenestration in specimen EC8 1.1a, but two specimens from EC7 (EC7 1.1a, 1.1b) show the distal part of the incisive foramen penetrating into the anterior part of the maxilla. More complete material is required to determine whether fenestration of the distal part of the palate was present or not in this species. There is a shallow, straight, groove for the palatine artery visible in specimens from EC7 (Fig. 8).

Upper dentition

The holotype right maxilla (Fig. 6, Table 3) retains all the teeth in moderate wear. The canine is two-rooted with a tall, bucco-lingually compressed main cusp positioned above the gap between the two roots, and low styles mesially and distally. The P1/ is smaller and lower than the canine and is separated from it by a short gap. It has two roots, and the main cusp is above the anterior root. The mesial style is minute, the distal one broader. The P2/ is a larger version of the P1/ and is separated from it by a short gap. It also has two roots and is slightly broader distally than in the middle. The P3/ has three roots, the lingual one supporting a prominent protocone. The paracone is larger and taller than the protocone. The metacone is low and reduced in size, and the hypocone is even smaller and lower. There is no buccal cingulum. The P4/ is molariform with four main cusps, the buccal ones taller than the lingual ones. It has four roots, the lingual ones coalescent. There is no cingulum. The mesial loph is slightly shorter mesio-distally than the distal loph.

The M1/ and M2/ are basically similar in morphology to the P4/ but are slightly smaller than it, the M2/ being smaller than the M1/. In M1/ and M2/, the mesial loph is slightly longer and broader than the distal loph. The metaconule is low and separates the trigon basin from the talon basin. The buccal and lingual sinuses are mesio-distally broad and relatively shallow. The M3/ has three roots and is considerably smaller than the M2/. There are two mesial cusps and a single distal cusp.

The maxilla EC7 1.1a, has the M2/ *in situ*, and preserves the partial alveoli of P4/ and M3/ and complete alveolus of M1/ (Fig. 7). The infraorbital canal is large and emerges onto the face of the maxilla above the P4/. The anterior root of the zygomatic process of the maxilla is in line with the middle of M1/ and its rear is in line with the middle of M2/. The partly preserved alveolus of the P4/ indicates that the tooth was almost as large as the M1/. These features conform to other brachyodont macroscelideans.
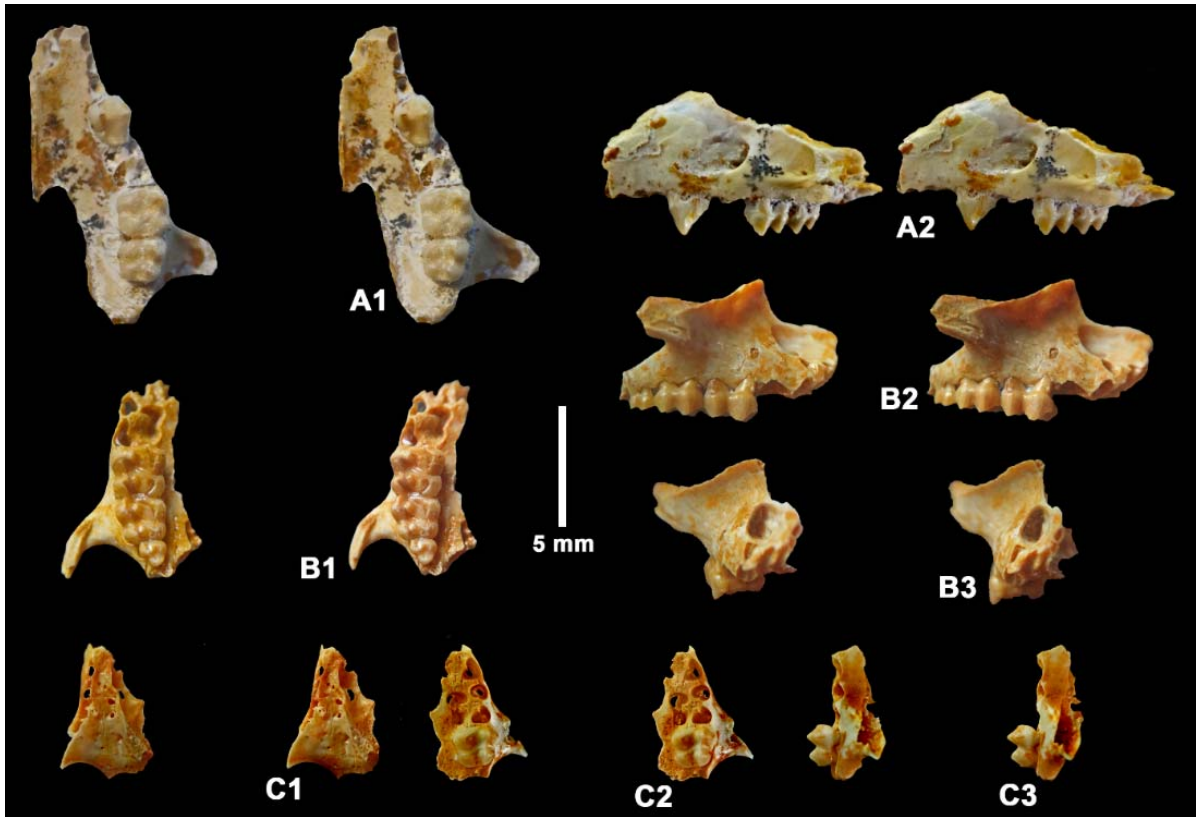
Figure 7. Stereo images of maxillae of *Namasengi mockeae* from Eocliff, Namibia. A) EC8 1.1a, left maxilla with P3/, M1/-M2/, A1 - occlusal view, A2 - lateral view, B) EC9 1.1a, right maxilla with M1/-M3/, B1 - occlusal view, B2 - lateral view, B3 - anterior view, C) EC7 1.1d, left maxilla with M2/, C1 - dorsal view to show the floor of the orbit and the course of the infraorbital canal, C2 - occlusal view, C3 - lateral view (scale : 5 mm).

Table 3. Measurements (in mm) of the teeth in the holotype right maxilla of *Namasengi mockeae*, EC10 1.1a.

Tooth	Mesio-distal length	Bucco-lingual breadth
Upper canine	1.5	0.7
P1/	1.3	0.6
P2/	1.7	0.8
P3/	2.1	1.8
P4/	2.3	2.2
M1/	2.0	1.7
M2/	2.3	1.7
M3/	1.4	1.1
C1/-M3/	14.8	--

The upper molars are tetracuspidate and brachyodont. The protocone has a preprotocrista that reaches the mesial cingulum. It has a slight swelling suggestive of a nascent paraconule. The postprotocrista is directed distally and very slighly buccally, and unlike other macroscelideans, there are no signs of a crista obliqua. The hypocone has a prehypocrista that extends mesio-buccally to terminate at the base of the junction between the paracone and metacone. There is no sign of a metaconule. The lingual sinus is deep and is not blocked off from the trigon basin. The buccal sinus is mesio-distally broad and shallow. The pre- and postcristae of the paracone and metacone are oriented mesio-distally, forming a sharp ectoloph. The parastyle and metastyle are small and about 60% of the height of the crown and there is no mesostyle. The two lingual roots are coalescent near the cervix and for most of their height, but are distinct at their apices. The incomplete alveoli of the P4/ indicate that it was also quadricuspidate and was somewhat smaller than the M1/. The M2/ is smaller than the M1/ while the M3/, of which only part of the alveolus is preserved, was smaller than the M2/ (Table 4).

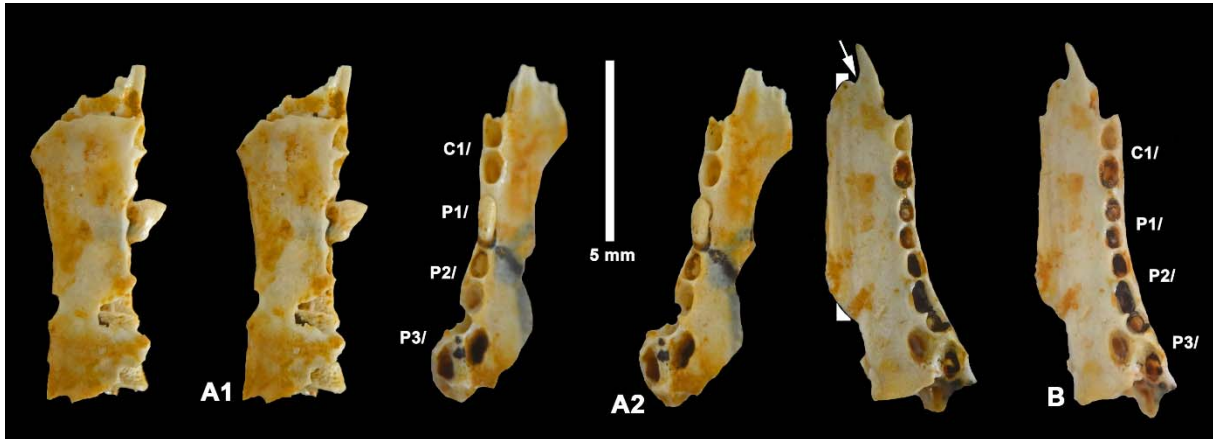Two other maxillae (Fig. 8) show the layout of the cheek tooth alveoli.

Figure 8. Stereo images of maxillae of *Namasengi mockeae* from Eocliff, Namibia. A) EC7 1.1b, right maxilla with P1/, A1 - buccal view, A2 - occlusal view with alveoli labelled, B) EC7 1.1a, edentulous left maxilla, occlusal view with alveoli labelled (white triangles are in line with the canal for the palatal artery, arrow shows part of the incisive foramen invading the maxilla) (scale : 5 mm).

Mandible

The mandible of *Namasengi mockeae* has a steeply oriented ascending ramus, the coronoid process rising some distance behind the rear of the m/3, thereby leaving a substantial retromolar space between the m/3 and the base of the coronoid process. There is no sign of a coronoid foramen in any of the adult specimens. The mandibular condyle is well above the occlusal surface of the cheek teeth, best seen in juvenile mandible EC10 1.2e (Figs 9-13).

In all the available fossils, there are two mental foramina, the anterior one beneath the p/1 and the posterior one beneath the p/4, both of them positioned at half the depth of the mandible. The ventral margin of the mandible is gently convex beneath the tooth row, but its profile becomes gently concave beneath the ascending ramus. The anterior margin of the masseteric fossa on the buccal side of the jaw is well behind the m/3.

In occlusal view the mandible is slender and straight, with no signs of fusion between the two hemi-mandibles. The lower tooth row, measured from the alveolus of i/1 to the rear of m/3 ranges in length from 14.6-17.1 mm (n = 5).

In lingual view of the mandible, the area of insertion of cartilages which held the mandibles together reach distally as far as the p/1. The mandibular foramen is located at the level of the occlusal surface of the cheek teeth. The i/2 is a peg-like tooth with a small heel distally. It is oriented rather procumbently in the mandible.

Figure 9. Stereo images of mandibles of *Namasengi mockeae* from Eocliff, Namibia. A) EC9 1.2f, right mandible with p/3-m/3, A1 - lingual, A2 - occlusal, A3 - buccal views, B) EC9 1.2d, left mandible with m/2, B1 - buccal, B2 - occlusal, B3 - lingual views (arrow shows the mandibular foramen), C) EC9 1.2e, left mandible with m/2, C1 - buccal, C2 - occlusal, C3 - lingual views (scale : 5 mm).

On the basis of the alveoli, the lower canine is a single-rooted tooth. None of the mandibles contains the tooth, but there are many isolated canine-like teeth in the collection. However, because the canines and third incisors can resemble each other, we do not attribute any of the isolated specimens to this species. The p/1 has two roots. The main cusp is positioned above the front of the mesial root and it has a prominent mesial stylid. There is a posterior stylid which rises to about half the height of the main cusp. The p/2 is a larger version of the p/1 with more prominent mesial and distal stylids, the mesial one rising almost as high as the main

cusp, the distal one is lower. The p/3 is larger than the p/2 but is constructed along the same morphological lines, with a tall main cusp, a tall mesial stylid and a lower distal stylid. The p/4 is molariform, the crown comprising two crescentids. The mesial crescentid (trigonid) has a large paraconid antero-lingually, the protoconid on its bucco-distal corner and the metaconid in its disto-lingual corner. The preprotocristid extends mesio-lingually to join the paraconid, and the postprotocristid is directed lingually where it joins the metaconid. The posterior crescentid (talonid) has a small metacristid close to the metaconid, a large

104

hypoconid in the disto-buccal corner and the entoconid on the disto-lingual corner. The prehypocristid is obliquely oriented, running from disto-buccal to mesio-lingual, thereby leaving a broad buccal sinusid between the two crescents. The talonid basin is larger than the trigonid basin.
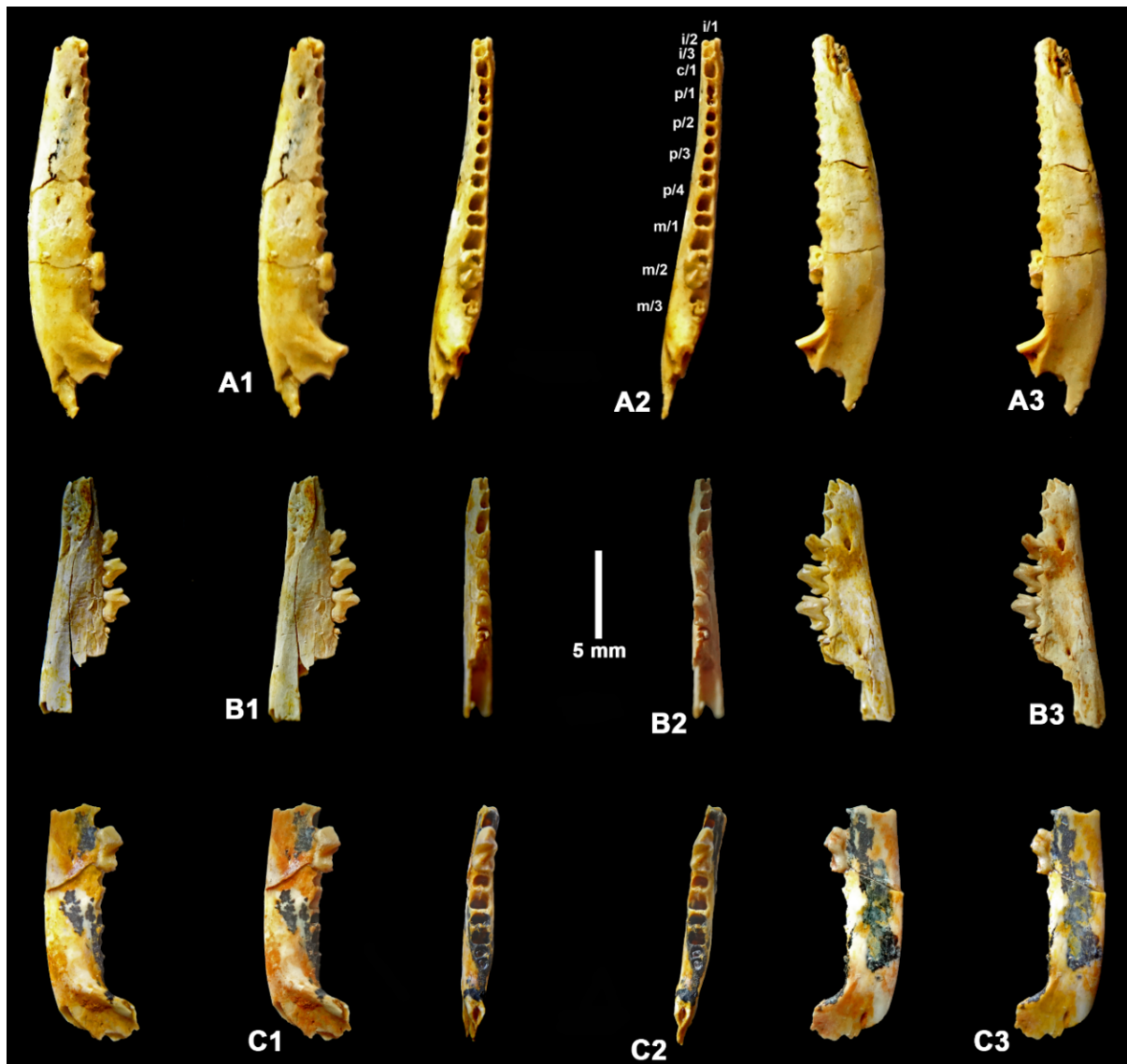
Figure 10. Stereo images of lower jaws of *Namasengi mockeae* from Eocliff, Namibia. A) EC10 1.2b, left mandible with m/2, A - buccal view, A2 - occlusal view with alveoli labelled, A3 - lingual view, B) EC9 1.2k, right mandible with p/1-p/3, B1 - lingual, B2 - occlusal, B3 - buccal views, C) EC9 1.2j, left mandible with p/4, C1 - buccal, C2 - occlusal, C3 - lingual views (scale : 5 mm).

The m/1 and m/2 are comprised of two crescentids, as in the p/4, but the mesial crescentid (trigonid) is more compressed mesio-distally than it is in the p/4. There is a cristid leading mesially from the entoconid, forming a subtle *tuberculum intermedium*. The preprotocristid and prehypocristid extend towards the midline of the crown, but the latter does not reach the metacristid. The postprotocristid and posthypocristid, in contrast, are directed lingually, forming a transverse loph-like structure. The m/3 is much reduced, but has two roots and two small crescentids, the distal one being half the breadth of the mesial one (Fig. 14). Measurements are provided in Table 5.

Figure 11. Stereo images of mandibles of *Namasengi mockeae* from Eocliff, Namibia. A) EC7 1.2b, right mandible with d/4 (p/4 and m/2 in crypt), A1 - occlusal view, A2 - buccal view, B) EC7 1.2c, left mandible with d/3, d/4, m/1 and m/2, B1 - occlusal view, B2 - lingual view, B3 - buccal view, C) EC4 1.2e, left mandible with p/4, occlusal view, D) EC4 1.2d, right mandible fragment with molar in crypt, occlusal view (scale : 5 mm).
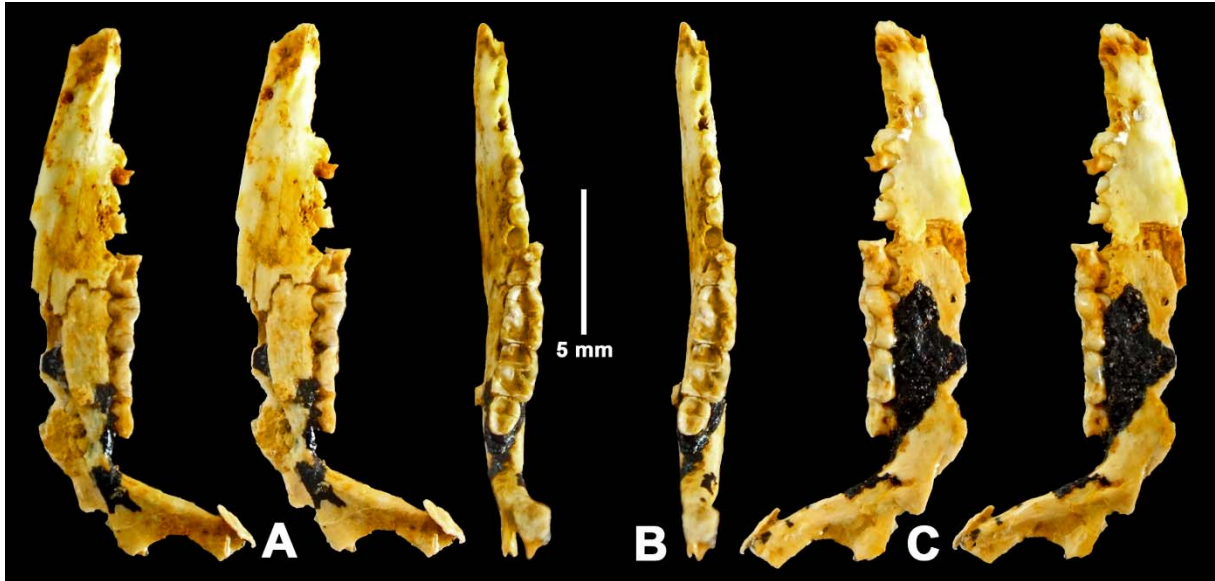
Figure 12. Stereo images of EC7 1.2g, right mandible with p/4-m/3 of *Namasengi mockeae*, A) lingual view B) occlusal view, C) buccal view (scale : 5 mm).
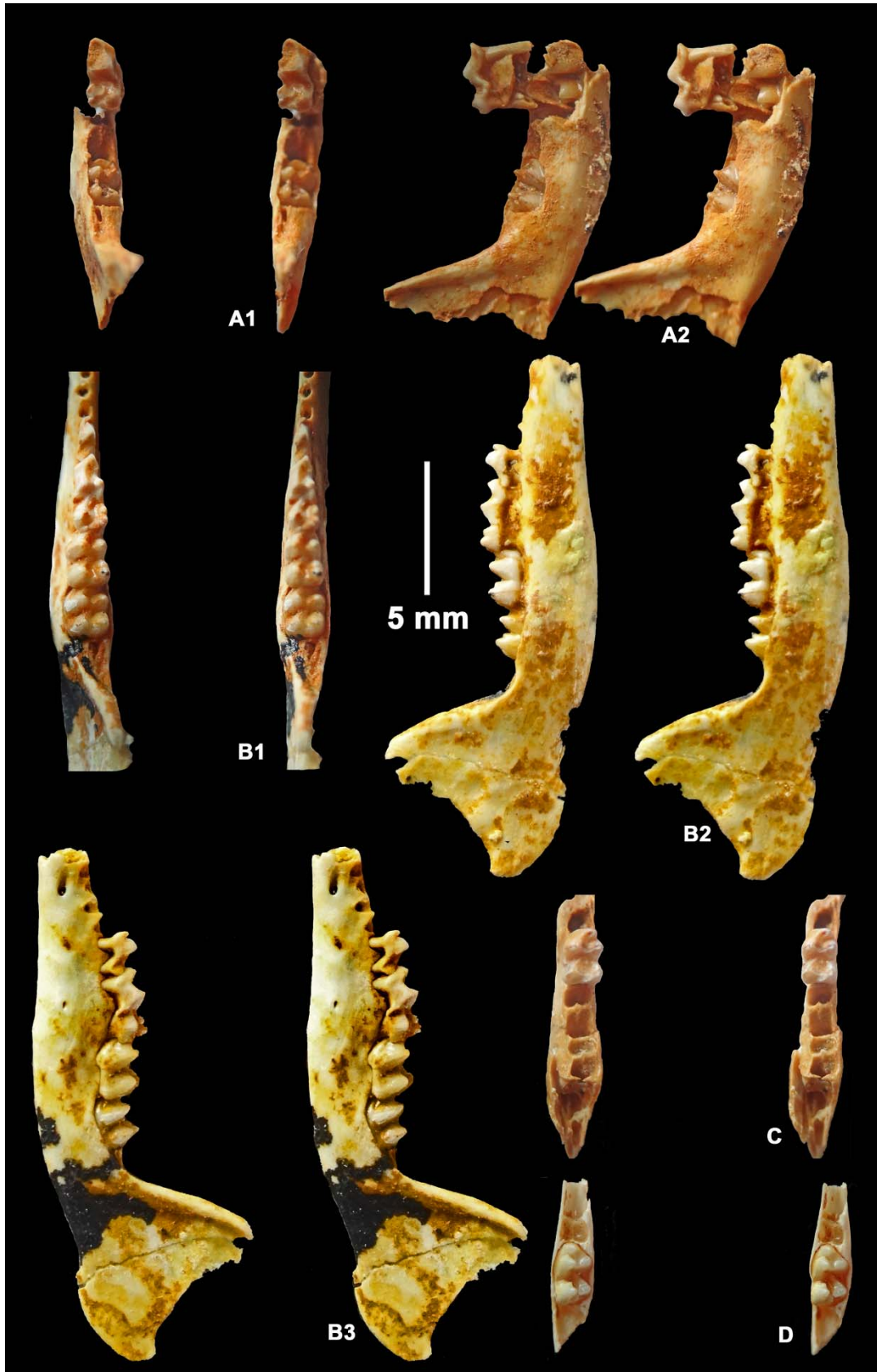

Figure 13. Stereo images of mandibles of *Namasengi mockeae* from Eocliff, Namibia. A) EC9 1.2g, left mandible with m/1 (m/3 in crypt) A1 - occlusal view of mandible, A2 - enlarged occlusal view of m/1, B) EC9 1.2o, right mandible with p/4, m/1, occlusal view, C) EC9 1.2q, left mandible with d/4 (m/1 in crypt), occlusal view (scale : 1 mm).
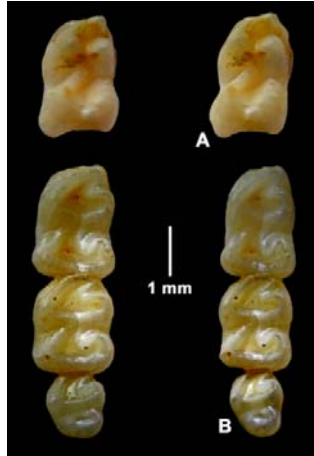
Figure 14. Stereo occlusal views of permanent lower cheek teeth of *Namasengi mockeae* from Eocliff, Namibia. A) EC8 1.2h, left m/1, B) EC10 1.2a, left m/1-m/3 (scale : 1 mm).

Deciduous dentition

The D2/ is tricuspid, with the three cusplets in line with each other and disposed in line with the long axis of the tooth row and it has two roots. The paracone is the largest cusp and is accompanied by a low, small parastyle and a somewhat larger metacone. There is no sign of a cingulum (Fig. 15).

The D3/ has three large cusps, two buccally (paracone, metacone) and one disto-lingually (protocone). The protocone is large but is lower than the paracone and metacone. The hypocone is rudimentary, being just a small swelling at the base of the postprotocrista. The parastyle is low but quite distinct at the mesial end of the preparacrista. There is a minuscule metaconule (sometimes absent) between the anterior cristae of the metacone and protocone, positioned at the rear of the small trigon basin. At the distal end of the postprotocrista there is a low, weak hypocone which is joined to the metastyle by a distal cingulum, which walls off the rear of the large talon basin. On the buccal side of the metacone there is a prominent ectostyle, behind which there is a notch into which the parastyle of the D4/ fits. There are no signs of a buccal cingulum in this tooth.

Figure 15. Stereo occlusal views of upper deciduous teeth of *Namasengi mockeae* from Eocliff, Namibia. A) EC10 1.1i, right D3/, B) EC10 1.1i, right D3/, C) EC10 1.1i, right D4/, D) EC10 1.1h, left D2/-D4/, E) EC10 1.1i, left D3/, F) EC10 1.1i, left D4/, G) EC7 1.1k, right D4/ in fragment of maxilla (scale : 1 mm).

108

The D4/ has four main cusps (protocone, paracone, metacone, hypocone) and three prominent cusplets (parastyle, paraconule (variably developed) and metaconule). The buccal main cusps are slightly taller than the lingual ones. The metaconule is slightly larger than the hypocone and the parastyle is bilaterally inflated and projects strongly mesially. The metastyle is low and is positioned in line with the parastyle, paracone and metacone and projects slightly distally. The postprotocrista (crista obliqua) descends towards the metaconule, but is separated from it by a narrow gap. The lingual and buccal sinuses are mesio-distally broad but shallow. There is no buccal cingulum.

Table 4. Measurements (in mm) of upper teeth of *Namasengi mockeae* from Eocliff, Namibia.

Catalogue	Tooth	Mesio-distal length	Bucco-lingual breadth
EC10 1.1h	D2/ left	2.0	0.6
EC10 1.1h	D3/ left	2.6	1.8
EC10 1.1h	D4/ left	2.8	2.1
EC4 1.1e	M1/ left	1.6	1.5
EC7 1.1f	M2/ left	1.9	2.0
EC7 1.1d	M2/ left	1.8	2.0

Figure 16. Stereo images of juvenile mandibles of *Namasengi mockeae* from Eocliff, Namibia. A) EC10 I.2e, left mandible with d/4, A1 - buccal, A2 - occlusal, A3 - lingual views, B) EC10 1.2f, right mandible with d/4, B1 - buccal, B2 - occlusal, B3 - lingual views (scale : 5 mm).
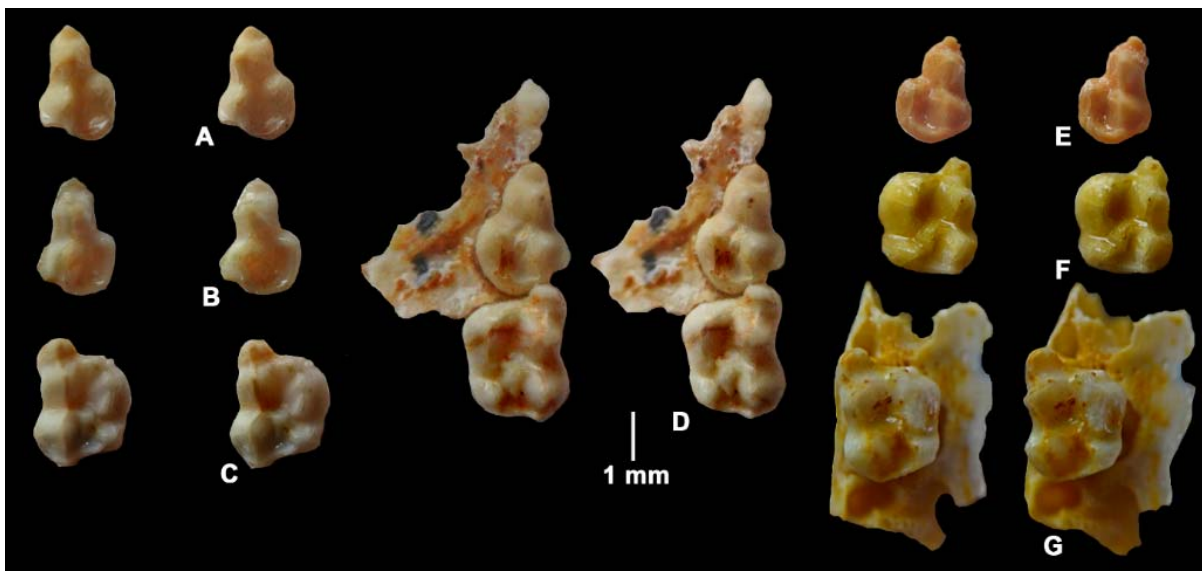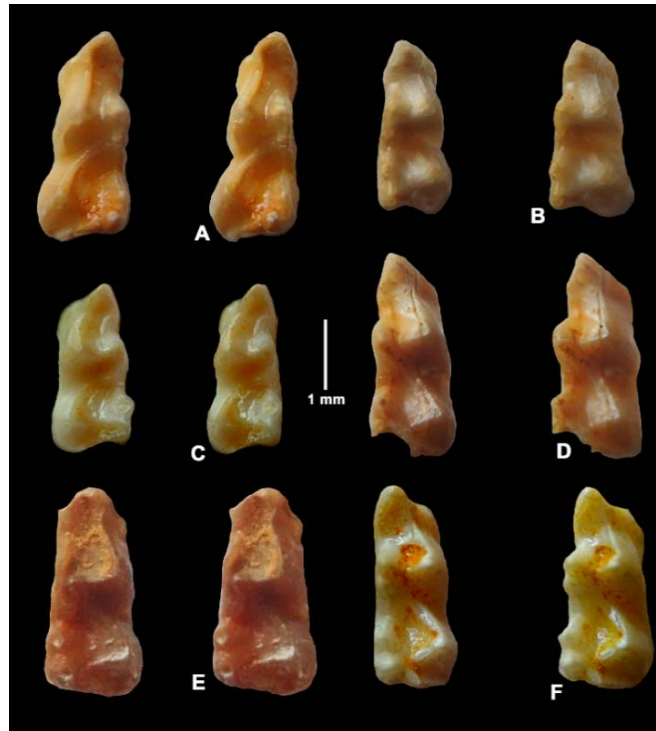
Figure 17. Stereo occlusal views of lower deciduous teeth of *Namasengi mockeae* from Eocliff, Namibia. A) EC9 1.2s, left d/4, B) EC9 1.2t, right d/4, C) EC8 1.2e, left d/4, D) EC9 1.2r, right d/4, E), EC6 1.2h, right d/4, F) EC7 1.2m, right d/4 (scale : 1 mm).

Figure 18. Stereo occlusal views of d/4s of *Namasengi mockeae* from Eocliff, Namibia. A) EC10 1.2e, left d/4, B) EC10 1.2f, right d/4 (scale : 1 mm).

There are several deciduous lower fourth molars from Eocliff, some of which are in mandibles (Figs 16-18). The mesial and distal roots are splayed apart mesially and distally, as is usual in mammalian deciduous teeth. One mandible has the d/4 in occlusion with the p/4 exposed beneath it (Fig. 11A). The mesial half of the crown of d/4 is slightly narrower than the distal half. The paraconid, protoconid and metaconid are arranged in a bucco-lingually compressed triangle, as are the metastylid, hypoconid and entoconid in the distal

crescentid. The paraconid is prominent and pointed, bordered on its buccal side by a precingulid. The metaconid is accompanied distally by a prominent, tall metastylid, slightly distinct at the apex. The protoconid is tall and robust with a long precristid extending towards the paraconid, and a short postcristid reaching lingually towards the metaconid. The prehypocristid descends obliquely mesio-lingually towards the base of the metastylid. The entoconid is small but is accompanied anteriorly by a *tuberculum intermedium* and

buccally by the postcingulid. The trigonid basin is slightly smaller than the talonid basin.

In specimen EC7 1.2c, a left mandible with d/3, d/4, m/1 and m/2, the d/3 is submolariform with a narrow mesial half and a broader distal half (Fig. 11B).

Dental specimens tentatively referred to Namasengi mockeae

There are several denticulate incisiform teeth from Eocliff, some of which probably belong to *Namasengi mockeae* (Figs 19, 20). However, none are *in situ* in mandibles or premaxillae, so there remains doubt about their taxonomic appurtenance and their meristic positions. On the basis of comparisons with extant macroscelidids, these incisors are most likely from the lower jaw, and some of them are likely to be deciduous.

In brief, these incisiform teeth are single-rooted with somewhat spatulate crowns which have from three to seven denticulations along the apical edge.
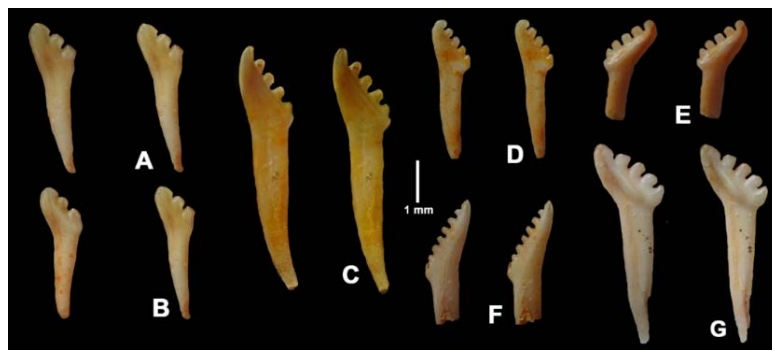
Figure 19. Stereo lingual views of denticulate incisiform teeth provisionally referred to *Namasengi mockeae* from Eocliff, Namibia. A-E) EC10 1.3a. A) three tined form, B) three-tined form, C) six-tined form, D) five-tined form, E) six-tined form, F) seven-tined from, G) EC14 1.2a, five-tined form (scale : 1 mm).
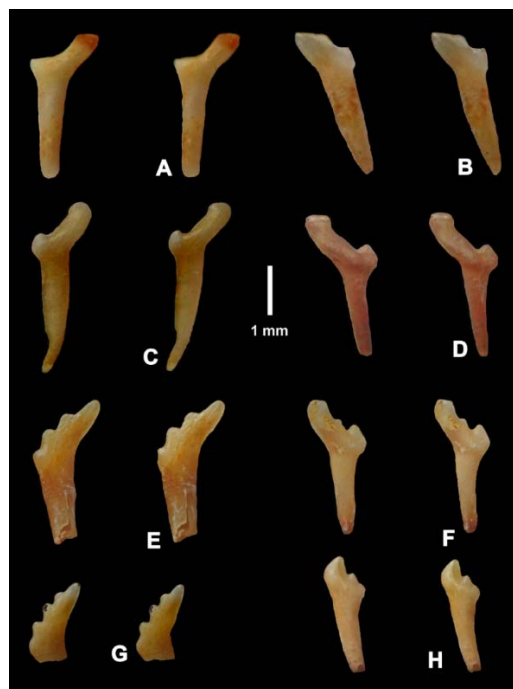
Figure 20. Stereo side views of lower canines and/or i/3s from Eocliff, Namibia, provisionally attributed to *Namasengi mockeae*. A-F) EC10 1.3d, G-H) EC10 1.3a (scale : 1 mm).

There are several isolated teeth from Eocliff that could represent lower canines or i/3s of this species, but so far none have been found *in situ* in mandibles. The teeth are single-rooted, with a crown that is canted mesially with respect to the root such that the mesial end of the tooth would be positioned rather far in front of its alveolus. The teeth have a prominent distal heel which rises occlusally, and there is a similar cusplet at the mesial end of the crown. One specimen has a small cusplet in the middle of the crown, slightly lower than the mesial and distal cusplets. One specimen has four cusplets apically.

Table 5. Measurements (in mm) of lower teeth of *Namasengi mockeae* from Eocliff, Namibia.

| Catalogue	Tooth	Mesio-distal length	Bucco-lingual breadth
EC7 1.2c	d/4 left	3.0	1.3
EC10 1.2e	d/4 left	2.9	1.2
EC10 1.2f	d/4 right	3.0	1.4
EC9 1.2s	d/4 right	2.9	1.1
EC9 1.2u	d/4 right	2.8	1.2
EC9 1.2q	d/4 left	3.0	1.3
EC9 1.2r	d/4 left	3.1	1.3
EC9 1.2t	d/4 left	2.7	1.3
EC9 1.2k	p/1 right	1.2	0.4
EC9 1.2k	p/2 right	1.4	0.6
EC9 1.2k	p/3 right	2.0	0.8
EC9 1.2o	p/4 right	2.3	1.1
EC9 1.2d	m/2 left	2.1	1.7
EC9 1.2e	m/2 left	1.9	1.7

Discussion

Namasengi mockeae is extremely common at Eocliff, being represented by hundreds of cranio-dental and post-cranial elements. The dimensions of the maxilla and mandibles indicate that it was slightly smaller than the smallest known extant macro-scelideans. Many of the fossils attributed to this species represent juveniles in which the deciduous dentition was still in occlusion, or even in the process of erupting, and the distal epiphysis of the tibio-fibula was unfused to the diaphysis (see below, the section on post-cranial skeleton). The diaphyses of the tibia and fibula are strongly synostosed even at this juvenile stage of development, the fusion extending over ca 66% of the length of the bone, as in extant macroscelideans in general. These observations indicate that the Eocliff forms were already fully adapted to a micro-cursorial locomotor mode.

Family Myohyracidae Andrews, 1914

Genus *Promyohyrax* nov.

Type species :- *Promyohyrax namibiensis* nov.

Diagnosis :- A genus of macrosclidean intermediate in dimensions between *Nasilio* and *Petrodromus* (i/1-m/3 measures 20.5 mm); semi-hypsodont cheek teeth, thick molar enamel; well-developed paraconule and metaconule in upper molars closing off deep fossettes distinct from the trigon and talon basins; deep, slit-like lingual sinus connecting to the trigon basin; robust, shallow mandible; strongly developed roots in the molars and premolars; large infra-orbital foramen (canal) associated with a prominent facial fossa; spatulate and pectinate upper central incisors, single-rooted upper canine, i/2 with distal heel; d/4 with well-developed entoconid complex comprising large, cusp-like *tuberculum intermedium*, large entoconid and cusp-like post-cingulid; upper and lower dental formula is three incisors, one canine, four premolars and three molars; ascending ramus of mandible steeply oriented.

Differential diagnosis :- *Promyohyrax* differs from *Myohyrax* and *Protypotheroides* by the less developed degree of hypsodonty in the cheek teeth, the presence of three roots in the

M3/ (two in *Protypotheroides*, one in *Myohyrax* (Patterson, 1965)), the presence of a large infra-orbital canal which opens onto the face of the maxilla low down (above the roots of the P4/), the presence of a facial fossa associated with the infra-orbital canal, and the shallower, broader,

more robust mandible. It differs from *Afrohypselodontus* by its lower crowned, rooted teeth. It differs from *Eorhynchocyon* by possessing a steeper ascending ramus of the mandible and the m/3 is not suppressed.

Etymology :- *Pro* for 'primitive' or 'before', with the suffix *myohyrax* for the well-known genus of Neogene hypsodont macroscelidids.

Species *Promyohyrax namibiensis* nov.

Diagnosis :- as for the genus.

Type locality and age :- Eocliff 9, Namibia, Bartonian-Priabionian.

Etymology :- The species epithet refers to the country, Namibia.

Holotype :- EC9 2.1h, right maxilla containing M1/ and M2/ and preserving the alveoli of P4/ and M3/ (Fig. 21A, Table 6).

Synonymy :- Macroscelididae hypsodont form related to *Myohyrax*, in Pickford, 2015a (figs 46A, C).

Description

The holotype right maxilla is preserved from the middle of the alveolus of the P4/ to the M3/ (Fig. 21). The palatine is partly preserved, the anterior part diverging away from the alveolar process of the maxilla at the level of the middle of M2/. The palatine has no signs of fenestration. The alveolus of the P4/ indicates that it was as large as the M1/, whereas the alveoli of the M3/ reveal that it was extremely reduced in size. The root of the zygomatic process of the maxilla is located opposite the middle of M1/ and M2/ and it sweeps rearwards at a shallow angle as a slender sliver of bone. Its lateral surface is marked by sutural ridges where the zygomatic bone articulated with it. The anterior and ventral margin of the orbit was

comprised of the zygomatic bone, which is absent, but leaving a narrow groove in the maxilla to reveal its extent.

In dorsal view the infra-orbital canal traverses the floor of the orbit to emerge onto the facial surface of the maxilla above the anterior roots of P4/. The floor of the orbit is traversed by numerous pin-hole foramina. In lateral and anterior views the infra-orbital foramen is seen to be large and to be associated with a capacious facial fossa. In the edentulous maxilla EC7 2.1b, the infra-orbital foramen is partly preserved above the roots of P4/ and it emerges into a facial fossa that fades out anteriorly.
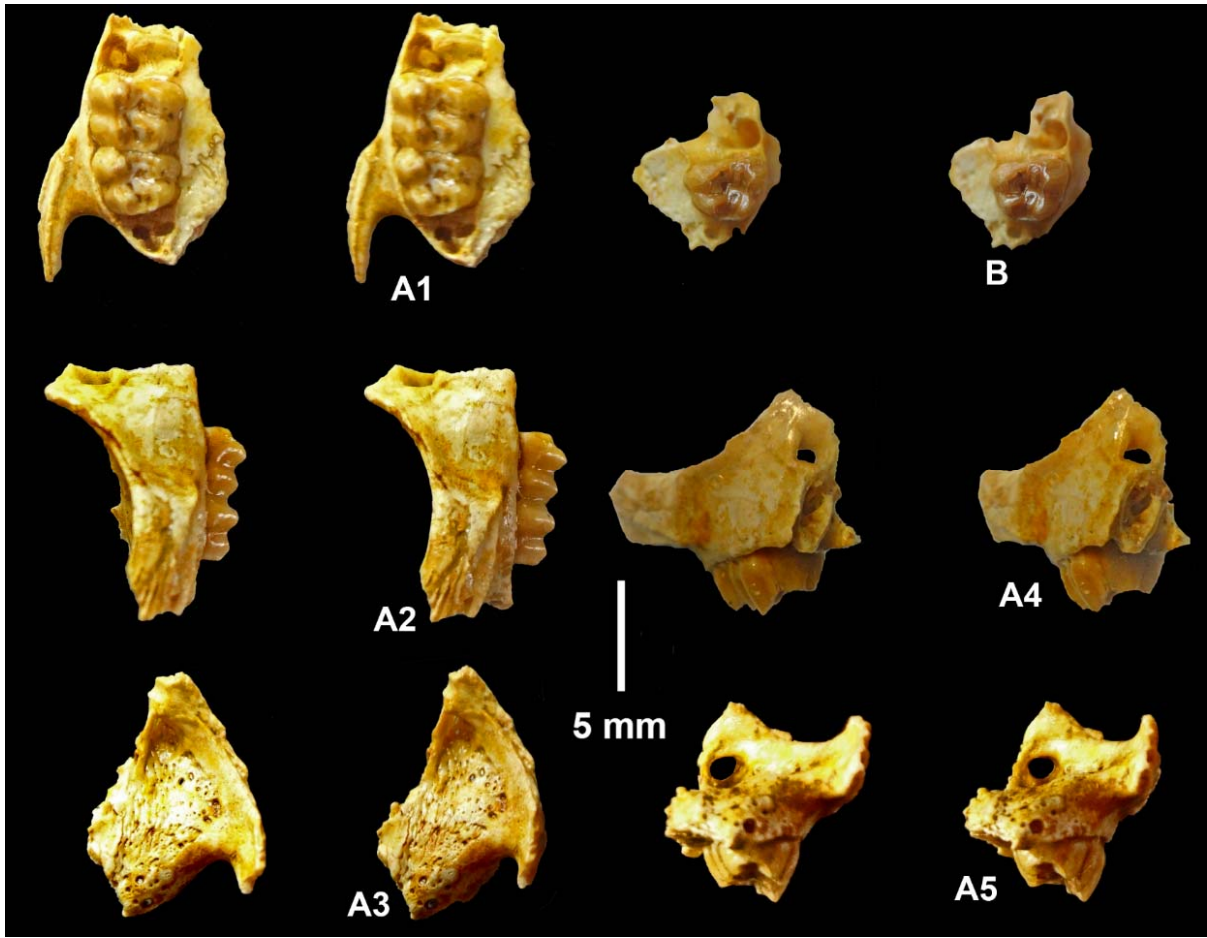
Figure 21. Stereo images of *Promyohyrax namibiensis* from Eocliff, Namibia. A) EC 9 2.1h, holotype right maxilla containing M1/-M2/ and alveoli of P4/ and M3/, A1- occlusal view, A2 - lateral view, A3 - dorsal view, A4 - anterior view, A5 - posterior view, B) EC9 2.1a, left maxilla with M2/, occlusal view (associated with 'A' and possibly representing the same individual) (scale : 5 mm).
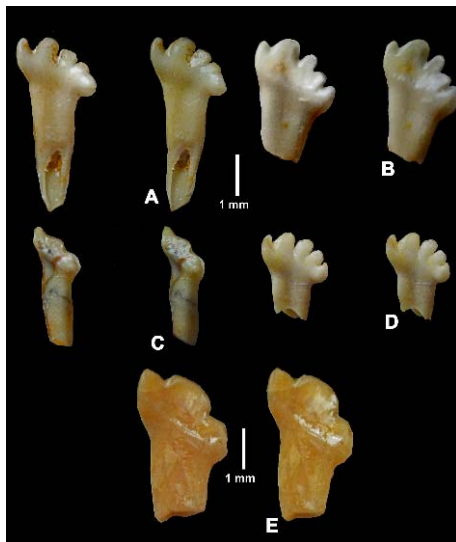
Figure 22. EC10 2.1g, stereo lingual views of incisors attributed to *Promyohyrax namibiensis* from Eocliff, Namibia. A, B, D) probably deciduous upper left central incisors, C) lower canine or p/1, E) upper left central incisor (scale : 1 mm).

Several upper incisors from Eocliff are attributed to *Promyohyrax namibiensis*, although none has been found *in situ* in premaxillae (Fig. 22). A possible permanent I1/ has a spatulate crown with three broad tines, tilted slightly distally. The lingual surface is shallowly concave. Three specimens are interpreted to be deciduous central incisors because their enamel is white instead of brown and they possess five tines, and are slightly smaller than the permanent counterpart. A possible lower canine or p/1 has the crown canted mesially on the root and its crown shows three apical swellings.
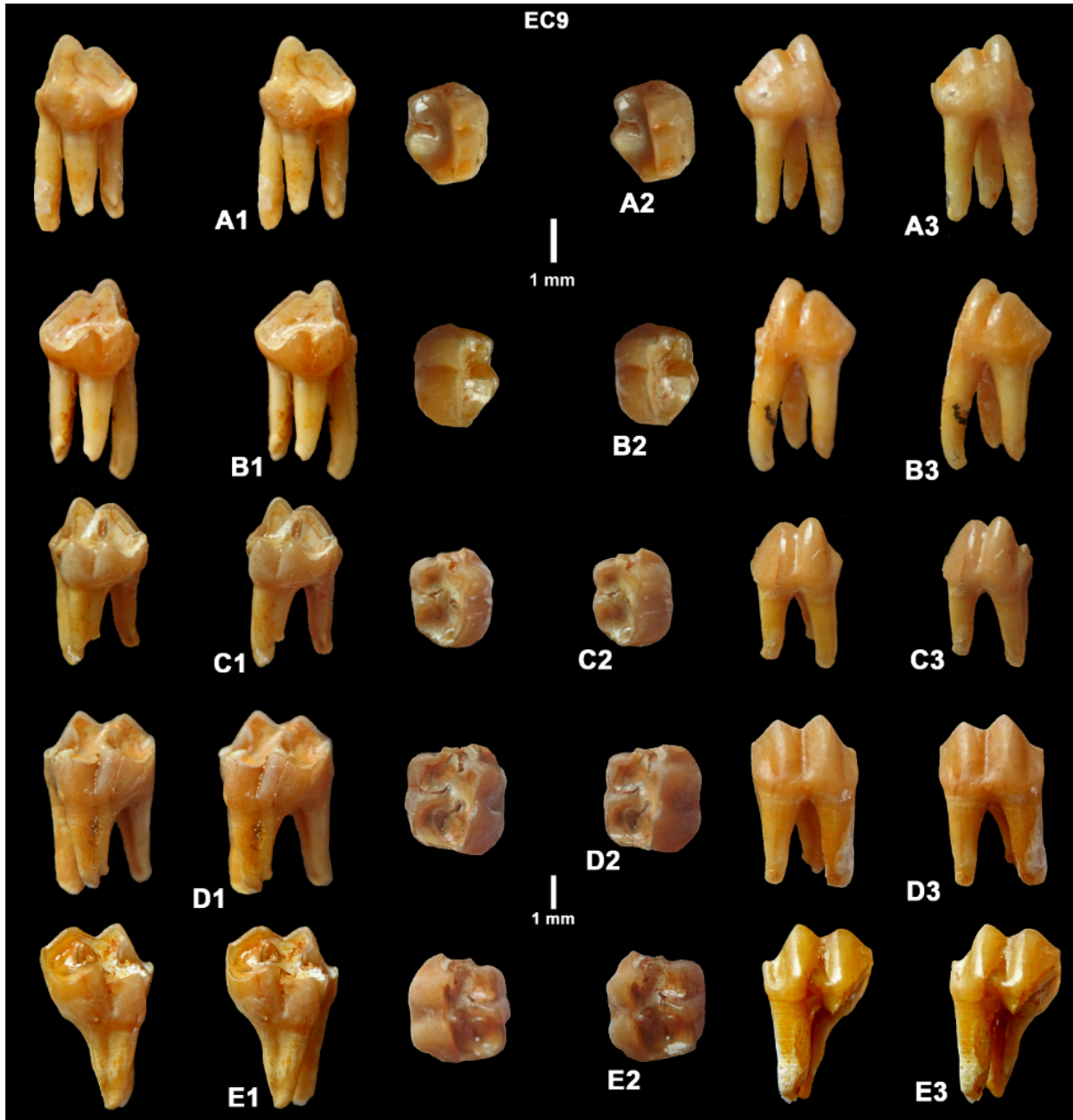
Figure 23. EC9 2.1, stereo images of upper premolars of *Promyohyrax namibiensis* from Eocliff, Namibia. A) left P3/, B) right P3/, C) left P3/, D) left P4/, E) right P4/ (1 - lingual, 2 - occlusal, 3 - buccal views) (scale :1 mm).

The upper third premolars possess three roots, two cylindrical ones on the buccal side supporting the paracone and metacone, and a bucco-lingually compressed 8-shaped root lingually supporting the protocone and hypocone (Fig. 23). The lingual root occasionally shows a sulcus on its lingual aspect indicating incipient development of a second root which is coalescent with the main one. The crown consists of a well-developed, tall ectoloph comprised of a tall paracone and a slightly lower metacone with low, small parastyle and metastyle. The buccal sinus is mesio-distally broad near the apex, but fades out towards the cervix. The lingual half of the crown consists of two low lingual cusps, a mesio-distally short protoconal part and a longer hypoconal part, separated from each other by a narrow but deep lingual sinus. The trigon and talon basins are shallow and disappear with moderate wear.

The P4/ possesses three roots, but in contrast to the P3/, the lingual root has a clear 8-shaped section, with the large part beneath the protocone and the smaller part beneath the hypocone (Fig. 23). The crown is molarised with sub-equal paracone and metacone forming the ectoloph accompanied by clear parastyle and metastyle which are tall but terminate below the level of the main cusps. The buccal sinus reaches almost to the cervix and there are shallow sulci between the paracone and parastyle mesially, and the metastyle and metacone distally. The lingual cusps are lower than the buccal ones, and the protocone is smaller than the hypocone, the two being separated by a deep but narrow lingual sinus that is slightly mesial to the buccal sinus. The trigon and talon basins are moderately deep and they are accompanied by fossettes between the parastyle and paraconule mesially, and the metaconule and premetacrista in the middle of the crown. The enamel of the P4/ is relatively thick. Measurements of the teeth are provided in Table 6.
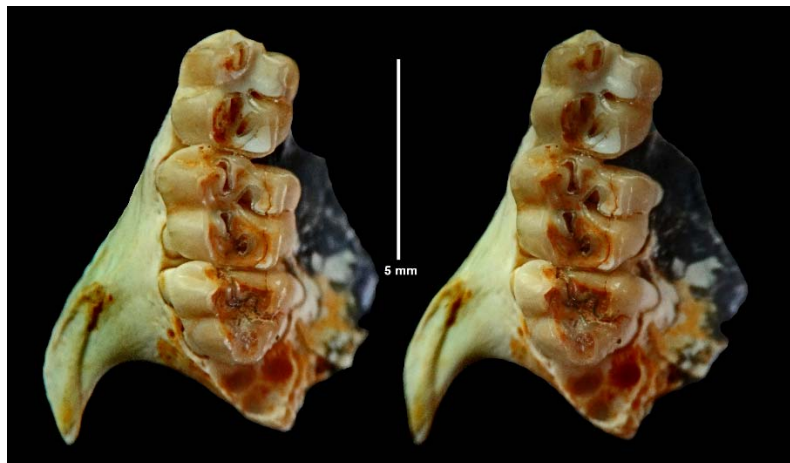
**Figure 24** Stereo occlusal view of EC7 2.1a, right maxilla of *Promyohyrax namibiensis* from Eocliff, Namibia containing P4/, M1/-M2/ and alveoli of M3/ (scale : 5 mm).

The M1/ is broader than the P4/. The M1/ and M2/ are similar in morphology, although the M2/ is smaller than the M1/ and is more trapezoidal in occlusal outline than the almost square outline of the M1/, its distal loph being narrower than the mesial one (Fig. 24). There are four main cusps (paracone, protocone, metacone and hypocone) plus well-developed paraconule and metaconule. There are no signs of buccal cingula in the upper cheek teeth. The trigon basin is small but deep and is connected to the lingual sinus which is narrow and deep, thereby forming an anterior fossette which opens lingually. The talon basin is small and deep, forming a posterior fossette. In addition, there are small but deep fossettes between the paracone and paraconule, and between the metacone and metaconule. The parastyle and metastyle are small, and there is no mesostyle. The enamel in the cheek teeth is thick, and this has contributed to the reduction of the dimensions of the occlusal basins, which, as a result, resemble fossettes rather than basins. There are four roots, the two lingual ones being connected to each other.

The P4/ (EC7 2.1g, germ) is comprised of two lophs, a short one anteriorly and a larger one posteriorly (Fig. 26C). The mesial loph is

slightly narrower than the distal one. The mesial loph is comprised of the protocone and paracone which are accompanied by well-developed parastyle and paraconule between which is a small but deep fossette. The trigon basin is small and is connected to the lingual sinus by a deep, narrow slit. The posterior loph is comprised of the metacone and hypocone, which are accompanied by a prominent metaconule. There is a small but deep fossette between the premetacrista and the metaconule, and the talon basin forms an additional fossette between the metacone, metaconule and hypocone.

A germ of a right M2/ (EC 9 2.1d) shows the layout of the cusps and fossettes clearly (Fig. 26B). The tooth is comprised of two lophs, the distal one narrower than the mesial one. The paracone and metacone are larger and taller than the protocone and hypocone. The parastyle is prominent and it projects a short distance mesially. The paraconule is well developed and between it, the parastyle and the paracone, there is a narrow but deep fossette. The protocone is separated from the paracone by the trigon basin, in the form of a deep fossette which is connected to the narrow but deep lingual sinus. The metacone is smaller than the paracone and the hypocone is even smaller, and between them there is a well-formed metaconule. Between the buccal side of the metaconule and the lingual side of the premetacrista, there is a small but deep fossette. The talon basin is small and fossette-like and is located between the hypocone and metacone. The metastyle is clearly expressed but is low and joined to the post-hypocrista by the cingulum-like distal margin of the tooth. There are no signs of buccal cingula in the upper cheek teeth. The lingual and buccal sides of the upper molars flare moderately from cusp apex to cervix.
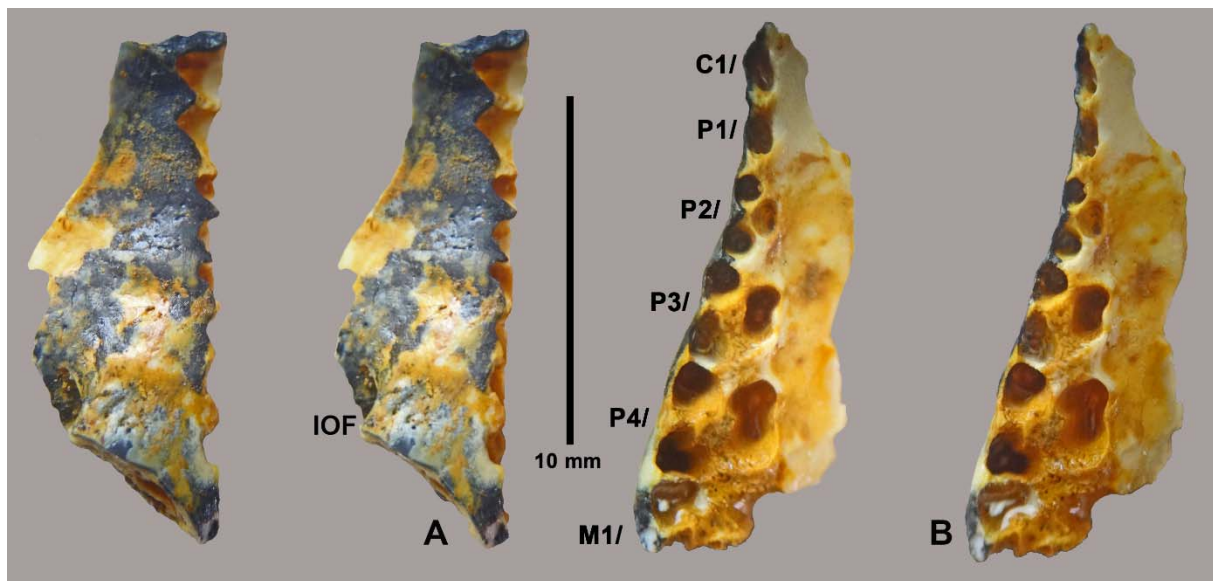
Figure 25. Stereo images of EC7 2.1b, edentulous right maxilla of *Promyohyrax namibiensis* to show the morphology of the cheek tooth alveoli and the facial surface of the maxilla. A) lateral view (IOF - infra-orbital foramen), B) occlusal view with alveoli labelled (scale : 10 mm).

Specimen EC7 2.1b is informative about the layout of the roots of the maxillary teeth (Fig. 25). The canine alveolus is single with a bilaterally compressed oval outline. The alveolus of the P1/ is smaller than that of the canine, but of similar compressed outline. There is a short gap between the alveoli of the P1/ and P2/. The latter tooth has three roots, two buccally with circular outlines and one lingually with a bucco-lingually compressed oval outline. The P3/ has three alveoli, two buccally which are circular in outline and one lingually which is comprised of two coalescent parts forming an 8-shaped outline. The P4/ alveoli are like those of the P3/ but are larger. Only the anterior alveoli of the M1/ are preserved and they also show that the two lingual roots were joined to each other.

117
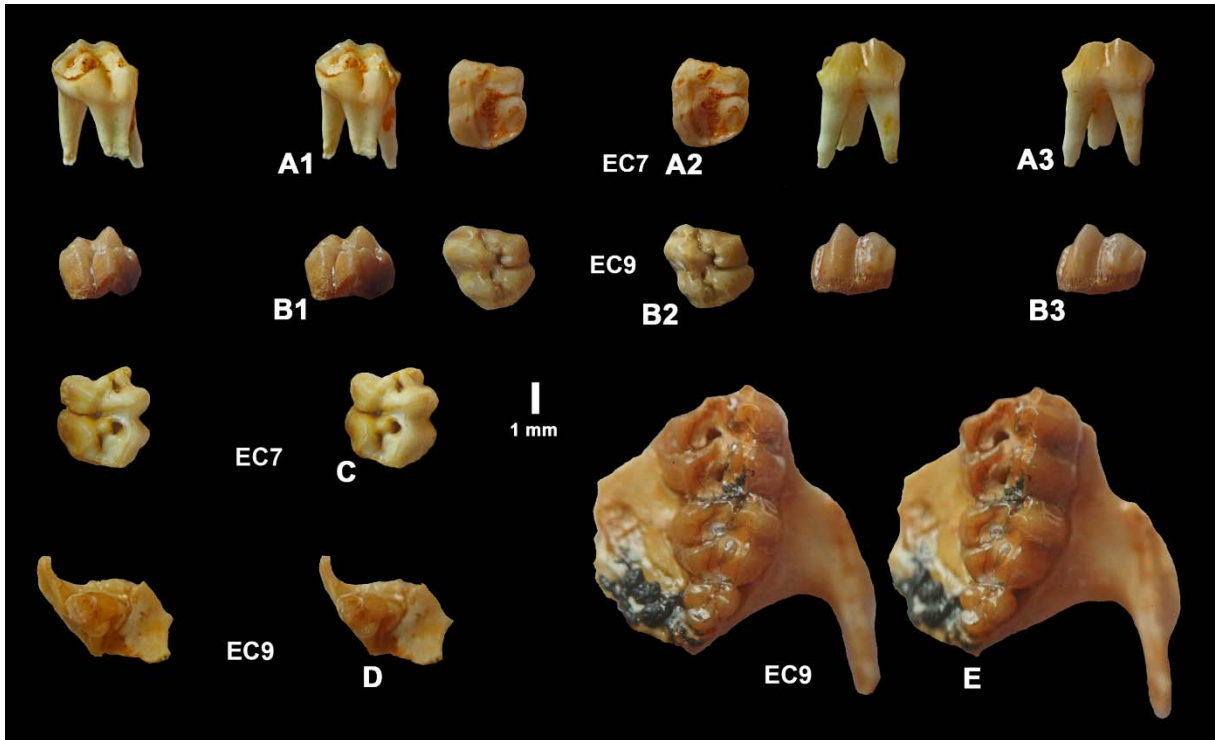
Figure 26. Stereo images of upper teeth of *Promyohyrax namibiensis* from Eocliff, Namibia. A) EC7 2.1f, right P4/, A1 - lingual view, A2 - occlusal view, A3 - buccal view, B) EC9 2.1d, germ of right M2/, B1 - lingual view, B2 - occlusal view, B3 - buccal view, C) EC7 2.1g, germ of left P4/, occlusal view, D) EC9 2.1b, right maxilla fragment with M3/, occlusal view, E) EC9 2.1h, left maxilla with M1/-M3/, occlusal view (scale : 1 mm).
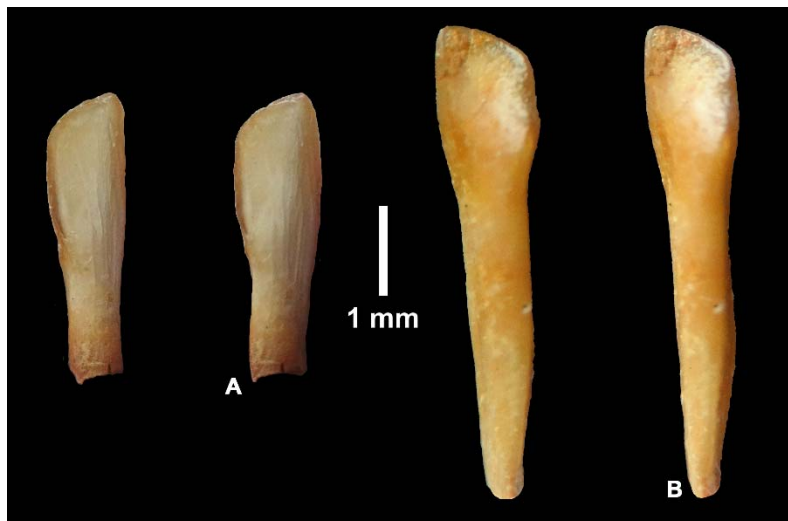
Figure 27. Stereo lingual views of lower central incisors attributed to *Promyohyrax namibiensis* from Eocliff, Nambia. A) EC9 3.2e, left i/1, B) EC6 3.3, right i/1 (scale : 1 mm).

The first lower incisors possess elongated roots and relatively low crowns (Fig. 27). The lingual side of the crown of the i/1 is shallowly concave and appears to lack an enamel cover, and there is no sign of sulci or ornamentation of the crown.

118
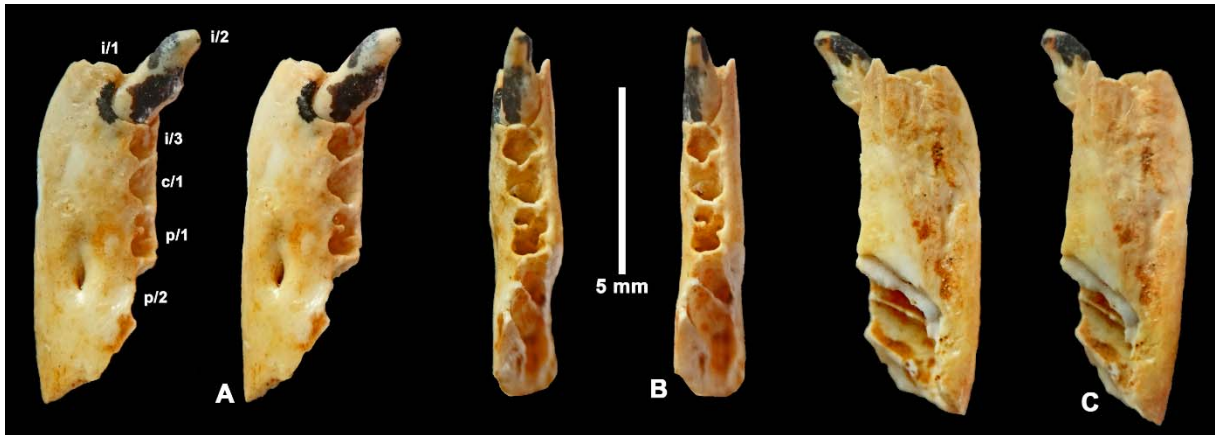
Figure 28. Stereo images of EC7 2.2l, left mandible fragment with i/2 of *Promyohyrax namibiensis*, A) buccal view with alveoli labelled, B) occlusal view, C) lingual view (scale : 5 mm).

One of the mandibles from Eocliff 7 (EC7 2.2l) retains the left i/2 (Fig. 28). The tooth is canted at an angle of ca 45° relative to the occlusal surface, and it has an elongated root and a moderately tall crown which is conical save for a swelling distally resembling a heel.
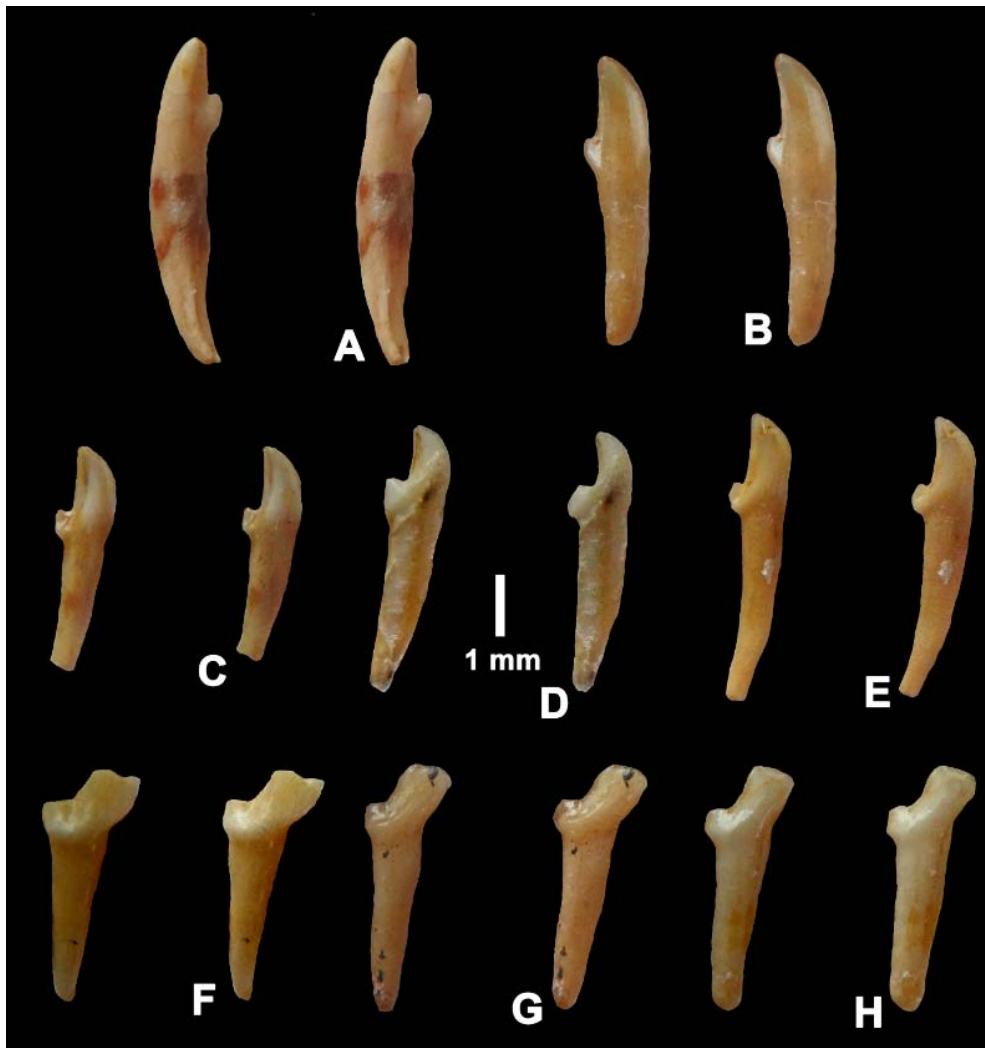
Figure 29. EC10 2.2j, A-E) stereo views of i/2, F-H) i/3 or canines attributed to *Promyohyrax namibiensis* from Eocliff, Namibia (scale : 1 mm).

Several isolated lower incisors are attributed to *Promyohyrax namibiensis* (Fig. 29). The root is elongated and the crown conical with a distinct, pointed distal cusp or heel. These teeth could represent i/2s, but until one is found *in situ* in a mandible, there will remain some doubt about their meristic positions. A second kind of incisiform tooth is common in the collections and comprises a crown that is canted on the root, thereby partly overlapping the tooth mesial to it. The main cusp is thus mesial to the root, and is accompanied by a small but tall mesial stylid, and a lower distal cusp. The root is long and cylindrical, tapering apically. These teeth could be i/3s or lower canines (Figs 29F-H).

Figure 30. Stereo views of EC9 2.2a, right mandible with unerupted m/3 of *Promyohyrax namibiensis* from Eocliff, Namibia. A) lingual view, B) occlusal view with alveoli labelled (arrows show the tiny remnants of the distal alveoli of the d/4), C) buccal view (scale : 5 mm).

A mandible from EC9 has the m/3 in its crypt, but the other teeth are absent (Fig. 30). An interesting aspect of this specimen is that the alveoli of the p/4 are fully formed, yet show the remnants of the posterior roots of the d/4 just behind the distal alveoli of the p/4. This conformation indicates that the d/4 was retained in the jaw even when the p/4 was almost fully erupted, the m/1 and m/2 had erupted and had developed their roots and the m/3 was still in its crypt.

In occlusal view, the tooth-bearing part of mandibles of *Promyohyrax namibiensis* is straight, but the ascending ramus diverges laterally at a low angle. In lateral view the body of the mandible is convex ventrally, but becomes gently concave beneath the ascending ramus. The anterior pole of the masseteric fossa is in line with the distal part of the m/3. There is a foramen beneath the p/4, located at about half the depth of the body of the mandible and another beneath the p/1.

The most complete mandible of this species indicates that there were three incisors, a canine, four premolars and three molars. Measurements of the teeth are provided in Table 7.

120
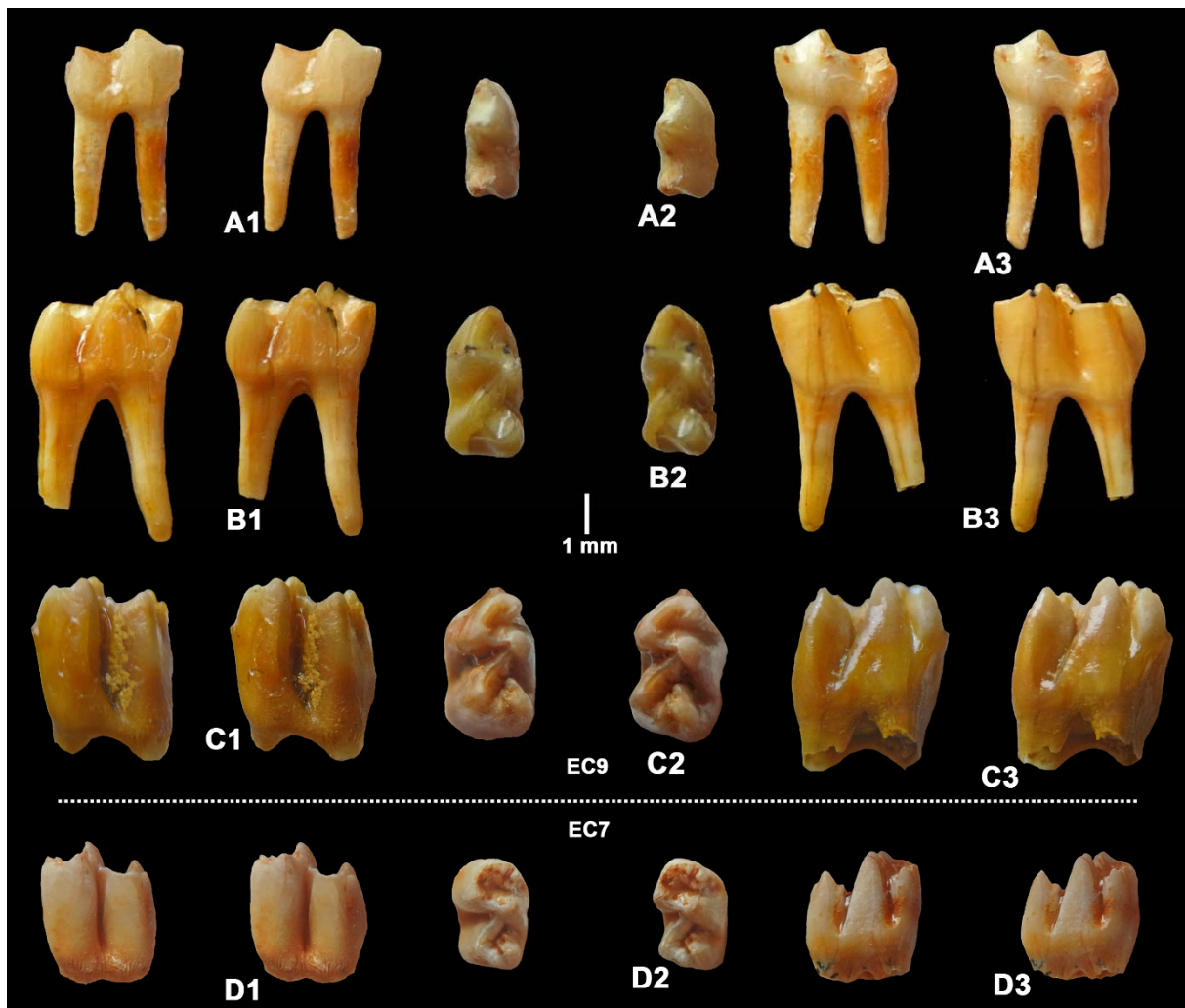
Figure 31. Stereo images of lower cheek teeth of *Promyohyrax namibiensis* from Eocliff, Namibia. A) EC9 2.2d, right p/3, A1 - buccal, A2 - occlusal, A3 - lingual views, B) EC9 2.2e, left p/4, B1 - lingual, B2 - occlusal, B3 - buccal views, C) EC9 2.2f, left m/1, C1 - buccal, C2 - occlusal, C3 - lingual views, D) EC7 2.2j, left m/2, D1 - buccal, D2 - occlusal, D3 - lingual views (scale : 1 mm).

The lower p/3 of *Promyohyrax namibiensis* is comprised of two crescentids, the anterior one smaller than the posterior one (Fig. 31a). The paraconid is mesio-lingually positioned and is joined to the protoconid by the preprotocristid. The metaconid and protoconid are close together without obvious signs of being two separate cusps. The distal crescentid is almost as tall as the mesial one, and comprises a hypoconid in the midline from which the prehypocristid extends mesio-lingually towards the base of the metastylid. The distal part of the hypoconid is swollen bilaterally, but does not produce separate cusplets. The entoconid is small and lower than the hypoconid. The trigonid basin is shallow and wide open lingually, as is the talonid basin. The buccal sinusid is mesio-distally broad and slightly mesially tilted, and fades out towards the cervix.

The p/4 is formed of two clear crescentids, each with a V-shaped buccal edge (Figs 31B, 32). The mesial crescentid is comprised of a mesio-lingually positioned paraconid, a disto-buccal protoconid and a lingually positioned metaconid which is clearly separated from the protoconid. The distal crescentid is comprised of a mesio-lingually positioned metastylid which is close to the metaconid, a disto-buccally positioned hypoconid and a distinct entoconid in the disto-lingual corner of the crown. The cristids between the main cusps are tall and sharp. The buccal sinusid is deep and broad apically and is tilted somewhat mesially, and basally it almost reaches the cervix. The trigonid and talonid basins open lingually. The two roots are tall and slender and are well separated from each other at cervix.
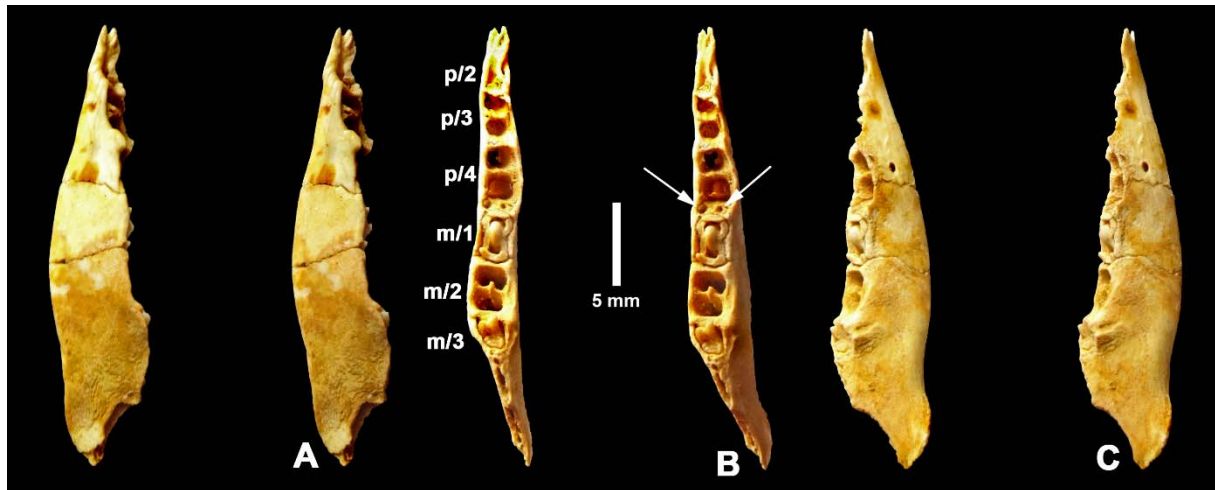
121

Figure 32. Stereo views of EC7 2.2c, left mandible fragment with p/4 of *Promyohyrax namibiensis* from Eocliff, Namibia. A) buccal view, B) occlusal view, C) lingual view (scale : 5 mm).
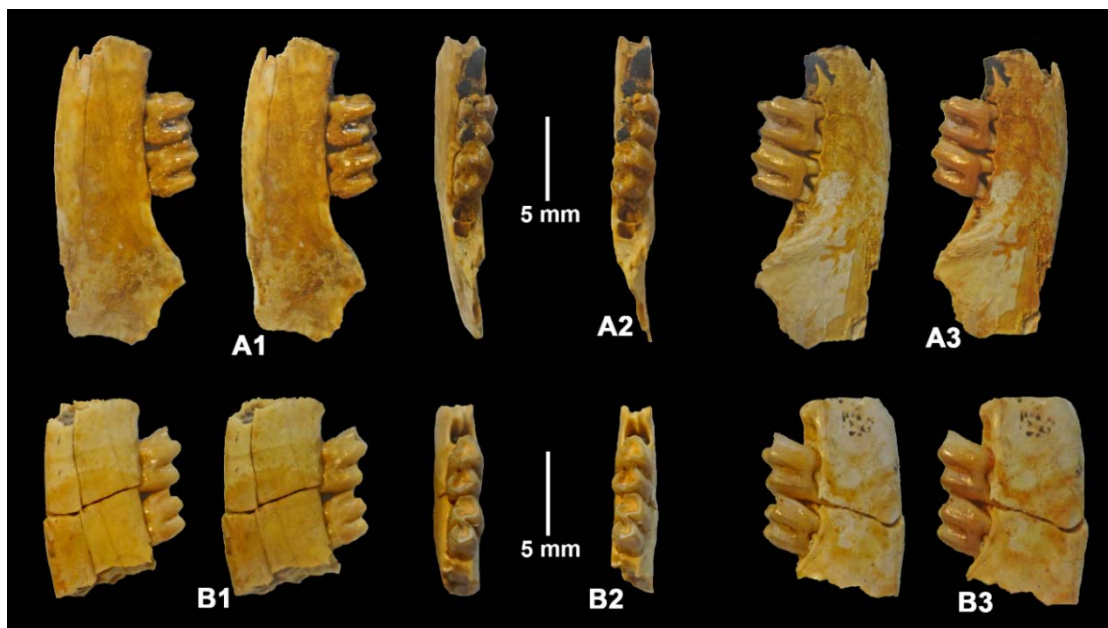
Figure 33. Stereo images of mandibles of *Promyohyrax namibiensis* from Eocliff, Namibia. A) EC9 2.2g, right mandible with m/1-m/2, A1 - lingual view, A2 - occlusal view, A3 - buccal view, B) EC9 2.2h, right mandible with m/1-m/2, B1 - lingual view, B2 - occlusal view, B3 - buccal view (scale : 5 mm).
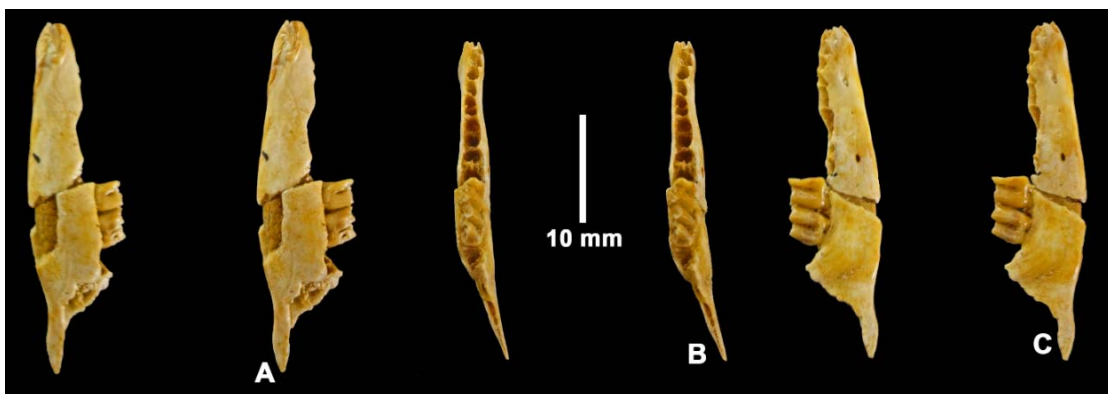
Figure 34. Stereo views of EC9 2.2h, right mandible with m/2-m/3 of *Promyohyrax namibiensis* from Eocliff, Namibia, A) lingual view, B) occlusal view, C) buccal view (scale : 10 mm).

122

The m/1 and m/2 of *Promyohyrax namibiensis* are stout, semi-hypsodont teeth comprised of two, tall crescentic lophids posed on robust roots (Figs 33, 34). The basic layout of the crown is like that of the p/4 described above, but the crowns are slightly more mesio-distally compressed and the paraconid is more strongly developed and curves slightly distally on the lingual side, thereby crowding the trigonid basin and producing an incipient fossettid. The entoconid is also more strongly developed than in the p/4 and shows a small *tuberculum intermedium* mesially which reduces the capacity of the talonid basin, likewise forming an incipient fossettid. The result of these modifications to the paraconid and entoconid is that, in lingual view, the trigonid and talonid basins appear as slit-like vertical valleys. The buccal sinusid is vertically oriented but fades out a short distance above the cervix. There is no sign of buccal or lingual cingulids in the lower cheek teeth of *Promyohyrax namibiensis*.
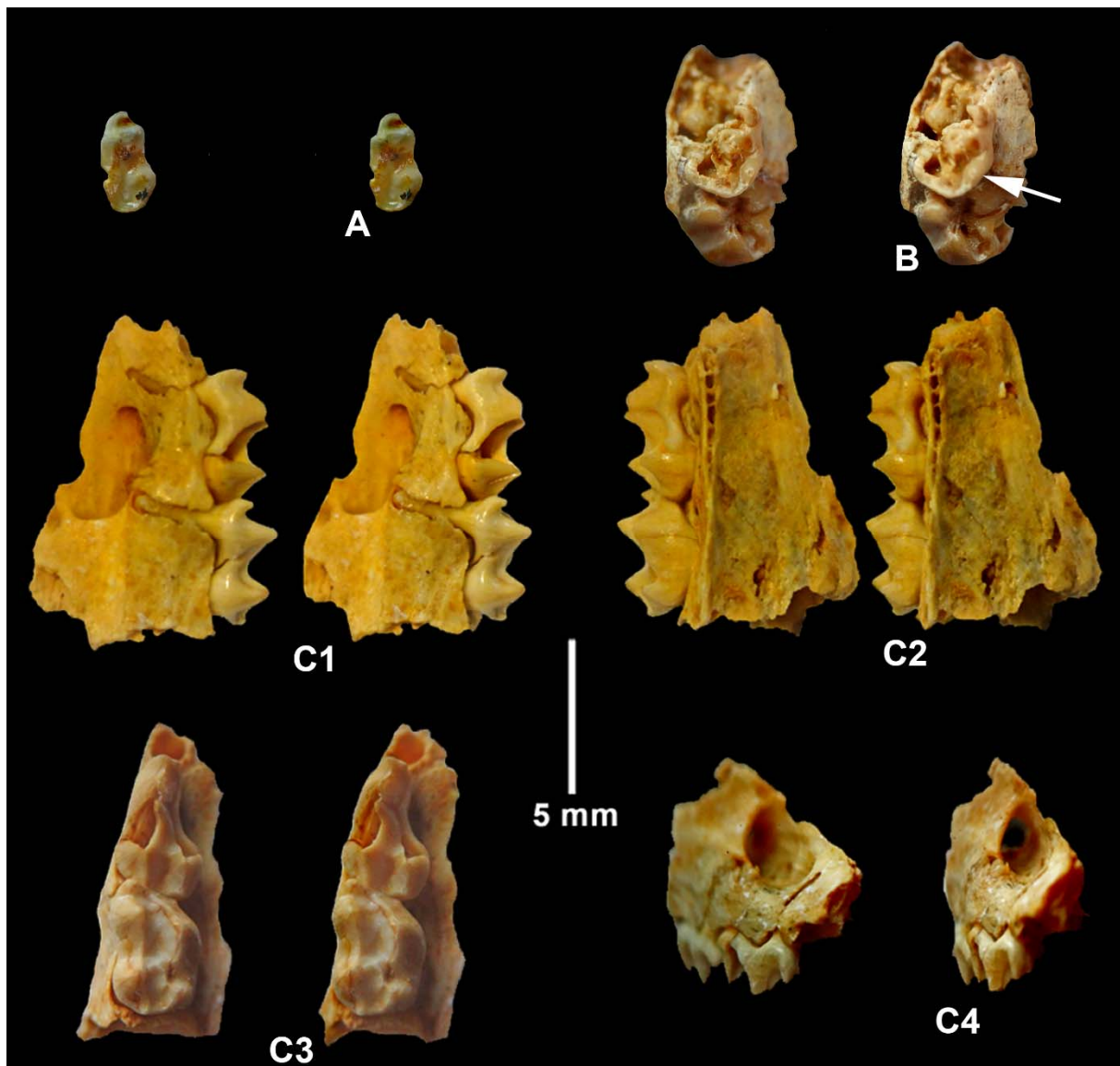
Figure 35. Stereo views of deciduous upper teeth of *Promyohyrax namibiensis* from Eocliff, Namibia. A) EC10 2.1d, right D2/, occlusal view, B) EC10 21a, juvenile right maxilla with D4/ in occlusion, and P4/ and M1/ in crypto, occlusal view (arrow points to the hypocone of the D4/), C) EC9 5.1a, right maxilla with D3/ and D4/, C1 - buccal view, C2 - lingual view, C3 - occlusal view, C4 - anterior view (scale : 5 mm).

The D2/ attributed to *Promyohyrax namibiensis* has an oval occlusal outline (Fig. 35A). It is slightly damaged on its disto-buccal corner, but the ectoloph is comprised of large

but quite low paracone and metacone with a distinct parastyle projecting mesially. The lingual cusps are comprised of a prominent protocone and a larger hypocone. The mesial fovea between the parastyle and the protocone is shallow and opens lingually. The trigon and talon basins are confluent with each other, there being no metaconule. The trigon basin opens lingually at a broad sinus. The buccal sinus is shallow.

A juvenile right maxilla fragment from EC10 has a damaged D4/ in occlusion, with the M1/ just beginning to erupt, and the P4/ still fully inside its crypt (Fig. 35B). The buccal cusps of the D4/ are broken, but part of the protocone is preserved as is the hypocone. The latter cusp is much smaller than the protocone and is low. The posthypocrista extends disto-buccally and overhangs the distal roots of the tooth.

EC9 5.1a is a right maxilla fragment containing the D3/ and D4/ (Fig. 35C). The specimen is remarkable for its large dimensions, and for the impressive facial fossa that it possesses above the D3/. The large infra-orbital canal opens above the mesial edge of D4/. The capacious facial fossa has a blind anterior pocket above the anterior root of the D3/, after which the fossa shallows anteriorly.

The D3/ is slightly damaged, but its basic morphology can be discerned. The occlusal outline is triangular with a concave lingual side, narrow mesially and broad distally. It has three large cusps, the paracone and

metacone on the buccal side, and the protocone in the disto-lingual corner of the crown. The strong parastyle projects anteriorly and is tall, whereas the metastyle is small and low. There is a small style at the end of the postprotocrista, possibly corresponding to a minute hypocone.

The D4/ has a trapezoidal occlusal outline. The ectoloph is comprised of tall paracone and metacone accompanied by a prominent parastyle and a small, low metastyle. There is a mesio-distally broad buccal sinus, separated from the trigon basin by the postparacrista and premetacrista. The lingual cusps – protocone and hypocone – are well formed but are slightly lower than the paracone and metacone. There is a paraconule between the protocone and parastyle which closes off a small fovea between the paracone, parastyle and paraconule. The protocone is slightly distal to the level of the paracone and has a strong postcrista that extends distally and slightly buccally to meet the metaconule which separates the trigon basin from the talon basin. The preprotocrista extends mesio-buccally towards the paraconule and parastyle. On its mesio-lingual side there is a low swelling, corresponding in position to the precingulum. The hypocone is smaller than the protocone and sends a precrista towards the metaconule and a postcrista towards the metastyle, thereby forming the low distal wall of the talon basin. The distal fovea is small and shallow. There are no signs of buccal cingula in either the D3/ or the D4/.
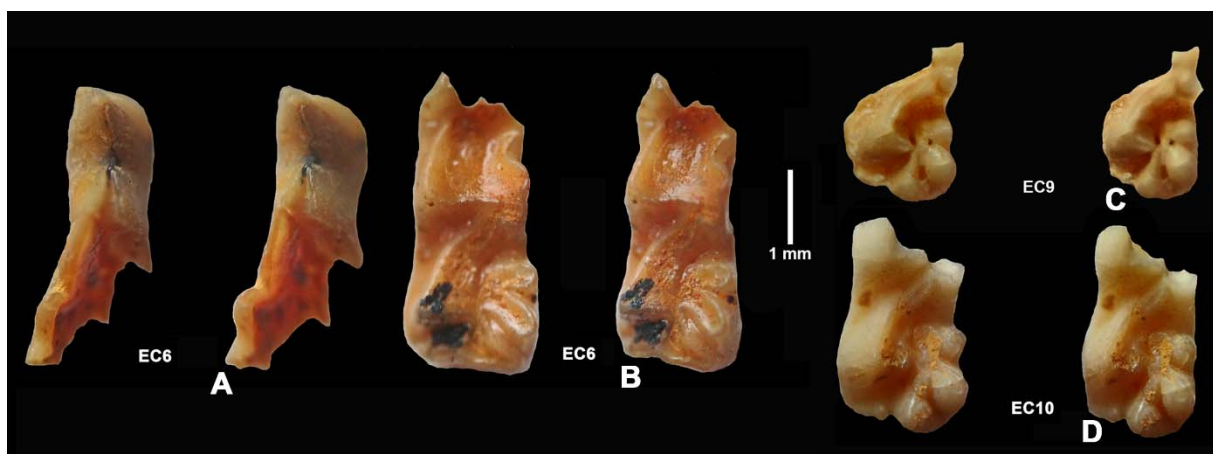
Figure 36. Stereo occlusal views of deciduous lower molars of *Promyohyrax namibiensis* from Eocliff, Namibia. A) EC6 2.2d, anterior half of right d/3, B) EC6 2.2c, left d/4, C) EC9 2.2m, distal lophid of left d/4, D) EC10 2.2c, distal lophid of left d/4 (scale : 1 mm).

Several lower deciduous molars of *Promyohyrax namibiensis* are present in the

Eocliff collection (Fig. 36). A damaged d/3 is mesio-distally elongated and shows a prominent

pointed paraconid at its mesial end that is separated by a notch from the preprotocristid, thereby recalling a carnivore carnassial. There is a precingulid on the mesio-buccal corner.

The d/4s are mesio-distally elongated trapezoidal teeth, slightly narrower mesially than distally. The d/4 has roots at its mesial and distal extremities. The paraconid is not preserved in any of the specimens due to damage, but one specimen preserves the disto-buccal part of the cusplet, separated from the preprotocristid by a sinusid. The post-protocristid is transversely oriented and joins the metaconid. The distal crescentid of the d/4 is comprised of the hypoconid, the metastylid and the entoconid complex. The latter complex consists of three distinct, pointed cuspids, the *tuberculum intermedium* on the mesial side of

the entoconid, the entoconid itelf, and the post-cingulid, which is developed into a conical cuspid at its apex. In addition, there is a small, low cingular cusplet behind the hypoconid. The metastylid is close to the metaconid, but is distinct at its apex. The hypoconid has two cristids, the mesial one (prehypocristid) extending mesio-lingually towards the meta-stylid, and the posterior one (posthypocristid) extending disto-lingually towards the ento-conid, but separated from it by a slit. The buccal sinusid is broad and apically it extends as far as the metastylid. The talonid basin is crowded by the entoconid complex but opens lingually between the metastylid and the *tuberculum intermedium*. There is a prominent distal fovea between the hypoconid and the postcingulid.
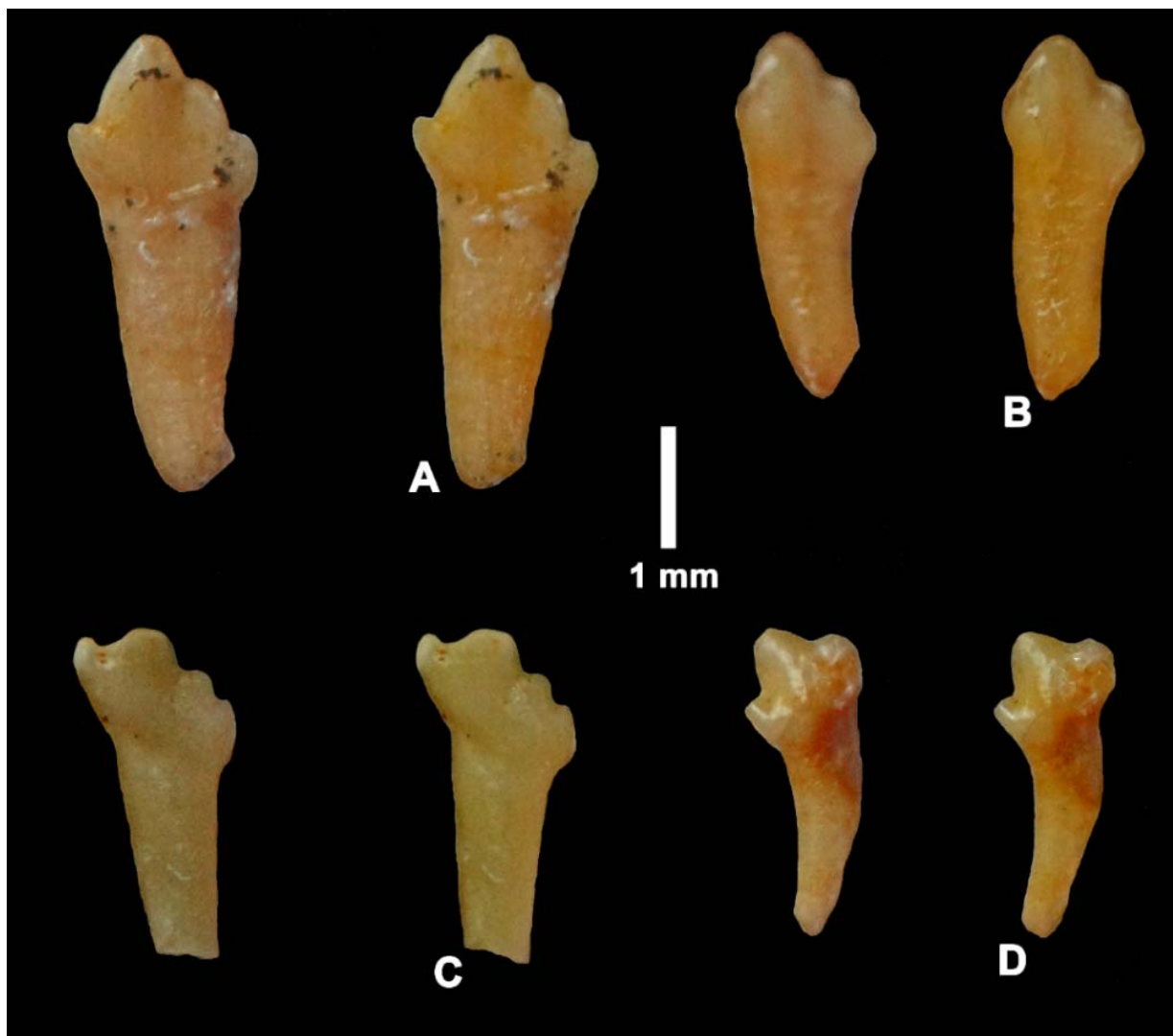
Figure 37. EC10, stereo images of anterior teeth of unknown meristic position attributed to *Promyohyrax namibiensis* from Eocliff, Namibia (scale : 1 mm).

To complete the description of the teeth attributed to *Promyohyrax namibiensis*, we illustrate some teeth that probably belong to this species, but there is doubt about their meristic positions (Fig. 37). They are single rooted teeth so could be incisors, canines or first premolars.

The crowns are appreciably longer mesio-distally than the roots, and with digitations or pectinations along the apices of the crowns. Two specimens have curved roots, the other two have straight roots.

Table 6. Measurements (in mm) of upper cheek teeth of *Promyohyrax namibiensis* from Eocliff, Namibia (holotype is in bold).

| Catalogue	Tooth	Mesio-distal length	Bucco-lingual breadth
EC10 2.1d	D2/ right	3.4	1.8
EC9 5.1a	D3/left	4.3	2.7
EC9 5.1a	D4/ left	4.2	2.8
EC10 2.1a	D4/ right	--	2.7
EC9 2.1c	P3/ left	2.3	2.0
EC9 2.1c	P3/ right	2.3	2.0
EC9 2.1c	P3/ left	3.0	2.4
EC9 2.1c	P4/ left	3.2	3.0
EC9 2.1c	P4/ right	3.2	3.0
EC9 2.1h	M1/ right	3.6	3.8
EC9 2.1h	M2/ right	2.5	3.5
EC9 2.1h	M1/ left	3.6	3.6
EC9 2.1h	M2/ left	2.4	3.1
EC9 2.1h	M3/ left	1.2	1.5
EC9 2.1d	M2/ right unworn	2.5	2.5

Table 7. Measurements (in mm) of lower cheek teeth of *Promyohyrax namibiensis* from Eocliff, Namibia.

Catalogue	Tooth	Mesio-distal length	Bucco-lingual breadth
EC9 2.2d	p/3 right	2.8	1.2
EC9 2.2e	p/4 left	3.0	1.8
EC9 2.2e	p/4 right	3.2	1.9
EC9 2.2g	m/1 right	3.0	2.0
EC9 2.2g	m/2 right	2.7	2.1
EC9 2.2h	m/1 right	2.9	2.0
EC9 2.2h	m/2 right	2.6	2.0
EC9 2.2i	m/2 left	2.8	1.8
EC9 2.2j	m/1 right	--	2.0
EC9 2.2j	m/2 right	2.5	1.9
EC9 2.2f	m/1 left unworn	3.2	2.1
EC7 2.2a	m/1 left	3.2	2.1
EC7 2.2a	m/1 right	2.8	2.1

Discussion

In a paper describing the Palaeogene strata of the Sperrgebiet, Pickford (2015a, fig. 46A, C illustrated two specimens of macro-scelidean teeth *in situ* in the tufas at Eocliff which were identified as « forms related to *Myohyrax* ». These specimens belong to *Promyohyrax namibiensis*.

The cheek teeth of *Promyohyrax* are semi-hypsodont, being much lower-crowned than those of *Myohyrax* and *Protypotheroides* from the early Miocene of Namibia (Senut, 2003, 2008) but they are taller than the teeth of extant macroscelideans. An important feature of the cheek dentition of *Myohyrax* is the presence of narrow but deep fossettes in the molars, both upper and lower (Andrews, 1914; Butler, 1984; Patterson, 1965) which persist even when the

teeth are heavily worn. This indicates that the hypsodonty in *Myohyrax* is of the crown apex category (cuspal hypsodonty of White, 1959). This contrasts with the category known as crown base hypsodonty, in which the cuspal part of the tooth, along with the trigon and talon basins, wear away early, leaving a tooth that has no fossettes and a single ring of enamel surrounding the dentine core. In this respect, the presence of deep fossettes in upper and lower molars of *Promyohyrax* indicates a close relationship between it, *Myohyrax* and *Protypotheroides*.

The lower molars of *Promyohyrax* have incipient closure of the lingual openings of the trigonid and talonid basins. In most macroscelideans the lingual openings of these

basins are broad, but in *Promyohyrax*, the paraconid curves lingually and distally at its apex shortening the distance between it and the metaconid. In the distal lophid, the *tuberculum intermedium* reaches towards the prehypocristid, thereby crowding the talonid basin. In both lophids, the basins are deep. This morphology possibly represents the initial stages of the formation of deep fossettids in the lower molars as seen in *Myohyrax*. In addition, the crowns and roots of the lower molars of *Promyohyrax* are oriented parallel to each other in the jaw, as in *Myohyrax*, unlike their fan-like arrangement in *Afrohypselodontus*, in which the cervical parts of the teeth are well separated from each other.

In the upper molars of *Promyohyrax*, the trigon and talon basins are deep and fossette-like and, unusual for a mammal, the mesial and distal foveae also develop into deep fossettes. These additional fossettes are related to the strong development of the paraconule and metaconule, which separate the trigon basin from the mesial fovea and talon basin from the distal fovea respectively. An additional resemblance between the upper molars of *Promyohrax* and *Myohyrax* concerns the lingual sinus, which is deep and narrow and extends far into the middle of the crown.

Thus, even though the cheek dentition of *Promyohyrax* is not nearly as hypsodont as those of *Myohyrax* and *Protypotheroides*, it could represent an initial stage in the evolution of the latter genera.

Family Afrohypselodontidae nov.

Type genus :- *Afrohypselodontus* nov.

Diagnosis :- small to medium-sized macroscelideans; hypselodont, ever-growing, rootless cheek teeth and central incisors; no facial fossa; shallow fossettes and fossettids in cheek teeth which wear away after about 1 mm of occlusal wear; cementum covering the outer surfaces, sinuses and sinusids of the cheek teeth.

Differential diagnosis :- Afrohypselodontidae differs from all other macroscelideans by the presence of ever-growing, rootless cheek teeth and upper and lower central incisors; upper and lower molars arranged in a fan-like fashion, with the occlusal apices in contact with each other but the cervices separated from each other; m/2 and m/3 with crowns curved (concave distally) from apex to cervix.

Genus *Afrohypselodontus* nov.

Type species :- *Afrohypselodontus minus* nov.

Diagnosis :- small to medium-sized macroscelideans; central incisors and cheek teeth are hypselodont (ever-growing, rootless teeth with mid-crown hypsodonty); M3/ and m/3 only slightly smaller than M2/ and m/2 respectively; zygomatic process of maxilla opposite M2/, extending a short way laterally before sweeping distally as a slender sliver of bone; fenestrae in the palatine bone; infra-orbital foramen opens high on the snout above the cervix of P4/; wall-like alveolar process for the M2/ and M3/ in the anterior portion of the orbit; lower cheek teeth with cervices close to the base of the mandible; enamel of cheek teeth thin; cementum in upper and lower cheek teeth, especially in the lingual sinus of upper molars and buccal sinusids of lower molars; occlusal basins (fossettes, fossettids) of premolars and molars shallow, disappearing with ca 1 mm of occlusal wear; facial fossa shallow; in buccal view, P4/ and p/4 vertical to the occlusal surface, M1/ and m/1 slanting slightly distally, M2/ and m/2 slanting at about 30° from the vertical and M3/ and m/3 slanting at almost 45° from the vertical; p/4 and m/1 straight-sided in lateral view, m/2 and m/3 concave distally in lateral view; in anterior view, P4/ and the upper molars tilted at ca 45° such that their cervices are closer to the sagittal plane than their occlusal surfaces; upper and lower central incisors without apical sulci.

Differential diagnosis :- *Afrohypselodontus* differs from hypsodont macroscelidean genera *Myohyrax* and *Protypotheroides* by the possession of hypselodont, ever-growing, rootless cheek teeth and upper and lower central incisors, absence of fossettes and fossettids in the cheek teeth, apex of I1/ not subdivided by sulci, M3/ and m/3 not as reduced relative to the M2/ and m/2 respectively, m/2 and m/3 concave distally in lateral view and not disposed parallel to each other; thinner enamel in the cheek teeth. It differs from all herodotines by the lack of buccal cingula in the upper molars, by its hypselodont cheek teeth, by its extremely shallow facial fossa and the elevated opening of the infra-orbital foramen. It differs from all Macroscelididae and Rhynchocyonidae by its ever-growing cheek teeth and central incisors, by its shallow facial fossa and the elevated opening of the infra-orbital foramen.

Etymology :- the genus name is a latinised combination of *Afro* for the African continent, *hypselos*, Greek for tall, and *odous*, Greek for tooth.

<div align="center">

Species *Afrohypselodontus minus* nov.

</div>

Diagnosis :- Small species of the genus, intermediate in size between *Nasilio*, which is larger and *Macroscelides* and *Elephantulus* which are smaller; length of mandible from i/1 to m/3 ca 18.5-19.5 mm; C1/-M3/ ca 14.4 mm long.

Holotype :- GSN EC10 3.1a, snout containing right P4/-M2/ and left M1/-M2/ and alveoli of C1/-P3/ (Fig. 38, Table 8).

Description

The holotype snout (EC10 3.1a) comprises the left and right maxilla and both frontals which have been crushed downwards and backwards. Small parts of the left zygomatic bone and the left parietal are preserved, and both palatine bones are present but damaged (Fig. 38). The maxillo-palatine suture is close to the alveolar process distally, but diverges medially at an angle of ca 45° opposite the middle of M2/. There is a fenestrum in the palatine, in line with the canal for the palatal artery in the maxilla. The right maxilla contains the P4/-M2/ and preserves the complete alveoli of P1/-P3/ and M3/. Part of the right canine alveolus is preserved. The left M1/-M2/ are *in situ*, the alveolus of the M3/ is complete, that of the P4/ is broken anteriorly. A

Type locality and age :- Eocliff 10, Namibia, Bartonian-Priabonian.

Etymology :- *minus* refers to the small dimensions of the species.

Synonymy :- Macroscelididae hypsodont form related to *Myohyrax,* in Pickford (2015a, fig. 46B).

small part of the left zygomatic bone is attached to the margin of the orbit.

This snout contains hypselodont cheek teeth that are so tall that their cervices reach close to the dorsal surface of the maxillae. The alveolar process is, as a consequence, very tall, the part within the maxillary recess of the orbit forming a wall-like structure within it, subdividing the anterior part (the maxillary recess) into two. The infraorbital canal is on the interior side of the alveolar process starting low down at the rear of the palatine bone, but rising sharply anteriorly to emerge onto the facial surface of the maxilla close to the nasals, above the cervix of the P4/.

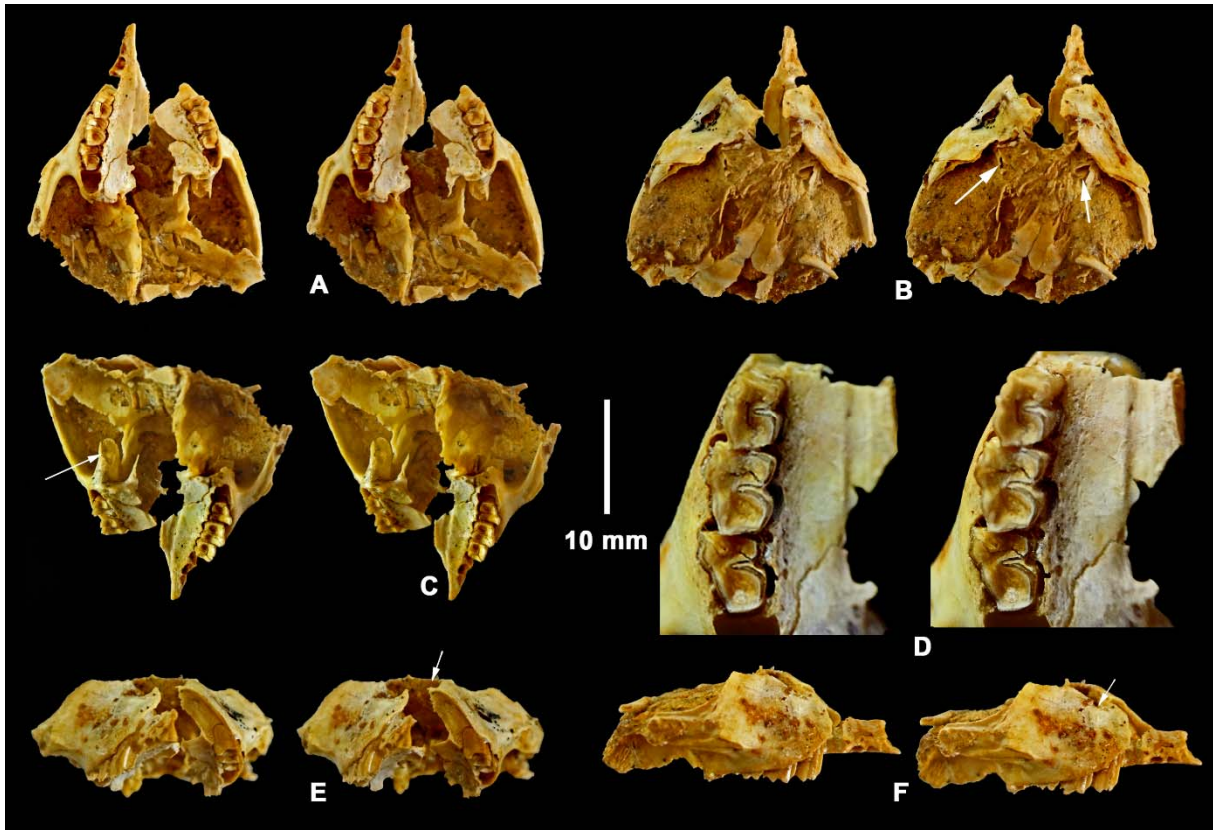Measurements of the teeth are provided in Table 8.

Figure 38. Stereo images of GSN EC10 3.1a, holotype snout of *Afrohypselodontus minus* from Eocliff, Namibia. A) ventral view (note fenestrae in palatine), B) dorsal view (arrows show the cervical ends of the M2/s), C) oblique distal view (arrow shows the tall left alveolar process of the M3/, broken at its apex), D) enlargement (x3) of right P4/-M2/ (note cementum cover), E) anterior view (arrow shows the outlet of the infraorbital canal above the cervix of the P4/), F) right lateral view (arrow shows the outlet of the infraorbital canal above the cervix of the P4/) (scale : 10 mm).

In ventral view, the root of the zygomatic process of the maxilla is observed to lie opposite the M2/, its anterior pole being at the level of the contact between M1/ and M2/, and the anterior pole of the maxillary recess being at the level of the rear of M2/. The root of the zygomatic process of the maxilla extends slightly laterally before sweeping distally as a long, slender sliver of bone. The bone anterior to the root of the zygomatic process is thin and is pierced by several small holes that penetrate into the narrow maxillary sinus that separates the alveolar process from the lateral surface of the maxilla.

In lateral and dorsal views, there is a shallow fossa associated with the infraorbital canal. The snout narrows rapidly anteriorly. The ventral and anterior margins of the orbit are formed of a thin sliver of the zygomatic (absent on the right side, but partly preserved on the left).

The left and right palatine bones are largely preserved. They show a posterior encoche, and a hook-like process anteriorly which defines the distal margin of the posterior fenestra. The palatal artery emerges from a canal in the palatine via the posterior fenestra and then courses in a prominent but shallow furrow in the palatal surface of the maxilla that extends in a straight line anteriorly.

The frontal bones are displaced backwards and ventrally relative to the maxilla, their vertical walls now occupying the orbits. The minimum distance between the orbits dorsally is 5.8 mm. The fronto-nasal sutures are preserved on the frontal and they suggest that the nasals extended backwards as far as the anterior margin of the orbits.

The cheek teeth in the holotype are hypselodont (ever-growing, rootless teeth, also described as euhypsodont (Mones, 1982; Garcia Lopez & Powell, 2011) or as « enamel-band hypsodonty » by Von Koenigswald (2020)). The cervical ends of the P4/-M2/ extend almost to the dorsal surface of the maxilla, and that of the M3/ is housed in a tall, wall-like alveolar

process in the anterior part of the orbital cavity. The alveolus of the P3/ indicates that it too was probably hypselodont, but the alveoli of the upper canine, P1/ and P2/ are considerably smaller and lower, although the P2/ is also hypselodont. The cheek tooth enamel is thin. The M3/ is slightly smaller than the M2/, the P4/ is slightly smaller than the M1/ which is the largest of the cheek teeth. The mesial and distal edges of the M3/ are curved such that its cervical end is separated from that of the M2/ by a short gap. The mesial and distal edges of the other upper molars and premolars are almost straight, but the buccal and lingual surfaces of the teeth are gently curved, such that the lingual surface is slightly concave.

The occlusal surfaces of worn cheek teeth show no signs of fossettes, which indicate that they fall into the category of morphology known as sub-basinal (or mid-crown) hypsodonty (White, 1959) or enamel-band hypsodonty (Von Koenigswald, 2020). In this type of tooth, the apical part of the crown in which the trigon basin and the talon basin are formed, soon wears away, leaving only the mid-crown part, which comprises a ring of thin enamel with a dentine infilling (both primary and secondary dentine). This is especially evident in unworn specimens of P2/, P4/ and M2/ in which the trigon basin and talon basin are preserved (Fig. 39). These two basins are less than a mm deep, for a crown height of 2 mm or more as preserved in the germs but as tall as 6 mm in fully formed teeth (Fig. 39D). The outer surface of the enamel shows narrow vertical ridges and grooves corresponding to styles, cusps and sinuses and there is a thin cementum cover (often missing in the fossils).

Table 8. Measurements (in mm) of the teeth and alveoli in the right maxilla of the holotype of *Afrohypselodontus minus* from Eocliff, Namibia (EC10 3.1a).

Tooth	Mesio-distal length	Bucco-lingual breadth
C1/ alveolus	0.6	0.3
P1/ alveolus	0.6	0.4
P2/ alveolus	1.1	0.7
P3/ alveolus	1.2	1.0
P4/	2.0	1.6
M1/	2.5	2.0
M2/	2.1	1.9
M3/ alveolus	2.1	1.9
C1/-M3/	14.4	
P1/-M3/	13.4	
P1/-M2/	11.2	
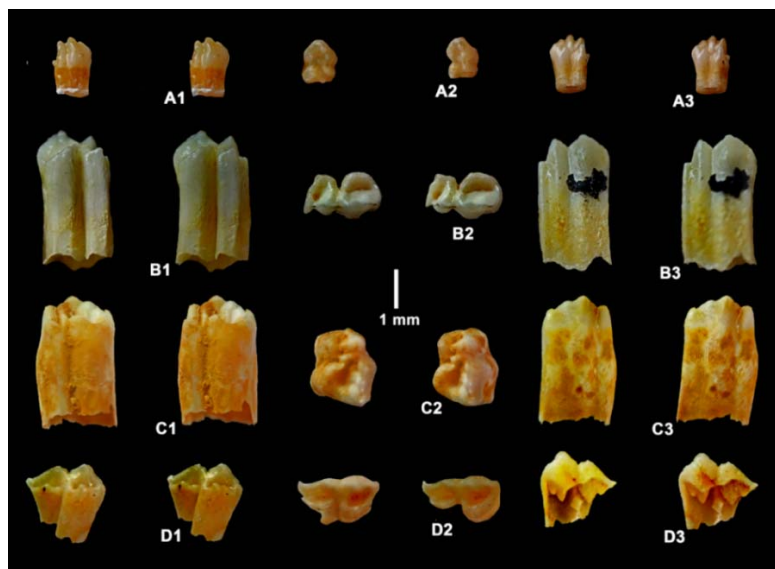
Figure 39. Stereo images of upper cheek teeth of *Afrohypselodontus minus* from Eocliff, Namibia. A) EC10 3.2, left P2/ germ, A - buccal view, A2 - occlusal view, A3 - lingual view, B) EC10 3.3, right P4/ germ, B1 - lingual view, B2 - occlusal view, B3 - buccal view, C) EF7 3.2f, left P4/ germ, C1 - lingual view, C2 - occlusal view, C3 - buccal view, D) EC10 3.3h, right M2/ germ, D1 - buccal view, D2 - occlusal view, D3 - lingual view to show base of trigonid and talonid basins (scale : 1 mm).
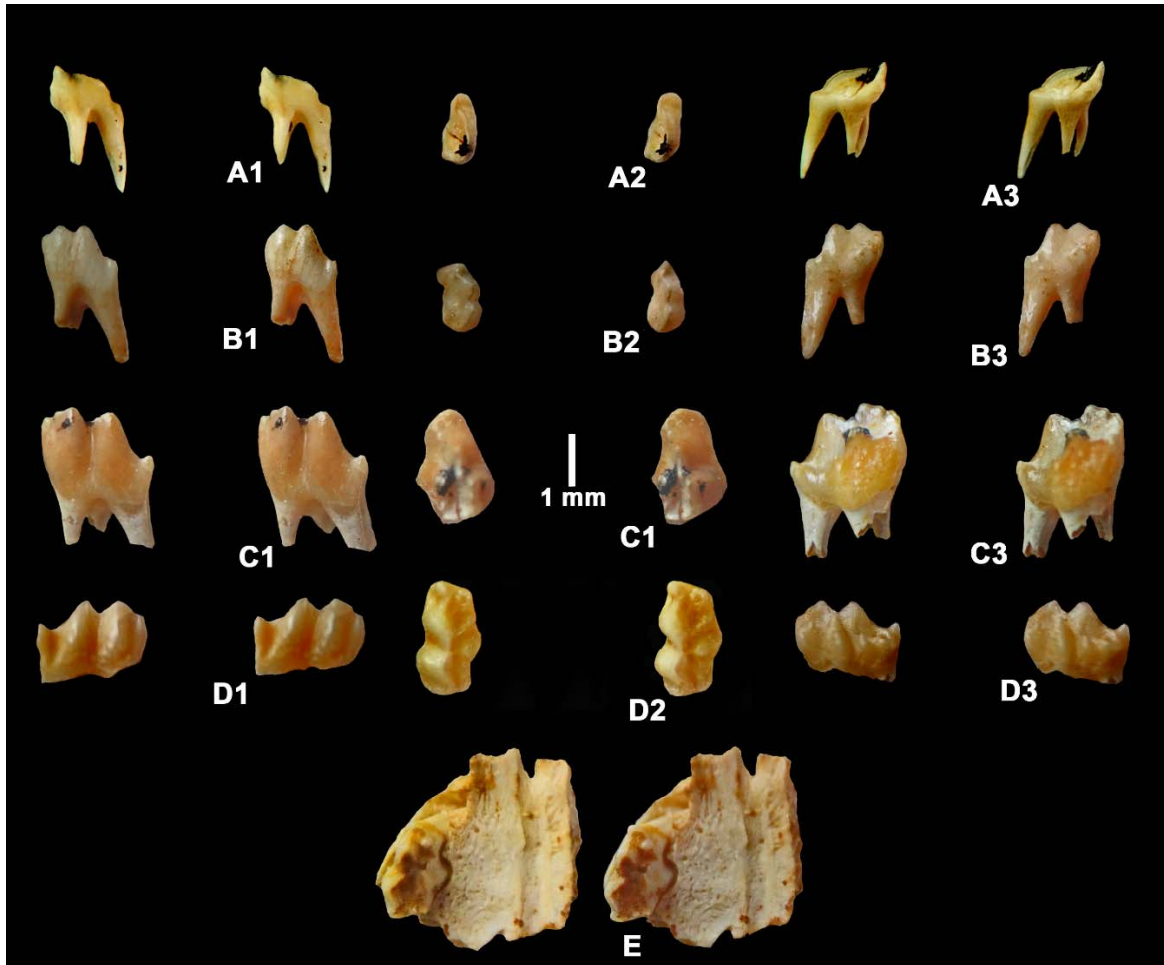
Figure 40. Stereo images of deciduous molars and P1/ of *Afrohypselodontus minus* from Eocliff, Namibia. A) EC9 3.1d, left D1/, B) EC10 3.2d, left P1/, C) EC10 3.2d, left D3/, D) EC10 3.2d, right D4/, (1 - buccal view, 2 - occlusal view, 3 - lingual view) E) EC8 3.1, right maxilla with D4/, occlusal view (scale : 1 mm).

The deciduous upper cheek teeth of *Afrohypselodontus minus* are reasonably well represented at Eocliff (Fig. 40). Some specimens of the D4/ are *in situ* in maxillae which are close in morphology to the type specimen in which the canal for the palatal artery is prominent.

The crown of the D4/ is semi-hypsodont and it develops three roots, two buccally and one lingually. The crown is sub-rectangular in occlusal outline, being mesio-distally long and bucco-lingually narrow. The ectoloph is comprised of large and tall paracone and metacone accompanied by a prominent parastyle anteriorly and a smaller, lower metastyle distally. There are four lingual cusps. The anteriormost cusp on the lingual side of the D4/ is the paraconule, but it is well separated from the protocone and parastyle and occupies a position at the mesio-lingual corner of the crown. The protocone is somewhat reduced in

size and is positioned lingual to the paracone. The crista obliqua is sharp and extends towards the base of the postparacrista. The metaconule is larger than the protocone and is positioned in a very lingual position in line with the buccal sinus. The hypocone is small and low and occupies the disto-lingual corner of the tooth. There is no sign of a buccal cingulum in the D4/.

The D3/ is triangular in occlusal view and it has three roots. The crown is semi-hypsodont with a tall ectoloph comprised of prominent paracone and metacone and small but tall parastyle and a low, distally projecting metastyle. The lingual cusps are reduced to a single main cusp in line with the buccal sinus (probably the protocone) with an undulatory distal surface.

The D1/ is a three rooted tooth, two on the buccal side and one lingually. As is usual in deciduous teeth the roots are splayed out from each other. There is a single main cusp

131

accompanied by a low mesial style and a tall distal style. Wear is predominantly on the lingual side, which imparts a sectorial aspect to the crown.

The P1/ has two roots and the crown is dominated by the ectoloph which has tall paracone and metacone closely applied to each other, a small parastyle and a low metastyle. The lingual cusps are so reduced that they make only small swellings of enamel mesially and distally.

Figure 41. Stereo lingual views of upper incisors of *Afrohypselodontus minus* from Eocliff, Namibia. A) EC8 3.1a, left I1/, B) EC8 3.1a, left I1/, C) EC8 3.1a, right upper incisor, D) EC10 3.9, right upper incisor, E) EC10 3.9, left upper incisor, F) EC10 3.9, left upper incisor (scale : 1 mm).

Upper incisors attributed to *Afro-hypselodontus minus* are hypselodont (Fig. 41). The central incisors are transversely concave lingually and curved from apex to cervix. Unworn specimens have no denticulation at the apex. Upper second and third incisors, if correctly attributed to this species, are denticulate (or pectinate) with five or six low tines evenly spread along the cutting edge of the crown. There are no signs of roots in any of the upper incisors.

As for the upper incisors, the i/1 is hypselodont and has no roots. The right mandible fragment, EC10 3.3c, has the i/1 in situ, but the apex of the crown is broken (Fig. 42C), The crown shows no signs of subdivision or sulci, unlike lower incisors of *Myohyrax* and *Protypotheroides* which do. Judging from the size of its alveolus, the i/3 was minuscule.
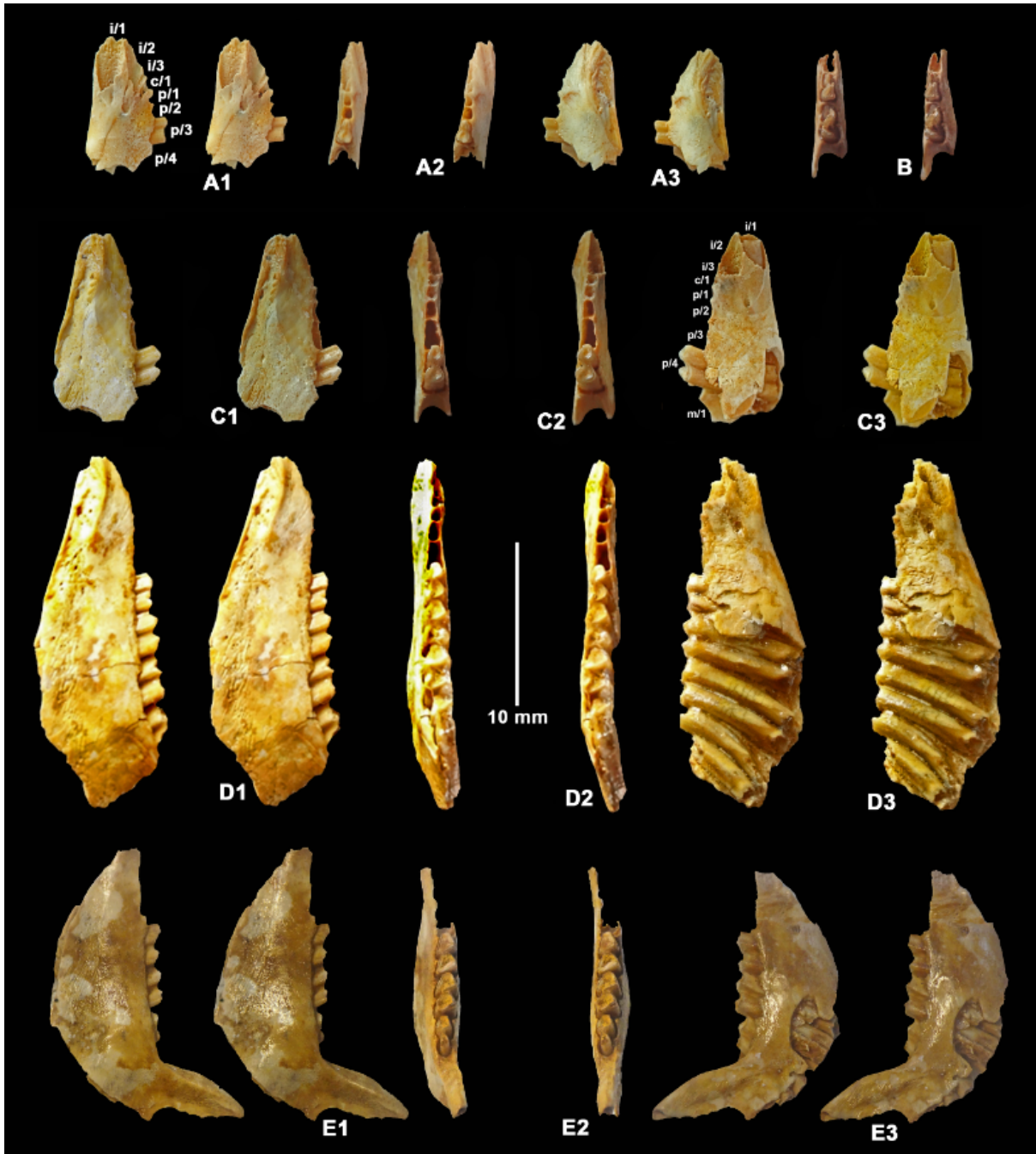
Figure 42. Stereo images of mandibles of *Afrohypselodontus minus* from Eocliff, Namibia. A) EC9 3.2a, left mandible fragment containing p/3, A1 - buccal view with alveoli labelled, A2 - occlusal view, A3 - lingual view, B) EC10 3.3d, left mandible fragment containing p/3-p/4, occlusal view, C) EC10 3.3c, right mandible fragment with p/4, alveoli labelled, B1 - lingual, B2 - occlusal, B3 - buccal views, D) EC10 3.3a, right mandible containing p/4-m/3 and alveoli of i/1-p/3, D1 - lingual view, D2 - occlusal view, D3 - buccal view, E) EC10 3.3b, right mandible containing m/1-m/3, E1 - lingual view, E2 - occlusal view, E3 - buccal view (scale : 10 mm).

Mandibles of *Afrohypselodontus minus* have a steeply oriented ascending ramus which rises immediately behind the m/3 but without hiding it in lateral view (Fig. 42). There is no coronoid foramen at the base of the coronoid process. In occlusal view, the tooth row is straight. In lateral view, the ramus deepens rapidly from the incisors to the m/2 where it is deepest. There are two mental foramina, one beneath the p/1, and the other beneath the p/4. The symphysis is unfused, but the marks left by the ligamentous attachments extend as far distally as the p/3. The p/4 is almost vertical in the jaw, but the m/1, m/2 and m/3 are inclined such that the cervix of each tooth is increasingly further to the rear than its apex. The apices of

133

the teeth are in contact with each other, but the cervices are separated at the base of the mandible, that of the m/3 terminating behind the base of the ascending ramus. In addition, the mesial and distal surfaces of the m/2 and m/3 are gently concave distally, more so in the m/3 than the m/2. The m/1 in contrast has straight, sub-parallel mesial and distal surfaces.

Measurements of the teeth are provided in Table 9.

Table 9. Measurements (in mm) of the teeth and alveoli of right mandible EC10 3.3a, *Afrohypselodontus minus* from Eocliff, Namibia.

Tooth	Mesio-distal length	Bucco-lingual breadth
i/1 alveolus	1.3	0.6
i/2 alveolus	1.1	--
i/3 alveolus	0.4	0.3
c/1 alveolus	0.4	0.4
p/1 alveolus	0.9	0.5
p/2 alveolus	1.4	0.6
p/3 alveolus	1.4	0.6
p/4	2.3	1.3
m/1	2.7	1.5
m/2	2.8	1.7
m/3	2.5	1.4

A lower central incisor, EC1bis 3.2, is hypselodont and slightly twisted from apex to cervix (Fig. 43). The section of the tooth is a compressed oval with a right-angled disto-lingual corner. The tooth is 7.6 mm tall, by 1.3 mm mesio-distal diameter, by 0.6 mm labio-lingual breadth.

Figure 43. Stereo lingual view of EC1bis 3.2, right i/1 of *Afrohypselodontus minus* from Eocliff, Namibia (scale :1 mm).
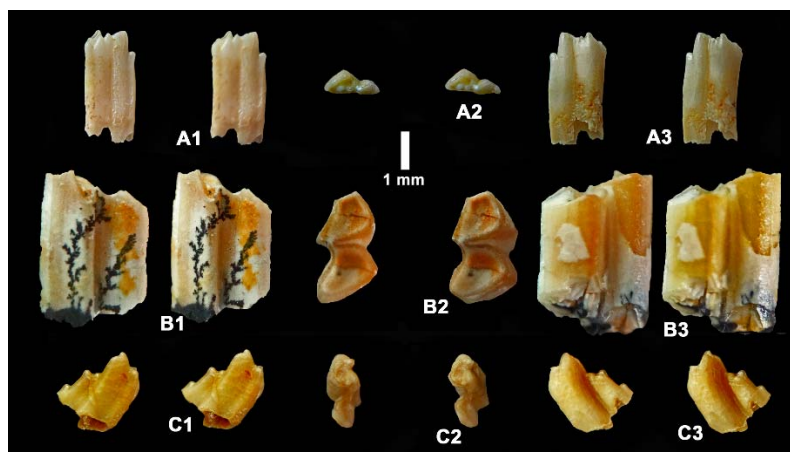
Figure 44. Stereo images of isolated lower teeth of *Afrohypselodontus minus* from Eocliff, Namibia. A) EC10 3.2f, left p/1 germ, A1 - lingual view, A2 - occlusal view, A3 - buccal view, B) EC7 3.2a, right m/1, B1 - lingual view, B2 - occlusal view, B3 - buccal view (note the cementum and thin enamel), C) EC9 3.2h, left m/3 germ, C1 - lingual view, C2 - occlusal view, C3 - buccal view (note the tilted orientation which brings the talonid and trigonid cusps almost to the same level as the occlusal surface) (scale : 1 mm).

The lower p/1-m/3 are hypselodont, rootless teeth (Fig. 44). Unworn specimens of p/1 and m/3 reveal that the crown is comprised of two crescentic lophids with extremely shallow trigonid and talonid basins. In the p/1, the mesial crescentid is smaller than the distal one. The mesial crescentid has three cusps (paraconid, protoconid, metaconid) arranged in a bucco-lingually narrow triangle. The distal crescentid is comprised of four cusps (metastylid, hypoconid, entoconid and *tuberculum intermedium*) also arranged in a bucco-lingually narrow triangle. These two crescentids are joined together close to the lingual side of the tooth, which results in a shallow lingual sinusid and a deeper buccal one.

In fully preserved cheek teeth there is a layer of cementum covering the lingual and buccal surfaces of the crown and infilling the lingual sinusid (Fig. 44B).

The m/3 is also comprised of two crescentids, but the mesial one is larger and taller than the distal one. The mesial crescentid is tricuspid (paraconid, protoconid, metaconid) and the distal one is quadricuspidate. The metastylid, *tuberculum intermedium* and hypoconid are the same height as each other and form a triangle, but the entoconid is much lower and forms a low cusp at the rear of the tooth. The m/3 slants distinctly to the rear, its mesial edge is convex and its distal edge is concave.

Measurements of the teeth are provided in Table 10.

Table 10. Measurements (in mm) of teeth of *Afrohypselodontus minus* from Eocliff, Namibia.

Catalogue	Tooth	Mesio-distal length	Bucco-lingual breadth	Crown height
EC7	I1/	1.9	0.7	6.4
EC 10 3.9	I1/ right	2.0	0.8	5.0
EC10 3.9	I1/ left	2.0	0.7	4.8
EC4 3.1	I1/ right	2.0	1.0	6.7
EC8 3.1a	I1/ left	1.9	0.8	5.4
EC8 3.1b	I1/ left	1.7	0.8	5.2
EC9 3.2	I1/ left	1.8	0.8	6.6
EC10 3.9	I2/ left	1.1	0.4	4.0
EC9 3.1	D1/ left	1.3	0.7	
EC10	D4/ right	2.1	1.1	
EC7 3.2f	P4/ right	1.9	1.5	
EC1 3.2	P4/ right	2.0	1.7	
EC4 3.1a	i/1	1.1	0.6	4.1
EC1bis 3.2	i/1 right	2.1	0.7	8.0
EC6 3.2	i/2 right	1.2	0.7	5.3
EC9 3.2f	d/4 left	2.1	1.1	
EC9 3.2h	d/3 left	1.5	0.6	
EC9 3.2h	d/3	2.0	0.9	2.4
EC10 3.3d	p/3 left	1.5	0.7	
EC10 3.3d	p/4 left	2.1	1.0	
EC2 3.3	p/4 right	2.4	1.5	
EC10 3.3c	p/4 right	2.3	1.2	
EC2 3.3	p/4 right	2.4	1.5	
EC7 3.2	m/1 right	2.6	1.4	
EC7 3.2a	m/1 right	2.6	1.4	
EC10 3.3h	m/3 right	2.1	1.1	

Discussion

Afrohypselodontus minus is slightly smaller than extant *Nasilio*, and somewhat larger than species of *Macroscelides* and *Elephantulus*. Its body weight is estimated to have been ca 60 grams. Its hypselodont central incisors and cheek teeth indicate that it was probably an obligate grazer. Because of the presence of exceptionally tall P4/ and upper molars, the maxillary opening of the infra-orbital canal has been displaced upwards to the

dorsal limits of the maxilla. It opens above the P4/ as is usual in macrocelideans and its origin in the orbital cavity is low down, just above the floor of the orbit in the maxillary recess. The anterior portion of the orbit is partly infilled with a tall, wall-like alveolar process containing the M2/-M3/. These teeth are in contact occlusally, but their cervical ends are separated by gaps, such that in lateral view, they are splayed out like an open fan. The upper molars

and P4/ are also canted in the maxilla, such that their cervical ends are appreciably closer together than their occlusal surfaces. The P4/, M1/ and M2/ are so tall that their cervices are close to the dorsal surface of the snout.

The mandible of *Afrohypselodontus minus* is shallow anteriorly, deepening rapidly beneath the p/3-m/3. It has two mental foramina, one beneath the canine-p/1, the other beneath the p/4. This disposition is characteristic of macroscelideans in general. In lateral view, the cervical ends of the p/4-m/3 are splayed apart fan-wise, but there are no gaps between these teeth at the occlusal surface. In addition, unlike any other macroscelideans, the m/2 and m/3 are curved such that their distal surfaces are concave from crown to cervix. This unusual morphology mirrors to some extent the situation in South American « ungulates » which are, however, much larger mammals (Agnolin & Chimento, 2011; Cassini *et al*. 2017).

Species *Afrohypselodontus grandis* nov.

Holotype :- EC 4 4.1a, right maxilla with P4/-M2/ (Fig. 45B, Table 11).

Type locality and age :- Eocliff 4, Namibia, Bartonian-Priabonian

Diagnosis :- large species of the genus, ca 30% larger than the type species.

Etymology :- *grandis* refers to the large dimensions when compared to the type species.

Description

The maxilla of *Afrohypselodontus grandis* is constructed along similar lines to the holotype of A*frohypselodontus minus*, but is appreciably larger than it (ca 130-140% +/-). The root of the zygomatic process of the maxilla is opposite the M2/, its anterior surface departing from the face at a low angle before curving medially to lie parallel to the lingual margin of the tooth row (Fig. 45C). The lateral surface of the zygomatic process of the maxilla is marked by ridged sutures for the zygomatic bone. The bone anterior to the root of the zygomatic process above the M1/ and M2/ is pierced by several holes which connect to a narrow but tall maxillary sinus which occupies the zone between the alveolar process and the lateral surface of the maxilla. The anterior wall of the maxillary recess is likewise pierced by several holes that connect with the same maxillary sinus. The palatine is preserved in EC9 4.1a. The maxillo-palatine suture is close to the tooth row and it extends anteriorly as far as the anterior margin of M2/ before curving medially. Its anterior part is broken off. In line with the rear of the M2/ the palatine is pierced vertically by a prominent foramen, and it is fenestrated. The alveoli of the M1/-M3/ indicate that these teeth were hypselodont, with a lingual sinus forming a vertical ridge in the lingual surface of the alveolus. The cervical parts of successive alveoli are separated from each other, but the occlusal parts are close together, indicating that the teeth were inclined with respect to each other.
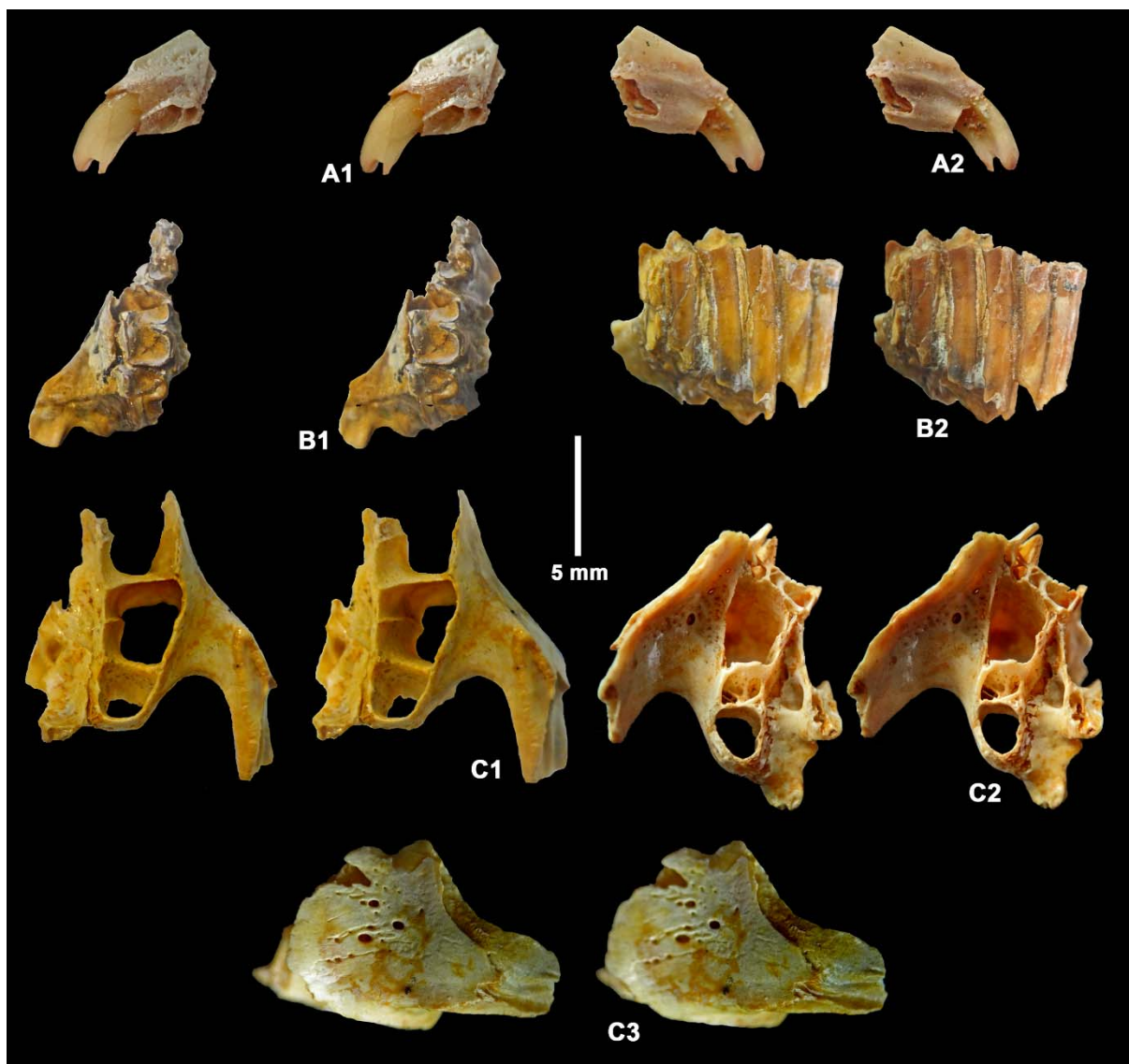
Figure 45. Stereo images of premaxilla and maxillae of *Afrohypselodontus grandis* from Eocliff, Namibia. A) EC4 4.1b, left premaxilla containing the I1/ and alveoli of I2/ and I3/, A1 - lateral view, A2 - lingual view, B) EC4 4.1a, holotype right maxilla with P4/-M2/, B1 - occlusal view, B2 - lingual view, C) EC9 4.1a, edentulous left maxilla with alveoli of M1/-M3/, C1 - palatal view (note the fenestrum and foramen in the palatine), C2 - dorsal view, C3 - lateral view to show the holes piercing the lateral surface of the maxilla anterior to the root of the zygomatic arch (scale : 5 mm).

The P4/ in the maxilla EC4 4.1a is missing the buccal half, but the remaining lingual half shows a relatively short mesial loph and a longer distal loph, with a clear lingual sinus infilled with cementum (Fig. 45B). The M1/ is more complete than the P4/ but is missing its paracone and parastyle. The mesial and distal lophs are sub-equal in dimensions. There is a prominent lingual sinus infilled with cementum. The teeth are heavily worn yet the buccal cusps are taller than the lingual ones. There are no signs of fossettes in the occlusal surfaces of the upper cheek teeth. The M2/ lacks the distal loph but what remains of the crown is similar to the M1/. None of these teeth possess roots. They are clearly hypselodont.

Measurements are provided in Table 11.

Table 11. Measurements (in mm) of teeth of *Afrohypselodontus grandis* from Eocliff, Namibia (holotype in bold) (e - estimated, * - meristic position uncertain).

Catalogue	Tooth	Mesio-distal length	Bucco-lingual breadth	Crown height
EC10 4.1	I1/ right	2.0	0.9	6.8
EC10 4.1	I1/ right	2.0	0.9	7.7
EC 9 4.1	I2/ left	1.7	0.8	8.9
EC4	I1/ left, *in situ*	2.0	0.9	7.4
EC4	I1/ left	2.0	0.9	7.4
EC10 4.2	D4/ left	2.4	1.5	
EC10 4.2	D4/ right	2.1	1.5	
EC9 4.1	M1/ left aveolus	--	3.2	
EC9 4.1	M2/ left alveolus	3.5	3.2	
EC9 4.1	M3/ left alveolus	2.2	2.1	
EC10 4.3s	M*/ right	3.1	1.9	10.4
EC4 4.1a	P4/ right	3.0	-	
EC4 4.1a	M1/ right	3.2	2.4	8.7
EC4 4.1a	M2/ right	-	2.4	
EC7 4.1a	P4/ left	2.3	1.8	
EC8 4.1a	M2/ left	2.6	2.1	8.7
EC8 4.1a	M2/ right	3.0	2.0	8.8
EC9 4.4b	M3/ right	2.6	2.2	8.4
EC7 4.2b	m/3 left	2.7	1.2	6.9e
EC10 4.3a	m/* left	2.7	1.6	8.3
EC10 4.3b	m/* left	2.6	1.6	8.8
EC10 4.3c	m/* right	2.3	1.4	8.1
EC10 4.3d	m/* left	2.5	1.4	8.6

The premaxilla, EC4 4.1b, is a short, narrow wedge of bone (Fig. 45A). On its lingual side there is a large incisive foramen running the length of the bone, thus resembling a fenestra more than a foramen, but it is much smaller than the fenestra in *Macroscelides* and *Elephantulus*. Its lateral surface is marked by several pin-prick foramina.

The I1/ is *in situ* and consists of a labio-lingually compressed hypselodont tooth with a C-shaped section, with a longitudinally concave lingual surface. The cervical part is oriented horizontally but the cutting edge is oriented at ca 60° from the horizontal. The cervical part of the I1/ terminates distally close to the premaxillo-maxillary suture, and the alveoli of the I2/ and I3/ are close to that of the I1/, such that their cervical ends are anterior to the cervical end of the I1/. The crowns of the three incisors probably touched each other to form a continuous cutting edge.

The I2/, EC4 4.1 is hypselodont and like the I1/, has a C-shaped section, and a sharp cutting edge. It is longitudinally curved from apex to cervix (concave lingually), but its mesial and distal edges are straight (Fig. 46).

The alveolus of I3/ is minute.
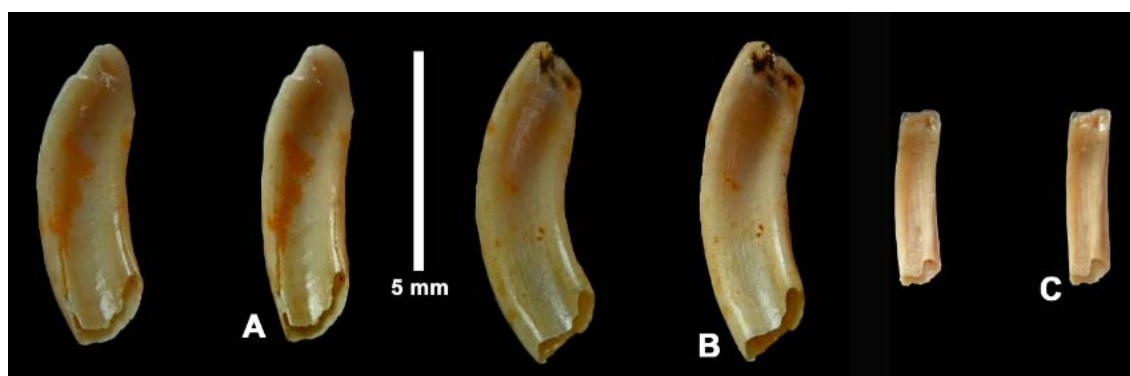
Figure 46. Stereo lingual images of upper incisors of *Afrohypselodontus grandis* from Eocliff, Namibia. A) EC10 4.1a, right I1/, B) EC10 4.1b, right I1/, C) EC4 4.1, left I2/ (scale : 5 mm).
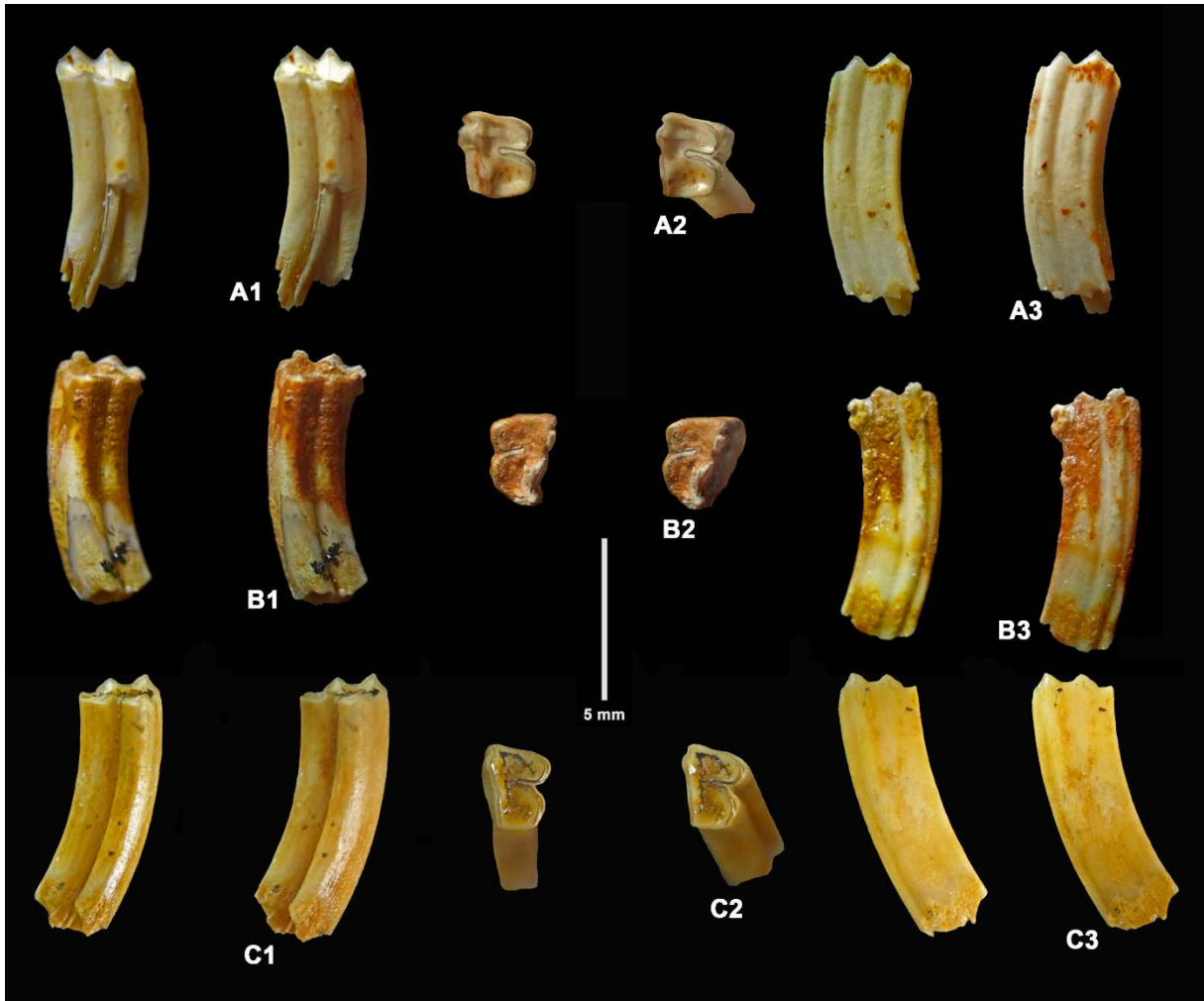
Figure 47. Stereo images of upper cheek teeth of *Afrohypselodontus grandis* from Eocliff, Namibia. A) EC8 4.1, right M2/, A1 - lingual view, A2 - occlusal view, A3 - buccal view, B) EC8 4.1, left M2/, B1 - lingual view, B2 - occlusal view, B3 - buccal view, C) EC9 4.1b, right M2/, C1 - lingual view, C2 - occlusal view, C3 - buccal view (scale : 5 mm).

Figure 48. Stereo lingual view of EC9 4.2a, left i/2 of *Afrohypselodontus grandis* from Eocliff, Namibia (scale : 5 mm).

An isolated hypselodont incisor from Eocliff 9 is slender, tall and slightly twisted longitudinally with a compressed oval section (Fig. 48). It is interpreted to be a left lower second incisor. The cutting edge is oriented at 60° with respect to the height axis of the tooth.
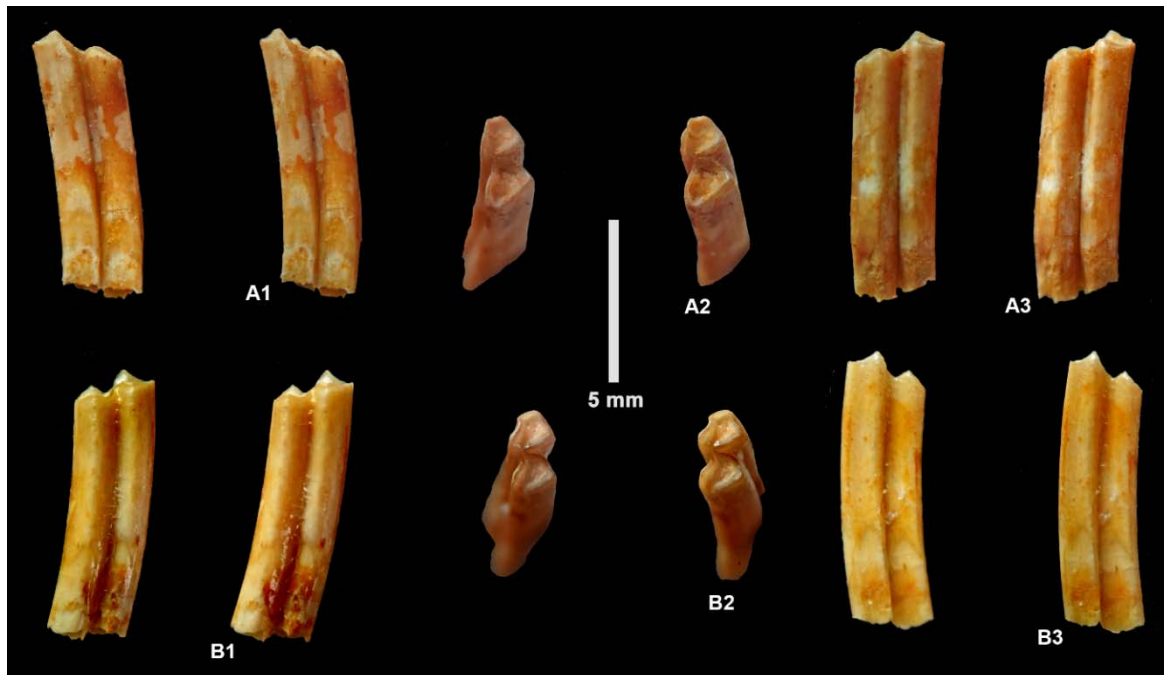
Figure 49. Stereo images of lower molars of *Afrohypselodontus grandis* from Eocliff, Namibia. A) EC10 4.3a, left lower molar, A1 - lingual view, A2 - occlusal view, A3 - buccal view, B) EC10 4.3b, left lower molar, B1 - buccal view, B2 - occlusal view, B3 - lingual view (scale : 5 mm).

Lower molars of *Afrohypselodontus grandis* from Eocliff are hypselodont and when worn show no sign of fossettes in the occlusal surface (Figs 49, 50). They are comprised of two crescentids joined to each other close to the lingual side of the tooth, with sinusids on the lingual and buccal sides, the buccal sinusid being bucco-lingually deeper and mesio-distally broader than the lingual one. In lateral view, the second lower molars are gently curved from apex to cervix, the distal edge being concave. The buccal and lingual sides of the teeth are straight and sub-parallel to each other.

Figure 50. Stereo images of EC7 4.2b, left mandible fragment with m.3 of *Afrohypselodontus grandis* from Eocliff, Namibia. A - buccal view (note the swelling of the surface of the mandible where the m/3 slants distally in its alveolus), B - occlusal view, C - lingual view (scale : 5 mm).

The ascending ramus of the mandible EC7 4.2b rises steeply a short distance behind the m/3 (Fig. 50) and has a sharp ridge on its lateral side. The anterior pole of the masseteric fossa terminates behind the level of the m/3. There is no sign of a coronoid foramen at the base of the coronoid process. The mandibular body is deepest beneath the m/2. The lingual part of the alveolus of the m/2 is broken, and shows that the cervix of the tooth was close to the ventral base of the mandible and that it was tilted slightly distally. The m/3 is comprised of two crescentids, the distal one slightly smaller than the mesial one. It is inclined in the mandible more than the m/2, such that its cervix underlies the base of the coronoid process.
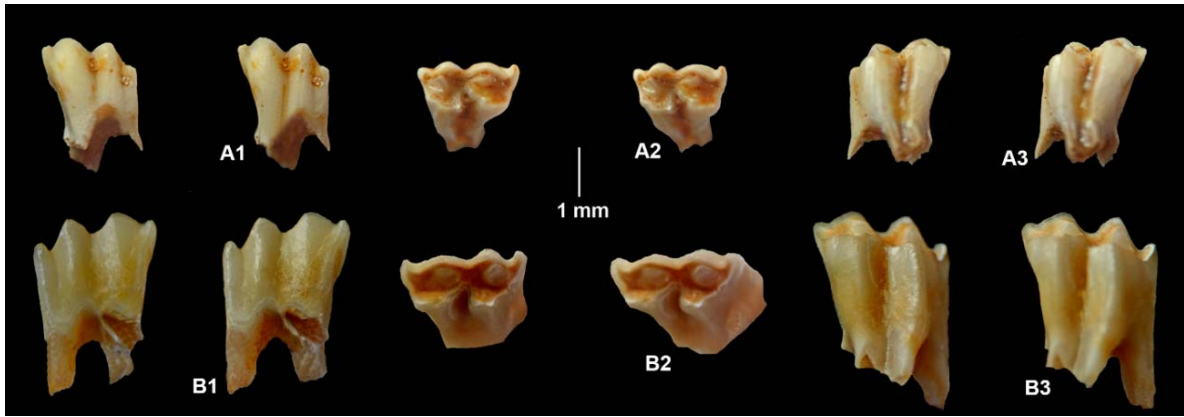
Figure 51. Stereo images of D4/s attributed to *Afrohypselodontus grandis* from Eocliff, Namibia. A) EC10 4.2a, right D4/, A1 - buccal view, A2 - occlusal view, A3 - lingual view, B) EC10 4.2b, left D4/, B1 - buccal view, B2 - occlusal view, B3 - lingual view (scale : 1 mm).

Eocliff 10 yielded two hypsodont teeth with short, slender, partly resorbed, splayed out roots, which are interpreted to be deciduous upper fourth molars (D4/) of *Afrohypselodontus grandis* (Fig. 51). The teeth are comprised of two lophs, with a deep lingual sinus and a shallower buccal sinus between them, but are strongly joined to each other in the middle. The teeth are slightly worn and show shallow trigon and talon basins which would disappear with additional wear. The paracone is taller than the protocone, and the metacone is taller than the hypocone. The parastyle is prominent and almost as high as the paracone, projecting anteriorly from the preparacrista. The metastyle is prominent but is lower than the metacone. On the buccal surface, the paracone and metacone form strong « ribs » separated from the parastyle and metastyle by shallow sulci. From apex to cervix, the crown increases slightly in breadth and decreases slightly in length. The lingual root, which is comprised of two coalescent roots, curves lingually, the buccal ones are splayed out mesially and distally. There is no sign of a buccal cingulum, and the mesostyle is absent.

Discussion

Afrohypselodontus grandis is morphologically similar to the type species of the genus, but is ca 30% larger, implying a body weight in the region of 220 grams : in other words, about the same as *Petrodromus* and smaller than *Rhynchocyon*. Such a degree of size difference is unlikely to represent sexual bimodality. Fossils of this large form are much more scarce in the Eocliff fossil collection than those of the small form, possibly because it was too large to be swallowed whole by owls. The skeletal remains are rather more broken up than those of the small species, suggesting that predators tore the body into pieces while consuming it.

In some features of the cranio-dental morphology, the two species of *Afrohypselodontus* differ so much from other described taxa of Macroscelidea that one can legitimately ask whether the genus belongs to this order. The fact that the P4/ and p/4 are fully molariform and as large as the first molars, and the upper and lower third molars are somewhat smaller than the second molars indicate however, that it is more likely to belong to this order of mammals than to any other. The presence of a fenestrum in the palatine also align it with some of the extant genera of this order. The position of the infraorbital foramen above the cervix of P4/ is another resemblance to macroscelideans. The general form of the mandible and the position of the two mental foramina, recall those of Myohyracidae, but the dental differences between *Afrohypselodontus* on the one hand, and *Myohyrax* and *Protypotheroides* on the other, indicate that it does not belong to this family. Myohyracidae molars are rooted and they exhibit fossettes and fossettids, whereas those of *Afrohypselodontus* are ever-growing, rootless teeth, without fossettes and fossettids. Furthermore, in lateral view, the lower molars of Myohyracidae and straight-sided and are disposed in the mandible sub-parallel to each other, whereas the lower molars of

Afrohypselodontus are curved and their cervices are splayed apart from each other as in a fan. In addition, the upper central incisors of *Afrohypselodontus* are ever-growing, rootless teeth without apical sulci or tines, unlike those of *Myohyrax* and *Protypotheroides* that are rooted teeth with sculpted crowns (Senut, 2008). For these reasons we erect a new family Afrohypselodontidae to accomodate this hypselodont macroscelidean genus.

Apart from possessing hypselodont molars and first incisors, there are other features unique to this family. The zygomatic process of the maxilla is located further to the rear - in line with the M2/ - than in other genera, in which it is opposite the middle of M1/ to the middle of M2/. The infraorbital foramen is located at the top of the snout, above the cervix of the P4/ instead of low down on the face and there is no facial fossa, unlike other macroscelideans in which there is a capacious fossa associated with the infra-orbital foramen.

Family *incertae sedis*

Genus and species *incertae sedis*

Description

The lower premolars *incertae sedis* are comprised of two crescentids, which are slender and lack the *tuberculum intermedium* in the distal crescentid (Fig. 52A, C). The paraconid is separated from the preprotocristid by a shallow notch. In one lower premolar the apex of the metaconid is distinct from the protoconid and the apex of the metastylid is detached from the metaconid. In two specimens the prehypocristid descends towards the base of the metaconid.
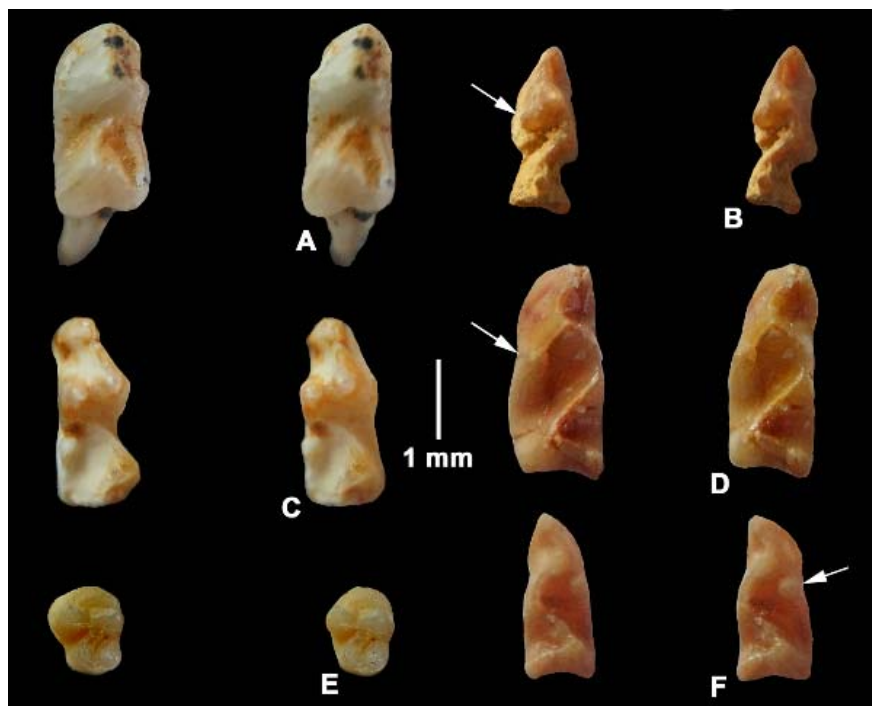
Figure 52. Stereo occlusal images of lower teeth *incertae sedis*. A) EC8 1.2g, left p/4, B) EC6, left m/1 germ, C) EC8 1.2e, right p/4, D) EC10 1.2g, left lower molar, E) EC8 1.2i, left m/3, F) EC10 1.2g, right m/14 (arrows show the accessory cuspid on the buccal cristid of the protoconid) (scale : 1 mm).

In three of the lower molars, the metastylid is closely joined to the metaconid and the prehypocristid is tall, extending right across to the apex of the metastylid without descending at all (Fig. 52B, D, F). In this kind of molar, the buccal edge of the protoconid is swollen and gives rise to a stylid that is detached at its apex. There is no *tuberculum intermedium*,

but the entoconid is tall and somewhat inflated, and is strongly linked to the hypoconid.

The lower third molar is reduced in dimensions (Fig. 52E) but retains two clear crescentids. The mesial crescentid is tricuspid (paraconid, protoconid, metaconid) and the distal crescentid has a clear entoconid and the hypoconid has well developed prehypocristid and post-hypocristid.

Measurements of the teeth are provided in Table 12.

Figure 53. Stereo images of lower deciduous teeth attributed to an unknown genus and species of macroscelidean from Eocliff, Namibia. A) EC9 3.2g, left d/3, A1 - lingual view, A2 - occlusal view, A3 - buccal view, B) EC9 3.2f, left d/4, B1 - lingual, B2 - occlusal, B3 - buccal view (scale : 1 mm).

The d/3 and d/4 attributed to this undetermined species each possess two slender roots that are splayed out mesio-distally (Fig. 53). The crowns are comprised of two crescentids with a deep buccal sinusid between them. The lingual sinusid is narrow and slit-like. The paraconid in the 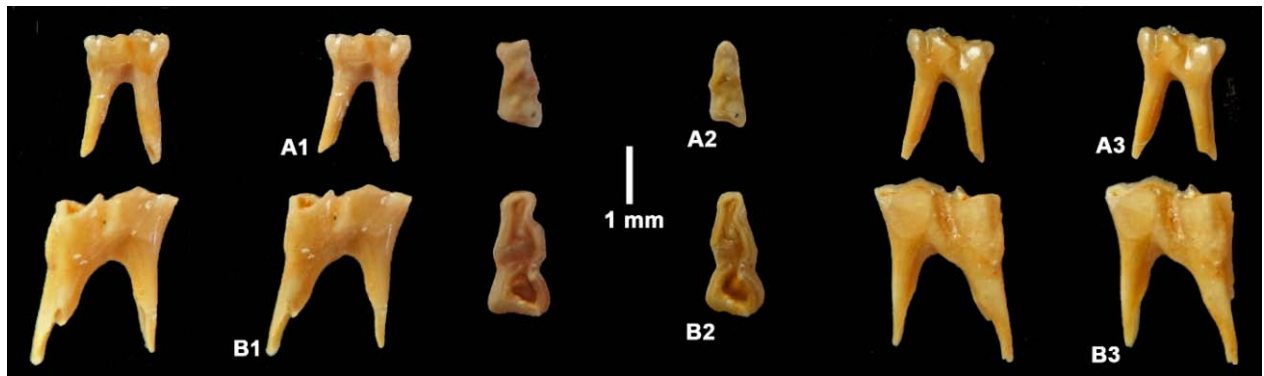d/3 projects anteriorly, and presumably the same applied to the d/4, but it is too worn to be sure. The d/3 shows a prominent *tuberculum intermedium*, but the d/4 is too worn to retain this structure. In both teeth the mesial crescentid is longer than the distal one, but is slightly narrower than it. The bucco-distal edge of the protoconid is sharply angular.

Table 12. Measurements (in mm) of teeth macroscelidean *incertae sedis* from Eocliff, Namibia.

Tooth	Mesio-distal length	Bucco-lingual breadth
EC10 m/1 right	2.1	1.0
EC10 m/2 left	2.7	1.1
EC6 m/2 left	2.5	1.0
EC9 3.2g d/3 left	1.6	0.6
EC9 3.2f d/4 left	2.1	1.1

Discussion

The macroscelidean gen. et sp. *incertae sedis* is the smallest of the order thus far found at Eocliff, and likely had a body weight of ca 30 grams. In some dental features its molars recall teeth of hyracoids. In other respects, such as the presence of a distinct cusplet on the disto-buccal angle of the protoconid, this lineage is unique, to our knowledge, such a cuspid never having been recorded in any other afrotherian.

The affinities of this small afrotherian will only be elucidated when better material becomes available.

Postcranial skeleton

The Eocliff tufas have yielded abundant post-cranial bones of macroscelideans. Among them there are some rather complete long bones which merit illustration and description, even though it is difficult to associate the specimens with any particular genus or species.

Measurements of the specimens indicate a wide range of body sizes falling roughly into three size groups.

Of particular interest are the bones of the ankle which demonstrate clear morpho-

logical characters that typify micro-cursorial mammals (Lovegrove & Mowoe, 2014).

We provide brief descriptions of the more complete postcranial elements, which will be treated in greater detail is a separate paper.
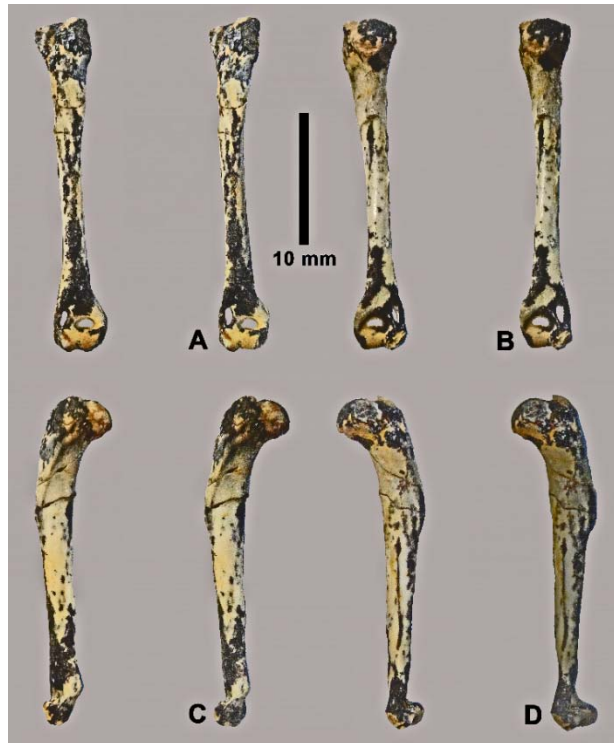
Figure 54. Stereo images of EC10 6.3, macroscelidean left humerus from Eocliff, Namibia, A) cranial view, B) caudal view, C) lateral view, D) medial view (scale 10 mm).

The macroscelidean humeri from Eocliff correspond closely in morphology to those of extant members of the order (Figs 54, 56). There is an entepicondylar foramen and the supratrochlear fossa is pierced through from cranial to caudal sides. The distal articulation is narrow with sharp edges to the trochlea and caput, indicating parasagittally constrained movements at the elbow joint. The proximal end of the humerus has well defined greater and lesser tuberosities and a globular head.

The complete humerus from EC10 (Fig. 54) is 25.5 mm long, which compares with 41.6 mm for *Rhynchocyon*, 29 mm for *Petrodromus*, 17.9 mm for *Nasilio* and 18.1 mm for *Petrosaltator* (= *Macroscelides rozeti*) Evans (1942).

Figure 55. Stereo anterior views of macroscelidean ulnae from Eocliff, Namibia. A) EC7 6.4, left ulna, B) EC9 6.4, right ulna (scale : 10 mm).

The proximal ulna and diaphysis of macroscelideans from Eocliff have a well-developed, tall olecranon process, a deep sigmoid notch and a prominent semi-circular fossa for the proximal radius (Figs 55, 56). The ulnar diaphysis narrows distally, as in extant forms of the order.

Figure 56. Ranges of metric variation in long bones of the forelimb of diverse macroscelideans from Eocliff. A) distal humerus articular breadth (n = 44), B) ulna olecranon height measured from the sigmoid notch to the proximal extremity (n = 19).

Figure 57. Stereo anterior views of macroscelidean femora from Eocliff, Namibia. A) EC7 6.6, right femur, B) EC9 6.6, left femur (scale : 10 mm).

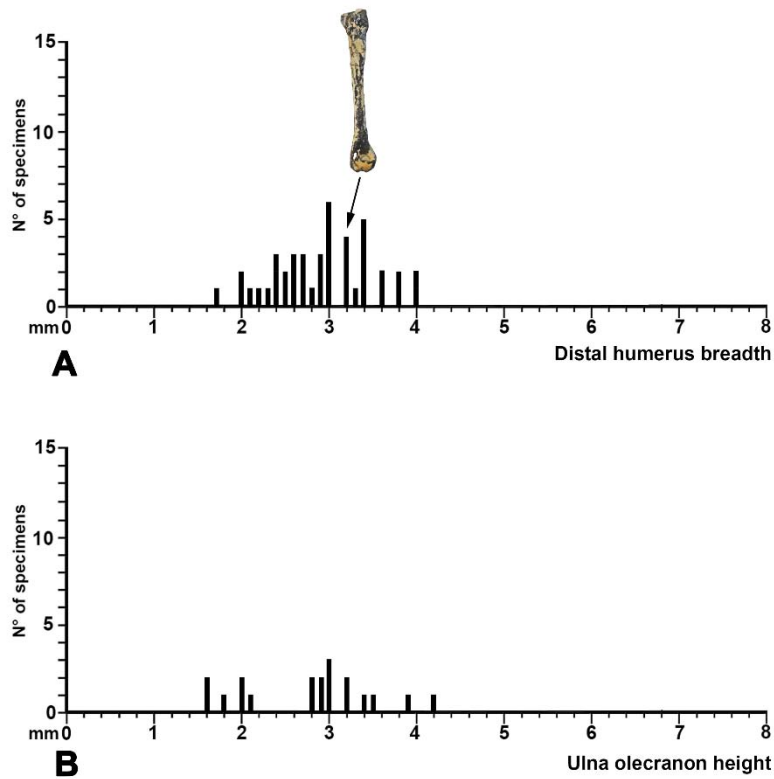The macroscelidean femora from Eocliff have a tall greater trochanter that projects above the femoral head (Fig. 57). The diaphysis is long and slender. There is a lesser trochanter close to the base of the femoral neck, and an expansive flattened third trochanter. The patellar groove is medio-laterally narrow and proximo-distally elongated, extending proximally onto the diaphysis for ca 20% of the length of the femur. In lateral view, the patellar groove is observed to extend disto-posteriorly a long way. The form and extent of the patellar groove indicate that movements of the knee joint were parasagittally constrained. The overall morphology of the Eocliff femora is typical of small cursorial mammals, but the specimens suggest that they were light and agile.

Measured from the apex of the greater trochanter to the distal condyles, the complete femur EC7 6.6 is 35.7 mm long and the smaller one EC9 6.6 is 22.4 mm long. Extant *Elephantulus rupestris* have femora that are 26.54+/-0.69 mm long for a body mass of 60.1+/-5.02 grams, while the femora of *Elephantulus edwardi* are slightly shorter (26.13+/-0.38 mm) for a body mass of 49.9+/-4.22 grams (Lovegrove & Mowoe, 2014). Evans (1942) gives the lengths of femora as follows :- *Rhynchocyon* - 59.8 mm, *Petrodromus* - 41.0 mm, *Nasilio* - 24.5 mm, *Petrosaltator* (*Macroscelides rozeti*) - 24.0 mm. From these figures it is inferred that the species represented by femur EC7 6.6 weighed appreciably more than 60 grams, whereas the species corresponding to specimen EC9 6.6 probably weighed less than 49 grams.

Figure 58. Stereo views of macroscelidean tibio-fibulae from Eocliff, Namibia. A) EC10 6.7, complete adult left tibio-fibula, anterior view, B) EC7 6.7, right diaphyses of juvenile tibio-fibula lacking the proximal and distal epiphyses, anterior view (scale : 10 mm).

There is a complete juvenile tibio-fibula from Eocliff 7 (EC7 6.7, Fig. 58B), which reveals that the diaphyses of the tibia and fibula are solidly fused to each other before the proximal and distal epiphyses become fused to them (Figs 58, 60). The degree of synostosis of the diaphyses of the tibia and fibula is similar to that observed in extant *Rhynchocyon* and *Elephantulus* (Lovegrove & Mowoe, 2014). In the two extant genera, the synostosis extends over the distal 2/3rds of the bone, as in the Eocliff fossil. This degree of synostosis is greater than that which occurs in leptictids (ca 33%, Rose, 2006) and apheliscids (ca 50%, Zack *et al.* 2005) but is close to that of the early Miocene myohyracids from Namibia (Senut, 2008). The distal epiphysis has two processes that project distally and curve slightly inwards towards their apices, indicating a tight fit to the cotylar fossa and medial surface of the talus.

The outcome is that the late Eocene macroscelideans of Eocliff possessed hind limbs and ankle joints that corresponded closely in proportions to those of extant genera, from which it is inferred that they were micro-cursorial, but possibly lighter and more agile than the early Miocene and extant forms of macroscelideans.

The complete adult tibio-fibula from Eocliff 10 (EC10 6.7, Fig. 58A) is 32 mm long and its talar facet is 1.5 mm broad. The bone thus corresponds to one of the smallest specimens from Eocliff. The length of the tibio-fibula compares with specimens of extant genera as follows :- *Rhynchocyon* - 73.5 mm, *Petrodromus* - 52.6 mm, *Nasilio* - 31.7 mm, *Petrosaltator* (= *Macroscelides rozeti*) - 34.7 mm (Evans, 1942). On the basis of these comparisons, it is inferred that the complete femur belongs to an animal about the same dimensions as *Nasilio* or *Petrosaltator*.

An interesting point about the Eocliff tibio-fibulae is that many of the distal epiphyses are not fused to the diaphysis. In the collection there are almost twice as many juvenile specimens as there are adults (Table 13). This observation is borne out by the large representation of deciduous cheek teeth among the dental samples from the tufa.

Table 13. Quantity of fused versus unfused distal epiphyses of macroscelidean tibio-fibulae from Eocliff, Namibia.

Fossiliferous patch	Unfused	Fused
EC4	2	2
EC6	4	0
EC7	16	11
EC8	5	1
EC9	9	6
EC10	10	4
Total	46	24

The macroscelidean tali from Eocliff have relatively long necks, deep cotylar fossae and the trochlea is pulley-like with raised margins (Figs 59, 60). There is no astragalar foramen. The neck of the Eocene tali appears to be proportionally longer relative to the trochlear body than that of the early Miocene species from Namibia.

The calcanea from Eocliff have an elongated tuber with a clear apical depression for the insertion of the achilles tendon (Figs 59, 60). The sustentaculum flares laterally, the ectal facet does not extend far onto the tuber calcis and the peroneal process is not salient. The calcaneo-cuboid process is quite long and the cuboid facet is at right angles to it.

The form of the calcaneum, talus and distal tibia indicate that they were tightly packed together such that movements at the ankle joint were well constrained to the parasagittal plane.

The calcanea from the early Miocene deposits of Namibia appear to have shorter tuber calci than those from Eocliff, which suggests that the Eocene taxa were perhaps lighter and more agile that the Miocene ones.
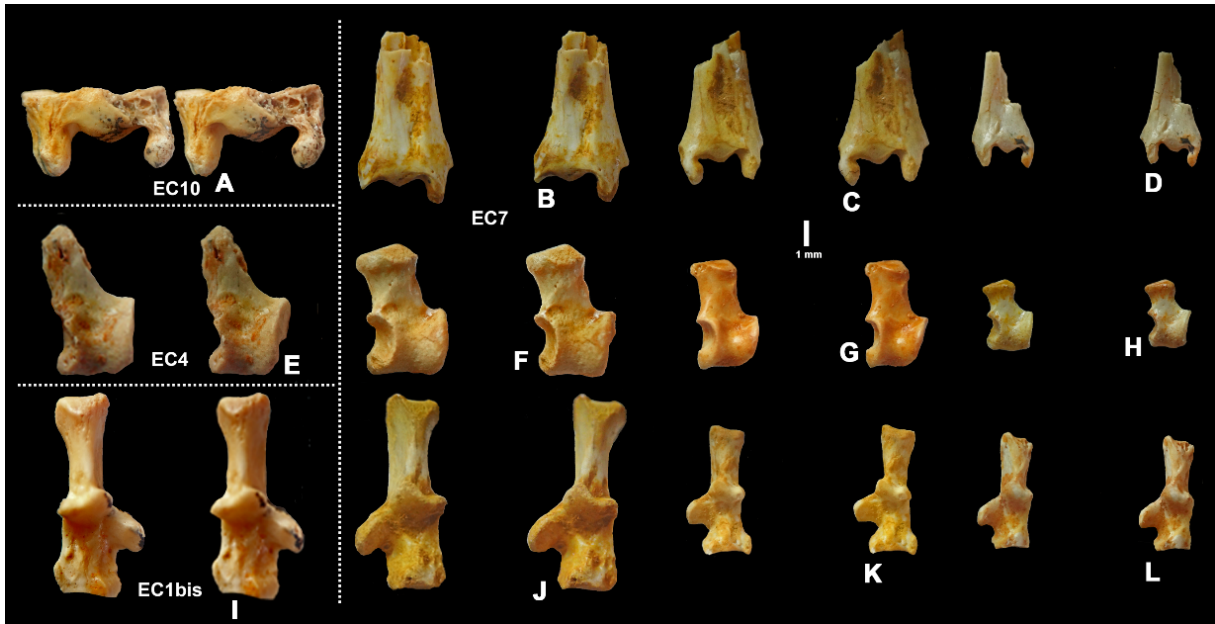
Figure 59. Stereo views of diverse macroscelidean distal tibio-fibulae, tali and calcanea from Eocliff, Namibia arranged with largest to the left and smallest to the right. A-D) distal tibio-fibula anterior views, A - EC10 6.7, B-D - EC7 6.7, E-I) right talus superior views, E - EC4 6.8, F-H – EC7 6.8, I-L) calcanea anterior views, I - EC1bis 6.9, right calcaneum, J-L - EC7 6.9, left calcanea (scale : 1 mm).
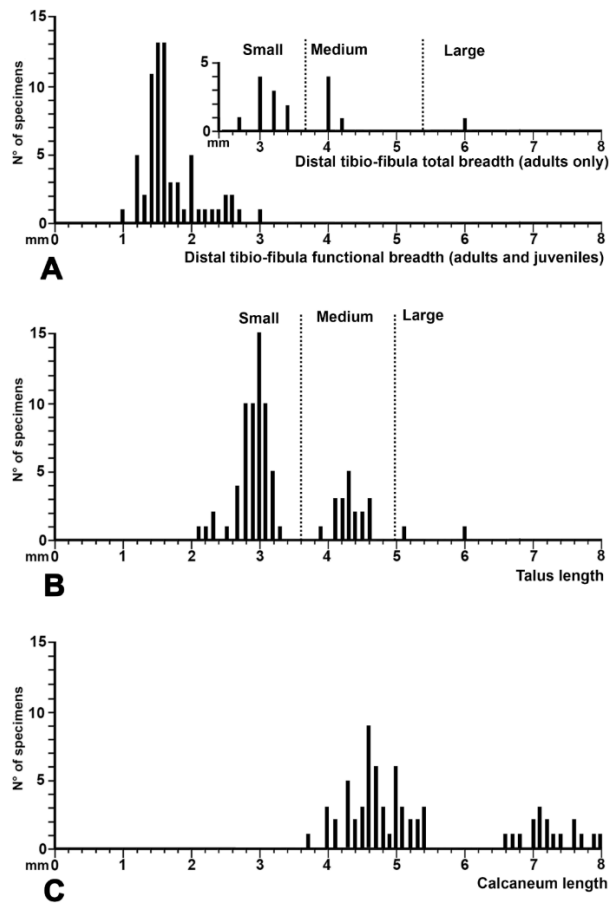
Figure 60. Ranges of metric variation in hind limb skeletal elements of diverse macrocelideans from Eocliff, Namibia. A) functional breadth (talar articulation) of distal tibio-fibula (n = 67) and total breadth of distal tibio-fibula (n = 16, adults only), B) talus length (n = 81), C) calcaneum length (n = 68).

Discussion

Diversity and affinities of Eocliff macroscelideans

The abundant macroscelidean fossils from Eocliff are herein classified into six species in five genera, one of which is *incertae sedis* (Table 14). One medium-sized taxon has mandibles in which the ascending ramus slants at a shallow angle to the rear as in extant *Rhynchocyon* as well as in *Miorhynchcyon* from the early Miocene of East Africa (Butler, 1984) and *Hypsorhynchocyon* from the early Miocene of Namibia (Senut, 2008). *Eorhynchocyon* is therefore classified in the family Rhynchocyonidae.

One of the small species from Eocliff that has approximately the same dimensions as extant *Macroscelides* and *Elephantulus*, is classified in a new subfamily (Namasenginae) of the family Macroscelididae (new rank). *Namasengi* differs from other Macroscelididae by the absence of palatal fenestrae and by the presence of upper and lower third molars, among other features.

The extinct family Myohyracidae is represented at Eocliff by a semi-hypsodont form which, in other respects, is similar to fully hypsodont *Myohyrax* and *Protypotheroides*. It is classified in a new genus *Promyohyrax*.

Unique to Eocliff is a genus of macroscelidean in which the cheek teeth and incisors are hypselodont (ever-growing crowns, with no development of roots) herein classified in a new family Afrohypselodontidae. *Afrohypselodontus* is represented at Eocliff by two species that differ in size.

Finally, at Eocliff there is a poorly represented, small taxon with unique molar and premolar morphology. It is currently left in open nomenclature, pending recovery of more informative specimens.

Comparisons between the Eocliff macroscelideans and Palaeogene herodotiine « macroscelideans » from North Africa reveal no close relationship to them, as previously mentioned by Senut (2008). Among the « macroscelideans » from North Africa, the only one that might be a true member of the order is the metoldobotine, *Metoldobotes*, but this genus is extremely poorly known (one upper molar, one incomplete mandible, some unpublished specimens).

The conclusion is that the Eocliff macroscelidean fauna is considerably more diverse than any of the Palaeogene and Neogene fossil assemblages described from Central and North Africa, which suggests that Southern Africa was a major evolutionary hotspot for this order. The early Miocene macroscelidean fauna from Namibia was also quite diverse (Senut, 2008) more so than the contemporaneous faunas of East Africa (Butler, 1995).

It has been said that Southern Africa was an evolutionary cul-de-sac but the Eocliff fauna provides evidence that it was, in contrast, a major centre of evolutionary activity, not only of plants, of which the Cape Floral Zone, despite its small area, is one of the six floral kingdoms of the world, but also of animals (Pickford, 2004; Pickford *et al*. 2016).

Table 14. Distribution of macroscelideans at the various fossiliferous patches at Eocliff. Absences at some spots are probably due to the small volume of tufa treated (- not present in sample, x present).

Taxon	EC1	EC2	EC4	EC6	EC7	EC8	EC9	EC10	EC14
Eorhynchocyon rupestris	-	-	-	x	x	-	x	-	-
Namasengi mockeae	x	x	x	x	x	x	x	x	x
Promyohyrax namibiensis	-	-	x	x	x	x	x	x	-
Afrohypselodontus minus	x	x	x	x	x	x	x	x	x
Afrohypselodontus grandis	-	-	x	-	x	x	x	x	-
Small sp. *incertae sedis*	-	-	-	x	-	x	x	x	-

Bunodonty, brachyodonty, hypsodonty and hypselodonty in Eocliff macroscelideans

The macroscelidean fossils from Eocliff show a high diversity of dental morphologies, presumably reflecting the principal focus of their diets. There are two

medium-sized to large forms with bunodont to brachyodont cheek dentitions, a small form with brachyodont cheek teeth, a medium-sized form with semi-hypsodont teeth as well as small and medium sized forms in which the cheek teeth are hypselodont.

The upper premolars of the bunodont rhynchocyonid from Eocliff has shallow occlusal basins, and the paraconule and metaconule are low and poorly expressed. The ectoloph is taller than the lingual cusps, and the hypocone is reduced in dimensions. The enamel in this form appears to be relatively thin. When deeply worn the occlusal surface of the cheek teeth is almost without relief. This suggests that the dentition was mainly of a crushing kind, presumably soft foods that did not require strong chewing forces, such as earth worms, termites and other soft bodied animals or soft plants.

Namasengi, the small brachyodont macroscelidean from Eocliff has low cusps in the posterior cheek teeth and rather thick enamel. The P4/ is fully molarised and the P3/ semi-molarised, but the anterior premolars are sectorial (bilaterally compressed, with tall mesial and distal stylids in the p/1-p/3). The diet of this form likely included small prey with hard-shelled bodies such as beetles.

Promyohyrax has cheek teeth that are semi-hypsodont, the increase in crown height resulting in apical hypsodonty (cusp hypsodonty of White, 1959, or multicusped hypsodonty of Von Koenigswald, 2020). The occlusal basins are retained into advanced wear, and have become deepened so as to resemble fossettes. The paraconule separates the talon basin from the mesial fovea, which itself is developed into a fossette, and the metaconule is enlarged and forms the wall of a fossette between it and the talon basin, the latter of

which is also fossette-like. This morphology heralds the situation present in the hypsodont early Miocene genera *Myohyrax* and *Protypotheroides*. In all three genera, strong roots develop. It is likely that *Promyohyrax* included some grass in its diet, but that its main food resources were probably of animal origin. *Myohyrax* and *Protypotheroides* from the early Miocene, in contrast, were probably obligate grazers but may have included a proportion of other food types, such as insects or fruit, in their diet (Senut, 2008).

None of the macroscelideans from Eocliff show classic sub-basinal hypsodonty in the restricted sense of the term (or tooth base hypsodonty of White, 1959) in which the apical, cuspal part remains brachyodont whereas the part below the talon and trigon basins is heightened, and roots are developed. In general mammals with hypsodont cheek teeth are grazers, either obligate or sometimes mixed feeders (White, 1959).

Two species of macroscelideans from Eocliff developed hypselodont dentitions, which are ever-growing teeth without the development of roots, even in senile individuals. Hypselodonty refers to teeth in which the apical cusp part remains low-crowned (unlike true hypsodonty) while the crown base is ever-growing (i.e. no roots develop). The term corresponds to « enamel-band hypso-donty » of Von Koenigswald (2020). The apical cusps and basins wear away soon after eruption, and from then onwards the teeth are ever-growing and do not develop roots. In *Afrohypselodontus* from Eocliff, not only did the two species possess hypselodont cheek teeth, but the central and lateral incisors were also hypselodont. These two species were probably obligate grazers.

Mandibular robuscticity and palatal fenestration

All the Eocliff macroscelideans possess mandibles with relatively robust bodies. The bone either side of the roots of the teeth is quite thick. This contrasts with the exceptionally thin bone that typifies the mandibles of extant *Elephantulus* and *Macroscelides*, in which the bone is so thin that the roots of the teeth can be observed through it.

In the Eocliff taxa for which the palatal process of the maxilla and the palatines are preserved, with the exception of *Afrohypselo-*

dontus minus there is no sign of palatal fenestration. This contrasts with the extensive fenestration that occurs in the extant genera of macroscelideans, not counting *Rhynchocyon* which lacks fenestra. The outcome is that the upper and lower jaws of extant macroscelideans (with the exception of *Rhynchocyon*) contain much less bone mass than their Eocene precursors. The selective pressures that resulted in this evolutionary trend are poorly understood, but it could be related to bone mass

redistribution in the skeleton keeping the total mass of the skeleton relative to total body mass, constant (Morales *et al.* 1992; Potter, 1986; Prange *et al.* 1979) or, less likely, it could be related to a reduction of skeletal mass relative to body mass in a swift-moving micro-cursorial mammal.

Body size estimates of Eocliff macroscelideans

Four complete macroscelidean long bones yield information about limb length and thus about possible body weights (Fig. 61). A humerus and a femur from EC10 are intermediate in length between those of *Petrodromus*, which is larger, and the group of genera comprising *Petrosaltator*, *Nasilio*, *Elephantulus*, *Macroscelides* and *Galegeeska*, which are smaller. On this basis a body weight of ca 100 grams is estimated for the taxon represented by these fossils. EC9 and EC10 yielded a femur and a tibio-fibula that are smaller than those of *Petrosaltator* etc. suggesting a body weight of ca 20-30 grams for the species concerned.
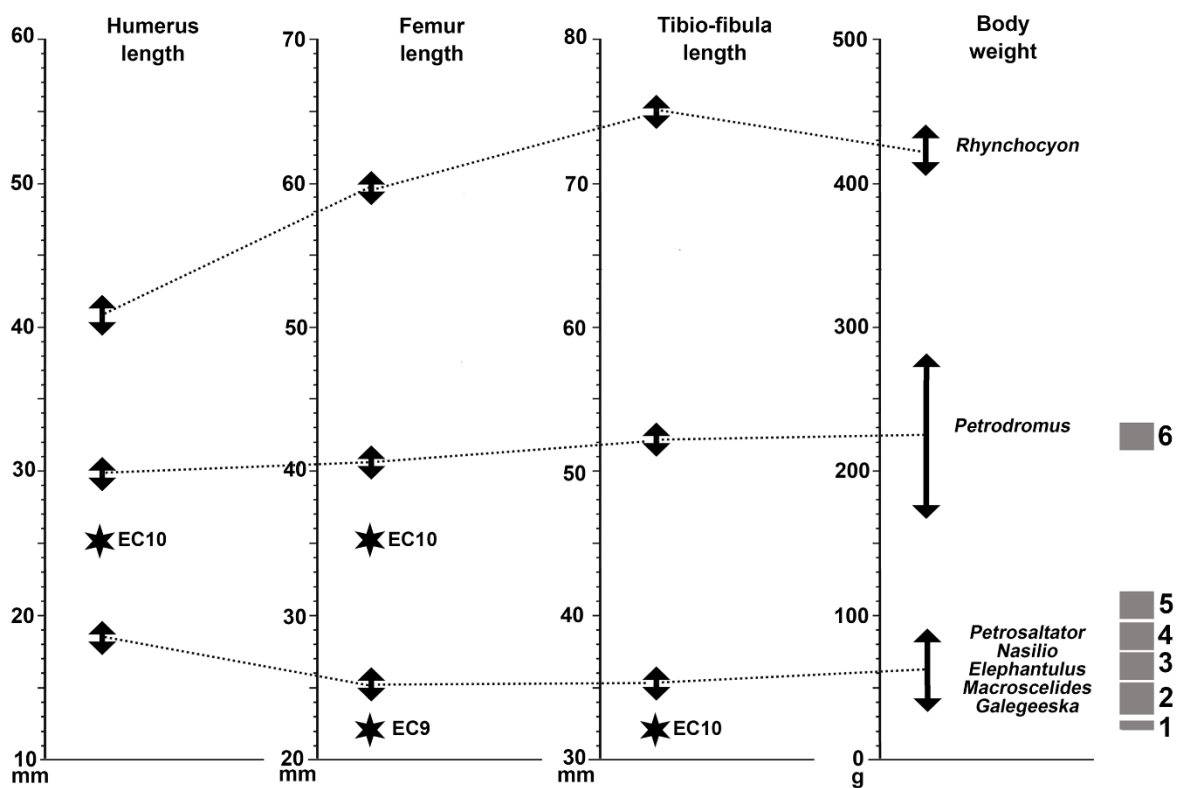
Figure 61. Long bone lengths and body weights of extant macroscelideans and some fossil specimens from Eocliff (data for extant taxa are from Evans, 1942; Skinner & Smithers, 1990; Kingdon, 1997, and Haltenorth & Diller, 1984). The right hand column provides approximate body weight estimates of the six described taxa from Eocliff. 1 - *Incertae sedis*, 2 - *Namasengi mockeae*, 3 - *Afrohypselodontus minus*, 4 - *Promyohyrax namibiensis*, 5 - *Eorhynchocyon rupestris*, 6 - *Afrohypselodontus grandis*.

Among the broken humeri, femora and tibio-fibulae from Eocliff, there are several specimens, the extremities of which are considerably larger than the largest of the complete bones. For example, an unfused (juvenile) distal tibio-fibula from EC10 is 6.0 mm broad medio-laterally, which compares with a breadth of 2.7 mm for the complete tibio-fibula from the same site. Other adult specimens from Eocliff (n = 5) are 4.0 to 4.2 mm broad and correspond to the metric range of variation of *Petrodromus*. The majority of adult distal tibio-fibulae from Eocliff (n = 9) range in breadth from 3.0 to 3.2 mm and thus correspond in dimensions to the group comprising *Petrosaltator*, *Nasilio*, *Elephantulus*, *Macroscelides* and *Galegeeska*.

The largest of the Eocliff macroscelideans is considered to have had approximately the same body weight as *Petrodromus* (ca 230 grams), but five of the taxa were smaller, with body weights ranging from ca 30 to ca 100 grams. The latter five taxa were therefore about the same dimensions as extant *Petrosaltator*, *Nasilio*, *Macroscelides*, *Galegeeska* and *Elephantulus*.

Locomotor adaptations of Eocliff macroscelideans

Abundant post-cranial skeletal elements from Eocliff are attributed to Macroscelidea because they accord closely with extant examples of this order. Limb bones are well represented, in particular elements of the ankle joint. The diaphyses of the tibia and fibula are synostosed over 60% of their length as in extant sengis, and the distal epiphyses of the tibia and fibula are strongly fused together, even if, in many individuals, they are not fused to the diaphysis. The talus has a prominent cotylar fossa, its neck is relatively long, and the trochlear margins are well defined, indicating that movement at the tibio-fibular-talar articulation was relatively constrained to the parasagittal plane. The calcanea from Eocliff have a long tuber calcis and the distance between the ectal facet and that for the navicular and cuboid is almost as great as the length of the tuber above the ectal facet.

The humeri and ulnae from Eocliff are similar to those of extant macroscelideans, the distal articulation of the humerus being bilaterally compressed with sharp trochlear margins, deep fossae cranially and caudally that pierce the bone completely above the trochlea, and the presence of an entepicodylar foramen.

On the basis of these specimens it is inferred that all the taxa described from Eocliff were micro-cursorial in much the same way as extant sengis (Lovegrove & Mowoe, 2014) but they may have been more lightly built and more agile.

North African « macroscelideans »

Comparisons between the Eocliff macroscelidean assemblage and fossils from North Africa that have been attributed to this order at one time or another, reveals that none of them show close derived dental and cranio-mandibular affinities with them. The only post-cranial elements of the North African forms comprise a talus and a calcaneum attributed to *Chambius kasserinensis* by Tabuce *et al*. 2007, which resemble those of macroscelideans.

In all the Eocliff forms, the mandible shows two mental foramina, an anterior one beneath the canine or p/1 and the posterior one beneath the p/4-m/1. *Herodotius* from the Fayum, Egypt, reportedly has two foramina, one beneath the canine, the other beneath the p/1 (Simons *et al*. 1991). In the maxilla of *Herodotius*, the root of the zygomatic process is opposite the M2/, whereas in the Eocliff macroscelideans, with the exception of *Afrohypselodontus*, the zygomatic arch leaves the face of the maxilla further forwards, the anterior part of the root being in line with the middle of M1/. The facial opening of the infra-orbital canal in *Herodotius* is located above the P3/ whereas in all the Eocliff macroscelideans the opening is above the P4/. With the exception of *Afrohypselodontus*, the bunodont, brachyodont and semi-hypsodont Eocliff macroscelideans possess a facial fossa associated with the infra-orbital opening, whereas the facial fossa is absent in *Herodotius*. The upper molars of *Herodotius* possess buccal cingula, but none of the Eocliff genera do.

Chambius, from the middle Eocene of Tunisia (Hartenberger, 1986) likewise shows a number of crucial differences from all the Eocliff macroscelideans. The anterior mental foramen of the mandible is further to the rear in *Chambius* than it is in any of the Eocliff taxa, being located beneth the p/2. The upper molars of *Chambius* are endowed with well-developed buccal cingula, unlike any of the Eocliff forms, and in P4/ the protocone is significantly larger than the hypocone, the opposite of the situation in the Eocliff species. On the face of the maxilla, in *Chambius*, the infra-orbital canal emerges above the front of M2/, which is further to the rear than its position in any of the Eocliff forms, where it is located above the P4/. With the exception of *Afrohypselodontus*, the root of the zygomatic arch is further to the rear in *Chambius* than it is in the Eocliff taxa. Another major difference between *Chambius* and the

Eocliff macroscelideans concerns the lower molars. None of the Eocliff specimens possesses buccal cingulids on the lower molars, whereas *Chambius* does (Tabuce, 2018). A further difference concerns the calcaneum, which, in *Chambius*, has a prominent, laterally projecting peroneal process (Tabuce *et al*. 2007) whereas in none of the Eocliff tali (n = 68) is the process as large nor does it project as far laterally.

The holotype upper molar of *Eotmantsoius* from Dur At-Talah, Libya, possesses a distinct entostyle attached to the hypocone, and a low cingular cusplet (pericone) in front of the protocone (Tabuce, 2018). These structures are not present in any of the Eocliff specimens.

Upper molars of *Nementchatherium* from Algeria possess buccal cingula and the hypocone of the P4/ is smaller than the protocone (Tabuce, 2018; Tabuce *et al*. 2001). None of the Eocliff macrosclideans has a buccal cingulum and in all of them the protocone of the P4/ is smaller than the hypocone. Tabuce (2018) documents the presence of a coronoid foramen at the base of the ascending ramus behind the m/3 in *Nementchatherium*. None of the Eocliff species has such a foramen.

Metoldobotes from the Fayum, Egypt, is poorly known (Schlosser, 1910, 1911; Patterson, 1965) but its upper molar shows some resemblances to the brachyodont and semi-hypsodont taxa from Eocliff, such as a deep, narrow lingual sinus that connects to the trigon basin, and a well-developed metaconule, but it lacks the paraconule (Simons *et al*. 1991) which is present in the Eocliff forms. *Metoldobotes*, like the Eocliff forms, lacks a buccal cingulum in the upper molars.

In summary, the only North African Palaeogene taxon hitherto included in Macroscelidea that might belong to the group is *Metoldobotes*, but its fossil record is so scanty (a mandible and an isolated upper molar) that its affinities will remain obscure until more informative material becomes available. Seiffert (2003, 2007) mentions the existence of an undescribed species of *Metoldobotes* from the Fayum, Egypt, but few details are available.

As concerns the genera *Herodotius*, *Nementchatherium*, *Chambius* and *Eotmantsoius*, previous interpretations linking them to Macroscelidea require support from a more substantial fossil record, including post-cranial skeletal elements. The resemblances to Macroscelidea are possibly primitive characters or convergences, and the differences from the Eocliff fossils outlined above, indicate that any relationships between the North African and Southern African Palaeogene lineages are likely to be remote. In conclusion the proposed inclusion of the North African forms in the order Macroscelidea requires more convincing support over and above the resemblances already evoked in the literature.

Origins of Macroscelidea

The order Macroscelidea has had an exceptionally convoluted history of inter-pretation. Patterson (1965) summarised the anatomical evidence which formed the basis for the various points of view concerning its systematic position within Mammalia. Starting with its inclusion in Insectivora, this grouping was subsequently subdivided into two major groups on the basis of the presence or absence of a caecum. Macroscelideans thereby became linked to colugos and tupaiids because they lack a caecum. Links to tupaiids, which at the time were included in Primates, were generally accepted for a long time, but Patterson (1965) considered that macroscelideans were an ancient group that originated early in the Cenozoic, if not towards the end of the Mesozoic. He emphasised that they « *may well have been members of this 'old African'* » fauna which comprised hyracoids, arsinoitheres, moeritheres, barytheres, proboscideans and catarrhine primates. This was a prescient inference, because, with the development of molecular biology, macroscelideans have become firmly embedded within the Afrotheria, which, with the exception of the primates, includes all the members of the 'old African' faunas listed by Patterson (1965).

However, the origins of the order are still not settled, with authors linking macroscelideans to diverse lineages from Eurasia and North America, thereby suggesting that the order dispersed to Africa from a neighbouring continent (Hooker & Russell, 2012; Novacek, 1984). During the past two decades, among the groups that have been linked more or less closely to Macroscelidea are the Hyopsodontidae (Halliday *et al*. 2017; Zack

et al. 2005), the Apheliscidae (Penkrot *et al.* 2008; Tabuce *et al.* 2001, 2006) and the Louisinidae (Hooker & Russell, 2012). Most of these hypotheses accept that the North African herodotiines are stem group macroscelideans (Tabuce *et al.* 2007) which, as argued above, may not strictly be the case.

Links to South American mammals have also been proposed (Agnolin & Chimento, 2011) and considering the dental and mandibular resemblances between some of the Eocliff macroscelideans and some of the South American notoungulates, this is possibly a more likely hypothesis than those linking them to European, Asian or North American groups. If so, then it is possible that macroscelideans originated in Africa (in particular Southern Africa) prior to the Eocene, and then dispersed to South America during the mid-late Eocene, more or less at the same times as rodents and primates.

Novacek (1984) in particular stressed the presence of deep fossettes and fossettids in the molars of some Macroscelideans (his characters 25 and 26), morphology that also occurs in a variety of South American notoungulates (Agnolin & Chimento, 2011).

Links to South America

By naming one of the early Miocene fossils from Namibia *Protypotheroides*, Stromer (1922) implied two things. Although not stated as such, the first was that it didn't represent a typical hyracoid (at the time the closely related genus *Myohyrax* was thought to be a hyracoid). The second, which was more strongly implied was that the species was possibly related to *Protypotherium* from South America. This point was evinced by Du Toit (1944) while he was responding to criticism by G.G. Simpson (1943) concerning the hypothesis of continental drift. Stromer (1922) recognised that the bulk of the Namibian early Miocene faunas indicated affinities with North and Central Africa, but according to Du Toit (1944) he considered that the « specialised hyracoid *Protypotheroides* is allied to the Miocene *Protypotherium* from Patagonia ».

Patterson (1965) dismissed the possibility that macroscelidids were related to South

The Eocliff macroscelidean post-cranial elements, and those from the early Miocene of Namibia (Senut, 2008) are so similar to those of extant sengis, that they call into doubt some of the phylogenetic interpretations based on the ankle joint of other groups that have at one time or another been viewed as ancestral to Macroscelidea, such as the Hyopsodontidae (Halliday *et al* 2017), Louisinidae (Hooker & Russell, 2012; Tabuce *et al.* 2006) and Apheliscidae (Penkrot *et al.* 2008). In the abstract of their paper, Lovegrove & Mowoe (2014) reported that early Eocene *Prodiacodon* from North America was the earliest macroscelid, but the results of their analyses demonstrate that it is unlikely that this genus belongs to the order.

The new evidence from Eocliff strengthens Patterson's (1965) point of view that the '*old African fauna*' (Primates excepted) originated in Africa, rather than Europe, Asia or North America. We thus ascribe to an African origin of the Afrotheria, followed by dispersal of some groups to other continents during the Palaeogene and Neogene.

American notoungulates, although he did mention that the myohyracines, like the notoungulates, had achieved the « ungulate » grade independently from the true ungulates which he considered were descended from Condylarthra.

Pickford (2018) demonstrated that similarities existed between tufamyid rodents from Eocliff and certain ctenohystrican lineages from South America, indicating that some small mammals somehow managed to disperse from Africa to South America during the Bartonian. It is not beyond the realms of possibility that forms of macroscelideans such as *Promyohyrax* or *Afrohypselodontus* were also implicated in a similar dispersal process. Further research is warranted, especially given that the Eocliff macroscelidean fossils are remarkably complete, and that further fossil discoveries will surely be made.

Conclusions

The richly fossiliferous tufa dome at Eocliff has yielded immense quantities of small mammal remains, as well as some birds and reptiles. Large mammals are rarer, but hyracoids are present. On the basis of the few large mammals found at Eocliff and Eoridge, the tufas are estimated to have accumulated during the Bartonian-Priabonian (Pickford, 2015a, 2020) and younger than the Black Crow carbonates (Ypresian-Lutetian, Pickford *et al.* 2008). Among the micro-mammals from Eocliff, macroscelideans are particularly abundant, currently represented by over 1,000 cranio-dental and post-cranial elements.

There are at least six species of macroscelideans at Eocliff. Small taxa are common, larger ones rare. The assemblage contains bunodont, brachyodont, hypsodont and hypselodont taxa indicating a great variety of dietary adaptations.

A new genus, of Rhynchocyonidae, *Eorhynchocyon*, is erected for a species that is much smaller than the extant genus, but which shares similar mandibular morphology. There are some similarities between the mandible of this genus and those of Orycteropodidae, but unlike the enamel-free teeth of this family, the teeth of *Eorhynchocyon* possess enamel.

A new subfamily of Macroscelididae (Namasenginae) is erected for *Namasengi* nov. gen., the main distinguishing characters being the lack of fenestration of the palate, and the retention of upper and lower third molars.

A new genus of Myohyracidae, *Promyohyrax*, is erected for a semi-hypsodont lineage that has lower crowned teeth than *Myohyrax* and *Protypotheroides*, but like them, possesses fossettes and fossettids in the upper and lower cheek teeth respectively, and like them, develops strong roots. This new genus is possible the ancestor of both *Protypotheroides* and *Myohyrax*.

A new family, Afrohypselodontidae is erected for the new genus *Afrohypselodontus*, which is characterised by the presence of hypselodont cheek teeth and incisors, these teeth being ever-growing and rootless. The sinuses and outer surfaces of the cheek teeth are covered in cementum (not always preserved in some of the fossils). In this lineage there is an extremely shallow facial fossa, and the infra-orbital canal emerges at the dorsal surface of the maxilla above the cervical part of the P4/. The palatine in *Afrohypselodontus* has fenestrae. There are two size groups in this genus, interpreted to represent distinct species, *Afrohypselodontus minus* and *Afrohypselodontus grandis* the dimensions of which differ by ca 30%.

The sixth species of macroscelidean at Eocliff is too poorly represented to name, but it shows several unique dental features such as the presence of accessory cuspids on the buccal angle of the protoconid and reduced *tuberculum intermedium* in the lower molars and premolars.

Many post-cranial elements from Eocliff are typical of macroscelideans, in particular the tibio-fibula, which is strongly synostosed over 60% of its length, and the distal epiphysis of the tibia-fibula, which is strongly synostosed even in juveniles in which it has not yet fused to the diaphysis. The talus has a prominent cotylar fossa, an elongated neck and raised trochlea margins. The femur has a large third trochanter, and the patella groove is long and narrow, extending well onto the diaphysis. The post-cranial bones indicate that all of the Eocliff taxa were adapted for micro-cursoriality.

Comparisons with North African fossils attributed to Macroscelidea reveal deep differences from most of them, the only genus that partly accords with the Eocliff forms is *Metoldobotes*, but this genus is still poorly known. The other genera (*Herodotius*, *Chambius*, *Nementchatherium*, *Eotmantsoius*) possess buccal cingula on the upper molars (and some of them on the lower molars as well), a structure that is unknown at Eocliff and in all younger genera of the order.

There are some morphological resemblances between the teeth and mandible of *Afrohypselodontus* and some South American groups (hypsodont notoungulates) (Agnolin & Chimento, 2011; Cassini *et al.* 2017). In both groups the posterior lower molars are arranged in the jaw such that the cervices are far apart while the occlusal parts are in contact with each other, and the distal margins of the m/2 and m/3 are slightly concave.

There are also a few dental similarities between *Promyohyrax* and some notoungulates, notably the presence of deep fossettes between the paraconule and paracone, and between the metaconule and metacone, in addition to those formed of the trigon and talon basins.

A revision of the systematics of the order Macroscelidea suggests that the ranks of some of the supra-generic groups need to be increased. What used to be commonly accepted as subfamilies are herein increased in rank to families. For example, in its mandibular morphology (slanting ascending ramus) and suppression of the m/3, the genus *Eorhynchocyon* is close to extant *Rhynchocyon*, despite its considerably smaller dimensions. It is also comparable in this respect to *Hypsorhynchocyon* from the early Miocene of Namibia (Senut, 2008). All the other genera of Eocliff macroscelideans have steep ascending rami and retain upper and lower third molars. These differences indicate a deeper subdivision between the groups than is suggested by subfamilial distinctions. Thus, four families of Macroscelidea are recognised in this work - Rhynchocyonidae, Macroscelididae, Myohyracidae and Afrohypselodontidae.

In the revised systematic scheme presented herein, the Macroscelididae contains four subfamilies - Macroscelidinae, Elephantulinae, Mylomygalinae and Namasenginae nov.

Apart from *Metoldobotes*, which might be a macroscelidean (a more comprehensive fossil record is required to settle its status) the North African « macroscelideans » are considered to be of doubtful or uncertain status, as are the relations of the Hyopsodontidae, Louisinidae and Apheliscidae to the Macroscelidea.

The Afrotheria thus appear to have originated in Africa (Patterson, 1965; Butler, 1995) and some of them, but not the Macroscelidea, then dispersed to other continents during the Palaeogene and Neogene.

Acknowledgements

References

Agnolin, F.L. & Chimento, N.R. 2011. Afrotherian affinities for endemic South American « ungulates ». *Mammalian Biology*, **76**, 101-108.

Andrews, C.W. 1914. On the lower Miocene vertebrates from British East Africa, collected by Dr Felix Oswald. *Quarterly Journal of the Geological Society of London*, **70,** 163-186.

Avery, M. 2019. *A Fossil History of Southern African Land Mammals*. Cambridge, Cambridge University Press, 315 pp.

Bonaparte, C.L. 1838. Synopsis vertebratorum systematis. *Nuovi Annali delle Scienze Naturali*, **1**, 105-133.

Broom, R. 1948. Some South African Pliocene and Pleistocene mammals. *Annals of the Transvaal Museum*, **21**, 1-38.

Butler, P.M. 1956. The skull of *Ictops* and the classification of the Insectivora. *Proceedings of the Zoological Society of London,* **126**, 453-481.

Butler, P.M. 1969. Insectivores and bats from the Miocene of East Africa : new material. *Fossil Vertebrates of Africa*, **1**, 1-37.

Butler, P.M. 1984. Macroscelidea, Insectivora and Chiroptera from the Miocene of East Africa. *Palaeovertebrata*, **14**, 117-200.

Butler, P.M. 1987. Fossil insectivores from Laetoli. *In*: Leakey, M.D. & Harris, J.M. (Eds) *Laetoli : A Pliocene Site in Northern Tanzania*, Oxford, Clarendon Press, pp. 85-87.

Butler, P.M. 1995. Fossil Macroscelidea. *Mammal Review*, **25 (1-2)**, 3-14.

Butler, P.M. & Greenwood, M. 1976. Lower Pleistocene elephant-shrews (Macroscelididae) from Olduvai Gorge and Makapansgat. *Fossil Vertebrates of Africa,* **4**, 1-56.

Butler, P.M. & Hopwood, A.T. 1957. Insectivora and Chiroptera from the Miocene rocks of Kenya Colony. *British Museum of Natural History, London, Fossil Mammals of Africa*, **13**, 1-35.

Cassini, G.H., Hernandez Del Pino, S., Muñoz, N.A., Acosta, M.V.W.G., Fernandez, M., Bargo, M.S. & Vizcaino, S.F. 2017. Teeth complexity, hypsodonty and body mass in Santacrucian (Early Miocene) notoungulates (Mammalia). *Earth and Environmental Science Transactions of the Royal Society of Edinburgh*, **106**, 303-313.

Corbet, G.B. & Hanks, J. 1968. A revision of the elephant-shrews, family Macroscelididae. *Bulletin of the British Museum of Natural History (Zoology)* **16**, 47-111.

Corvinus, G. & Hendey, Q.B. 1978. A new Miocene vertebrate locality at Arrisdrift in Namibia (South West Africa). *Neues Jahrbuch für Geologie und Paläontologie, Monatshefte*, **1978**, 193-205.

De Graaf, G. 1961. A preliminary investigation of the mammalian microfauna in Pleistocene deposits of caves in the Transvaal System. *Palaeontologia Africana,* **7**, 59-118.

Dumbacher, J.P., Carlen, E.J. & Rathbun, G.B. 2016. *Petrosaltator* gen. nov., a new genus replacement for the North African sengi *Elephantulus rozeti* (Macroscelidea; Macroscelididae). *Zootaxa*, **4136 (3)**, 567-579.

Du Toit, A. 1944. Tertiary Mammals and Continental Drift. A Rejoinder to George G. Simpson. *American Journal of Science*, **242**, 145-163.

Evans, F.G. 1942. Osteology and relationships of the elephant shrews (Macroscelididae).

Bulletin of the American Museum of Natural History, **80**, 85-125.

Garcia Lopez, D.A. & Powell, J.E. 2011. *Griphotherium peiranoi*, gen. et sp. nov. ; a new Eocene Notoungulata (Mammalia, Meridiungulata) from Northwestern Argentina. *Journal of Vertebrate Paleontology*, **31** (**5**), 1117-1130.

Gill, T. 1872. Arrangement of the Families of Mammals with analytical tables. *Smithsonian Miscellaneous Collections*. **230**, 1-98, Washington, Smithsonian Institution.

Gregory, W.K. 1920. Studies in comparative myology and osteology: N° 4. A review of the evolution of the lacrymal bone of vetebrates with special reference to that of mammals. *Bulletin of the American Museum of Natural History*, **42**, 95-263.

Grossman, A. & Holroyd, P.A. 2009. *Miosengi butleri*, gen. et sp. nov., (Macroscelidea) from the Kalodirr Member, Lothidok Formation, early Miocene of Kenya. *Journal of Vertebrate Paleontology*, **29**, 957-960.

Halliday, J.D., Upchurch, P. & Goswami, A. 2017. Resolving the relationships of Paleocene placental mammals. *Biological Reviews*, **92**, 521-550.

Haltenorth, T. & Diller, H. 1984. *A Field Guide to the Mammals of Africa including Madagascar*. London, Collins, 400 pp.

Hartenberger, J.-L. 1986. Hypothèse paléontologique sur l'origine des Macroscelidea (Mammalia). *Comptes rendus de l'Académie des Sciences, Paris*, **302**, 247-249.

Hendey, Q.B. 1978. Preliminary report on the Miocene vertebrates from Arrisdrift, South West Africa. *Annals of the South African Museum*, **76 (1)**, 1-41.

Heritage, S. & Rayaleh, H. 2020. *In*: Heritage, S., Rayaleh, H., Awaleh, D.G. & Rathbun, G.B. 2020. New records of a lost species and a geographic range expansion for sengis in the Horn of Africa. *PeerJ* 8:e9652 DOI 10.7717/peerj.9652. 38 pp.

Holroyd, P. 2009. Past records of *Elephantulus* and *Macroscelides* : geographic and taxonomic issues. *Afrotherian Conservation*, **7**, 3-7.

Holroyd, P. 2010. Macroscelidea. *In*: Werdelin, L. & Sanders, W.J. (Eds) *Cenozoic Mammals of Africa*, University of California Press (Berkeley, Los Angeles, London) pp. 89-98.

Hooker, J.J. & Russell, D.E. 2012. Early Palaeogene Louisinidae (Macroscelidea,

Mammalia), their relationships and north European diversity. *Zoological Journal of the Linnean Society*, **164**, 856-936.

Hopwood, A.T. 1929. New and little known mammals from the Miocene of Africa. *American Museum Novitates*, **334**, 1-9.

Kingdon, J. 1997. *The Kingdon Field Guide to African Mammals*. London, Academic Press, 464 pp.

Krásová, J., Mikula, O., Šumbera, R., Horáková, S., Robovský, J., Kostin, D.S., Martynov, A.A., Lavrenchevko, L.A. & Bryja, J. 2021. The Rufous Sengi is not *Elephantulus* – Multilocus reconstruction of evolutionary history of sengis from the subfamily Macroscelidinae. *Journal of Zoological Systematics and Evolutionary Research*, doi.org/10.1111/jzs.12460.

Lovegrove, B.G. & Mowoe, M.O. 2014. The evolution of micro-cursoriality in mammals. *Journal of Experimental Biology*, **217**, 1316-1325.

Matthew, W.D. 1915. A revision of the lower Eocene Wasatch and Wind River faunas: Part II. Order Condylarthra, Family Hyopsodontidae. *Bulletin of the American Museum of Natural History,* **34**, 311-328.

Mein, P., Pickford, M. & Senut, B. 2000b. Late Miocene micromammals from the Harasib karst deposits, Namibia. Part 2a - Myocricetodontinae, Petromyscinae and Namibimyinae (Muridae, Gerbillidae). *Communications of the Geological Survey of Namibia*, **12**, 391–401.

Mones. A. 1982. An equivocal nomenclature: What means hypsodonty? *Paleontological Journal*. **56** (**1-2**), 107-111.

Morales, J., Pickford, M. & Soria, D. 1992. Pachyostosis in a Lower Miocene giraffoid from Spain, *Lorancameryx pachyostoticus* nov. gen. nov. sp. and its bearing on the evolution of bony appendages in artiodactyls. *Geobios*, **26** (**2**), 207-230.

Mourer-Chauviré, C., Pickford, M. & Senut, B. 2014. Stem group galliform and stem group psittaciform birds (Aves, Galliformes, Paraortygidae and Psittaciformes, family *incertae sedis*) from the Middle Eocene of Namibia. *Journal of Ornithology*, DOI: 10.1007/s10336-014-1224-y, 12 pp.

Mourer-Chauviré, C., Pickford, M. & Senut, B. 2018. New data on stem group Galliformes, Charadriiformes, and Psittaciformes from the middle Eocene of Namibia. Paleontología y Evolución de las Aves. *Contrib-*

uciones Cientificas del Museo Argentino de Ciencias Naturales "Bernardino Rivadavia", **7**, 99-131.

Novacek, M. 1984. Evolutionary stasis in the Elephant-Shrew, *Rhynchocyon*. *In*: Eldredge, N. & Stanley, S.M. (Eds) *Living Fossils*, New York, Springer-Verlag, pp. 4-22.

Patterson, B. 1965. The fossil elephant shrews (family Macroscelididae). *Bulletin of the Museum of Comparative Zoology, Harvard*, **133**, 295-335.

Peters, W.K.H. 1846. Neue Säugethier-gattungen aus den Ordnungen der Insectenfresser und Nagethiere. *Bericht über die zur Bekanntmachung geeigneten Verhandlungen der Königlichen Preussischen Akademie der Wissenschaften zu Berlin*, **1846**, 257-259.

Peters, W.K.H. 1847. Neue Säugethiergattung aus der Ordnung der Insektenfresser. *Bericht über die zur Bekanntmachung geeigneten Verhandlungen der Königlichen Preussischen Akademie der Wissenschaften zu Berlin*, **1847**, 36-38.

Pickford, M. 2004. Southern Africa: a cradle of evolution. *South African Journal of Science*, **100**, 205-214.

Pickford, M. 2015a. Cenozoic Geology of the Northern Sperrgebiet, Namibia, accenting the Palaeogene. *Communications of the Geological Survey of Namibia*, **16**, 10-104.

Pickford, M. 2015b. Late Eocene Potamogalidae and Tenrecidae (Mammalia) from the Sperrgebiet, Namibia. *Communications of the Geological Survey of Namibia*, **16**, 114-152.

Pickford, M. 2015c. Late Eocene Chrysochloridae (Mammalia) from the Sperrgebiet, Namibia. *Communications of the Geological Survey of Namibia*, **16**, 153-193.

Pickford, M. 2015d. Late Eocene Lorisiform Primate from Eocliff, Sperrgebiet, Namibia. C*ommunications of the Geological Survey of Namibia*, **16**, 194-199.

Pickford, M. 2015e. New Titanohyracidae (Hyracoidea: Afrotheria) from the Late Eocene of Namibia. *Communications of the Geological Survey of Namibia*, **16**, 200-214.

Pickford, M. 2015f. *Bothriogenys* (Anthracotheriidae) from the Bartonian of Eoridge, Namibia. *Communications of the Geological Survey of Namibia*, **16**, 215-222.

Pickford, M. 2018. Tufamyidae, a new family of hystricognath rodents from the

Palaeogene and Neogene of the Sperrgebiet, Namibia. *Communications of the Geological Survey of Namibia*, **19**, 71-109.

Pickford, M. 2019. Orycteropodidae (Tubuli-dentata, Mammalia) from the Early Miocene of Napak, Uganda. *Münchner Geowissen-schaftliche Abhandlungen, Reihe A, Geologie und Paläontologie*, **47**, 1-101.

Pickford, M. 2020. Two new rodents (Rodentia, Mammalia) from the late middle Eocene of Eocliff, Namibia. *Communications of the Geological Survey of Namibia*, **22**, 21-46.

Pickford, M., Senut, B., Mocke, H., Mourer-Chauviré, C., Rage, J.-C. & Mein, P. 2014. Eocene Aridity in southwestern Africa: timing of onset and biological consequences. *Transactions of the Royal Society of South Africa* pp. 1-6, doi: 10.1080/0035919X.2014.933452,

Pickford, M., Senut, B., Morales, J., Mein, P. & Sanchez, I.M. 2008. Mammalia from the Lutetian of Namibia. *Memoir of the Geological Survey of Namibia*, **20**, 465-514.

Potter, B. 1986. The allometry of Primate skeletal weight. *International Journal of Primatology*, **7**, 457-466.

Prange, H.D., Anderson, J.F. & Rahn, H. 1979. Scaling of skeletal mass to body mass in birds and mammals. *American Naturalist*, **113**, 103-122.

Rathbun, G.B. & Dumbacher, J.P. 2016. *In*: Dumbacher, J.P., Carlen, E.J. & Rathbun, G.B. 2016. *Petrosaltator* gen. nov., a new genus replacement for the North African sengi *Elephantulus rozeti* (Macroscelidea; Macroscelididae). *Zootaxa*, **4136 (3)**, 567-579.

Rose, K.D. 2006. The postcranial skeleton of early Oligocene *Leptictis* (Mammalia: Leptictida), with a preliminary comparison to *Leptictidium* from the middle Eocene of Messel. *Palaeontographica Abteilung A* **278**, 37-56.

Schlosser, M. 1910. Über einige fossile Säugetiere aus dem Oligocän von Ägypten. *Zoologischer Anzeiger*, **35**, 500-508.

Schlosser, M. 1911. Beiträge zur Kenntnis der oligozänen Landsäugetiere aus dem Fayum, Ägypten. *Beiträge zur Paläontologie und Geologie Österreich-Ungarns*, **24**, 51-167.

Seiffert, E.R. 2003. *A Phylogenetic Analysis of Living and Extinct Afrotherian Placentals*. Unpublished PhD Dissertation, Duke University, North Carolina.

Seiffert, E. 2007. A new estimate of afrotherian phylogeny based on simultaneous analysis of genomic, morphological, and fossil evidence. *BMC Evolutionary Biology*, **7**, 1-13, doi:10.1186/1471-2148-7-224.

Senut, B. 2003. The Macroscelididae from the Miocene of the Orange River, Namibia. *In*: Pickford, M. & Senut, B. (Eds), Geology and Palaeobiology of the Central and Southern Namib. Volume 2: Palaeontology of the Orange River Valley. *Memoir of the Geological Survey of Namibia*, **19**, 119-141.

Senut, B. 2008. Macroscelididae from the lower Miocene of the Northern Sperrgebiet, Namibia. *Memoir of the Geological Survey of Namibia*, **20**, 185-225.

Senut, B. & Georgalis, G. 2014. *Brevirhyncho-cyon* gen. nov., a new name for the genus *Brachyrhynchocyon* Senut, 2008 (Mamm-alia, Macroscelidea) preoccupied by *Brachyrhynchocyon* Loomis, 1936 (Mamm-alia, Carnivora). *Communications of the Geological Survey of Namibia*, **15**, 69.

Senut, B., Pickford, M., de Wit, M., Ward J., Spaggiari R. & Morales, J. 1996. Biochron-ology of sediments of Bosluis Pan, Northern Cape Province, South Africa. *South African Journal of Science*, **92**, 249-251.

Simons, E.L., Holroyd, P. & Bown, T.M. 1991. Early Tertiary elephant-shrews from Egypt and the origin of the Macroscelidea. *Proceedings of the National Academy of Science, USA*, **95**, 9967-9972.

Simpson, G.G. 1943. Mammals and the nature of continents. *American Journal of Science*, **241**, 1-31.

Skinner, J.D. & Smithers, R.H.N. 1990. *The Mammals of the Southern African Subregion*, 2nd edition. University of Pretoria, Republic of South Africa, CTP Book Printers Cape, pp. i-xxxii + 1-771.

Smith, A. 1829. Contributions to the natural history of South Africa. *Zoological Journal of London*, **4 (16)**, 433-444.

Stromer, E. 1922. Erste Mitteilung über Tertiäre Wirbeltier-reste aus Deutsch-Sudwestafrika. *Sitzungsberichte der Bayerische Akademie der Wissenschaften,* **1921 (2)**, 331-340.

Stromer, E. 1926. Reste Land- und Süss-wasserbewohnender Wirbeltiere aus den Diamantfeldern Deutsch-Südwestafrikas. *In*: Kaiser, E. (Ed.) *Die Diamantenwuste Südwest-Afrikas*, Berlin, Reimer, volume **2**, 107-153.

Stromer, E. 1931a. Reste Süsswasser und Land bewohnender Wirbeltiere aus den Diamantfeldern Klein-Namaqualandes (Südwestafrika). *Sitzungsberichte der mathematisch Physikalischen Klasse, Bayerische Akademie der Wissenschaften,* **1931**, 17-47.

Stromer, E. 1931b. *Palaeothentoides africanus* nov. gen. nov. spec. ein erstes Beuteltier aus Afrika. *Sitzungsberichte der Bayerischen Akadamie der Wissenschaften,* **1931**, 177-190.

Sudre, J. & Russell, D.E. 1982. Les mammifères montiens de Hainin (Paléocène moyen de Belgique). Part II: Les condylarthres. *Palaeovertebrata*, **12**, 173-184.

Tabuce, R. 2018. New remains of *Chambius kasserinensis* from the Eocene of Tunisia and evaluation of proposed affinities for Macroscelidea (Mammalia, Afrotheria). *Historical Biology*, **30** (**5**), 251-266.

Tabuce R., Coiffait, B., Coiffait, P.-E., Mahboubi, M. & Jaeger, J.-J. 2001. A new genus of Macroscelidea (Mammalia) from the Eocene of Algeria: A possible origin for elephant-shrews. *Journal of Vertebrate Paleontology*, **21**, 535-546.

Tabuce, R. & Jaeger, J.-J. 2012. *In*: Tabuce, R., Jaeger, J.-J., Marivaux, L., Salem, M., Bilal, A.A., Benammi, M., Chaimanee, Y., Coster, P., Marandat, B., Valentin, X. & Brunet, M. 2012. New stem elephant-shrews (Mammalia, Macroscelidea) from the Eocene of Dur At-Talah, Libya. *Palaeontology*, **55** (**5**), 945-955.

Tabuce, R., Jaeger, J.-J., Marivaux, L., Salem, M., Bilal, A.A., Benammi, M., Chaimanee, Y., Coster, P., Marandat, B., Valentin, X. & Brunet, M. 2012. New stem elephant-shrews (Mammalia, Macroscelidea) from the Eocene of Dur At-Talah, Libya. *Palaeontology*, **55** (**5**), 945-955.

Tabuce, R., Marivaux, L., Adaci, M., Bensalah, M., Hartenberger, J.-L., Mahboubi, M., Mebrouk, F., Tafforeau, P. & Jaeger, J.-J. 2007. Early Tertiary mammals from North Africa reinforce the molecular Afrotheria clade. *Proceedings of the Royal Society B*. **274**, 1159-1166.

Tabuce, R., Telles Antunes, M., Smith, R. & Smith, T. 2006. Dental and tarsal morphology of the European Paleocene/Eocene 'condylarth' mammaml *Microhyus*. *Acta Palaeontologica Polonica* **51** (**1**), 37-52.

Thomas, O. & Schwann, H. 1906. The Rudd exploration of South Africa - V. List of mammals obtained by Mr Grant in North East Transvaal. *Proceedings of the Zoological Society of London*, **1906**, 575-591.

Von Koenigswald, W. 2020. Construction and wear of mammalian teeth in terms of heterochrony. *In*: Martin, T. & Von Koenigswald, W. (Eds) *Mammalian Teeth - Form and Function*. München, Friedrich Pfeil Verlag, pp. 171-186.

Wanas, H., Pickford, M., Mein, P., Soliman, H. & Segalen, L. 2009. Late Miocene karst system at Sheikh Abdallah, between Bahariya and Farafra, Western Desert, Egypt: Implications for palaeoclimate and geomorphology. *Geologica Acta*, **7** (**4**), 475-487.

White, T.E. 1959. The endocrine glands and evolution, N° 3: Os cementum, hypsodonty, and diet. *Contributions from the Museum of Paleontology, The University of Michigan*, **13** (**9**), 211-265.

Whitworth, T. 1954. The Miocene hyracoids of East Africa. *Fossil Mammals of Africa,* **7**, 1-58.

Zack, S.P., Penkrot, T.A., Bloch, J.I. & Rose, K.D. 2005. Affinities of 'hyopsodontids' to elephant shrews and a Holarctic origin of Afrotheria. *Nature*, **434**, 497-50.

Taxonomic revision of the genus *Leptoplesictis* (Viverridae, Mammalia) with description of new fossils from Grillental VI (Namibia) and Moratilla 2 (Spain)

Jorge Morales[1] & Martin Pickford[2]

1. Departamento de Paleobiología, Museo Nacional de Ciencias Naturales-CSIC - C/José Gutiérrez Abascal 2, 28006, Madrid, Spain (jorge.morales@mncn.csic.es)
2. Sorbonne Université - CR2P, MNHN, CNRS, UPMC - Paris VI, 8, rue Buffon, 75005, Paris, France (martin.pickford@mnhn.fr)

Abstract : The early Miocene locality of Grillental VI (21-19 Ma) has yielded an interesting assemblage of fossil carnivores, including a new mandible of the small viverrid classified as *Leptoplesictis senutae* Morales *et al.* 2008, which permits a better idea of the species to be obtained. In addition an unpublished mandible from the Spanish locality Moratilla 2, provisionally identified as *Leptoplesictis aurelianensis* Schlosser, 1888, gives us the possibility to make direct comparisons between these fossils, which, because of their small dimensions have not been well figured in the literature. Comparisons are made with mandibles of *Leptoplesictis filholi* Gaillard 1899, from the French locality of La Grive-Saint-Alban curated at the NHMUK, London, upon which Forsyth Major, 1903, based the new genus *Leptoplesictis*. The result is that the less hypercarnivorous African species can be segregated into a different genus from *Leptoplesictis,* for which a new genus is proposed, *Dunictis* nov. gen., with *Dunictis senutae* (Morales *et al.* 2008) as the type species, which is from Grillental VI, Namibia. Contrary to general opinion, the European forms of *Leptoplesictis* do not constitute a homogeneous assemblage, but instead comprise two divergent lineages. The first of these, from the locality of La Grive-Saint-Alban, represented by *Leptoplesictis filholi* Gaillard, 1899, has a less-reduced m/2, a robust m/1 and gracile premolars, which is joined by a second species of the genus, *Leptoplesictis peignei* from the late middle Miocene of Thailand, which even though it has relatively more robust premolars, shows an overall morphology which is closer to this genus than to any other. The second lineage is characterised by strong reduction of the m/2, a very sectorial m/1 and more robust premolars, for which we propose a new genus *Forsythictis* nov. gen., of which the type species is *F. ibericus* from the locality of Moratilla 2, and which includes the classic species *Forsythictis aurelianensis* (Schlosser, 1888) and the poorly known species *Forsythictis atavus* (Beaumont, 1973).

Key Words : Carnivora, Feliformia, Viverridae, Miocene, Africa, Eurasia, Biochronology, Biogeography

Introduction

There has been a certain amount of debate about the systematic classification of the various species of Early Miocene African Feliformia. The problem was particularly grave when attempts were made to relate the fossil feliformes in the broad sense, to the extant families, Viverridae and Herpestidae, and with the extinct family, Stenoplesictidae. The separate family status of Herpestidae from Viverridae is currently widely accepted, supported as it is by a wide range of morphological and biomolecular characters (Hunt, 1989; Hunt & Tedford, 1993; Veron, 2010; Eizirik *et al.* 2010; Nyakatura & Bininda-Emonds, 2012; Zhou *et al.* 2017). However, the skeletal differences between these families, except for the more derived tympanic bulla of Herpestidae, are difficult to determine. In addition, the fossil remains available from the Early Miocene of Africa are predominantly represented by more or less complete dento-gnathic material. The dentitions of some extant herpestids and viverrids show a really notable abundance of adaptations, occupying a broad range which includes many species of hypocarnivores and hypercarnivores, with

highly diverse adaptations (carnivores, myrmecophages, piscivores, frugivores, etc.). Under these circumstances it is difficult to establish clear criteria based solely on the dentition to distinguish the extant families, but as was pointed out above, this is the situation with which we are confronted in the present state of knowledge of the African early Miocene fossil record. A particularly complex case concerns the genus *Leptoplesictis* Forsyth Major, 1903, considered to belong either to Herpestidae or to Viverridae, which had a vast geographic distribution during the early and middle Miocene of the Old World (Beaumont, 1973; Schmidt-Kittler, 1987; Roth, 1988; Morales *et al*. 2008; Grohé *et al*. 2020). The description of new fossils from the early Miocene of Grillental VI (Namibia) and from the beginning of the middle Miocene of Moratilla 2 (Spain) attributed to *Leptoplesictis* prompts us to undertake a revision of the taxonomic status of this genus.

Geological Context and Age

Grillental VI is located in the fossiliferous valley-fill sediments of the Northern Sperrgebiet, Namibia, which are faunally similar to East African sites such as Songhor, Koru and Napak and to other Sperrgebiet sites such as Langental, Elisabethfeld and Grillental I-V, that are attributed to the Early Miocene (East African Faunal Set I, Pickford, 1981, 1986) dated about 21-19 Ma (Pickford & Senut, 2003). Moratilla 2 is located in the Calatayud-Teruel Basin, Spain, dated about 15.8 Ma (Lower Middle Aragonian, local zone Db (Van der Meulen & Daams, 1992; Daams *et al*. 1999).

Material and Methods

The new material from Grillental (GT) described herein is curated at the Earth Science Museum of the Geological Survey of Namibia (GSN Windhoek, Namibia). The specimen from Moratilla 2 is curated at the Museo Nacional de Ciencias Naturales (MNCN)-CSIC, Madrid. Specimens from La Grive-Saint-Alban, France are curated in the Natural History Museum (London) (NHMUK).

The teeth were measured with a Nikon Measuroscope 10 5x microscope with an incorporated micrometer. Scans were made by the Servicio de Técnicas No Destructivas: Microscopía Electrónica and Confocal and Espectroscopía del MNCM-CSIC, Madrid. Images of Tomographic Scans were obtained with VGStudio MAX 3.0 software.

Systematic Palaeontology

Order Carnivora Bowdich, 1821

Suborder Feliformia Kretzoi, 1945

Family Viverridae Gray, 1821

Genus *Dunictis* nov.

Type species :- *Dunictis senutae* (Morales *et al.* 2008)

Locality :- Grillental VI, Sperrgebiet, Namibia.

Age :- Early Miocene.

Derivatio nominis :- From "dune", a geomorphological entity common at Grillental.

Holotype :- GT VI 1'06, right mandible with p/1-m/2.

Included species :- *Dunictis rangwai* (Schmidt-Kittler, 1987); *Dunictis peignei* (Grohé *et al*. 2020) and (?)*Dunictis mbitensis* (Schmidt-Kittler, 1987)

Diagnosis :- Viverridae of small dimensions, with reduced m/2, m/1 large in comparison with the premolar series, with compressed paraconid lower than the protoconid, tall metaconid, almost as high as the paraconid; broad talonid comprised of similar-sized peripheral cuspids which surround a deep central valley; p/4 with cusps aligned oblique to the long axis of the mandible and the talonid enlarged, lingually closed by a tall lingual cristid, strong in the type species, but weaker in other species of the genus; p/3 with cuspids aligned along a mesio-distal axis of the mandible, p/3 with weak anterior cuspid, talonid broadening disto-lingually similar to that of the p/4, but smaller; p/2 lacking mesial cuspid, with small distal accessory cuspid and vestigial talonid, but similar in shape to those of the p/3 and p/4, uniradiculate p/1 separated by a diastema from the p/2.

Differential diagnosis :- *Dunictis* differs from *Leptoplesictis* Forsyth Major (1903) by the less sectorial character of the premolar row, with short, more robust premolars, and with greater lingual development of the talonid. The m/1 is also more robust, differing from that of the type species *L. filholi* (Gaillard, 1889) by the less-developed cuspids and its peripheral position which results in a larger talonid valley.

Species *Dunictis senutae* (Morales *et al*. 2008)

Synonymy :-
2008 *Leptoplesictis senutae* Morales *et al*. p. 303.
2010 *Leptoplesictis senutae* Werdelin & Peigné, p. 630.

Description of new material

GT VI 5'18 is a left mandible lacking the ascending ramus (Fig. 1). The m/2 is lost, but its alveolus indicates that it was reduced in dimensions and was uniradiculate. The m/1 has a tall trigonid, with a quite mesio-buccally compressed paraconid, the protoconid is taller than the paraconid and is also compressed such that its mesial and disto-lingual cristids are sharp and form a cutting blade. The metaconid is partly broken, but judging from its base it must have been well-developed (similar to the m/1 in the holotype GT VI 1'06). The talonid is short (ca 31% of the total length of the tooth) and broad, with a deep valley, somewhat displaced lingually, surrounded by a crestifom hypoconid which continues as a peripheral cristid extending to the base of the metaconid in which the hypoconulid and entoconid are indistinguishable.

The p/4 is an elongated tooth with a large main cusp, the accessory mesial cusplet is relatively small, the distal accessory cuspid larger and taller. These three cusps are aligned with each other but are oblique (ca 20º) to the long axis of the jaw. Buccally, the talonid is short, but lingually it is well developed and is closed by a tall lingual cristid which terminates at mid-height of the main cusp, without forming a separate cuspid (analogous to the position of the metaconid in the m/1). The p/3 has the cuspids aligned along the mesio-distal axis of the mandible, the mesial accessory cusplet is weak, the talonid is disto-lingually broadened similar to the morphology described for the p/4, but more reduced. The p/2 has no mesial cusplet, the distal accessory cusplet is very small and the talonid is vestigial, although similar in form to those of the p/3-p/4. The p/1 is eroded. It has a single tiny root. The canine is strong but the crown is damaged. Its transverse section is oval, quite compressed and its root is long, extending into the mandible as far as the base of the p/2.
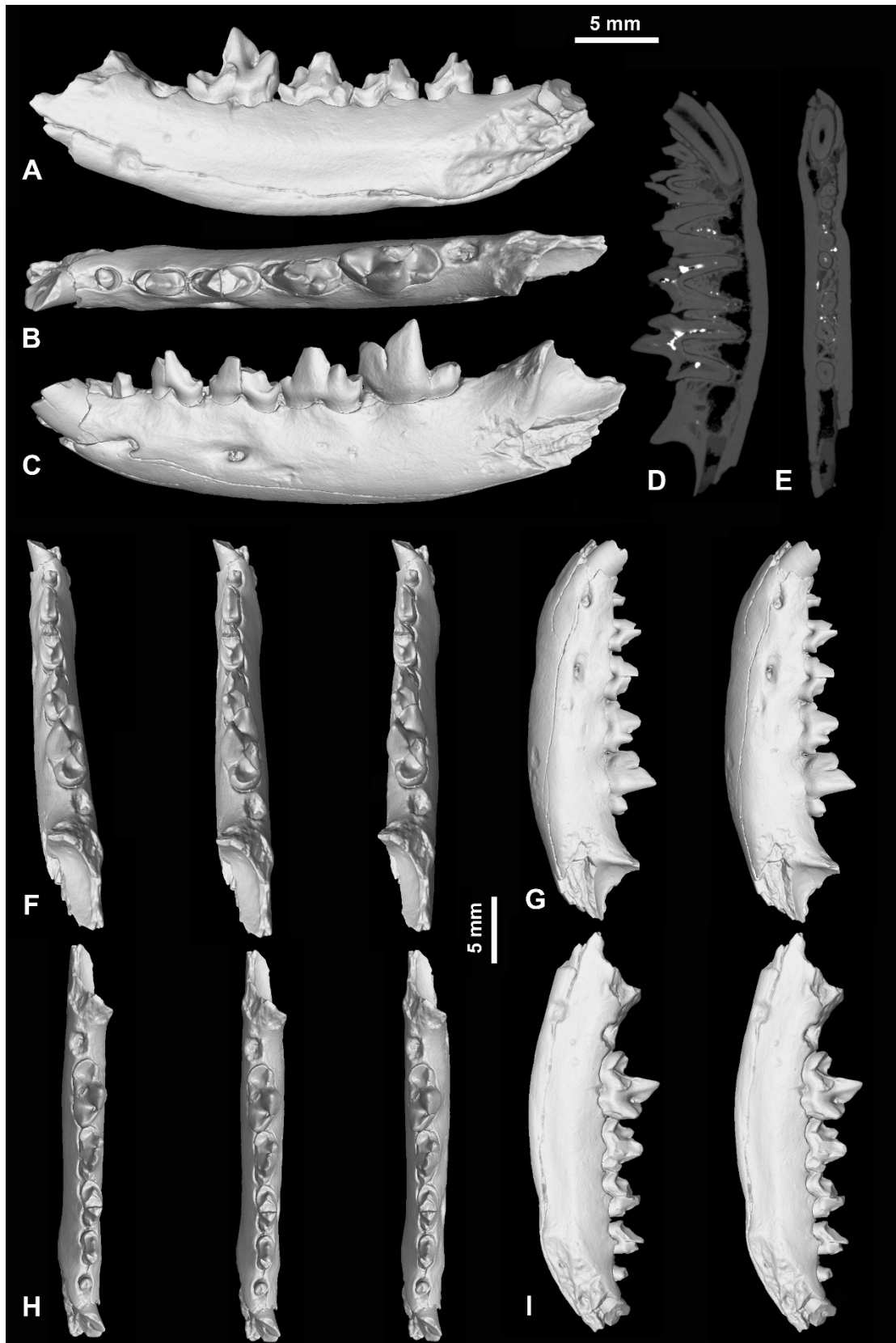
Figure 1. GSN GT VI 5'18, *Dunictis* nov. gen. *senutae* (Morales *et al*. 2008) from Grillental VI, Namibia, right mandible with canine root, p/1-m/1 and alveolus of m/2. A) lingual view, B) occlusal view, C) buccal view D) mesio-distal cross section, E) transverse section near the base of the tooth roots, F) occlusal stereo pairs (oblique distal view), G) buccal view (stereo pair), H) occlusal stereo pairs, I) lingual view (stereo pair).

Discussion

Dunictis senutae was originally related by Morales *et al.* (2008) to *Leptoplesictis rangwai* and *Leptoplesictis mbitensis* (Fig. 2) based on the morphology of its p/4, in which the strong development of the talonid stands out, as does the alignment of the cusps oblique to the long axis of the mandible, as was pointed out by Schmidt-Kittler (1987). The three species share the m/1 with short talonid, formed of a hypoconid endowed with an anterior cristid and a peripheral entoconid. The presence of a uniradiculate, reduced p/1 is another feature shared by *D. senutae* and *L. rangwai* (Fig. 2) but the condition of this tooth is unknown in *L. mbitensis* (Morales *et al.* 2008). However, *D. senutae* differs from *L. rangwai* by the smaller dimensions of the m/2 (represented only by its alveolus in *D. senutae*), the more compressed and sectorial morphology of the trigonid of the m/1 and of the premolars, although it is only possible to affirm this for the p/4, but judging from the alveoli of the p/3-p/2 in the holotype mandible of *L. rangwai* it is probable that the two premolars were more robust than those of *D. senutae*. Because of the hypercarnivorous morphology of the Grillental species, Morales *et al.* (2008) related it to *Leptoplesictis aurelianensis*, and suggested a generic distinction between these species and the less sectorial ones *L. rangwai* and *L. mbitensis*. However, the generic separation between *Dunictis senutae* and *Leptoplesictis filholi*, added to the taxonomic re-evaluation of *Leptoplesictis aurelianensis*, drastically changes the scenario, reducing the morphological variation which *a priori* could justify the generic distinction between *L. rangwai* and *Dunictis senutae*. For this reason we propose that the former species should be transferred to the same genus, and be classed as *Dunictis rangwai* (Schmidt-Kittler, 1987). It is more difficult to extend the proposition to *L. mbitensis*, which has a short p/4 with a subtriangular occlusal outline, a large talonid which has developed a lingual cuspid adjoining the mesio-buccal accessory cusplet, thereby approaching this p/4 to the situation in *Orangictis gariepensis* Morales *et al.* (2001). The morphology of the m/1 is difficult to interpret, because in the holotype, the protoconid is broken, the metaconid being almost as tall as the paraconid, and the two cusps are joined basally. According to Schmidt-Kittler (1987) the m/1 is morphologically very close to that of *D. rangwai*, and is thus distinct from the morphology in *O. gariepensis*. In the meantime we propose to leave it in an open taxonomic position as (?)*Dunictis mbitensis* (Schmidt-Kittler, 1987), the same as for the Langental species (?)*Dunictis namibiensis* (Morales *et al.* 2008).
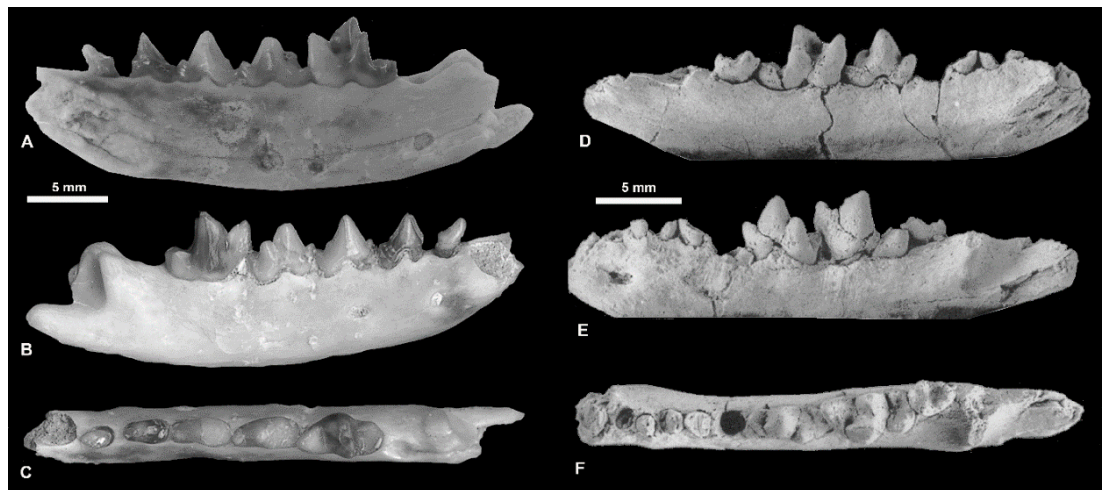
Figure 2. Comparison of GSN GT VI 1'06, the holotype left mandible of *Dunictis* nov. gen. *senutae* (Morales *et al.* 2008) from Grillental VI, Namibia, with KNM RU 15990, the holotype left mandible of *Dunictis rangwai* (Schmidt-Kittler, 1987) from Rusinga, Kenya. A-C) *Dunictis* nov. gen. *senutae* mandible with p/1-m/2, A) lingual view, B) buccal view, C) occlusal view. D-F) *Dunictis rangwai* mandible with p/4-m/2 and roots of canine-p/3, D) lingual view, E) buccal view, F) occlusal view.

Genus *Leptoplesictis* Forsyth Major, 1903

Type species :- *Leptoplesictis filholi* (Gaillard, 1899).

Diagnosis :- Forsyth Major (1903), Roth (1988), Werdelin & Peigné (2010).

Notes on the taxonomy of *Leptoplesictis* Forsyth Major, 1903

Leptoplesictis was proposed by Forsyth Major (1903) who based his diagnosis on five mandibles from La Grive-Saint-Alban, France, curated at the NHMUK (previously abbreviated BMNH) (Fig. 3), for the similar-sized fossils ascribed to the species described by Gaillard (1889) as *Herpestes filholi*, and the smaller ones to a second species which he named *Leptoplesictis minor*. Forsyth Major (1903) did not discuss the new genus in depth, limiting his remarks to its proximity to *Stenoplesictis* from the Phosphorites of Quercy by the slenderness of its teeth, "*but its other characters assign to it decidedly a position within Viverridae*". Previously Schlosser (1888) defined a new species *Stenogale aurelianensis*, on the basis of descriptions and figures of a mandible called *Plesictis* by Gervais (1867-69) from Suevres, France, which he related to an edentulous mandible from La Grive-Saint-Alban identified as *Mustela* sp. by Filhol (1888). Mayet (1908) followed the identification by Schlosser (1887-88) without adding any new data, and ignoring the work of Gaillard (1899) who described *Herpestes filholi* from the locality of La Grive. Stehlin & Helbing (1925) proposed a new taxonomic combination *Herpestes aurelianensis* and pointed out that the preservation characters of the specimen indicate that it probably did not come from Suevres, but was more like fossils from Pontlevoy. These two authors discussed the relationships of *H. aurelianensis* to the fossils from La Grive attributed by Gaillard (1899) to *Herpestes filholi,* concluding that the differences that were observed between them could be explained by individual variation, and thus the species from La Grive would be a synonym of *H. aurelianensis*. They did not pronounce an opinion on the validity of *Leptoplesictis*, but evidently discounted keeping the species in *Herpestes*. This position was maintained by Viret (1951) in his monograph on the carnivores of La Grive, considering that the species present in the locality should be called *Herpestes aurelianensis*, and therefore considered that *Leptoplesictis filholi* Gaillard (1899) and *Leptoplesictis minor* Forsyth Major (1903) were synonyms of the species defined by Schlosser (1888). Viret (1951) attributed a maxilla with P4/-M1/ and alveolus of M2/ to this species. Beaumont (1973) revalidated *Leptoplesictis* but only at the subgeneric rank, as *Herpestes* (*Leptoplesictis*) *aurelianensis*, in which he included two subspecies; *Herpestes* (*Leptoplesictis*) *aurelianensis atavus* for two molars from Vieux Collonges and *Herpestes* (*Leptoplesictis*) *aurelianensis aurelianensis* for the species from La Grive, a denomination that runs against the International Code of Zoological Nomenclature, in that the nominal subspecies must apply to *Leptoplesisctis aurelianensis*, either with the type locality Suevres or alternatively Pontlevoy, but not La Grive. A thorough revision of the genus was undertaken by Roth (1988) who raised the subspecies from Vieux Collonges to species rank as *Leptoplesictis atavus*. However, she considered *Leptoplesictis filholi* Gaillard (1899) to be valid, and to be the type species of the genus and indirectly noted that it could not be *Leptoplesictis aurelianensis* Schlosser (1889). Prior to the study by Roth (1988) Schmidt-Kittler (1987) as discussed above, included two new species from the early Miocene of Kenya in the genus *Leptoplesictis*, *L. rangwai* and *L. mbitensis,* both from Rusinga. Morales *et al*. (2008) described two new species from Namibia, *L. senutae* from Grillental and *L. namibienses* from Langental. McKenna & Bell (1997) and Werdelin & Peigné (2010) included the genus in the family Herpestidae. A new species *Leptoplesictis peignei* from the late middle Miocene of Thailand was recently defined by Grohé *et al*. (2020), who expressed their conviction that the type species of the genus is *Leptoplesictis filholi* (Gaillard, 1899).

Species *Leptoplesictis filholi* (Gaillard 1899)

Synonymy :-
1899 *Herpestes filholi* Gaillard, p. 62.
1903 *Leptoplesictis filholi* Forsyth Major, p. 535.
1925 *Herpestes aurelianensis* Stehlin & Helbing, p. 61.
1951 *Herpestes aurelianensis* Viret, p. 76.
1988 *Leptoplesictis filholi* Roth, p. 338.
1999 *Leptoplesictis filholi* Ginsburg, p. 131.
2012 *Leptoplesictis filholi* Peigné, p. 625.
2020 *Leptoplesictis filholi* Grohé *et al.* p. 39.

Type locality :- La Grive-Saint-Alban, France.

Age :- Middle Miocene, Upper Aragonian (MN 6-7/8).

Holotype :- LGr 1372 mandible with p/3-m/2, figured by Gaillard 1899, pl. III, fig. 4.

Diagnosis :- Roth (1988).

Discussion

Inclusion of the species *Herpestes aurelianensis* in *Leptoplesictis* has caused a great deal of confusion in the taxonomy of the genus, considering that the type species of the genus, *L. filholi* is a synonym of the species described by Schlosser (1888), which is represented only by a mandible fragment containing m/1-p/4. The pooling of the two taxa into a single species greatly increased the range of intraspecific variation, to the extent of turning the genus into a waste-basket taxon. Roth (1988) as discussed above, separated out the two species and added a third *L. atavus*, which had been defined as a subspecies by Beaumont (1973). A detailed comparison between *Leptoplesictis filholi* from La Grive (including the material used by Forsyth Major, 1903) and the material from Petersbuch 2 (Germany) described by Roth (1988) as *Leptoplesictis aurelianensis*, together with an unpublished mandible from Moratilla 2 (Spain) and the holotype of *Herpestes aurelianensis* (Schlosser, 1888) figured by Mayet (1908) and Stehlin & Helbing (1925) shows clearly the specific distinction between *Leptoplesictis filholi* and *Herpestes aurelianensis*, which could even extend to the level of the genus. *Leptoplesictis filholi* has a relatively robust m/1, in particular compared with the gracility and elongation of the premolars. The m/2, even though reduced, retains a complete trigonid and a narrow talonid. However, the forms included in *Leptoplesictis aurelianensis* are characterised by the great reduction of the m/2, the m/1s are elongated and bucco-lingually compressed, whereas the premolars (in the forms in which they are known) even though gracile, do not show the specialisation seen in *L. filholi*. It is evident that the divergence between the two species, even if they had a common ancestor, is sufficiently great to separate them at the generic level. In consequence, the European species of this genus, hitherto identified as *L. aurelianensis* and *L. atavus* must be removed from this genus, and for this reason a new genus is erected, for which we propose the name *Forsythictis* nov. gen.
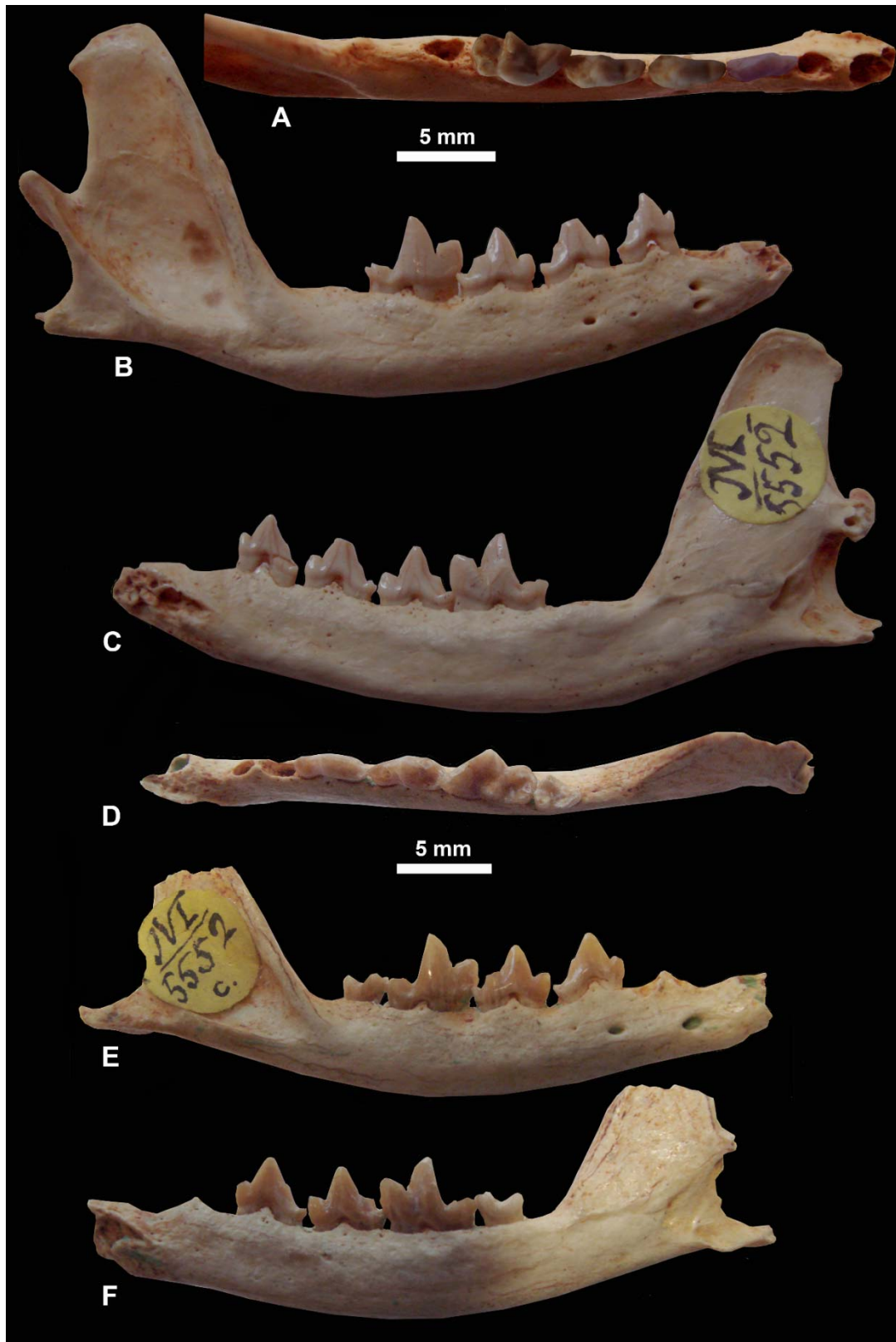
Figure 3. *Leptoplesictis filholi* (Gaillard, 1888) and *Leptoplesictis minor* Forsyth Major (1903) from La Grive-Saint-Alban, France. Mandibles employed by Forsyth Major (1903) to diagnose the genus *Leptoplesictis*. NHMUK M-5552 right mandible of *Leptoplesictis filholi* with alveoli of the canine and p/1, complete p/2-m/1 and alveolus of m/2. A) occlusal view, B) buccal view, C) lingual view. NHMUK M-5552c right mandible of *Leptoplesictis filholi* (=*Leptoplesictis minor*) with alveoli of canine and p/2, and complete p/3-m/2. D) occlusal view, E) buccal view, F) lingual view.

Species *Leptoplesictis peignei* Grohé *et al.* 2020

Type locality :- Mae Moh, Thailand.

Age :- Middle Miocene (ca. 13.2-13.4 Ma).

Holotype :- MM-51, fragment of mandible with alveolus of p/2, complete p/3-m/1, Grohé *et al.* 2020, Fig. 7.

Diagnosis :- Grohé *et al.* (2020)

Discussion

When erecting the species *Leptoplesictis peignei* from Thailand Grohé *et al.* (2020) pointed out the differences between it and *Leptoplesictis filholi*. In general *Leptoplesictis peignei* differs from *L. filholi* by the greater robusticity of the premolars. The morphology of the p/4 is very close to that of extant *Genetta genetta* L., and the same applies to the simple morphology of the p/3 and p/2, with the accessory cusplets greatly reduced, as in the extant form. The morphology of the m/1 of *L. peignei* is close to that of *Leptoplesictis filholi* and also close to that of *G. genetta*, with a reduced, bucco-lingually narrow talonid compared to the trigonid; which conserves the tall and strong metaconid; in the talonid the hypoconid stands out from the rest of the cusplets, which are little different from each other and positioned disto-lingually. The differences between the species from Mae Moh, Thailand, and *Forsythictis* are marked, particularly by the more sectorial carnassial of the species of this genus. With respect to *Dunictis* the differences are also important, in particular in the construction of the talonid of the premolars, much larger and disto-lingually accentuated, while the m/1 shows distinct differences; in *Dunictis* the talonid is proportionally broader bucco-lingually and as a consequence, the talonid valley is larger.

Genus *Forsythictis* nov.

Type species :- *Forsythictis ibericus* nov. sp.

Other species :- *F. aurelianensis* and *F. atavus.*

Diagnosis :- Very small viverrid, lower post-canine dental series comprised of four premolars and two molars, with strong reduction of m/2; m/1 with clear sectorial tendency, elongated, trigonid narrow, metaconid variable depending on the species, very reduced in the type species, although well-developed in other species of the genus. Where known, the premolars in the species are moderately elongated; p/4 with well-developed accessory distal and mesial cusplets, the disto-lingual expansion weakly developed; p/3 with a mesial accessory cusplet but the distal cusplet is variable, absent in the type species.

Derivatio nominis :- Dedicated to British palaeontologist Charles Immanuel Forsyth Major.

Species *Forsythictis ibericus* nov.

Holotype :- (MNCN 87000) fragment of left mandible with alveolus of m/2 and complete m/1-p/3.

Type locality :- Moratilla 2, Zaragoza, Spain

Age :- Middle Miocene, Middle Aragonian MN 4 (local zone Dd).

Diagnosis :- *Forsythictis* with metaconid of the m/1 greatly reduced, accessory cuspids of the p/4 small, p/3 without a distal accessory cuspid.

Derivatio nominis :- From the Iberian Peninsula.

Description

(MNCN-87000) is a fragment of left mandible with the alveolus of the m/2, and complete m/1-p/3 (Fig. 4). The mandible is deep and robust, lacking the ascending ramus, the symphysis and the alveolar part of the p/1 and the mesial root of the p/2. There is a strong mental foramen beneath the p/3. The distal root of the p/2 is clearly reduced in comparison with those of the p/3, and it is possible to discern that the canine root ends beneath the p/3. The p/3 is a simple tooth with a tall main cusp, a low, but well-developed mesial accessory cusplet, and no distal accessory cusplet, or if one is present it is a small talonid elevated distally. The p/4 has a well-developed distal accessory cusplet, and a more developed talonid somewhat

.

extended lingually, the mesial accessory cusplet is tall and strong. The m/1 has a paraconid which is quite a bit lower than the protoconid, but the two cusps are of similar length. The base of the paraconid has an ample contact with the lingual part of the talonid of the p/4. The metaconid is small, and is positioned at mid-height of the disto-lingual cristid of the protoconid, and barely stands out lingually. The talonid is low, small compared to the trigonid. The hypoconid, hypoconulid and entoconid are crestiform, being barely differentiated from each other and are located peripherally around the talonid valley. The alveolus of the m/2 is small, uniradiculate and almost circular in section.
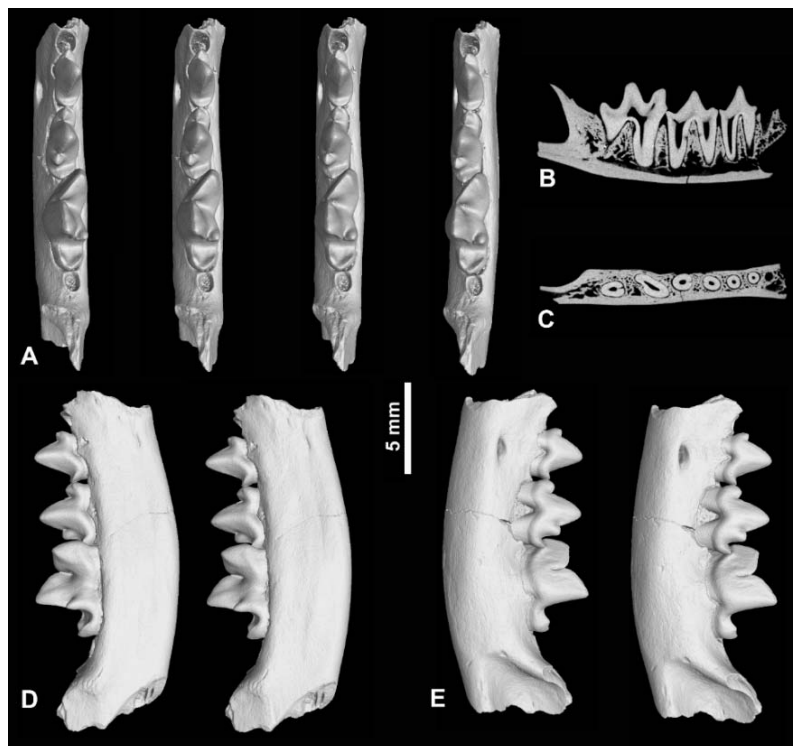

Figure 4. MNCN 87000, *Forsythictis* nov. gen. *ibericus*. nov. sp. from Moratilla 2, Spain. Left mandible with partial canine root, distal root of p/2, p/3-m/1 and alveolus of m/2. A) occlusal view (stereo pairs), B) mesio-distal cross section, C) transverse section near the base of the tooth roots, D) lingual view (stereo pair), E) buccal view (stereo pair).

Discussion

The mandible from Moratilla 2, selected to be the holotype of *Forsythictis ibericus*, eliminates ambiguities in the taxonomy of *Leptoplesictis* as well as *Forsythictis*; which could occur if it were

secondary to *Forsythictis aurelianensis* (mandible from Suevres or from Pontlevoy). The latter mandible lacks the mesial premolars (p3-p/1), which, as was discussed above, are crucial for distinguishing between these two

genera. According to the illustrations published by Mayet (1908) and Stehlin & Helbing (1925) *F. aurelianensis* appears to have an m/1 that is somewhat less sectorial than that in the most complete mandible from Petersbuch 2, identified by Roth (1988) as *Leptoplesictis aurelianensis*. *Forsythictis ibericus* is clearly more advanced towards a hypercarnivorous adaptation, which is why they are here separated into two genera. This runs counter to the affirmation by Viret (1951, p. 79) that "*Grâce à un moulage de la mandibule de Pontlevoy, j'ai pu me convaincre que celle-ci a appartenu à un fort sujet d'*H. filholi". However, this supposed similarity seems improbable, a revision and more precise illustration of the mandible from Pontlevoy may aid in throwing light on the relation between the species included in *Forsythictis*.

Species *Forsythictis aurelianensis* (Schlosser, 1889)

Synonymy :-
1889 *Stenogale aurelianensis* Schlosser, p. 153.
1908 *Stenogale aurelianensis* Mayet, p. 223.
1925 *Herpestes aurelianensis* Stehlin & Helbing, p. 59.
1951 *Herpestes aurelianensis* Viret, p. 76.
1958 *Herpestes aurelianensis* Mein, p. 51.
1987 *Leptoplesictis aurelianensis* Schmidt-Kittler, p. 105.
1988 *Leptoplesictis aurelianensis* Roth, p. 335.
1999 *Leptoplesictis aurelianensis* Ginsburg, p. 131.
2002 *Leptoplesictis aurelianensis* Ginsburg, p. 130.
2008 *Leptoplesictis aurelianensis* Morales *et al.* p. 303.
2020 *Leptoplesictis aurelianensis* Grohé *et al.* p. 39.

Type locality :- Suevres (Schlosser, 1888); Ginsburg (2002), Stehlin & Helbing (1925) wrote that the type locality was Pontlevoy.

Other localities :- Petersbuch 2 and Erkertshofen 2, Germany (Roth, 1988), Artenay and Aerotrain, France (Ginsburg, 2002).

Age :- Middle Miocene, Middle Aragonian MN 4 (ca. 17-18 Ma).

Diagnosis :- Roth (1988).

Differential diagnosis :- *Forsythictis aurelianensis* differs from *F. ibericus* by the greater development of the metaconid of the m/1, which is displaced distally with respect to the protoconid, the greater development of the accessory cusplets in the p/4 and the presence in p/3 of a well-developed distal accessory cusplet (Fig. 5).
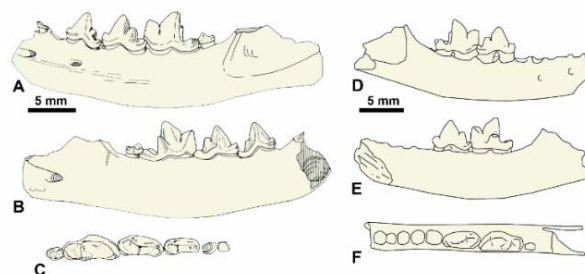

Figure 5. Comparison between the mandible with alveolus of p/2 and complete p/3-m/2 of *Forsythictis* nov. gen. *aurelianensis* (Schlosser, 1887) from Petersbuch 2, Germany (after Roth, 1988) and the holotype of the species, a mandible with alveoli of p/1-p/3, complete p/4-m/1 and alveolus of m/2 (Pontlevoy 20) from Pontlevoy (after Stehlin & Helbing, 1925). A-C) *Forsythictis* nov. gen. *aurelianensis* from Petersbuch 2, A) buccal view, B) lingual view, C) occlusal view. D-F) *Forsythictis* nov. gen. *aurelianensis* from Pontlevoy, D) buccal view, E) lingual view, F) occlusal view.

Table 1 Measurements (in mm) of the teeth of species of *Leptoplesictis*, *Forsythictis* and *Dunictis*. Data from : 1: Gaillard (1889) holotype of *Leptoplesictis filholi* Forsyth Major (1903). 2: measurements taken by the authors. 3: Roth (1988). 4: Peigné (2012). 5: measurements estimated by the authors in Viret (1951, Fig. 21). 6: Ginsburg (2002). *alveolus measurement. ** Mandibles from La Grive identified as *Leptoplesictis minor* Forsyth Major (1903). (BLB – bucco-lingual breadth, MDL – mesio-distal length). (BSPG - Bayerische Staatssammlung für Paläontologie und Geologie, Munich; FSL - Faculty of Science, University of Lyon; GSN - Geological Survey of Namibia, Windhoek; MNHN - Muséum National d'Histoire Naturelle, Paris; NHMUK - Natural History Museum of the United Kingdom, London; SMNS - State Museum of Natural History, Stuttgart).

Species	Catalogue	Locality	c/1 MDL	c/1 BLB	p/2 MDL	p/2 BLB	p/3 MDL	p/3 BLB	p/4 MDL	p/4 BLB	m/1 MDL	m/1 BLB	m/2 MDL	m/2 BLB	Data source
Leptoplesictis filholi	MNHN LGr 1372	La Grive			3*		4		4.5		5	2.5	2.5	2	1
Leptoplesictis filholi	NHMUK M 5308	La Grive			3	1.1	3.1	1.5	3.5	1.6	4.5	2.5			2
Leptoplesictis filholi	NHMUK M 5552a	La Grive			3.3	1.1	3.6	1.3	3.5	1.7	5.1	2.4			2
*Leptoplesictis minor***	NHMUK M 5552c	La Grive					3.5	1.3	3.8	1.6	4.7	2.6	2.4	1.6	2
*Leptoplesictis minor***	NHMUK M 5552b	La Grive							3.6	1.6	4.4	2.6			2
Forsythictis aurelianensis	Pontlevoy 20	Pontlevoy							4.6		5.3				3
Forsythictis aurelianensis	BSPG 1976 XXII 3669	Petersbuch 2			2.9		3.7	1.4	4.5	2	5.6	2.5	1.6	1.2	3
Forsythictis aurelianensis	SMNS 44366	Petersbuch 2							4.7	2.1					3
Forsythictis atavus	FSL 65580 VxC	Vieux-Collonges									5.1	2.4			3
Forsythictis atavus	MNHN Sa 940	Sansan					3.3	1.3	3.6	1.5					4
Forsythictis atavus	MNHN Ss 5340	Sansan									4.7	2.5			3
Forsythictis ibericus	MNCN 87000	Moratilla 2					3.1	1.7	4.3	1.9	5.6	2.8			2
Dunictis senutae	GSN GT 10'06	Grillental VI			3.4	2	4.3	2.1	5	2.5	6	3	2*		2
Dunictis senutae	GSN GT 5'18	Grillental VI	3	2.5	2.9	1.6	3.9	1.8	4.9	2.2	5.5	2.8	1.5*	1.6*	2
?Dunictis namibiensis	GSN LT 30'07	Langental									8.3	4.4			2

Species	Catalogue	Locality	C1/ MDL	C1/ BLB	P2/ MDL	P2/ BLB	P3/ MDL	P3/ BLB	P4/ MDL	P4/ BLB	M1/ MDL	M1/ BLB	M2/ MDL	M2/ BLB	Data Source
Leptoplesictis filholi	MNHN LGr 1375	La Grive							5.1	3.3	2.7	5.1	0.7*	2.5*	5
Forsythictis aurelianensis	MNHN AR 2403	Artenay			2.8	1.65	4.5	2.2	7	3.65	2.7	5			6
Forsythictis atavus	FSL 65580 VxC	Vieux-Collonges									2.5	4.5			3

Species *Forsythictis atavus* (Beaumont, 1973)

Synonymy :-
1973 *Herpestes* (*Leptoplesictis*) *aurelianensis atavus* Beaumont, p. 293.
1987 *Leptoplesictis atavus* Roth, p. 181.
1988 *Leptoplesictis atavus* Roth, p. 339.
1999 *Leptoplesictis atavus* Ginsburg, p. 131.
2012 *Leptoplesictis atavus* Peigné, p. 625.

Type locality :- Vieux Collonges, France

Age :- Middle Miocene, MN 5.

Diagnosis :- In Roth (1988).

Discussion

The species is so poorly represented that it is difficult to be precise about its validity, comprising the material described by Beaumont (1973) from Vieux Collonges (Mein, 1958), to which Roth (1988) added a mandible from Sansan in which only the m/1 is preserved, that Ginsburg (1961) identified as *Herpestes aurelianensis*. Nevertheless, the size of the

alveolus of the m/2, is greater than that of *Forsythictis*, and the apparently greater robusticity of the m/1 could indicate a closer relationship to *Leptoplesictis filholi*. Peigné (2012) added a fragment of mandible with p/3-

p/4 to the hypodigm which could provide additional support in that, at least the fossils from Sansan resemble *Leptoplesictis filholi* from La Grive (Fig. 6).
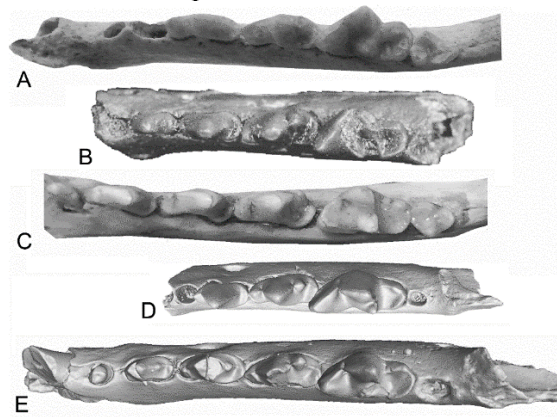

Figure 6. Mandibles in occlusal views; A) NHMUK M 5552, *Leptoplesictis filholi* (Gaillard, 1888) from La Grive-Saint-Alban, France; B) MM-51, *Leptoplesictis peignei* Grohé *et al.* (2020) from Mae Moh, Thailand; C). *Genetta genetta* Linnaeus, 1758, extant from Spain; D) MNCN 87000, *Forsythictis* nov. gen. *ibericus*. nov. sp. from Moratilla 2, Spain; E) GSN GT VI 5'18, *Dunictis* nov. gen. *senutae* (Morales *et al.* 2008) from Grillental VI, Namibia.
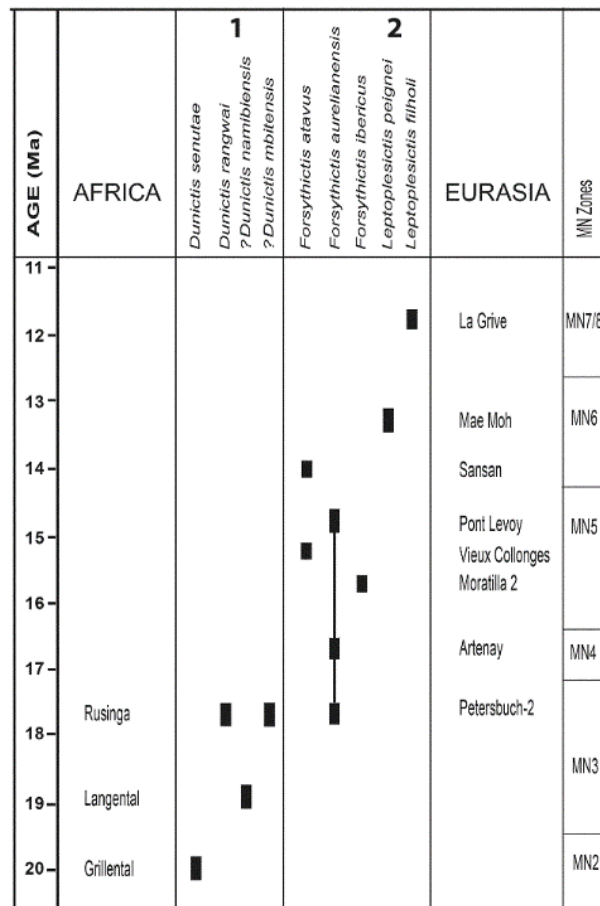

Figure 7. Biochronology of African and Eurasian Miocene localities, with the temporal ranges of the species of *Leptoplesisctis*, *Forsythicytis* and *Dunictis*. For correlations of African localities see Pickford (1986), Pickford & Senut (2003) and Werdelin & Peigné (2010); for European and Asian localities see Daams *et al.* (1999), Ginsburg (1999), Prieto & Rummel (2016) and Grohé *et al.* (2020). 1, African species. 2, Eurasian species. The time scale is from Hilgen *et al.* (2012).

Conclusions

The revision of *Leptoplesictis* exposes the heterogeneity of the species previously included in the genus (Fig. 6) already evoked by Schmidt-Kittler (1987) and Morales *et al.* (2008), who reduced the content to two; the type species erected by Forsyth Major (1903) *Leptoplesictis filholi* (Gaillard 1899) from La Grive-Saint-Alban, France, and the recently defined *Leptoplesictis peignei* Grohé *et al.* (2020) from the middle Miocene of Thailand (Fig. 7). These two species are evidently affiliated with extant *Genetta*. The other species previously included in *Leptoplesictis*, exhibit important differences indicating that they represent distinct genera. On the one hand, the European species are herein classified in the genus *Forsythictis*, defined on the basis of a new species *F. ibericus* from the middle Miocene of Spain which is the type species, whilst the oldest named species *Stenogale aurelianensis* Schlosser (1888) is today called *Forsythictis aurelianensis*, and with some uncertainty, a third species is included, *F. atavus* Beaumont (1973) which is poorly known (Fig. 7). *Forsythictis* is characterised by a hypercarnivorous dental adaptation, more derived than that of *Leptoplesictis* but comparable to that of *Stenoplesictis cayluxi* Filhol (1880) or *Semigenetta mutata* (Filhol, 1891) even if the lower carnassial has a lower and more extended trigonid with slight reduction of the talonid compared to the species of *Stenoplesictis* (Peigné & De Bonis, 1999) or

of *Semigenetta* (Ginsburg, 1961). Finally, the African species – the oldest of the group studied herein (Fig. 7) are classified in a new genus *Dunictis* with *D. senutae* from Grillental, Namibia, as the type species, to which are transferred two species from Kenya previously attributed to *Leptoplesictis* by Schmidt-Kittler (1987); today known as *Dunictis rangwai* and with an element of doubt (?)*Dunictis mbitensis*. *Dunictis* is clearly less hypercarnivorous than *Forsythictis*. It also differs from *Leptoplesictis* in the morphology of the talonid of the m/1, in which the central basin is well developed and the talonid of the premolars which broaden distally forming a shallow valley.

The genera discussed in this paper have been included in the family Viverridae but conscious of the ambiguity of this classification expressed by Veron (2010) who wrote "*The relationships within the Viverridae have been long debated, largely due to their large diversity of forms and also because this family was a dumping ground for all 'viverrid-like' species of feliforms*", a reflection that applies to the fossil forms, including those discussed herein. Without doubt, the three genera discussed in this contribution fall into a diffuse space comprising the grades "Stenoplesictinae" and "Viverridae/Herpestidae" which overlap, and as such they contribute to the resolution of one of the more interesting puzzles concerning the phylogeny and evolution of "*viverrid-like*" Feliformia.

Acknowledgements

References

Beaumont, G. de, 1967. Observations sur les Herpestinae (Viverridae, Carnivora) de l'Oligocène supérieur avec quelques remarques sur les Hyaenidae du Néogène. *Archives des Sciences, Genève*. **20**, 79-108.

Bowdich, T.E. 1821. *An Analysis of the Natural Classification of Mammalia for the use of Students and Travellers*. Paris, J. Smith. pp.

1-115 (+31).

Daams, R., Meulen, A.J. van der, Alvarez-Sierra, M.A., Peláez-Campomanes, P., Calvo, J.C., Alonzo Zarza, M.A. & Krigsman, W. 1999. Stratigraphy and sedimentology of the Aragonian in type area. *Newletters on Stratigraphy*, Berlin, **37** (**3**), 103-139.

Eizirik, E., Murphy, W.J., Koepfli, K.-P., Johnson, W.E., Dragoo, J.W., Wayne, R.K. & O'Brien, S.J. 2010. Pattern and timing of diversification of the mammalian order Carnivora inferred from multiple nuclear gene sequences. *Molecular Phylogenetics and Evolution*, **56** (**1**), 49-63. doi: 10.1016/j.ympev.2010.01.033.

Filhol H. 1888. Sur un nouveau genre d'Insectivore. *Bulletin de la Société Philomatique de Paris*, **1**, **12**, 24-25.

Filhol, H. 1891. Etude sur les mammifères fossiles de Sansan. *Annales de la Société géologique de France*. **21**, 314 pp.

Forsyth Major, C.I. 1903. New Carnivora from the Middle Miocene of La Grive-St-Alban, Isère, France. *Geological Magazine, London*, (4) **10**, 534-537.

Gaillard, C. 1899. Mammifères miocènes nouveaux ou peu connus de La Grive-Saint-Alban. *Archives du Muséum d'Histoire Naturelle de Lyon*, **7**, 78 pp.

Gervais, P. 1867-1869. *Zoologie et paléontologie générales 2ème série, Nouvelles recherches sur les animaux vertébrés dont on trouve les ossements enfouis dans le sol et sur leur comparaison avec les espèces actuellement existant*s. Arthus Bertrand, Paris, 263 pp.

Ginsburg, L. 1961. La faune de carnivores miocènes de Sansan. *Mémoires du Muséum National d'Histoire Naturelle,* série, C, **9**, 1-190

Ginsburg, L. 1999. Order Carnivora. *In*: Rössner, G.E. & Heissig, K. (Eds) *The Miocene Land Mammals of Europe*. Friedrich Pfeil, München, pp. 109-148.

Ginsburg L. 2002. Les carnivores fossiles des sables de l'Orléanais. *Annales de Paléontologie*, **88**, 115-146.

Gray, J.E. 1821. On the natural arrangement of vertebrose animals. *London Medical Repository*, **15**, 296-310.

Gray, J.E. 1864. A revision of the genera and species of viverrine animals (Viverridae) founded on the collection of the British Museum. *Proceedings of the Zoological Society of London*, **1864**, 502-579.

Grohé, C, de Bonis, L, Chaimanee, Y., Chavasseau, O., Rugbumrung, M., Yamee, C., Suraprasit, K., Gibert, C., Surault, J., Blondel, C. & Jaeger, J.-J. 2020. The late middle Miocene Mae Moh Basin of northern Thailand: the richest Neogene assemblage of Carnivora from Southeast Asia and a paleobiogeographic analysis of Miocene Asian carnivorans. *American Museum Novitates*, **3952**, 1-57.

Hilgen, F.J., Lourens, L.J., Van Dam, J.A., Beu, A.G., Boyes, A.F., Cooper, R.A., Krijgsman, W., Ogg, J.G., Piller, W.E. & Wilson, D.S. 2012. The Neogene Period. *In*: Gradstein, F.M., Ogg, J.G., Schmitz, M.D. & Ogg, G.M. (Eds) *The Geologic Time Scale 2012*. Elsevier, pp. 923-978.

Hunt, R.M. 1989. Evolution of the aeluroid Carnivora: significance of the ventral, promontorial process of the petrosal and the origin of basicranial patterns in the living families. *American Museum Novitates*, **2930**, 1-32.

Hunt, R.M. & Tedford, R.H. 1993. Phylogenetic relationships within the aeluroid Carnivora and implications of their temporal and geographic distribution. *In*: Szalay, F.S., Novacek M.J. & McKenna M.C. (Eds) *Mammal Phylogeny: Placentals*, New York, NY: Springer-Verlag, pp. 53-73.

Kretzoi, M. 1945. Bemerkungen über das Raubtiersystem. *Annales Historico-Naturales Mussei Nationales Hungarici*. **38**, 59-83.

Linnaeus, C. 1758. *Systema naturae per regna tria naturae, secundum classes, ordines, genera, species, cum characteribus, differentiis, synonymis, locis. Vol. 1: Regnum animale*. Editio decima, reformata. Stockholm: Laurentii Salvii.

Mayet, L. 1908. Etude des mammifères miocènes des Sables de l'Orléanais et des Faluns de la Touranies. *Annales de l'Université de Lyon*, 1, fascicule **24**, 326 pp.

McKenna, M. & Bell, S. 1997. *Classification of Mammals above the Species Level*. New York, Columbia University Press, 631 pp.

Mein, P.-R. 1958. Les mammifères de la faune sidérolithique de Vieux-Collonges. *Nouvelles Archives du Muséum d'Histoire Naturelle de Lyon*, *Publications du Musée des Confluences*, **5**, 3-122.

Morales, J., Pickford, M. & Salesa, M.J. 2008. Creodonta and Carnivora from the early

Miocene of the Northern Sperrgebiet, Namibia. *Memoir of the Geological Survey of Namibia*, **20**, 291-310.

Morales, J., Pickford, M. & Soria, D. 2007. New carnivoran material (Creodonta, Carnivora and *incertae sedis*) from the Early Miocene of Napak, Uganda. *Paleontological Research*, **11**, 71-84.

Morales, J., Pickford, M., Soria, D. & Fraile, S. 1998. New carnivores from the basal Middle Miocene of Arrisdrift, Namibia. *Eclogae Geologicae Helvetiae*, **91**, 27-40.

Morales, J., Pickford, M., Soria, D. & Fraile, S. 2001. New Viverrinae (Carnivora, Mammalia) from the basal Middle Miocene of Arrisdrift, (Namibia). *Palaeontologia africana*, **37**, 99-102.

Morales, J., Pickford, M., Fraile, S., Salesa, M.J. & Soria, D. 2003. Creodonta and Carnivora from Arrisdrift, early Middle Miocene of Southern Namibia. *Memoir of the Geological Survey of Namibia*, **19**, 177-194.

Nyakatura, K. & Bininda-Emonds, O.R.P. 2012. Updating the evolutionary history of Carnivora (Mammalia): a new species-level supertree complete with divergence time estimates. *BMC Biology*; **10** (**12**). https://doi.org/10.1186/1741-7007-10-12.

Peigné, S. 2012. Les Carnivora de Sansan. *In*: Peigné, S. & Sen, S. (Eds), Mammifères de Sansan. *Mémoires du Muséum National d'Histoire Naturelle*, Paris, **203** (**6**), 559-660.

Peigné, S. & Bonis, L. de, 1999. The genus *Stenoplesictis* Filhol (Mammalia, Carnivora) from the Oligocene deposits of the Phosphorites of Quercy, France. *Journal of Vertebrate Paleontology*, **19** (**2**), 566- 575.

Pickford, M. 1981. Preliminary Miocene Mammalian biostratigraphy for Western Kenya. *Journal of Human Evolution*, **10**, 73-97.

Pickford, M. 1986. The geochronology of the Miocene higher primate faunas of East Africa. *In*: Else, J.G. & Lee, P.C. (Eds) *Primate Evolution*, Cambridge, Cambridge University Press. pp. 19-33.

Pickford, M. & Senut, B. 2003. Miocene Palaeobiology of the Orange River Valley, Namibia. *Memoir of the Geological Survey of Namibia*, **19**, 1-22.

Prieto, J. & Rummel, M. 2016. Some considerations on small mammal evolution in Southern Germany, with emphasis on Late Burdigalian-Earliest Tortonian (Miocene) cricetid rodents. *Comptes Rendus Palevol*,

15, 837-854.

Roth, C. 1987. *Die Raubtierfauna aus den miozänen Spaltenfullungen Petersbuch 2 und Erkerteshofen, 2, Taxonomie, Stratigraphie, Ökologie*. Dissertationen, Institute für Geowissenschaften, Paläontologie, Johannes Gutenberg-Universität Mainz, 252 pp.

Roth, C. 1988. *Leptoplesictis* Major 1903 (Mammalia, Carnivora, Viverridae) aus dem Orleanium und Astaracium/Miozän von Frankreich und Deutschland. *Paläontologische Zeitschrift*, **62**, 333-343.

Schlosser, M. 1889. Die Affen, Lemuren, Chiropteren, Insectivoren, Marsupialer, Creodonten und Carnivoren des Europäischen Tertiär. *Beiträge zur Paläontologie Österreich-Ungarns und des Orients*, **7**, 226-386.

Schmidt-Kittler, N. 1987. The Carnivora (Fissipeda) from the lower Miocene of East Africa. *Palaeontographica*, **A197,** 85-126.

Stehlin, H.G. & Helbing, H. 1925. Catalogue des Ossements de Mammifères Tertiaires de la collection Bourgeois à l'Ecole de Pont-Levoy (Loir-et-Cher). *Bulletin de la Société d'Histoire naturelle et Anthropologie de Loir-et-Cher*, **18**, 77-277.

Van der Meulen, A.J. & Daams, R. 1992. Evolution of early-middle Miocene rodent faunas in relation to long-term palaeo-environmental changes. *Palaeogeography, Palaeoclimatology, Palaeoecology*, **93** (**3-4**), 227-253.

Veron, G. & Heard, S. 2000. Molecular systematics of the Asiatic Viverridae (Carnivora) inferred from mitochondrial cytochrome b sequence analysis. *Journal of Systematics and Evolutionary Research*, **38**, 209-217.

Viret, J. 1951. Catalogue critique de la faune de mammifères de La Grive-Saint-Alban: Chiroptères, Carnivores, Pholidotes. *Nouvelles Archives du Muséum d'Histoire Naturelle de Lyon*, **3**, 1-104.

Werdelin, L. & Peigné, S. 2010. Carnivora. *In*: *Cenozoic Mammals of Africa*, Werdelin, L. & Sanders, W.J. (Eds), Berkeley, University of California Press. Chapter **32**, 603-657.

Zhou, Y., Wang, S.-R. & Ma, J.-Z. 2017. Comprehensive species set revealing the phylogeny and biogeography of Feliformia (Mammalia, Carnivora) based on mitochondrial DNA. *PLoS ONE* **12**(3), 19 pp:0174902.https://doi.org/10.1371/journal. pone. 0174902.

A spiny distribution: new data from Berg Aukas I (middle Miocene, Namibia) on the African dispersal of Erinaceidae (Eulipotyphla, Mammalia).

Florentin Cailleux

Comenius University, Department of Geology and Palaeontology, SK-84215, Bratislava, Slovakia, and Naturalis Biodiversity Center, Darwinweg 2, 2333 CR Leiden, The Netherlands.
(email: cailleux1@uniba.sk)

Abstract : Material of Erinaceidae (Eulipotyphla, Mammalia) from Berg Aukas I (late middle Miocene, Namibia) is described. Originally identified as belonging to the gymnure *Galerix*, the specimens from Berg Aukas I are herein attributed to the hedgehog *Amphechinus* cf. *rusingensis*, and they represent the last known occurence of *Amphechinus* in Africa. Its persistence in Northern Namibia may have been favoured by its generalist palaeoecology and the heterogeneous aridification of southern Africa during the middle Miocene. In addition, an update of the data acquired on African Erinaceidae is provided: a migration of the Galericinae to southern Africa is no longer supported; all attributions of African middle Miocene to Pliocene material to the genus *Galerix* are considered to be improbable; at least two migratory waves of *Schizogalerix* are recognized in northern Africa with *S.* cf. *anatolica* in the late middle Miocene (Pataniak 6, Morocco) and *S.* aff. *macedonica* in the late Miocene (Sidi Ounis, Tunisia).

Key Words : Erinaceidae, *Amphechinus*, Biogeography, Miocene, Africa.

Introduction

While the family Erinaceidae (Eulipotyphla, Mammalia) is a frequent element of European and Asian Miocene faunas, little is known about the scarce African fossil record. Naturally, several factors have to be considered: the Palaeogene isolation of Africa, the highly heterogeneous distribution of known localities, the presence of already established insectivorous groups (e.g. Chrysochloridae, Tenrecidae) and the usual scarcity of Erinaceinae in small mammal deposits. Despite this, the suspected Miocene lineage *Gymnurechinus-Mellalechinus* suggests that Asian migrants evolved into better-adapted forms during their short stay in Africa.

The Otavi Mountains in Northern Namibia, yielded a rich quantity of fossiliferous cave breccias and fissure fillings with abundant remains of small mammals (Conroy *et al.* 1992; Senut *et al.* 1992; Rosina & Pickford, 2019; Peláez-Campomanes *et al.* 2020).

Unexpectedly, Eulipotyphla are poorly-represented. The only mentioned Erinaceidae is a specimen from Berg Aukas I (breccia block 63, extracted in 1991; middle Miocene) attributed to the well-known genus *Galerix*, whose subfamily had never previously been encountered in southern Africa. Another specimen, discovered in the breccia block 52 extracted in 1994, was considered to belong to the same species.

The occurrence of a Galericinae named *Galerix africanus* during the early Miocene of Eastern Africa (Butler, 1956, 1984) followed by the report of *Galerix* in Namibia (Conroy *et al.* 1992; Senut *et al.* 1992) led Butler (2010) to consider that *Galerix* may have dispersed throughout Africa. Since this genus already has a broad distribution in Europe and Asia (Van den Hoek Ostende, 2001), the first aim of the present note was to investigate the potential spread of *Galerix* in Africa.

Material and Methods

The material described here corresponds to two specimens extracted from breccias at the Namibian hominoid-bearing locality Berg

Aukas I (19°30'58"S, 18°15'10"E), during expeditions led in 1991 and 1994. The geological context was thoroughly described by

Pickford & Senut (2002, 2010), in which the oldest level of the palaeocave infilling at Berg Aukas I is estimated to date between 13 Ma and 12 Ma.

Engesser (1980) is followed for terminology and Prieto *et al.* (2010) for the measurement method of length (L), mesial width (W1) and distal width (W2). Measurements were obtained with a binocular LEICA MZ16 A, a digital camera LEICA DFC420, two optical lights sources LEICA CLS 150X, and the programm Leica Application Suite (v. 4.5.0). Drawings were obtained with the software Autodesk SketchBook (v. 8.7.1). Specimens are figured in left orientation and housed at the National Earth Science Museum, Geological Survey of Namibia, Windhoek, Namibia.

Systematic Palaeontology

Order Eulipotyphla Waddell, Okada & Hasegawa, 1999

Family Erinaceidae Fischer, 1814

Subfamily Erinaceinae Fischer, 1814

Genus *Amphechinus* Aymard, 1850

Type species :- *Amphechinus arvernensis* (Blainville, 1839)

Species *Amphechinus* cf. *rusingensis* Butler, 1956

Partial synonymy :-
1992 *Galerix* sp. - Conroy *et al.*
1992 *Galerix* sp. - Senut *et al.*

Type locality :- Hiwegi Formation, locality R.1, Rusinga Island, Kenya; early Miocene.

Original diagnosis :- A species of *Amphechinus* that differs from *A. edwardsi* (Filhol) in the following characters: size smaller (C1/-M3/ inclusive: 13.2-13.5 mm); C1/ and P2/-p/2 less reduced; P2/ with two roots; buccal edge of M1/ slightly longer than that of P4/; M2/ slightly larger in proportion to M1/ (length M2/ - length M1/: 0.82) (Butler, 1956, p. 54).

Material and measurements :- BA 63'91, right P4/ (L=3.28, W1=2.68, W2=3.39); BA 52'94, right m/1 (L=3.12, W1=2.01, W2=2.01).

Berg Aukas MM1, Otavi Mountains, Namibia; late middle Miocene (13-12 Ma) (Fig. 1).

Description

The P4/ has a slightly S-shaped buccal margin because of a rounded parastyle and a curved and elongated metastyle. The paracone is a strong, upright cusp with a subtriangular base. From it starts a high and sharp metaloph reaching the pointed bucco-distal border. The metacone is distinguishable at the center of the crest only by a more worn aspect. A parastyle is attached to the mesio-buccal base of the paracone, without being connected to it by a crest. The distal border of the premolar is concave. The circular protocone is the tallest cusp of the lingual extension of the tooth. A thin bucco-lingual crest is present at the buccal base of this cusp. Another thin ridge is found between the protocone and the small rounded hypocone, which is situated more lingually. A barely distinguishable bulge is also present at the disto-lingual border of the premolar, from which starts a short mesial cingulum. This cingulum is stopped by a distinct notch situated lingually to the metaloph wall. Very narrow cingula are visible at the lingual and mesial base of the metaloph.

The trigonid of the first lower molar is slightly longer than the talonid. The paraconid

177

is the smallest cuspid of the trigonid. Mostly included in the paralophid, it is still distinguishable at the mesio-lingual corner of the tooth. The paralophid is a two-segmented crest connecting the paraconid to a triangular protoconid, the strongest cuspid of the molar. The metaconid has a circular base, smaller dimensions than the protoconid and is situated in a slightly more mesial position than the latter cuspid. Two thin ridges start from the median side of both cuspids, ending at the border of the trigonid distal wall without touching each other. The trigonid basin is open on its lingual side and is characterised by three valleys, the largest one having an almost bucco-lingual orientation. The talonid is much lower than the trigonid. The subtriangular hypoconid is the smallest cuspid of the tooth. The smooth cristid obliqua is almost parallel to the lingual margin. The triangular entoconid is shorter than the paraconid. A weak hypolophid connects the two distal cuspids while a thin ridge joins the base of the entoconid to the base of the metaconid (there is no entocristid). This has led to a continuous closure of the deep and squared talonid basin. The postcingulid is large and connected to the entoconid without being in contact with the hypolophid. A narrow but continuous cingulid is present on the buccal margin.
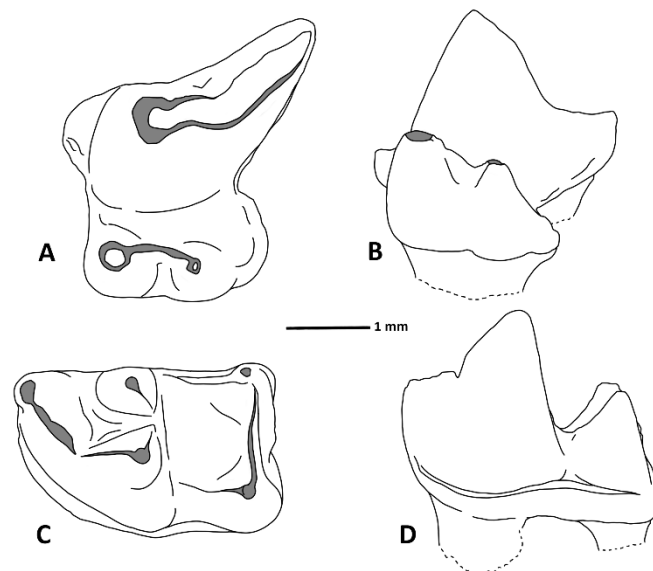

Figure 1. Interpretive line drawings of *Amphechinus* cf. *rusingensis* from Berg Aukas I. **A-B**) P4/ (BA 63'91, reversed). **C-D**) m/1 (BA 52'94, reversed). **A, C**) occlusal, **B**) lingual, **D**) buccal views (scale: 1mm).

Comparisons

While the species of Galericinae are known by their rounded and molarized P4/, the material from Berg Aukas I present a more angular shape with an elongated and sharp metaloph, which is the usual pattern found in Miocene Erinaceinae. A disto-lingual bulge is sometimes found in deciduous P4/ of Galericini (Ziegler, 1983), but the outline of this tooth is much more irregular than the described specimen. The distinctive notch present at the medio-distal margin ("anteroposteriorly compressed lingual region", according to Butler, 1984:146) is usually found in *Amphechinus*, and is more pronounced than in the European *A. baudeloti*. This notch is not similar to the constriction of the lingual area observed in *Mellalechinus salis*. There are no significant differences from the material of *A. rusingensis* from the Sperrgebiet (Mein & Pickford, 2008).

The two-segmented paralophid in m/1 is similar to that of Galericinae and *Amphechinus*, while *Gymnurechinus leakeyi* has a curved crest (Butler, 1984). The talonid of m/1 is lower and simpler than in Miocene Galericini. The postcingulid-entoconid connection is found in *Gymnurechinus*, *Mellalechinus* and *Amphechinus*, but also occurs in derived lineages of Galericini (Van den Hoek Ostende, 2001). The trigonid of the m/1 represents 58% of the total length of the tooth, while representing 60%-63% in *Amphechinus rusingensis* described by Butler

(1984). The first lower molar of *Mellalechinus salis* described by Lavocat (1961) is less compact, with a more stretched and open trigonid, as in *Gymnurechinus*. Moreover, the hypoconid of m/1 is situated in a more buccal position in *A. rusingensis* than in *M. salis*.

The dimensions of the two Berg Aukas specimens do not differ from the morphometric range of the early Miocene *Amphechinus rusingensis*. The size increase observed in the material from Arrisdrift (Mein & Pickford, 2003) is not present in the sample from Berg Aukas. Because it is not possible to compare the Berg Aukas I material with the fossils of *Amphechinus* sp. from Fort Ternan, Kenya (13.7 Ma; Butler, 1984) and the lack of adequate diagnostic features, the two specimens from Namibia are attributed to a young form named *Amphechinus* cf. *rusingensis*.

Discussion

Palaeoecology of *Amphechinus*

The presence of *Amphechinus* at Berg Aukas I occurred at a time of global aridification. While environments where humid and forested during the early Miocene, the hyperarid Namib Desert emerged at the beginning of the middle Miocene (Pickford & Senut, 2002) which probably favoured the success of grazing mammals in southern Africa earlier than in the North-Eastern part of the continent (Pickford, 2008). The desertification of southern Africa was however heterogeneous and the Kalahari-Otavi area seems to have maintained more humid conditions (Senut *et al.* 2009; Rosina & Pickford, 2019), helping the preservation of less adapted forms during the middle Miocene.

A clear evolutionary history of *Amphechinus* is difficult to establish since the generic attribution of several species cannot be fully supported (Ziegler, 2005; Van Dam *et al.* 2020). At least, *Amphechinus* is for now recognized in Asia, Europe, Africa and North America. This suggests that the generalist eco-morphology of this genus allowed it to prosper in a lot of environments during the Oligocene and the Miocene. For instance, the North-American occurrences (Martin & Lim, 2004) coincide with the estimated immigration of several other Asian Eulipotyphla (Rich, 1981) usually considered as inadapted to cold environments, while European forms persisted even after the middle Miocene cooling event with *A. golpae* and *A. robinsoni*. Also, *Amphechinus* is identified in the well-known Spanish fossil record slightly before 16 Ma and survived there although the conditions became drier (Van Dam *et al.* 2020). This ubiquity could explain the longer persistence of *Amphechinus* in southern Africa compared to other Erinaceidae.

Overview of the African fossil record of Erinaceidae

Amphechinus is found in the Miocene of Africa with two other Erinaceinae: *Gymnurechinus* and *Mellalechinus* (previously *Protechinus* Lavocat 1961; see Zijlstra, 2012). Based on the comparisons of Lavocat (1961), *Mellalechinus* probably emerged from an undiscovered *Gymnurechinus*. However, the paucity of the fossil record means that this idea needs to be treated with caution. The first occurrences of *Amphechinus rusingensis*, *Gymnurechinus* and *Galerix africanus* in the Kenyan Koru and Legetet Formations (Fig. 2) are explainable by a single wave of dispersal, before 20 Ma. As for *Galerix africanus* and *Gymnurechinus*, the ancestral shape of *Amphechinus rusingensis* suggests a non-European ancestor. The only African representative of *Amphechinus* is mostly found in the early Miocene but survived at least until the early middle Miocene (Mein & Pickford, 2003; Butler, 2010). While the material from Berg Aukas I confirms the survival of a form close to *A. rusingensis* in the late middle Miocene, the middle Miocene *Amphechinus* sp. from Fort Ternan indicates some morphological diversity and seems to highlight the acquisition of new characters in the African lineage.

From the middle Miocene to the early Pliocene, several occurrences of Erinaceidae are reported on the coastal side of northern Africa (Fig. 2). Almost all available data have been compiled by Stoetzel (2013) with the exception of the significant contribution of Engesser (1980). A large part of Erinaceidae occurrences are identified in the literature as *Galerix* and *Schizogalerix*, but since all the

described material show affinities with *Schizogalerix* (Engesser, 1980; Robinson *et al.* 1982; Ameur, 1984) the presence of the early to middle Miocene genus *Galerix* in the late Miocene and Pliocene of Africa is more than improbable. These materials attributed to *Galerix* should now be considered as "*Galerix*" indet. (or even as Galericinae indet.) since they probably correspond to *Schizogalerix*. Lavocat (1961) identified an incisor (or canine) from Beni Mellal (Morocco, middle Miocene) as belonging to *?Galerix*, and considered another incisor to belong to *Palaeoerinaceus?*

(=*Amphechinus*). It is now well known that such isolated antemolar teeth do not allow precise identification, especially since Beni Mellal is the type-locality of *Mellalechinus*, whose dental variability is unknown. These doubtful identifications are thus not followed here. The last occurrence of the enigmatic *Mellalechinus* (*Mellalechinus* cf. *salis*) coincides with the first occurrence of Galericinae in the Moroccan late middle Miocene locality of Pataniak 6 (Stoetzel, 2013) based on an isolated M2/ attributed to the Galericini *Schizogalerix* cf. *anatolica* by Engesser (1980).
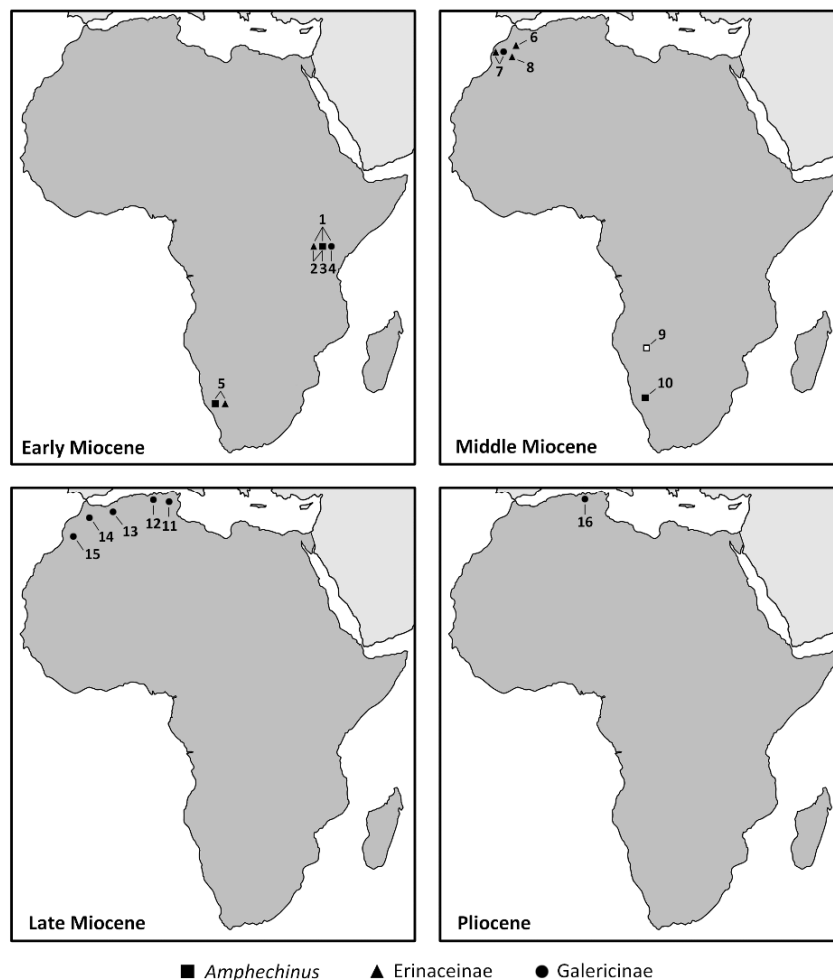

Figure 2. Updated distribution of Erinaceinae and Galericinae during the Miocene and Pliocene of Africa. *Amphechinus* is represented by squares, other Erinaceinae by triangles, and Galericinae by circles. **1**) Legetet Formation, Hiwegi Formation and Kapurtay Agglomerates; Kenya. **2**) Kulu Formation and Karungu; Kenya. **3**) Maboko; Kenya. **4**) Koru Formation; Kenya. **5**) Sperrgebiet localities; Namibia. **6**) Beni Mellal; Morocco. **7**) Pataniak 6; Morocco. **8**) Azdal 1, 3, 6 and 7; Morocco. **9**) Berg Aukas I; Namibia. **10**) Arrisdrift; Namibia. **11**) Amama 1 and 2, Argoub Kamellal 1, Bab el Ahmar, El Hiout, Guergour Ferroudi and Smendou 6; Algeria. **12**) Sidi Ounis; Tunisia. **13**) Bou Hanifia 5, Koudiet el Tine and Sidi Salem; Algeria. **14**) Oued Zra; Morocco. **15**) Afoud 6, Asif Assermo and Oued Tabia; Morocco. **16**) Amama 3; Algeria. Data are based on Engesser (1980), Ameur (1984), Butler (1984, 2010), Mein & Pickford (2003, 2008), Stoetzel (2013), Zouhri *et al.* (2017) and this work.

According to Robinson *et al.* (1982) the Turolian locality of Sidi Ounis (MDM locality, Tunisia) yielded a few teeth attributed by them to *Schizogalerix ?moedlingensis*. The Sidi Ounis specimens plot outside the metric range of variation of *S. moedlingensis*, and fit much better with *S. macedonica*, considered as belonging to the same lineage as *S. moedlingensis* by Doukas *et al.* (1995).

Robinson *et al.* (1982) mentioned the presence of a third cuspule on the lingual side of the M1/, between the protocone and the hypocone. This corresponds to a peculiar diagnostic feature of *S. macedonica*. Also, the trigonid of m/2 is not narrowed, compared to the trend observed in Turkish species (Furió *et al.* 2014). Despite this, it has to be noted that the extra cuspid found near the entoconid of m/1 and m/2 in *S. macedonica* and usually in *S. zapfei* is not described in Sidi Ounis lower molars. This lack also occurs in specimens from Pikermi (Greece) identified as *S. zapfei* by Rümke (1976). Moreover, Furió *et al.* (2014) had the opportunity to study the late Vallesian material of Kastellios Hill (Crete Island) and also found similarities with *S. macedonica* and *S. zapfei*, although the first discovered M2/ from this locality was attributed to *Schizogalerix sinapensis* by Van der Made (1996). The new clues from Kastellios Hill and Sidi Ounis imply a southward dispersal of the European lineage. The material from Sidi Ounis is here considered as belonging to a form named *Schizogalerix* aff. *macedonica*.

Engesser (1980) identified *Schizogalerix* in Oued Zra (Morocco), Amama 1 and Amama 2 (Algeria). The description of the small samples from Oued Zra and Amama 1 seems to imply the persistence into the Vallesian of the late middle Miocene migrant from Pataniak 6. The locality Bou Hanifia 5 (Morocco) may help to understand better the Vallesian record of *Schizogalerix* but only an unmeasured M3/ has been reported (Ameur, 1984). Apart from this, the even bigger *Schizogalerix* nov. sp. (*sensu* Engesser, 1980)

from the Turolian of Amama 2 is easily distinguished from all known species of the genus. It is clear that this material represents a new species that may have been derived from *Schizogalerix* aff. *macedonica*. Younger forms of *Schizogalerix* survived until the early Pliocene of Amama 3 (Algeria), where Galericinae are recorded for the last time in Africa (Stoetzel, 2013). Thus, at least two groups of *Schizogalerix* are identified in the late Miocene of Northern Africa and are related to two distinct dispersals. Finally, It is for now not possible to go further with the enigmatic fragment of M1/ found in the Lukeino Formation (Kenya, late Miocene) and attributed to an indeterminate Erinaceidae by Mein & Pickford (2006). A more southwards dispersal of the Galericini during the middle and late Miocene is considered to be unlikely.

While the ancestral Erinaceinae (*Amphechinus, Gymnurechinus, Mellalechinus*) disappeared during the Miocene, they were not immediately replaced by the recent dry-adapted genera *Atelerix* and *Paraechinus*. Even if the hypothesis of Mein & Ginsburg (2002) is correct by considering the existence of *Atelerix* in the French late Miocene of La-Grive-Saint-Alban (which is still a matter of debate), only a late diversification of *Atelerix* and also *Para-echinus* can be supported. Bannikova *et al.* (2014) estimated by molecular dating that the split between recent species of the two genera took place about 2.5 Ma. Concerning *Atelerix*, it seems to be related to a series of allopatric isolation events in northern Africa (Velo-Antón *et al.* 2019). The exclusively African distribution of recent *Atelerix* suggests an entrance of this genus before this split, during the Plio-Pleistocene transition, which is at least supported by the Plio-Pleistocene material from Ahl Al Oughlam (Zouhri *et al.* 2017). In southern Africa, the presence of *Atelerix* is only attested by a skull from an upper Pleistocene cave deposit of South Africa (Broom, 1937) attributed to *Atelerix major*.

Conclusion

The reassignment of Berg Aukas I fossil hedgehog material supports the persistence of ancestral erinaceids in southern Africa during the middle Miocene while greatly weakening the idea of a more southern expansion of Galericinae. The few occurrences of

Erinaceidae in Africa are mostly explained by a succession of dispersal events around the Mediterranean Basin during the early, middle and late Miocene while extant species seem to have emerged after the Plio-Pleistocene transition. Despite these clues, a large part of

Erinaceidae history in Africa still needs to be discovered.

Acknowledgements

References

Ameur, R. 1984. Découverte de nouveaux rongeurs dans la formation Miocène de Bou Hanifia (Algérie occidentale). *Geobios*, **17**, 167-175.

Bannikova, A.A., Lebedev, V.S. & Abramov A.V. 2014. Contrasting evolutionary history of hedgehogs and gymnures (Mammalia: Erinaceomorpha) as inferred from a multigene study. *Biological Journal of the Linnean Society,* **112**, 499-519.

Broom, R. 1937. Notices of a few more new fossil mammals from the caves of the Transvaal. *Annals and Magazine of Natural History,* Series 10, **20**, 509-514.

Butler, P.M. 1956. Erinaceidae from the Miocene of East Africa - *Fossil Mammals of Africa*, **11**. British Museum (Natural History), London, 75pp.

Butler, P.M. 1984. Macroscelidea, Insectivora and Chiroptera from the Miocene of East Africa. *Palaeovertebrata*, **14**, 117-200.

Butler, P.M. 2010. Neogene Insectivora, *In*: Werdelin, L., & Sanders, W.S. (Eds), *Cenozoic Mammals of Africa*. University of California Press, Berkeley, California, pp. 573-580.

Conroy, G.C., Pickford, M., Senut, B., Van Couvering, J. & Mein, P. 1992. *Otavipithecus namibiensis*, first Miocene hominoid from southern Africa. *Nature*, **356**, 144-148.

Doukas, C.S., Van den Hoek Ostende, L.W., Theocharopoulos, C.D. & Reumer, J.W.F. 1995. The vertebrate locality Maramena (Macedonia, Greece) at the Turolian-Ruscinian Boundary (Neogene). *Münchner Geowissenschaftliche Abhandlungen*, A**28**, 47-64.

Engesser, B. 1980. Insectivora und Chiroptera (Mammalia) aus dem Neogen der Turkei. *Schweizerische Paläontologische Abhandlungen*, **102**, 47-149.

Furió, M., Van Dam, J. & Kaya, F. 2014. New insectivores (Lipotyphla, Mammalia) from the Late Miocene of the Sivas Basin, Central Anatolia. *Bulletin of Geosciences*, **89**, 163-181.

Lavocat, R. 1961. Le gisement de vertébrés miocènes de Beni Mellal (Maroc). *Notes et Mémoires du Services géologique du Maroc*, **155**, 29-94, 109-120.

Martin, L.D. & Lim, J.D. 2004. New insectivores from the Early Miocene of Nebraska, USA and the Hemingfordian faunal exchange. *Mammalian Biology*, **69**, 202-209.

Mein, P. & Ginsburg, L. 2002. Sur l'âge relatif des différents dépôts karstiques miocènes de La Grive-Saint-Alban (Isère). *Publications du Musée des Confluences*, **5**, 7-47.

Mein, P. & Pickford, M. 2003. Insectivora from Arrisdrift, a basal Middle Miocene locality in southern Namibia. *Memoir of the Geological Survey of Namibia*, **19**, 143-146.

Mein, P. & Pickford, M. 2006. Late Miocene micromammals from the Lukeino Formation (6.1 to 5.8 Ma), Kenya. *Bulletin mensuel de la Société linnéenne de Lyon*, **75**, 183-223.

Mein, P. & Pickford, M. 2008. Early Miocene Insectivores from the Northern Sperrgebiet, Namibia. *Memoir of the Geological Survey of Namibia*, **20**, 169-183.

Peláez-Campomanes, P., Mein, P. & Pickford, M. 2020. Fossil Sciuridae (Rodentia, Mammalia) from Berg Aukas (Otavi Mountains,

Namibia). *Communications of the Geological Survey of Namibia,* **23**, 65-89.

Pickford, M. 2008. Diversification of grazing mammals in southern and equatorial Africa during the Neogene and Quaternary. *Memoir of the Geological Survey of Namibia*, **20**, 529-537.

Pickford, M. & Senut, B. 2002. The fossil record of Namibia. *Ministry of Mines and Energy, Geological Survey of Namibia,* Windhoek, Namprint, 39 pp.

Pickford, M. & Senut, B. 2010. Karst Geology and Palaeobiology of Northern Namibia. *Memoir of the Geological Survey of Namibia*, **21**, 1-74.

Prieto, J., Gross, M., Böhmer, C. & Böhme, M. 2010. Insectivores and bat (Mammalia) from the late middle Miocene of Gratkorn (Austria): biostratigraphic and ecologic implications. *Neues Jahrbuch für Geologie und Paläontologie Abhandlungen*, **258**, 107-119.

Rich, T.H.V. 1981. Origin and History of the Erinaceinae and Brachyericinae (Mammalia, Insectivora) in North America. *Bulletin of the American Museum of Natural History,* **171**, 1-116.

Robinson, P., Black, C.C., Krishtalka, L. & Dawson, M. 1982. Fossil Mammals from the Kechabta Formation, Northwestern Tunisia. *Annals of the Carnegie Museum*, **51**, 231-249.

Rosina, V.V. & Pickford, M. 2019. Preliminary overview of the fossil record of bats (Chiroptera, Mammalia) from the Miocene sites of Otavi Mountainland (Northern Namibia). *Communications of the Geological Survey of Namibia*, **21**, 48-58.

Rümke, C.G. 1976. Insectivora from Pikermi and Biodrak (Greece). *Proceedings Koninklijke Nederlandse Akademie van Wetenschappen*, **B79**, 256-270.

Senut, B., Pickford, M., Mein, P., Conroy, G. & Van Couvering, J.A. 1992. Discovery of 12 new late Cainozoic fossiliferous sites in palaeokarsts of the Otavi Mountains, Namibia. *Comptes Rendus de l'Académie des Sciences, Paris*, **314**, 727-733.

Senut, B., Pickford, M. & Ségalen L. 2009. Neogene desertification of Africa. *Comptes Rendus Geoscience*, **341**, 591-602.

Stoetzel, E. 2013. Late Cenozoic micromammal biochronology of northwestern Africa. *Palaeogeography, Palaeoclimatology, Palaeoecology*, **392**, 359-381.

Van Dam, J.A., Mein, P. & Alcalá, L. 2020. Late Miocene Erinaceinae from the Teruel Basin (Spain). *Geobios*, **61**, 61-81.

Van den Hoek Ostende, L.W. 2001. A revised generic classification of the Galericini (Insectivora, Mammalia) with some remarks on their palaeogeography and phylogeny. *Geobios*, **34**, 681-695.

Van der Made, J. 1996. Pre-Pleistocene land mammals from Crete. *In*: Reese, D.S. (Ed.). *Pleistocene and Holocene fauna of Crete and its First Settlers.* Prehistory Press, Madison, Wisconsin, pp. 69-79.

Velo-Antón, G., Boratyński, Z., Ferreira, C., Lima, V.O., Alves, P.C. & Brito, J.C. 2019. Intraspecific genetic diversity and distribution of North African hedgehogs (Mammalia: Erinaceidae). *Biological Journal of the Linnean Society*, **127**, 156-163.

Ziegler, R. 1983. Odontologische und osteologische Untersuchungen an *Galerix exilis* (Blainville) (Mammalia, Erinaceidae) aus den miozänen Ablagerugen vom Steinberg und Goldberg im Nördlinger Ries (Süddeutschland). Unpublished PhD thesis, University of Munich, 224 pp.

Ziegler, R. 2005. Erinaceidae and Dimylidae (Lipotyphla) from the Upper Middle Miocene of South Germany. *Senckenbergiana lethaea*, **85**, 131-152.

Zijlstra, J.S. 2012. A *nomen novum* for *Protechinus* Lavocat, 1961 (Mammalia, Erinaceidae), a junior homonym of the valid name *Protechinus* Noetling, 1897 (Echinoidea, Arbacioida). *Zootaxa*, **3233**, 67-68.

Zouhri, S., Benammi, M., Geraads, D. & El Boughabi, S. 2017. Mammifères du Néogène continental du Maroc: faunes, biochronologie et paléobiogeographie. *Mémoires de la Société Géologique de France*, **180**, 527-588.

COMMUNICATIONS OF THE GEOLOGICAL SURVEY OF NAMIBIA

INSTRUCTIONS FOR CONTRIBUTORS

General

1. Manuscripts must be written in English.

2. A short abstract of less than 200 words must accompany research papers and reports.

3. Short geological notes (commonly less than 1000 words) may also be submitted. Notes do not require an abstract.

4. Contributions have to be submitted in digital format. The preferred format for text is Microsoft Word, for figures jpg or tiff (350 dpi).

5. Papers will be reviewed by external and/or internal referees; reports will be reviewed by internal referees. Manuscripts submitted by students should be critically reviewed by their supervisors before submission. It is the responsibility of the supervisor to ensure that a high standard is maintained.

Text

1. A recent issue of *Communications* should be consulted for the general style and format to be adopted.

2. An alphabetical list of all references must follow the text, with a format as follows:

Blignault, H.J. 1977. *Structural-metamorphic Imprint on part of the Namaqua Mobile Belt in South-West Africa*. Ph.D. Thesis (unpublished), University of Cape Town, 197 pp.

Gevers, T.W. & Frommurze, H.F. 1929. The tin-bearing pegmatites of the Erongo Area, SWA. *Transactions of the Geological Society of South Africa*, **32**, 111-149.

Illustrations

1. Figures and photographs must be of good quality; ensure that lettering is readable after reduction.

2. Figures and tables may be included in the text document to indicate their positioning, but must also be provided separately in one of the above-mentioned formats (jpg/tiff).

3. Figure captions must be provided as a separate list.

4. Headings of tables and appendices should appear above the table.

5. All illustrations or photographs are termed figures, and are referred to as Fig. or Figs in the text.